Initiation and Growth of Cracks Near Fatigue Threshold in Plain Carbon Steels

N. Narasaiah

Initiation and growth of cracks near fatigue threshold in plain carbon steels

Thesis Submitted in Partial Fulfillment
of the Requirements for the Degree of

Doctor of Philosophy

in

Engineering

By

N. Narasaiah

Department of Metallurgical and Materials Engineering
Indian Institute of Technology, Kharagpur-721 302, India
February, 2004.

Department of Metallurgical and Materials Engineering
Indian Institute of Technology
Kharagpur – 721302, India.

CERTIFICATE

This is to certify that the thesis entitled *"**Initiation and growth of cracks near fatigue threshold in plain carbon steels"*** being submitted by **Mr. N. Narasaiah** to the Indian Institute of Technology, Kharagpur, for the award of the degree of **Doctor of Philosophy in Engineering** is a record of bonafide research work carried out under my supervision and guidance. The results presented in this thesis have not been submitted elsewhere for the award of any other degree or diploma.

This work, in my opinion, has reached the standard of fulfilling the requirements for the award of the degree of **Doctor of Philosophy** in accordance with the regulations of the institute.

February, 2004 (Professor K. K. Ray)

ACKNOWLEDGMENT

I would like to express my deep sense of gratitude to Professor Kalyan Kumar Ray, for his invaluable guidance and for the constant inspiration in each and every stage of this research program. In addition, his inspiration at every stage of this work and fatherly treatment built up a momentum inside me. My sincere thanks to him.

I would also like to express my sincere gratitude to Dr. S. Tarafder and Dr. V. R. Ranganath, and thanks to Dr. S. Sivaprasad and to Ms. Prabha Prasad, all from the Fatigue and Fracture group, Materials Evaluation Division, National Metallurgical Laboratory, Jamshedpur for their kind help in conducting a part of the crack initiation tests and for several critical discussion related to my project work. It would have been difficult to complete this work within the current time frame without the help of Dr. Pravash Chandra Chakraborti, Jadavpur University in conducting a few sets of crack initiation experiments. I remain grateful to him.

The author wishes to thank Prof. S.C. Panigrahi, Prof. A. K. Chakrabarti, Prof. U. K. Chatterjee, Prof. O. P. Gupta, Prof. P. G. Mukunda, Prof. S. K. Roy, Prof. M. Chakraborty and Dr. Rahul Mitra for their valuable suggestions during the course of this investigation. I also thank all the faculty of the Department of Metallurgical and Materials Engineering for shaping me up for advanced research. My special thanks are to Prof. B. S. Murty for his brotherly treatment and continued encouragement at all critical stages.

I have enjoyed the healthy research atmosphere in the Mechanical Metallurgy Group (Metal testing, Fatigue, Fracture, Failure analysis, Structure-property correlation etc.) where the cooperative attitude and the sense of togetherness made me feel this as an abode of researchers working together as members of the same family.

The author also wishes to thank Mr. Subhashis Roy and Mr. Basudev Bhattacharya for their help in fabrication of the specimens, Mr. Subhashis Ghosh for his help in conducting the fatigue tests and in some photography work, Mr. B. C. Jena, Mr. B. Deb for their help during the microstructural examinations, Mr. S. Bhattacharyya and V. Das for their help in conducting some of the mechanical tests, Mr. D. N. Mahato and Mr. A. K. Jha for their help in heat-treatment work. I remain

thankful to Dr. R. N. Maiti, Mr. S. Mitra and Mr. D. Sana for their excellent assistance during SEM examinations.

I remain grateful to Dr. A. Chakraborty, DMRL, Hyderabad, Mr. Anish Kumar and Mr. K. V. Rajkumar, IGCAR, Kalpakkam, and Dr. K. Sadananda, Naval Research Laboratory, Washington, USA for their valuable advises and helps in every possible manner in obtaining numerous reprints.

I am grateful to my Senior Research colleagues Dr. Asim Bag, Dr. C. K. Mukhopadhyaya, Dr. Subhadra Sen, Dr. Joydeep Joardar, Dr. M. K. Dutta and others for their friendly encouragement whenever they met me. I take this opportunity to express my heart-felt thanks to my contemporary research colleagues Panigrahi, Ashok Kumar, Kudari, Vinod, Sheela, Kallol, Prasad, Animesh, Shashank, Krishnaiah, Sarath, Kiran, Nandita, Sanjay, Veerababu, Sivakumar, Krishnan, Somnath, Rahul and all other friends for their kind help at the required moments and for making my stay at IIT a memorable one. It is my pleasure to acknowledge thanks to my old friends Sudheer Reddy, Srimannarayana, Nageswara Rao, Kanchan, Sriram, Rawat for their well wishes and constant encouragement at every moment.

Jayanta Das, Vijay Toppo and Prahlad helped me at the final stage of thesis preparation. I convey my special thanks to them. I remain grateful to N. Subba Reddy and A. K. Dutta for their brotherly treatment and helping me at all stages.

I am very grateful to Mrs. S. Sujata (w/o Prof. B. S. Murty), Mrs. N. Sujatha (w/o Mr. N.S. Reddy) and Mrs. Sanju Ray (w/o Prof. K. K. Ray) for their affectionate treatment and providing homely environment during the course of my stay at IIT, Kharagpur. The company of little masters, Mr. Sourya (s/o Mr. N. S. Reddy), Mr. Sasank and Mr. Siddharth (both are s/o Prof. B. S. Murty) and Mr. Ayan Ray (s/o Prof. K. K. Ray) provided joyful breaks from my long hours of continued work. I remain thankful to these little masters.

I remain deeply indebted to my parents, brothers and my sisters-in-law for their continued support. Without their strong support I could not have translated my dream to reality.

(N. Narasaiah)

PREFACE

This dissertation is submitted for the degree of Doctor of Philosophy at the Indian Institute of Technology, Kharagpur, India. This investigation has been carried out in the Department of Metallurgical and Materials Engineering, Indian Institute of Technology, Kharagpur. Except where acknowledgment to previous work is made, this dissertation is my own work assisted and guided by my supervisor at all stages, and no part of this work belongs to any other collaborative project.

This dissertation is divided into eight chapters. Chapter-1 addresses some of the current problems related to the study of crack initiation, short crack growth and fatigue threshold of structural materials. The literature pertaining to fatigue crack initiation, growth of short cracks, fatigue threshold for long cracks, non-propagating cracks and the factors which influence fatigue crack propagation, are outlined in Chapter 2. The chemistry and the microstructure of the steels, selected for this investigation, and their related mechanical properties have been described in Chapter 3. Examinations of crack initiation and its associated mechanisms in a ferritic (single phase) and in a ferrite-pearlite (multiphase) steel are given in Chapter 4. Short crack growth studies in three plain carbon steels, made using a developed technique, have been incorporated in Chapter 5. The long crack fatigue thresholds in four plain carbon steels, determined using a new procedure with the help of a rotating bending machine, have been discussed in Chapter 6. An attempt to model short crack growth behaviour using a new proposition is discussed in Chapter 7. Each of the chapters 3 to 7 includes the objective at the outset followed by details of the experimental work, the results obtained and their pertinent discussion prior to the conclusions drawn. Chapter 8 gives an overall view of the major conclusions drawn from this investigation and suggests the future work in this field.

N. Narasaiah

VITAE

Born on June 02, 1973 at Jallapur, Andhra Pradesh, the author obtained his graduation in Mechanical Engineering in 1997 through successful completion of the examinations required for the Associate Membership of The Institution of Engineers (India). In 1998 he was awarded the GATE scholarship to pursue Masters degree in the Department of Metallurgical and Materials Engineering, Indian Institute of Technology, Kharagpur. After successful completion of the Masters degree, the author was awarded an Institute Scholarship to pursue his Ph.D programme. The keen interest of the author for advanced research on mechanics of materials made him to continue with the same department. Prior to his graduation the author has obtained Diploma in Mechanical Engineering from the State Board of Technical Education and Training, Andhra Pradesh in 1993. During his graduation he has taken apprenticeship training in Hindustan Aeronautics Limited (HAL), Hyderabad for one year and between graduation and post graduation studies the author served Sab Nife Power System Ltd, Hyderabad for one year.

He is a life member of The Institution of Engineers (India), The Indian Institute of Metals and a student member of American Society of Metals International (ASM International). He was the Chairman of the ASM International Student Chapter, Kharagpur for the year 2002-2003 and was a member of executive committee of The Indian Institute of Metals, Kharagpur Chapter between 1999 and 2001. He has participated in several workshops, seminars/conferences related to studies on fatigue, fracture and structural integrity assessment during his Doctoral work. He is recipient of the best paper award at the Fourth National Symposium of Research Scholars (NSRS-4) held in September 2002, at Indian Institute of Technology, Chennai, India. He is also a recipient of the best paper award at the Conference of Research Scholars on Materials Science and Engineering (CRSMSE), held in August, 2003, at Indian Institute of Technology, Kharagpur, India. He possesses a few publications and presentations as listed at the end of the thesis.

Permanent Address

N. Narasaiah
Jallapur - 509153
Mahabubnagar,
Andhra Pradesh, INDIA.
narasaiah@metal.iitkgp.ernet.in
narasaiahn@yahoo.co.in

LIST OF SYMBOLS

Symbol	Description
a	Crack length
a_i	Initial crack length
a_f	Final crack length
a_o	Intrinsic crack length
Δa	Increment of crack extension
da/dN	Fatigue propagation rate
B	Thickness of test specimen
C	Experimental determined scaling constant (Paris equation)
d	distance between two consecutive barriers
E	Elastic (Young's modulus)
f	Fraction of dislocation participating in crack growth
f	Function of stress intensity factor range ΔK and load ratio R
f_{ij}	Dimensionless function of polar angle θ measured from crack
J_{IC}	J-integral value
K_c	Fracture toughness
K_{cl}	Closure stress intensity factor
K_c^m	Critical value of microscopic stress intensity at tip of slip band
K_I	Stress intensity factor in mode I loading
K_{II}	Stress intensity factor in mode II loading
K_{max}	Maximum stress intensity during cycle
K_{min}	Minimum stress intensity during cycle
K_{th}	Threshold stress intensity factor
K_1	Local mode I stress intensity factor for non-linear crack
K_2	Local mode II stress intensity factor for non-linear crack
ΔK	Nominal stress intensity factor range (Kmax - K_{min})
ΔK_{eff}	Effective stress intensity factor range (K_{max} - K_{cl})
ΔK_{eq}	Equivalent stress intensity range for short crack
ΔK_{th}	Threshold stress intensity factor range
L	Slip band length
m	Exponent in Paris power law
N	Number of cycles
N_f	Final number of cycles (N_i + N_p)
N_i	Number of cycles necessary to initiate macrocrack
N_p	Number of cycles necessary to propagate macrocrack subcritically
P_{cl}	Closure load during fatigue cycle

Symbol	Description
P_{max}	Maximum load during fatigue cycle
P_{min}	Minimum load during fatigue cycle
Q	Finite specimen correction factor
r	Radial distance from crack tip
r_p	Size of plastic zone
r_c^*	Critical value of cyclic plastic zone size
r_{rpz}	Reversed plastic zone size
R	Load or stress ratio (K_{min}/K_{max})
W	Width of specimen
X	Distance between crack tip and a grain boundary
w_o	Length of blocked slip band zone
α	Empirical constant
ξ	Factor related to mode mixicity
γ	Shear strain
θ_0, θ_1	Angles associated with crack deflection
ν	Poisson ratio
ϕ	Crack deflection factor
ρ	Notch root radius
σ	Local stress
σ^∞	Nominal stress
σ_{cl}	Closure stress
σ_{max}	Maximum stress
σ_e	Tensile stress corresponding to fatigue limit
σ_{fr}^*	Normal frictional stress for dislocation motion
σ_{ij}	Local crack tip stresses dependent on distance from crack tip and
σ_{th}	Threshold stress for no crack growth
σ_y	Yield stress
$\Delta\sigma$	Local stress range
$\Delta\sigma_{th}$	Threshold stress range for no crack growth
τ	Shear stress
ψ	Factor related surface characteristics of a specimen

Some of the symbols have been used to designate more than one parameter but in such instances the symbol definition has been provided.

LIST OF FIGURES

LIST OF TABLES

ABSTRACT

Fatigue crack initiation, short crack growth behaviour and fatigue thresholds of short and long cracks of a few plain carbon steels (0.003%C, 0.14%C, 0.25%C, 0.47%C and 0.62%C steels) have been studied. The phenomena of the formation of small cracks in 0.003%C (single phase) and 0.14%C (multiphase) steels have been studied on dumble-shaped plate type specimens under varied cyclic stress amplitudes at the load ratio of R = 0. Simple experimental techniques have been developed with new specimen configurations to examine short crack growth behaviour vis-à-vis microstructural features of materials and to determine the fatigue thresholds using a rotating bending machine. The fatigue thresholds have been estimated by load drop procedure and each crack profile is recorded together with the associated microstructures during these studies. The microstructures of the investigated steels have been characterized using optical and scanning electron microscopes. The influence of the microstructural features of these steels on the near threshold crack growth has been examined. Conventional mechanical properties like hardness and tensile parameters have been determined following standard procedures.

Studies on crack initiation revealed that ferrite-pearlite interfaces and/or ferrite-ferrite grain boundaries are preferred crack initiation sites in the investigated steels. The lengths of the initiated cracks at ferrite-pearlite interfaces or at grain boundaries are usually larger in size compared to those of grain body cracks. The formation of slip band inside the grain body, slip band impingement at grain boundary and elastic-plastic incompatibility are attributed as the main causes for crack initiation. The formation of irregular voids inside slip bands, initiation and growth of small voids at grain boundaries and subsequent joining of these are some interesting observations for fatigue crack initiation in 0.003%C steel. It is observed here for the first time that the angle between the direction of banding and the loading axis, has pronounced effect on the orientation and on the size of initiated cracks.

Studies on short crack growth have demonstrated that the developed technique (with new specimen configuration) can be used satisfactorily to understand short crack growth behaviour and to determine the transition length from short to long

cracks. The estimated critical crack lengths can be considered as function of the nature of the short cracks. Short crack growth rate decreases or gets arrested with increasing crack length under the same applied crack driving force. The fatigue threshold values obtained from short crack growth experiments are found to lie in a narrow range and are closer to long crack thresholds. The cracks were found to have affinity to grow through interfaces, but the length of a crack passing through a specific phase was found to be approximately proportional to its amount.

The developed technique to determine fatigue thresholds using a rotating bending machine yielded reliable results. The fatigue thresholds of four steels with carbon contents 0.003, 0.25, 0.47 and 0.62% were found to be 3.8, 4.2, 5.8 and 6.0 $MPam^{1/2}$ respectively. The developed procedure is based on the measurement of da/dN with high sensitivity of the order of 10^{-12} m/cycle and the obtained threshold values appear to represent effective fatigue thresholds determined by conventional technique. Analysis of the crack growth behaviour near the notch indicates occurrence of non-propagating cracks only in 0.25%C and 0.47%C steels. The occurrence of non-propagating cracks has been attributed to the presence of some secondary stress field at the crack tip. Fatigue threshold at R = -1 for plain carbon steels increases with increasing carbon content or the harder pearlitic constituent.

A new model for short fatigue crack growth has been proposed to overcome some of the limitations of the earlier models. The model accounts the effect of mixed mode loading and the surface characteristics of a specimen, and describes both short and long crack growth. A series of computations have been carried out to examine the influence of different parameters considered in the model to describe short crack growth rate. The generated experimental results as well as some reported results have been satisfactorily described using the proposed model.

CONTENTS

Chapter 1

Introduction

Advances in technology have brought the issue of structural integrity to the fore and the latter is intimately concerned with the fatigue damage in materials. An appreciation of the importance of fatigue crack initiation and its growth, and variables that influence fatigue crack propagation is being made for more than a century. The introduction of stress intensity factor concept and its application to fatigue in 1960's have led a great deal of research in various manners into studies related to fatigue crack propagation. The strengthening of fracture mechanics concepts has led investigators to analyse fatigue data through popular relationships between alternating stress intensity factor range (ΔK) and crack growth rate (da/dN); because these provide a strong rational basis for predicting fatigue lifetime and failures. Concepts related to short crack growth behaviour in materials have emerged in 1970's. Over the past three decades though there have been numerous investigations related to microcrack nucleation, short crack growth and fatigue thresholds, there exist several unanswered queries and difficulties to evaluate fatigue damage in this regime. The present investigation deals with the latter regime and aims to strengthen the understanding of fatigue damage below and near fatigue threshold values in structural materials.

Micro-crack nucleation in structural materials is considered to be the first stage in fatigue damage. By now it is well conceived that a large percentage of (high cycle) fatigue life of smooth specimens is spent in the domain of crack nucleation and small crack growth especially in the emerging clean (i.e. with very low inclusion content) structural materials. The existing studies related to the mechanisms of crack nucleation are found to be mostly associated with concepts related to sub-structural features e.g. dislocations, dislocation-vacancy complexes, dislocation dipoles etc. [1-3]. It is well known by now that the microstructure of a material significantly influences this stage of fatigue damage. But information related to the role of microstructure on micro crack nucleation are limited and scattered, and these have not resulted in any generalization plausibly because of the numerous variety of

microstructures encountered in the different investigated materials. The earlier attempts to probe this aspect, have usually laid more emphasis either on the investigated material system or on the mechanism of crack initiation rather than trying to reveal the effect of microstructure on the location of crack nucleation. Also at times two-phase materials exhibit banded microstructure. The existing literature does not indicate the role of such structures on the nucleation of small crack. The present study aims to achieve understanding about the location, characteristics and the associated initiation mechanisms of small cracks in single and two-phase materials with randomly distributed constituents and banded structures.

The second stage in fatigue damage is short crack growth (SCG). There has been an upsurge of interest to understand the behaviour of short cracks as it is well recognized by now that fatigue lifetime of several structural components is considerably influenced by the rate of growth of small cracks. When the fatigue behaviour of such short cracks was studied in late 1970's and early 1980's by several researchers, e.g. Pearson [4], Morris et. al. [5], Miller et. al. [6] and Newman [7], it was found that short crack growth rates exceed those of long cracks at same ΔK, and short cracks are observed to grow at stress intensities below the long crack threshold.

The earlier studies related to short crack growth are primarily directed to understand their mechanics and mechanisms with consequent attempts to model the growth of these cracks. It is well documented in several investigations that short crack exhibit several 'arrests' during their growth; these 'arrests' are often referred as short crack fatigue threshold (SCFTH). The maximum value of fatigue threshold for short cracks is referred here as near long crack fatigue threshold (NLFTH). The earlier studies related to short crack growth in different materials have not laid sufficient emphasis on the understanding NLFTH and its relationship with long crack fatigue threshold. One of the major aims of this investigation is to estimate and to understand this feature of short crack. The limited investigations on SCFTH and NLFTH are plausibly due to difficulties associated in their determination. Attempts are therefore directed in this study to determine these parameters with an alternate test procedure in a relatively simple manner.

There exist several attempts to describe short crack growth behaviour through modeling which takes into account a few physical phenomena. But two important

aspects have not been considered so far in modeling short crack growth behaviour. First, the nucleation and growth of a short crack cannot be assumed to occur perpendicular to the loading direction. This is evident from the fact that stage-I crack initiation usually occurs at an angle 45^o to the tensile or compressive loading direction. When the growth of such cracks gets retarded at a barrier with subsequent movement associated with deflection, the mean crack length can be considered to remain at some angle to the principle stresses. Secondly, short cracks are generally considered to nucleate inside slip bands. It is known that defect density and hence stresses at the surface of a specimen are different than that prevailing inside its bulk. Thus surface phenomena in solids are expected to influence growth of short cracks. These aspects have not been accounted in the earlier models. An attempt is also made here to model short crack growth behaviour incorporating the above factors.

The design of structural materials against fatigue damage requires the knowledge of the nature of variation of crack growth rate (da/dN) with alternating stress intensity factor (ΔK) and the magnitude of fatigue threshold (ΔK_{th}). The assessment of these engineering parameters is conventionally carried out following the ASTM standard E-647 [8]. The determination of ΔK_{th} usually requires significant time engagement of servo-hydraulic or electro-magnetic resonance type machines. As a result, studies on fatigue behaviour at crack growth rates $< 10^{-6}$ mm/cycle is considerably limited compared to that at da/dN$>10^{-6}$ mm/cycle. But fatigue studies at crack growth rates $<10^{-6}$ mm/cycle is important to explore the mechanics and mechanisms of crack growth behaviour in structural materials designed for safe-life applications. One of the major aims of this investigation is thus to search for alternative simple techniques for studying crack growth behaviour at low da/dN values, and thereby to estimate ΔK_{th} of structural materials.

The search for a possible quantitative relation between the lengths of crack paths and their associated microstructure has not been made so far. Studies of this nature can bring forth information about the weak links in a microstructure through which a crack prefers to pass through or the affinity of a crack to travel through any specific phase in a microstructure. This aspect has been examined for the first time in this investigation for both short and long crack growths.

The present investigation is founded on the issues highlighted above. This investigation aims to encompass a series of studies on microstructural aspects, conventional mechanical properties, fatigue crack initiation, short crack growth behaviour and thresholds of a few plain carbon steels. Five varieties of plain carbon steels having carbon content of 0.003%, 0.14%, 0.25%, 0.47% and 0.62% are chosen for this study.

The major objectives of this investigation and some details of the work to fulfill these are enumerated below.

1. To characterize microstructures and to evaluate the conventional mechanical properties of the selected steels

The characterization of the microstructures of the investigated steels incorporates (a) determination of the amount and distribution of the various phases in the microstructure (b) estimation of the cleanliness of the steels (c) measurement of ferrite grain size (d) determination of hardness and (e) evaluation of tensile properties of the selected steels.

2. To examine fatigue crack initiation in single and multiphase steels

This consists of (a) identification of the preferred crack nucleation sites in 0.003%C (single phase) and 0.14%C (multiphase) steels, (b) examination of the effect of banding on small crack initiation, (c) understanding the possible mechanisms of crack initiation in the investigated steels.

3. To develop a simple technique for short crack growth studies and to characterize short crack growth behaviour in plain carbon steels

This includes (a) design and development of a new specimen configuration to study short crack growth in structural materials using a rotating bending machine, (b) determination of short crack growth characteristics and their threshold values in 0.003%C, 0.25%C and 0.47%C steels, and (c) examination of the influence of the investigated microstructures on crack paths.

4. To develop a technique to determine long crack fatigue thresholds using a rotating bending machine and to evaluate threshold values of a few plane carbon steels

This aspect pertains to the estimation of fatigue thresholds of 0.003%C, 0.25%C, 0.47%C and 0.62% steels. This part of the investigation incorporates (a) development of a new technique for studying crack growth behaviour using a rotating bending machine, which primarily involves design and fabrication of a new specimen configuration, (b) determination of fatigue crack growth thresholds of 0.003%C, 0.25%C, 0.47%C and 0.62%C steels using the developed technique and to examine their appropriateness, (c) examination of the existence of non-propagating cracks in the investigated steels, and (d) assessment of the effect of microstructure on the crack paths.

5. To model short crack growth behaviour

This part of the investigation consists of (a) comparison of the available models to describe short crack growth behaviour, (b) proposition of a new model, and (c) assessment of the applicability of the model to the generated short crack growth data and to some available experimental data.

Chapter 2

Literature review

This chapter deals with the pertinent literature related to fatigue damage below and near fatigue threshold in structural materials and begins with an outline on the general aspects of the analyses of fatigue cracks in section 2.1. A brief description of the phenomenon of crack initiation and that of the mechanisms associated with initiation and growth of cracks in structural materials are given in section 2.2. At the start of section 2.3 the definition of short cracks and the terminologies associated with the anomalous behaviour of these cracks are given. Emphasis has been laid to describe the salient features of the test procedures, crack length measurements and problems associated with short crack growth studies in this section. At the end of this section, the existing literature pertaining to modeling of short cracks is summarized. The different types of measurements for long crack fatigue threshold, the role of load shedding procedure on its estimation and the factors that affect the estimated magnitudes of this parameter are discussed in section 2.4. Non-propagating cracks and their salient features are outlined in section 2.5. The role of mechanical, microstructural and environmental factors on crack propagation is outlined in section 2.6. The chapter is concluded with an appraisal of the present investigation.

2.1 Analysis of fatigue cracks – an outline

2.1.1 Approaches to fatigue analysis

The propagation of fatigue damage in a structural component consists of several sequential stages till catastrophic fracture occurs. These are (i) sub-structural changes causing nucleation of micro-cracks, (ii) creation of micro-cracks, (iii) growth and coalescence of micro-cracks to a dominant macro-crack, (iv) stable propagation of the dominant macro-crack, and finally (v) structural instability causing complete fracture. The design philosophy against fatigue damage either considers all the stages or it considers only the stable sub-critical propagation of the dominant macro-crack. The former one is referred as total-life approach whereas the latter one is termed as defect-tolerant approach.

The total life approach is the classical one used by practicing engineers for over a century. This classical approach involves characterization of total fatigue life to failure in terms of cyclic stress range (S-N curve approach) or plastic or total strain range (low-cycle fatigue). The number of stress or strain cycles necessary to cause fatigue failure in nominally smooth-surfaced laboratory specimens is estimated in this approach. The fatigue life estimated by this approach takes into account the number of fatigue cycles to initiate a dominant macro-crack and its subsequent propagation till catastrophic failure. Often the number of cycles to initiate a macro-crack is predominately significant than the number of cycles required to propagate it. But the exact proportion for the number of cycles to initiate a crack to the number of cycles for its propagation is uncertain and the ratio depends on specimen size, its geometry and its surface condition apart from the dependence on chemistry and microstructure of the material.

The defect-tolerant philosophy originates form the fracture mechanics principles and is based on the basic premise that all engineering components are inherently flawed. The useful fatigue life of a structural component is thus defined as the number of fatigue cycles or time to propagate a dominant macro-crack from its initial size to some critical dimension, based on the fracture toughness of the material. The prediction of crack propagation life using defect-tolerant approach involves empirical crack growth laws based on fracture mechanics. The apparent distinction can be summarized as: the total-life approach deals primarily with the resistance to fatigue crack initiation and its subsequent growth on nominally defect free laboratory specimens, whereas the defect-tolerant approach deals with the resistance to fatigue crack growth. Interestingly the design of alloys for these two approaches requires different considerations. For example, high strength material with fine grain microstructure leads to longer fatigue life by the total-life approach. On the other hand, the resistance to growth of a long fatigue crack generally increases with increasing grain size or decreasing yield strength.

2.1.2 Paris law

The fatigue crack growth rate (FCGR) data (da/dN) in defect-tolerant approach is generally examined against the corresponding stress intensity factor range (ΔK) in a manner suggested by Paris and Erdogan [9]. The concept of stress intensity

factor (K) is explained in Appendix-A [10-40]. A plot between d*a*/dN *vs* ΔK for various materials can be schematically represented as shown in Fig.2.1. Such a plot is usually subdivided into three regions as shown in Fig.2.1, and the data in regime II is generally expressed as:

$$\frac{da}{dN} = C(\Delta K)^m \qquad \ldots(2.1)$$

where C and m are considered as material constants. The expression (2.1) is commonly referred as Paris or Paris–Erdogan equation. The magnitudes of the constants in this equation are influenced by material, microstructure, environment, temperature and load-ratio.

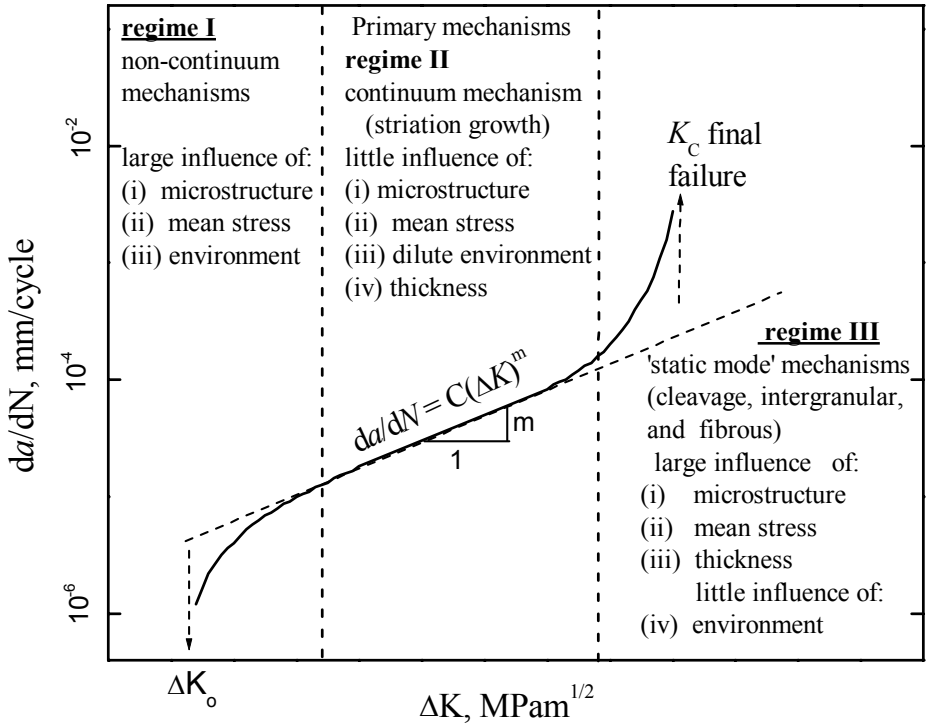

Fig.2.1. Schematic variation of da/dN with ΔK.

There has been some controversy about the form of fatigue crack growth law for long cracks and several investigators have preferred to describe crack growth rate by a two-parameter approach in which the second parameter is either K_{max} or R. Such a law can be expressed as [13]:

$$\frac{da}{dN} = f(\Delta K, R) \qquad \ldots(2.2)$$

$$\frac{da}{dN} = \frac{C(\Delta K)^m}{(1-R)K_c - \Delta K} \qquad \ldots(2.3)$$

where K_c is the cyclic fracture toughness

2.1.3 Short cracks

The practice of characterizing the growth of fatigue cracks on the basis of fracture mechanics primarily relies on data obtained from laboratory fatigue tests on specimens containing 'long' cracks, which are typically several millimeters in length. However, many defects encountered in service are significantly smaller in dimension, for example that in turbine discs and blades etc. Design for such critical engineering components requires an understanding of propagation of these small fatigue cracks. The fatigue behaviour of such short cracks has been studied experimentally and it is well-documented [41-45] that the growth rates of short cracks can be significantly greater than the corresponding rates of long cracks when characterized in terms of the same nominal driving force (Fig.2.2). The application of laboratory data (derived from experiments on long fatigue cracks) to design against the failure of safety-critical components containing short flaws can lead to dangerous overestimation of fatigue lives.

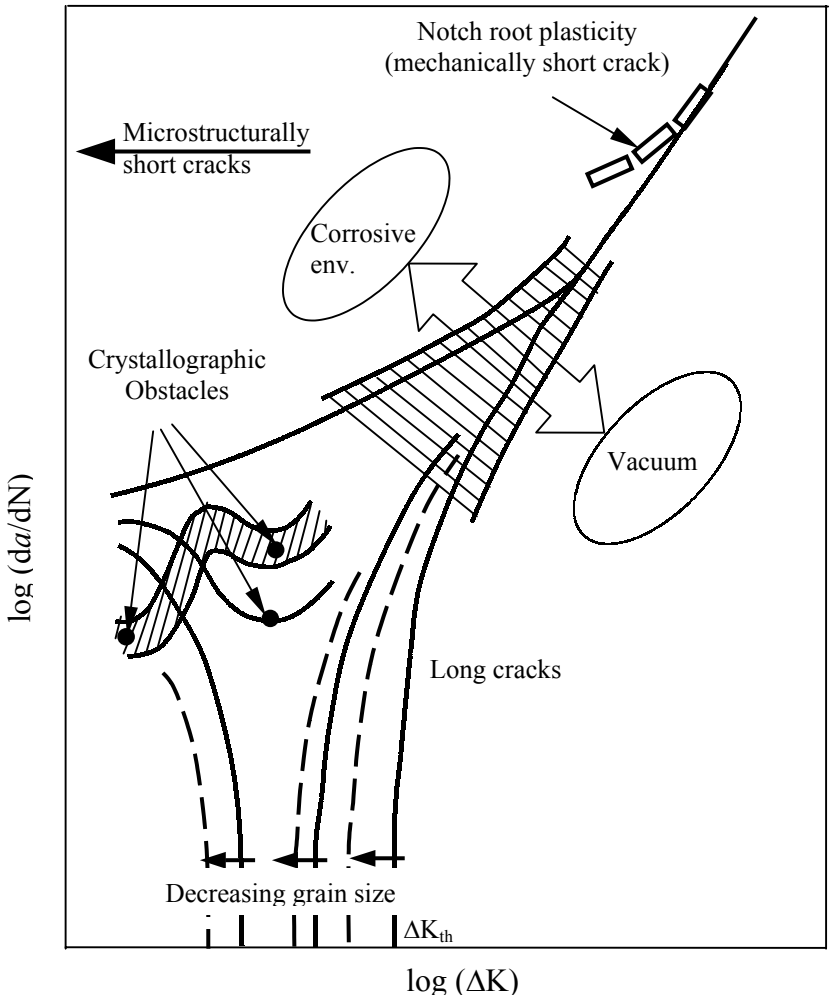

Fig.2.2 Characteristics of short cracks and its transition to long crack behaviour.

The practical significance of the 'short crack problem' can be better illustrated with the estimated fatigue life of a commercial alloy, Fig.2.3 [46]. This figure contains experimental data on the number of fatigue cycles to failure for cracks of different initial dimensions in a nickel-base superalloy. Current design methodology based on linear elastic fracture mechanics (LEFM) provides accurate estimates of fatigue life in this material when the initial size of the fatigue flaw is larger than 0.3 mm [1]. However, when the material contains defects that are smaller than this size, life predictions nominally based on LEFM may give non-conservative values. This complication arises because the actual growth characteristics, crack path tortuosity or closure processes for small flaws can be different from those of longer flaws.

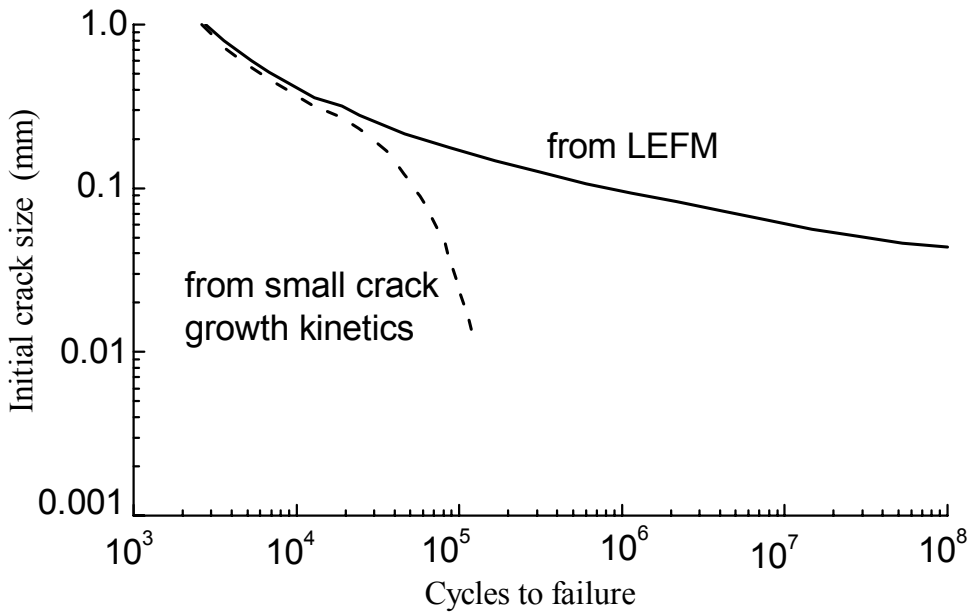

Fig.2.3 The number of fatigue cycles to failure estimated using LEFM and small crack growth kinetics as a function of initial flaw size for an Astroloy [46].

2.1.4 Fatigue thresholds

Fatigue crack propagation in regime-I (Fig.2.1) deals primarily with non-continuum failure processes, where the increment of average crack extension is smaller than lattice spacing. In this region, the stress intensity factor range approaches the fatigue crack growth threshold (ΔK_{th}). The defect-tolerant design takes into account that most of the engineering structures are inherently flawed. This design philosophy ensures that an existing flaw will not propagate to failure within foreseen

in-service time or between given inspection periods. The lifetime prediction is commonly done using the constants of Paris-type relations obtained from standard fatigue crack growth curves. But some components, for example, in the aerospace and automobile industries can experience a high number of load cycles within their in-service period and have to be designed for infinite life. For this condition, the defect-tolerant design has to describe the non-propagating condition of inherent cracks and needs to predict the fatigue limit of the components. The fatigue crack growth threshold, ΔK_{th}, is the characteristic value to determine this condition.

An operational definition for ΔK_{th} is commonly used in terms of a maximum crack growth rate (typically 10^{-8} mm/cycle), based on the accuracy of the crack monitoring system and the number of elapsed cycles. For example, if the method used for crack length measurement is accurate to at least 0.1 mm, and if no crack advance is detected for at least 10^7 cycles, a crack growth threshold is considered to have been reached. Near threshold crack growth rates and the value of the threshold ΔK_{th} are sensitive to several mechanical and microstructural and environmental factors, namely, mean stress, load ratio, prior stress history, crack size, cyclic frequency, number and nature of phases, grain size, grain boundary composition etc. From both the scientific and practical viewpoints, near threshold fatigue offers a challenging research topic in that large changes in the value of ΔK_{th} (and hence in the total fatigue life) can be effected by alterations in the above factors.

2.2 Initiation and propagation of fatigue cracks

2.2.1 Fatigue crack initiation

The process of fatigue inherently consists of cyclic deformation that leads to the formation of ridges (hills) and grooves (valleys) on the surface of a material. The valleys and hills formed on the surface are commonly referred as intrusions and extrusions respectively. The initial documentation of these phenomena was by Forsyth and Stubington [47]. Subsequent to the revelation of slip induced surface roughening during fatigue [47], the mechanism of fatigue crack formation in metals and alloys was rationalized by Wood [48]. The basic premise of Wood's postulate is that repeated cyclic straining of a material leads to different amounts of net slip on various glide planes. The irreversibility of shear displacements along the slip bands then results in the 'roughening' of the surface of a material. This roughening is

manifested as microscopic ‘hills’ and ‘valleys’ at sites where slip bands emerge at the free surface. The valleys so generated act as micro-notches and the effect of stress concentration at the root of the valleys promotes additional slip and fatigue crack nucleation. The fatigue crack nucleation during cyclic loading by this process is schematically illustrated in Fig.2.4.

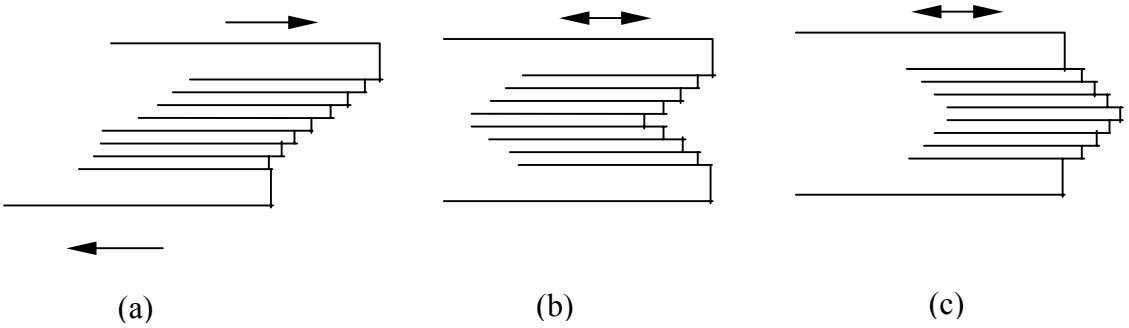

Fig.2.4 Wood’s concept of micro-deformation leading to formation of fatigue crack: (a) Static deformation, (b) Fatigue deformation leading to surface notch (intrusion), (c) fatigue deformation leading to slip-band extrusion [48].

Wood’s hypothesis is limited by the fact that it does not explain why intrusions progressively deepen. Mott [49] suggested that screw dislocations, moving along different paths in slip bands of a crystal during forward and reverse glide, repeat their path by cross slip. The screw dislocations complete a circuit during a fatigue cycle; the volume encompassed by the circuit is then translated parallel to the dislocation by a distance equal to its Burgers vector. This displacement manifests itself in the form of an extrusion at the specimen surface. The proposal of Mott is considered as one of the basic reasons for surface roughening.

2.2.1.1 Crack initiation along persistent slip bands (PSBs)

The interface between the PSB and the matrix is a plane, which exhibits a sharp gradient of dislocations. These interfaces serve as preferential sites for fatigue crack nucleation [2]. Direct experimental evidence of crack initiation at the interface has been obtained by Hunshe and Neumann [50] and Ma and Laird [51,52]. Strains within the PSB are highly inhomogeneous and localized at the PSB-matrix interface. Fatigue crack initiation gets strongly influenced by the roughening of the surface. The population of these fatigue cracks increases linearly with the number of cycles and the applied strains [1].

Direct evidence of crack initiation and early crack growth along PSBs has been obtained in fatigued polycrystalline Cu by Katagiri et. al. [53]. With high voltage TEM observation of dislocation arrangements ahead of pre-cracks, Katagiri et. al. [53] established that crack nucleation and early crack growth occur in the PSB.

2.2.1.2 Crack initiation along grain boundaries

The nucleation of fatigue cracks at grain boundaries occurs under the influence of embrittling environment (which preferentially attack grain boundaries and the second phase particles/inclusion particles, if any) and elevated temperature (at which grain boundary cavitation and sliding are promoted). Intergranular failure is also commonly observed in brittle solids due, at least in part, to the residual stresses induced by thermal contraction mismatch between adjacent grains. The occurrence of fatigue crack nucleation at grain boundaries in a ductile solid, in absence of grain boundary particles, creep deformation or environmental influence, is relatively less common. There have been some documentations of purely mechanical fatigue failure along grain facets [54-57].

Kim and Laird [55] noted that fatigue cracks may nucleate at grain boundaries if: (i) these boundaries separate highly misoriented grains, (ii) the active slip system of at least one of the grains is directed at intersection of the boundary with the specimen surface, and (iii) the traces of the high angle grain boundaries in the free surface make a large angle (30-90^{o}) with tensile stress axis.

In general, grain boundary cracking may arise from one of two mechanisms during cyclic loading: (i) at low to intermediate plastic strain amplitude, the impingement of PSBs at grain boundaries causes cracking [56,58] and (ii) at high plastic strain amplitudes grain boundary cracking occurs as a consequence of surface steps formed at the boundary [55].

In BCC metals such as commercially pure iron, intergranular crack nucleation has also been observed under reversed bending and push-pull axial loading over the cyclic frequency range 0.01-1000 Hz [59]. Asymmetry of slip associated with the glide of screw dislocation in tension and compression can induce shape changes in BCC single crystals. The surface roughness created by similar shape changes in the

near-surface grains of polycrystalline BCC metals, such as α-iron, can cause intergranular crack nucleation [60].

2.2.1.3 Crack nucleation in commercial alloys

In engineering components made of commercial materials, the principal sites of heterogeneous fatigue crack nucleation include voids, slag or gas entrapments, dents, scratches, forging laps and folds, macroscopic stress concentrations, as well as regions of microstructural and chemical non-uniformity. While surface grains are the most likely locations for crack initiation in metals and alloys of high purity, the formation of fatigue cracks is feasible at both near-surface and interior locations in commercial alloys.

The mechanism of fatigue crack initiation at defects depends upon a number of mechanical, microstructural and environmental factors. These factors involve the slip characteristics of the matrix, the relative strength values of the matrix and the defect, the strength of the matrix-inclusion interface, and the relative susceptibility of the matrix and the inclusion to corrosion in the fatigue environment. The effect of inclusions on fatigue crack initiation is often specific to the alloy system.

In high strength steels containing MnS particles the initial stage of fatigue damage is associated with the debonding of the inclusion from the matrix. This occurs by a quasi-static mode of failure in that the interfacial separation is induced during the very first tensile loading at far-field stress levels close to the threshold stress range for infinite fatigue life [61].

In aluminium alloys, constituent particles such as the S-phase (Al_2CuMg) and β-phase (Al_2Cu_2Fe), typically 1-10 μm in diameter, provide sites for fatigue crack nucleation. The type of cracking, however, is a function of microstructure and test conditions. In 2024-T4 aluminium alloy, Grosskreutz and Shaw [62] noticed the debonding of the particle-matrix interface after cyclic damage within the matrix over a large number of fatigue cycles. Another type of crack nucleation in the 2024-T4 alloys involves cracking along slip bands emanating from or terminating at the inclusions.

In high strength nickel-base superalloys, crack initiation has been identified with the existence of large defects, either pores or non-metallic inclusions [63]. At

room temperature, crystallographic cracking at or near the surface is initiated at the sites of the defects of both low and high strain ranges. At an elevated temperature of 760^{o}C, low strain range fatigue results in crack nucleation at the interior of a specimen.

2.2.1.4 Environmental effects on crack initiation

There is a wealth of experimental evidence indicating that the environment plays an important role in dictating the extent of slip irreversibility and fatigue life. Gough and Sopwith [64] and Thompson et. al. [65] demonstrated that the fatigue life is markedly improved in vacuum or in dry, oxygen-free media as compared to moist laboratory air. For fatigue in pure metals in vacuum or in an inert environment, single slip during the tensile loading cycle produces slip steps at the surface. The extent of surface slip offset can be diminished by reverse slip during unloading or subsequent compression loading in fully reversed fatigue. In inert environments, surface roughening during fatigue occurs primarily by a random process. On the other hand, when slip steps form during the tensile portion of a fatigue cycle in laboratory air or in a chemically aggressive medium, the chemisorption of the embrittling species (such as oxygen or hydrogen) or the formation of an oxide layer on the freshly formed slip step makes reverse slip difficult on the same slip plane upon load reversal. In the embrittling medium, this process (schematically shown in Fig.2.5) can provide a mechanism of enhanced surface roughening as well as easier transport of the embrittling species to the build of the material preferentially along the persistent slip bands, thereby facilitating crack nucleation.

If a cyclically loaded engineering component (made of commercial alloy) is exposed to a chemically aggressive environment during service, preferential attack of the environment at selected locations on the material surface may provide nucleating sites for fatigue crack. These sites are generally corrosion pits which form at surface locations where: (i) slip steps or intrusions are created at the surface, (ii) grain boundaries, either embrittled by tempering treatments (as in alloy steel) or surrounded by precipitate-free-zones (as in age-hardened alloys) intersect the surface, (iii) the protective oxide layer on the surface is partially broken, exposing the underlying fresh metal to preferential chemical attack, (iv) inclusions, such as MnS particles in steels,

debond from the surrounding matrix at near-surface locations, and (v) one of the constituent phases in a multiphase alloy is preferentially corroded.

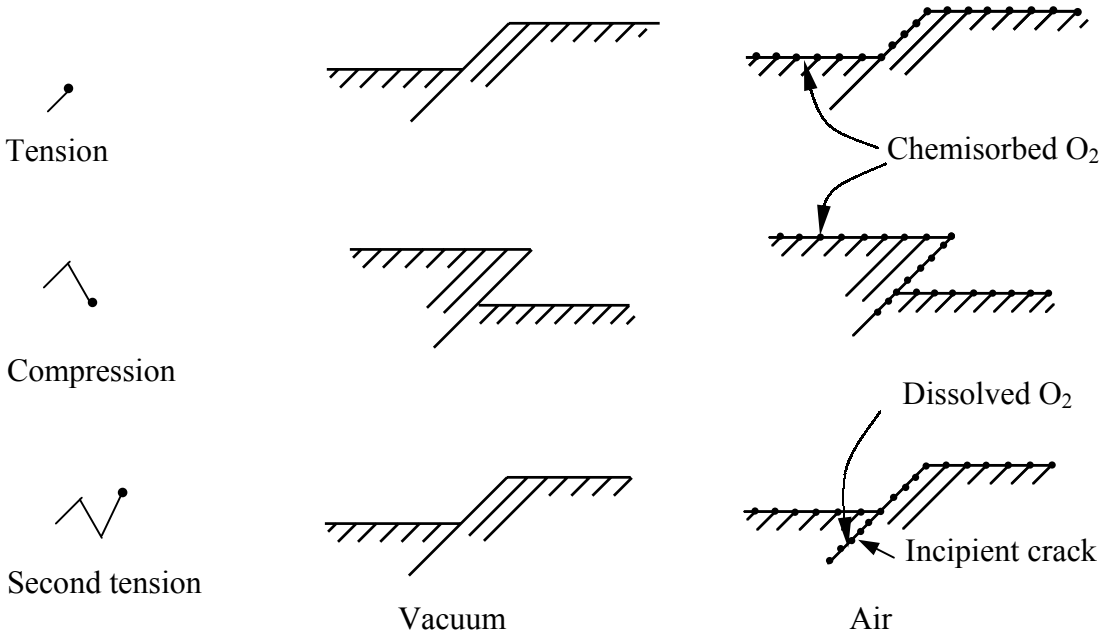

Fig.2.5 The model for fatigue crack nucleation near a free surface by the synergistic effect of single slip and environmental interactions due to Thompson et.al. [65].

Corrosion pits are typically smaller than a millimeter in depth and serve as micro-notches, which locally elevate the stress level. Furthermore, the PH level of the corrosive medium inside the pit can be more acidic than that in the bulk, causing possible acceleration in the rate of fatigue crack growth.

2.2.2 Crack growth mechanism

The mechanism of cracking during fatigue crack growth depends on the magnitude of ΔK. For low ΔK in stage-I the plastic deformation associated with the crack tip remains confined within a few grains, whereas at high ΔK such plastic deformation encompasses a large number of grains. In stage-I (low ΔK) deformation occurs by single slip, whereas in stage-II (intermediate or high ΔK) deformation occurs by duplex slip. The single slip leads to a zigzag crack path whereas the duplex slip results in a planar crack path. The difference in the nature of crack paths during stage-I and stage-II crack growth is shown in Fig.2.6.

The stage-II crack growth in most of the engineering alloys leads to the formation of fatigue striations. The popular model for the formation of fatigue

striation has been proposed by Laird [66]. The increment of crack extension in this model is visualized as successive plastic blunting and re-sharpening of crack under repeated load reversals. The blunting and opening of a crack occur under the tensile cycle whereas the re-sharpening and closure occur under compression cycle. The closure or re-sharpening of a crack cannot fully negate the blunting and its associated extension, and the net crack growth occurs during a fatigue cycle leading to the formation of striations. The model for formation of fatigue striations is schematically shown in Fig.2.7.

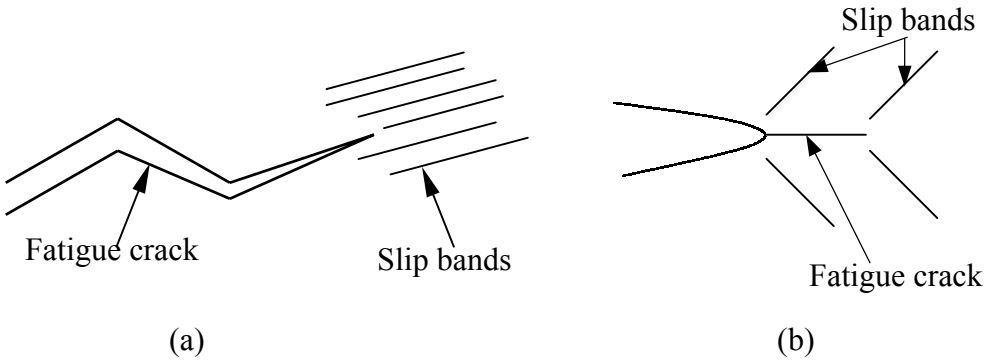

Fig.2.6 A schematic view of fatigue crack growth: (a) Stage I, (b) Stage II.

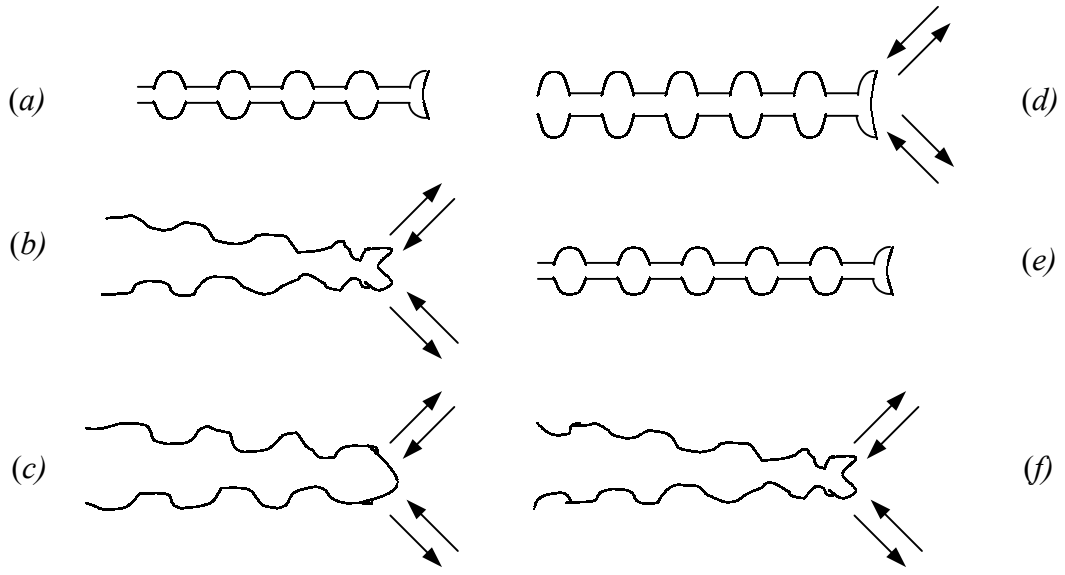

Fig.2.7 An illustration of plastic blunting and re-sharpening which leads to stage II fatigue crack growth in fully reversed fatigue: (*a*) zero load, (b) small tensile load, (c) peak tensile load, (d) onset of load reversal (e) peak compressive load, and (f) small tensile load in the subsequent tensile cycle. Arrows indicate slip direction.

2.3 Short cracks and their anomalous behaviour

2.3.1 Definition

The definition of short cracks originates from the experimental observations of abnormal crack growth as shown in Fig.2.8. The physical description of these cracks is not straightforward; however, following Suresh [1] these cracks can be defined as:

(i) cracks which are simply physically small having dimension of ≤ 0.5- 1 mm

(ii) cracks which are of a length comparable to the scale of the microstructural parameters like grain size

(iii) cracks which are of a length comparable to the scale of local plasticity like a crack embedded in the plastic zone of a notch

(iv) cracks of a length which are amenable to analysis by linear elastic fracture mechanics in neutral environment but exhibit anomalies in chemically aggressive environment.

A schematic view illustrating the physical nature of these cracks is given in Fig.2.2. In general short fatigue cracks can be defined as those, which are not amenable to an unambiguous characterization by linear elastic fracture mechanics parameters.

2.3.2 Similitude concept

The application of fracture mechanics to the propagation of fatigue cracks is based on the premise that the governing parameter, such as the stress intensity factor K_I or the J-integral, used to correlate growth rates fully describes the stress and deformation fields in the vicinity of the crack tip. In addition, it is implicitly assumed that the concept of similitude (Fig.2.9) is valid. This concept implies the fact that for a particular material-environment system subjected to some particular loading history, identical near-tip conditions will prevail in specimens of different sizes containing different crack geometries if the magnitude of the characterizing parameter (e.g., K_I in small-scale yielding) is same [1]. Since LEFM uniquely characterizes the growth of a linear elastic fatigue crack (in the absence of the crack retardation mechanisms), the crack propagation mechanisms in different specimens would be expected to be the same. However, the concept of similitude cannot be applied when [41]:

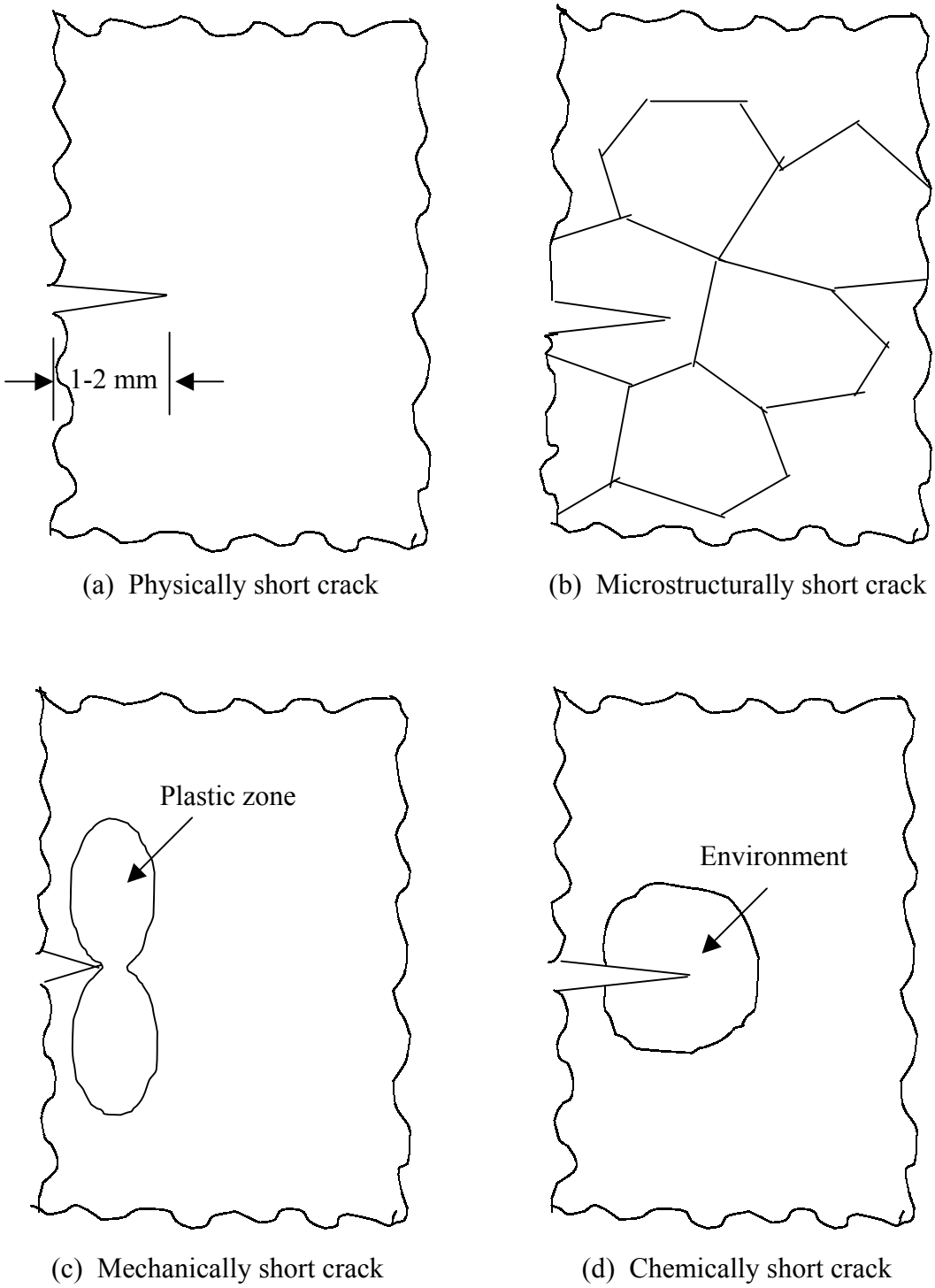

(a) Physically short crack (b) Microstructurally short crack

(c) Mechanically short crack (d) Chemically short crack

Fig.2.8 Schematic illustrations to define short crack.

(i) crack sizes approach the local microstructural dimensions,

(ii) crack sizes are comparable with the extent of local plasticity,

(iii) through thickness, out of plane stresses (which are independent of K_I) are different

(iv) crack extension mechanisms are different

(v) extensive fatigue crack closure is observed

(vi) external environments significantly influence crack growth.

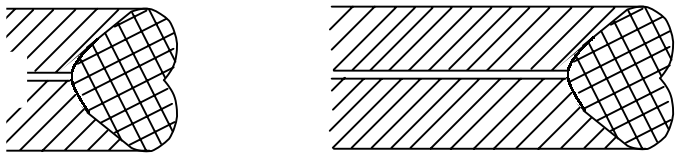

Fig.2.9 Schematic representation of similitude concept. This implies that cracks of differing length subjected to same nominal driving force, e.g. ΔK, have equal plastic zone sizes (r_p) ahead of crack and will therefore advance by equal increments per cycle.

Most of these mechanisms are specific to the short crack problem and thus contribute to differences in the growth rate behaviour of long and short cracks at nominally identical driving forces. In general their effect on the breakdown of the similitude concept for short cracks is that these influence (to varying degrees according to the crack length, for example) the local driving force (i.e. the characterizing parameter K_I or J effectively experienced in the region near tip). It is this 'near tip' parameter that governs crack advance, not the 'nominal' global value of this parameter computed by conventional analyses of externally applied loads and measurements of macroscopic crack lengths [41].

2.3.3 Transition crack size

The ΔK_{th} is dependent on crack length for the short cracks unlike that for long cracks. The conditions for the transition behaviour have been attributed to three possible phenomena:

(a) transition / intrinsic crack size,

(b) critical plastic zone size, and

(c) slip band grain boundary interaction.

The similitude concept of fracture mechanics implies that the intrinsic threshold stress intensity factor range, ΔK_{th}, for a long crack should be crack size independent. On the basis of the short crack growth rate data obtained for a wide variety of materials, Kitagawa and Takahashi [67] demonstrated that there exists a critical crack size a_0 below which ΔK_{th} decreases with decreasing crack length. For $a < a_0$, it is found from a survey of results for a large variety of engineering alloys (Fig.2.10) that the threshold condition is characterized by a critical stress $\Delta\sigma_{th}$ which approaches the smooth bar fatigue limit σ_e for vanishingly small crack sizes. For $a > a_0$, $\Delta K_{th} = \Delta K_0$ and ΔK_{th} is independent of crack size. Attempts have been made to establish link between the transition crack size and the characteristics microstructural dimension in a large number of engineering materials but the exact nature of a_o is yet to emerge [67-73].

The difference in rates between long and short fatigue crack propagations can be explained using transition crack size [74] and such an explanation appears to infer that crack propagation rates would be independent of crack size (by LEFM analysis) when one considers:

$$\Delta K = Q\Delta\sigma \sqrt{\pi\left(a + a_o\right)} \qquad \ldots(2.4)$$

where Q is a finite specimen correction factor. The limitations with the concept of transition crack size are that (i) this is an empirical approach and (ii) the physical meaning of a_o does not exist.

A different group of investigators [75-77] attribute the transition from long to short crack behaviour with the concept of a critical value of cyclic plastic zone size, r_c^*. These researchers indicate that r_c^* is constant for different crack sizes and can explain their results with this hypothesis as in Fig.2.10. But experimental verification of the nature of r_c^* is lacking. The magnitude of r_c^* is expressed as:

$$r_c^* = a\left(\sec\frac{\pi\Delta\sigma_{th}}{4\sigma_y} - 1\right) \qquad \ldots(2.5)$$

where σ_y is the yield stress. Despite the apparent success of this hypothesis to predict the overall variation of the threshold stress with crack size, the basic premise of the

model, namely that r_c^* is a constant for different crack sizes, remains to be established by experiments or by physical reasoning.

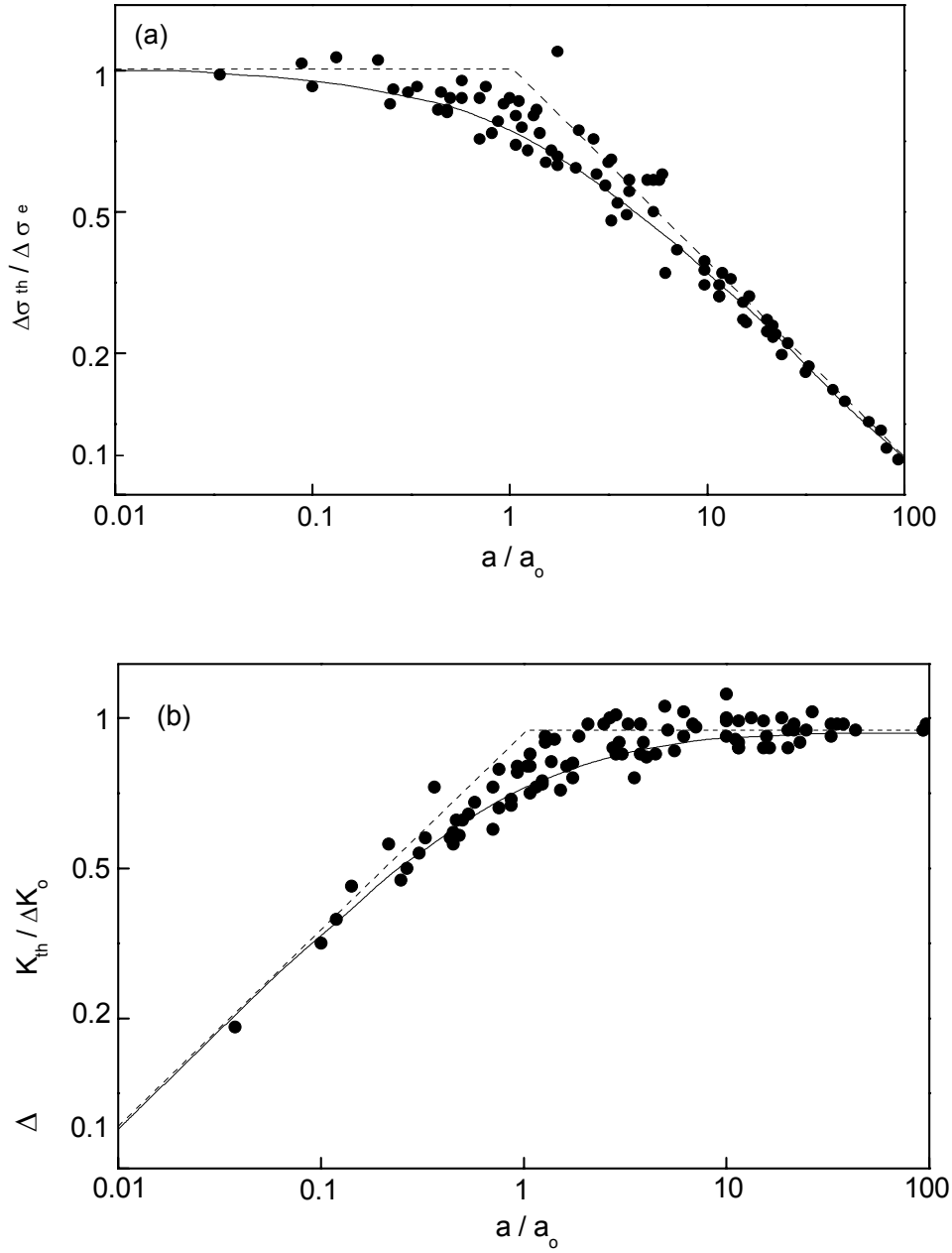

Fig.2.10 The effect of crack size on (a) threshold stress and (b) threshold stress intensity factor range for a wide variety of engineering alloys [68].

The threshold conditions of small fatigue cracks have also been explained in terms of interactions between the slip band at crack tip and grain boundary in a material. An analysis [68] of the condition for the blockage of slip band by grain boundaries (schematically shown in Fig.2.11) provides the following results for σ_{th} and K_{th}.

$$\sigma_{th} = \frac{K_c^m}{\sqrt{\pi b}} + \frac{2}{\pi}\sigma_{fr}^* \cos^{-1}\left(\frac{a}{b}\right) \qquad ...(2.6)$$

$$K_{th} = \sigma_{th}\sqrt{\pi a} = K_c^m \sqrt{\frac{a}{b}} + 2\sqrt{\frac{a}{\pi}}\sigma_{fr}^* \cos^{-1}\left(\frac{a}{b}\right) \qquad ...(2.7)$$

where b is the sum of the crack length a and the width of the blocked slip band zone w_o, σ_{fr}^* is the friction stress for dislocation motion in the band, and K_c^m is the microscopic stress intensity factor at the tip of the slip band. The threshold stress intensity is given by

$$K_o = K_c^m + 2\sqrt{\frac{2}{\pi}}\sigma_{fr}^* \sqrt{w_o} \qquad \text{for long crack } w_o << a \qquad \ldots(2.8)$$

For vanishingly small fatigue flaws, the fatigue limit σ_e is obtained by letting $a = 0$ in eqn.(2.6) such that

$$\sigma_e = \sigma_{fr}^* + \frac{K_c^m}{\sqrt{\pi w_o}} \qquad \text{for } a = 0 \qquad \ldots(2.9)$$

$$\sigma_{th} = \frac{K_o}{\sqrt{\pi(a + a_o)}} \qquad \text{and} \qquad K_{th} = \frac{K_o\sqrt{a}}{\sqrt{(a + a_o)}} \qquad \text{for } w_o = a_o \qquad \ldots(2.10)$$

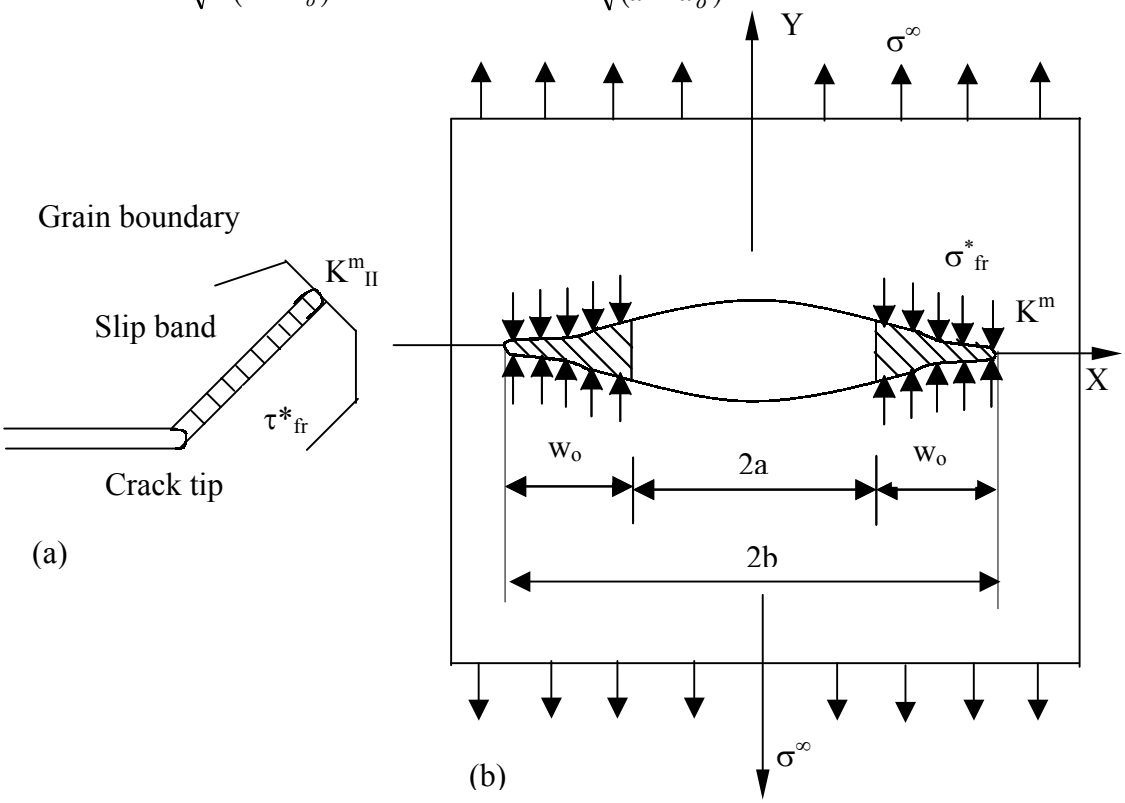

Fig.2.11 Schematic representation of the slip model proposed by Tanaka et. al. [68]: (a) slip band emanating from a crack tip is blocked by a grain boundary and (b) the crack and its dimensions. Nomenclature associated with the figure are given in list of symbols.

This approach explains the transition crack size a_o, and r_c* hypothesis as special conditions. But this analysis predicts that microstructural modifications like reducing grain size (and in turn increasing yield strength), which offer an enhanced resistance to the initiation and growth of small flaws, have a detrimental effect on long fatigue cracks. These expectations have been verified for different materials like maraging steel, cast iron [76], dual-phase steel etc.[78,79].

2.3.4 Procedures for measurement of short crack growth rate

2.3.4.1 Test procedure

The procedure for the measurement of fatigue crack growth rate (FCGR) of long cracks is well documented in ASTM standard E-647 [8]. FCGR can be determined from a wide range of specimen configurations, including all the types of specimens used for fracture toughness testing based on LEFM or EPFM principles. The configuration of specimens could be compact tension, CT, middle tension, MT or bend specimens in three or four-point loading modes. Standard CT and MT specimens recommended in the ASTM standard are shown in Fig.2.12. Tests can be carried out under ΔK-decrease or ΔK-increase methods, keeping R as constant or as variable. These different procedures are shown in Fig.2.13. During the FCGR test one measures the crack length and the number of cycles at some convenient intervals. The crack length can be measured by optical technique [41], by compliance technique [80] or by potential drop method [81,82]. The details of these techniques are available in the ASTM standard [8] and in several earlier reports [80,83-85]. A typical FCGR test result is shown in Fig.2.14.

The data analysis requires computation of da/dN and ΔK at different stages of crack growth. The values of da/dN are obtained either by direct calculation between successive pairs of readings or from slope of a curve fitted to subsets of the basic *a vs.* N data. The magnitude of ΔK is computed from the P_{max} and P_{min} values at any particular stage of crack growth together with the information of crack length at that point using eqns. (A.2) and (A.3) of Appendix.

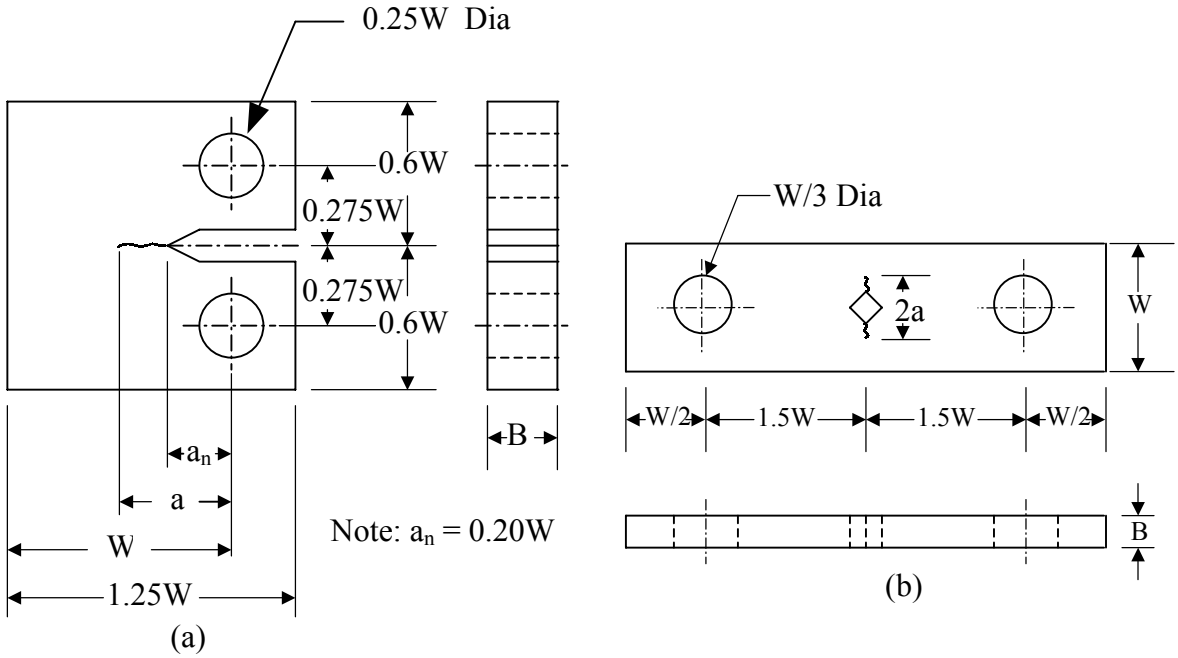

Fig.2.12 Standard Specimens for Fatigue crack growth rate testing: (a) Compact tension (CT) and (b) Middle tension (MT) specimen.

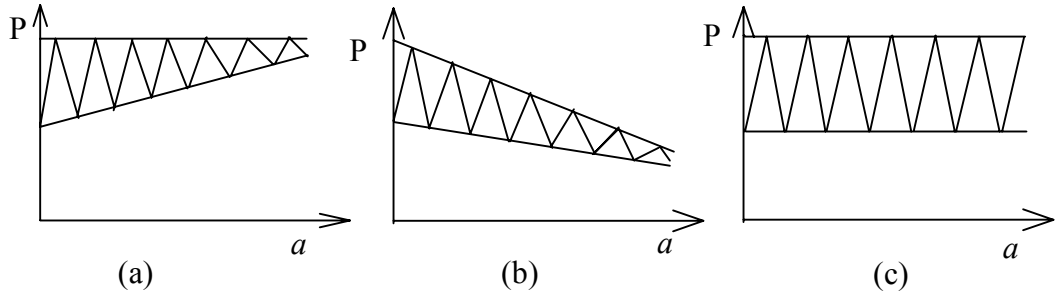

Fig.2.13 Schematic illustration of different types of loading sequence used for fatigue tests: (a) P_{max}-constant, ΔK-decreasing test, (b) R-constant, ΔK-decreasing test and (c) ΔP-constant, ΔK-increasing test.

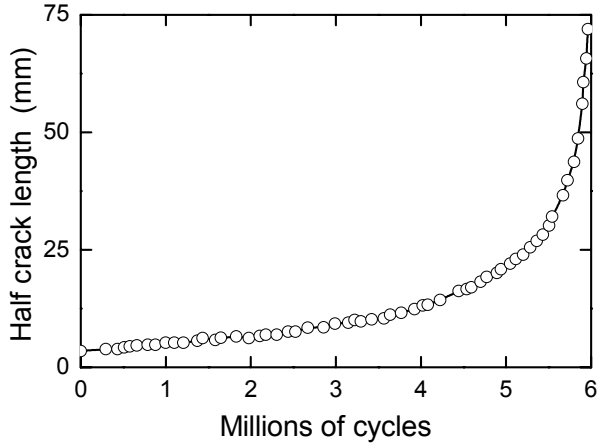

Fig.2.14 Typical crack growth curve for a central crack in a mild steel specimen [83].

2.3.4.2 Problems of short crack studies by experiments

The approaches for experimental study of crack growth rate and threshold behaviour of small fatigue cracks involve adopting procedures originally designed for measuring long cracks. The experimental techniques to monitor growth rates of long cracks are:

(i) optical (ii) potential drop
(iii) compliance (iv) acoustic emission
(v) ultrasonics (vi) eddy current

The first three methods are used widely for measurement of long cracks. The use of travelling microscope is considered quite suitable for measurement of long cracks, but such low magnification optical techniques are not suited to detect the presence and subsequently to monitor the growth of short cracks. The potential drop or compliance technique often does not possess the required resolution and reproducibility to characterize growth of short cracks of complex geometry.

The determination of fatigue threshold (ΔK_{th}) for a long crack is normally carried out using load shedding method or decreasing ΔK test. This method involves making continuous reduction in ΔK by not more than 10%, and the crack is allowed to propagate over a specific distance at each ΔK level. This load reduction scheme is repeated till the threshold ΔK_{th} is reached; this is the point at which no detectable long crack growth can be observed. The above method to estimate ΔK_{th} for long cracks is difficult to employ for similar measurements on short cracks. The difficulties are:

(i) the depth of a short crack can not be estimated with certainty and hence one can not obtain an appropriate formulation for ΔK,

(ii) in the load shedding technique, the crack continuously grows and as a result it may cease to be a short crack in nature, and

(iii) initiation stage of a short crack may involve linking up of several flaws at different locations.

Another major problem associated with short crack studies is to answer the question whether short crack behaviour should be examined using an artificial or a natural crack. It is difficult to insert an artificial notch in a specimen without damaging the material immediately ahead of the crack tip. The machined notches contain residual stresses whereas notches prepared by electro-discharge machining

exhibit a locally melted zone at the crack tip. Such residual stresses or local microstructural damage can introduce uncertainty on the growth behaviour of short cracks. As a consequence, reproducibility of growth behaviour of artificial short cracks is a major problem. In case of natural cracks, one encounters other type of difficulties, like introduction of a short crack exactly perpendicular to the loading direction is almost an impossibility and hence, mixed mode stress intensity factor of appropriate formulation may be required to examine such cracks.

2.3.4.3 Measurement of short cracks

The popular methods for measuring initiation and growth of short cracks are direct microscopic measurement and replication technique. Unlike examination of long cracks, the short cracks cannot be revealed by travelling microscopes or with the use of high-speed cameras. The measurement of short cracks has been usually carried out with the help of metallurgical microscopes having long working distances. Use of camera attachment has also been made to photographically record the progressive changes in the surface of specimens subjected to cyclic loading. Optical techniques have also been used to study short cracks at elevated temperatures using microscopes with long working distance [86]. Additionally short cracks can be examined using Scanning electron microscopes [87] by transferring a specimen under test at regular intervals.

The most widely used technique to monitor initiation and growth of small flaws has been the replication method. In this method, tests are generally interrupted periodically for replicating the surface structure of a specimen using pre-softened cellulose acetate tapes or blocks. The popularity of the direct and indirect microscopic measurements can be easily understood from a compilation (Table 2.1) of short crack techniques employed in earlier investigations.

In addition to direct or indirect microscopic examinations, alternate methods like electrical potential drop technique [88-90], surface acoustic technique [91] and electro-chemical methods [92] have also been employed to reveal initiation of short cracks and subsequently to estimate their growth behaviour. The use of optical or replication techniques are associated with the fact that these are difficult to apply in hostile environments such as in corrosive media or at elevated temperatures. These techniques provide information only about the surface lengths of cracks without any

details about the internal profile of the cracks. The use of electrical potential drop techniques is particularly suitable to overcome those limitations but this method requires suitable methods for calibration.

Table 2.1 Techniques used for short crack growth studies by some earlier authors.

Sl.No.	Material	Technique	References
01	Al 7075-T6	Optical	[93]
02	Low alloy steel	Optical	[94]
03	Ni-based super alloy	Optical	[95]
04	Al	Optical	[96]
05	Waspaloy	Optical	[97]
06	Copper	Optical	[98]
07	Titanium aluminides	Optical	[99]
08	Al	Optical	[100]
09	Al 5083 alloy	Optical	[101]
10	Hot rolled 45 steel	Optical	[102]
11	Al	SEM	[103]
12	Waspaloy	SEM	[104]
13	2024-T351 Al-alloy	SEM	[105]
14	316L Stainless steel	SEM	[106]
15	0.4 % carbon steel	Replica	[107]
16	Low carbon steel	Replica	[108]
17	Al-Li alloy	Replica	[109]
18	Al-LI-Cu-Mg-Zr alloy	Replica	[110]
19	Titanium	Replica	[111]
20	AL-Sic	Replica	[112]
21	Gray cast iron	Replica	[113]
22	Eutectoid steel	Replicas	[114]
23	Mg-Zn alloy	Optical and Replicas	[115]
24	Steel	Optical and Replicas	[116]
25	Pure titanium	SEM and Replicas	[117]
26	QIN (HY80) Steel	Potential drop	[118]
27	HY130 Steel	Potential drop	[119]
28	Ti-6Al-2Sn-4Zr-2Mo-0.1Si (Ti 6242) alloy	Replica	[120]

2.3.4.4 Fatigue crack closure

The crack closure in fatigue refers to a phenomenon that the applied load/stress/stress intensity factor is not fully efficient in driving the growth of a fatigue crack. The possibility that a fatigue crack remains closed upto some critical stress intensity factor level even under a tensile load cycle was first indicated by Elber [121,122] on the basis of a series of experimental results. The phenomenon can be described as one in which a crack remains partially closed for the portion of a loading cycle and does not open fully until a certain opening stress intensity factor, K_{op} ($=K_{cl}$), level is reached. The damaging portion of the cyclic load excursion, as a consequence, gets restricted to that part of the load cycle that acts on a fully opened crack. This phenomenon is illustrated in Fig.2.15, which indicates that fatigue crack growth is dictated by an effective stress intensity factor range ΔK_{eff}, which can be denoted by $K_{max} - K_{op}$ rather than by $K_{max} - K_{min}$. This fact indicates that crack growth rates are not only insensitive to compressive load excursion, but also to a part of the tensile load excursion.

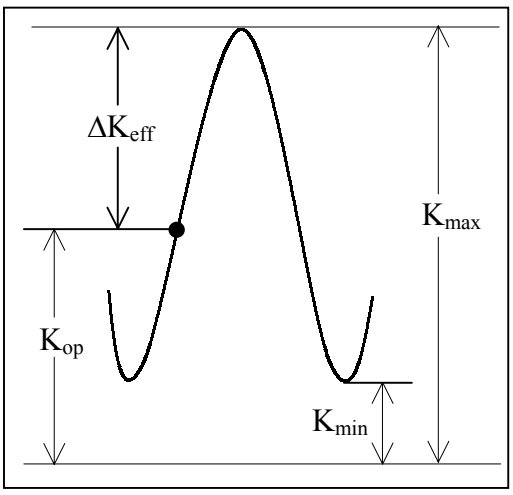

Fig.2.15 Schematic illustration of crack opening, K_{op}. $\Delta K_{eff} = K_{max}-K_{op}$.

Elber [121,122] explained the mechanism of crack closure with the consideration of a zone of residual tensile deformation in the wake of a fatigue crack tip. This zone gives rise to premature contact between the advancing crack faces. The

suggested mechanism of crack closure due to residual plastic stretch at crack wake has been popularly termed as 'plasticity induced crack closure' [123]. Several alternative mechanisms originate from: (i) corrosion layer in fatigue (oxide induced crack closure), (ii) microscopic asperities (roughness induced crack closure), (iii) viscous fluid penetrated inside a crack (viscous fluid induced crack closure), (iv) stress or strain-induced phase transformation at the crack tip (transformation induced crack closure), (v) crack deflection, (vi) crack-bridging by fibers, (vii) crack trapping by particles, and (viii) crack-shielding due to microcracking. All these mechanisms are schematically illustrated in Fig.2.16.

The techniques available for monitoring the premature closure of long fatigue cracks are:

(i) optical techniques, (ii) compliance techniques,

(iii) strain gauge method, (iv) acoustic method,

(v) ultrasonic techniques.

The methods adopted for measurement of closure associated with long cracks cannot be employed for measurement of closure associated with short cracks, because of insufficient resolution. Tanaka and Nakai [124,125] have demonstrated the use of compliance technique for measuring crack closure associated with the growth of short cracks. But such measurements can only be done for physically small cracks. For microscopically small cracks Morris and Buck [126] have suggested measurement of compliance by subjecting a crack under cyclic loading, while observing it under Scanning electron microscope. An alternative technique involves monitoring the behaviour of short crack propagation by stereo imaging [127,128].

The crack closure phenomenon indicates that the propagation rate of a crack will be slower if this phenomenon is operative. Because the nominal stress intensity range ΔK ($K_{max} - K_{min}$) computed from applied load and crack length reduces to a lower effective value ΔK_{eff} which is given as $K_{max} - K_{cl}$, where K_{cl} is the stress intensity at closure (usually > K_{min}).

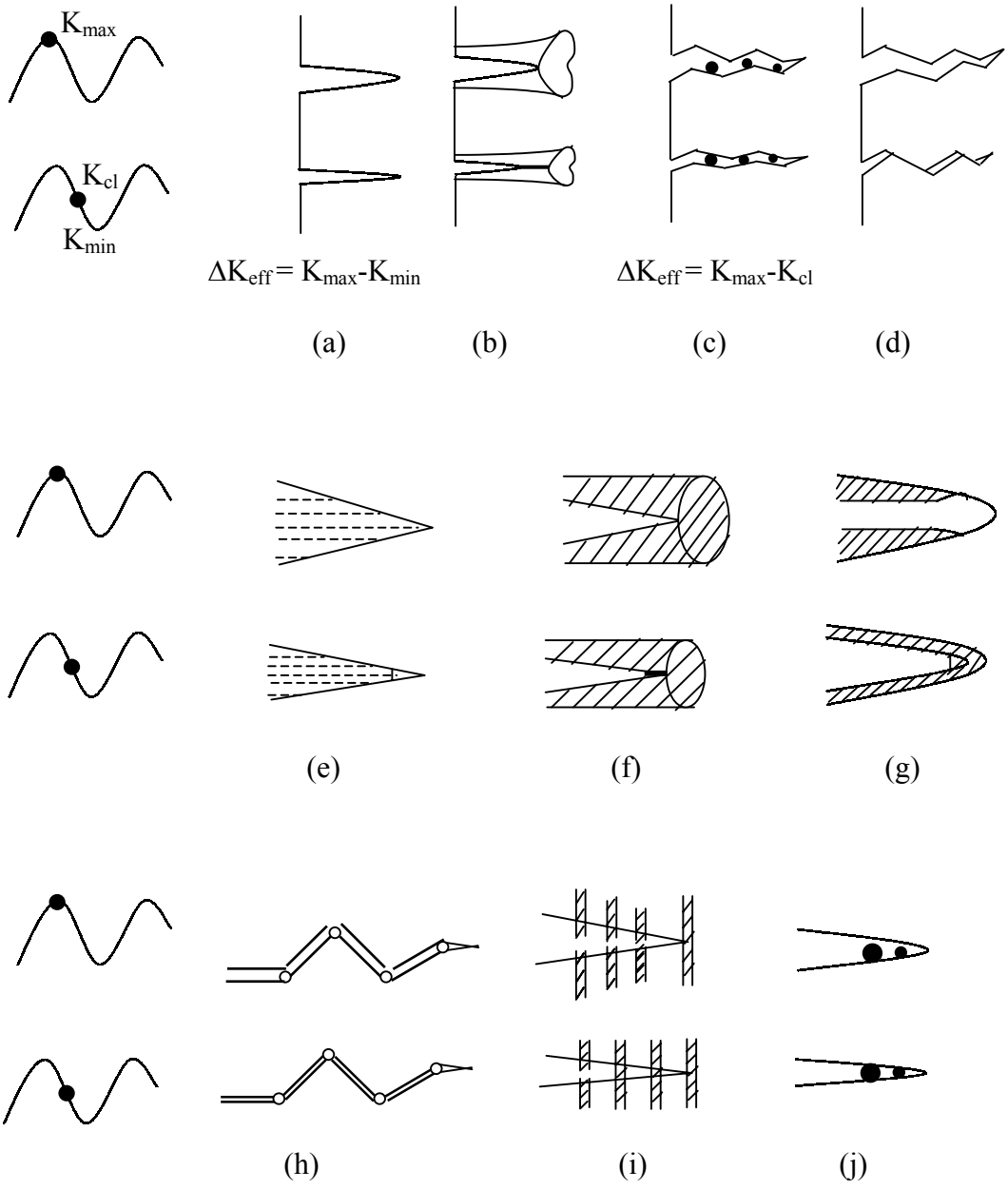

Fig.2.16 Schematic illustration of the mechanisms which promote retardation of fatigue crack growth in constant amplitude fatigue: (a) no closure, and closure induced by (b) cyclic plasticity, (c) corrosion deposites, (d) rough surface, (e) fluid, (f) phase transformation, (g) oxide-transformattion, (h) crack deflection, (g) crack-bridging by fibres and (h) crack bridging (or trapping) by particles.

Extensive studies on the behaviour of long crack particularly at near threshold stress intensity level have revealed that such crack closure mechanisms govern the crack growth rate by the influence of load ratio [129-132], yield strength [131], grain size [131], environment [129-131,133] and variable amplitude cycling [134]. Since the small cracks have a limited wake, it is expected that the effect of closure is different for long and short cracks. James and Morris [135] have extended evidence for the fact that crack closure is function of crack size (Fig.2.17). A similar evidence (Fig.2.18) on the effect of the environment on crack growth rate in short and long cracks in AISI 4130 steel has also been reported by Gangloff [88,90]. A schematic demonstration of K_{max}, K_{min} and K_{cl} in Fig.2.19 by the Liaw and Logsdon [136] indicates the generalized behaviour of short cracks compared to those of long cracks.

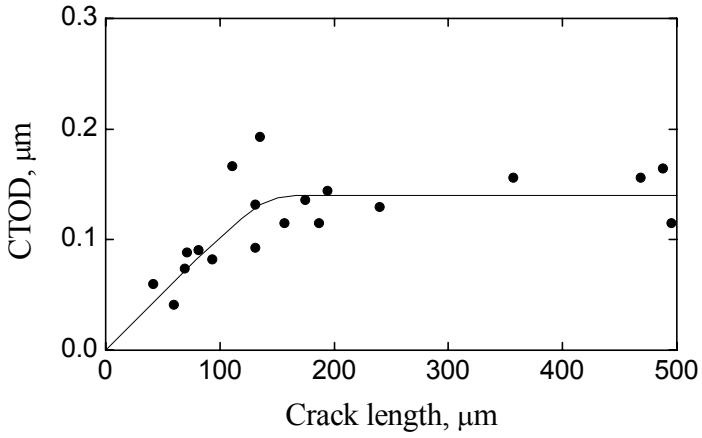

Fig.2.17 Variation of CTOD with length of small surface cracks in 6Al-2Sn-4Zn-6Mo titanium alloy showing reduction in crack closure with decreasing crack size [135].

2.3.5. Models for short fatigue crack growth rate

Several investigators [107,137-143] have attempted to model short crack growth behaviour over the last two decades. These models take into account several geometric and microstructural parameters apart from stress and stress intensity factor to predict short crack growth rate. A chronological account of these models together with the expressions used to describe short crack growth rate by these models are first summarized in Table.2.2 prior to some elaboration of these ones in the following discussion.

Table 2.2 Short crack growth rate models suggested by the earlier investigators.

Investigator	Expression for model
Hobson [137]	$da_s/dN = C_1(d - a_s)$ for microstructurally short crack …(2.11) $da_s/dN = C_2 a - D_1$ for physically short crack …(2.12)
Chan and Lankford [138]	$da/dN = C_1 \Delta K^n \left[1 - k\phi\left[(D-2X)/D\right]^m\right]$ …(2.13) $k\phi = 1-\tau_B/\tau_A$, $\Delta K = 1.12\,\Delta\sigma\sqrt{\pi a/Q}$
Rios et. al.[139]	$da/dN = f\dfrac{\tau(L-a)}{\mu}$ …(2.14)
Rios et. al.[107]	$da/dN = f(2\pi aD)^{1/2}\left(1-\phi\left[\dfrac{D-X}{D}\right]\right)^m \dfrac{\tau}{\mu}$ …(2.15)
Navarro et. al. [140]	$da/dN = f\phi_1$, $\phi_1 = \dfrac{2k}{G}\sqrt{\dfrac{1-n^2}{n}}\,\sigma\, a$ …(2.16) $n = n_c = \cos\left(\dfrac{\pi}{2}\dfrac{\sigma-\sigma_{Li}}{\sigma_{comp}}\right)$, $\sigma_{Li} = \dfrac{\sigma_{FI}}{\sqrt{i}}$ for first grain $n = n_s = n_c\left[i/(i+2)\right]$ after crossing first grain
McEvily et. al.[144]	$da/dN = A\left\{\left\{\sqrt{2\pi r_e} + Y\sqrt{\left[\dfrac{\pi}{2}a\left(\sec\dfrac{\pi\sigma}{2\sigma_y}+1\right)\right]}\right\}\Delta\sigma - \left(1-e^{-kl}\right)K_{op\max} - \Delta K_{eff}\right\}^2$ …(2.17)
Hussain et. al.[141]	$da/dN = f_2\phi^*$, $\phi^* = \dfrac{k}{G}\dfrac{\sqrt{1-n^2}}{n}\Delta\sigma\, a_s$ …(2.18) $n = n_c = \cos\left(\dfrac{\pi}{2}\dfrac{\sigma-\sigma_{Li}}{\sigma_{comp}}\right)$ --for first grain $n = n_s = n_c\left[i/(i+2)\right]$, $\sigma_{li} = \sigma_{FI}/i^{1/2}$, --after crossing first grain $n = \cos[(\pi\sigma/2\sigma_{comp})]$ -- for long crack
Murtaza and Akid [142]	$da_s/dN = C_s(d_i - a_s)$ ---for short crack …(2.19) $C_s = A_i(\Delta\gamma_t)^{\alpha}{}_I$ $da/dN = C_l a - D_1$ ---for long crack …(2.20) $C_l = B(\Delta\gamma_t)^{\beta}$, $D_l = B(\Delta\gamma_{fl})^{\beta} d_m$

a = crack length, a_o = transition crack length, d = distance between two consecutive barriers, K_I = stress intensity factor in mode I, K_{II} = stress intensity factor in mode II, ΔK = stress intensity factor range, ΔK_{th}, = threshold stress intensity factor range, ΔK_{eff} = effective stress intensity factor range, da/dN = crack growth rate, X = distance between crack tip and a grain boundary, L = slip band length, f = fraction of dislocation participating in crack growth, ϕ = crack deflection factor, τ and σ = applied stress, θ = angle between the loading axis and the mean crack plane, μ = shear modulus, γ = shear strain, ξ= factor related to mode mixicity, ψ= factor related surface characteristics of a specimen and C_1, C_2, D_1, A, B are material constants.

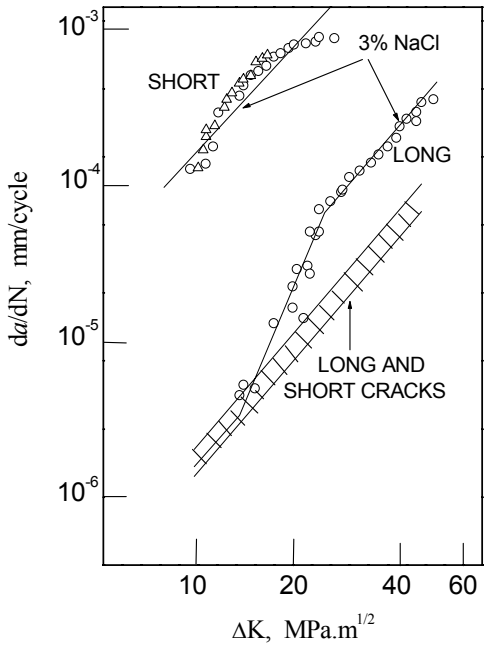

Fig.2.18 Fatigue crack propagation rate, da/dN as function of ΔK for long and physically short cracks in AISI 4130 steel, tested in moist air and in aqueous 3% NaCl solution [88].

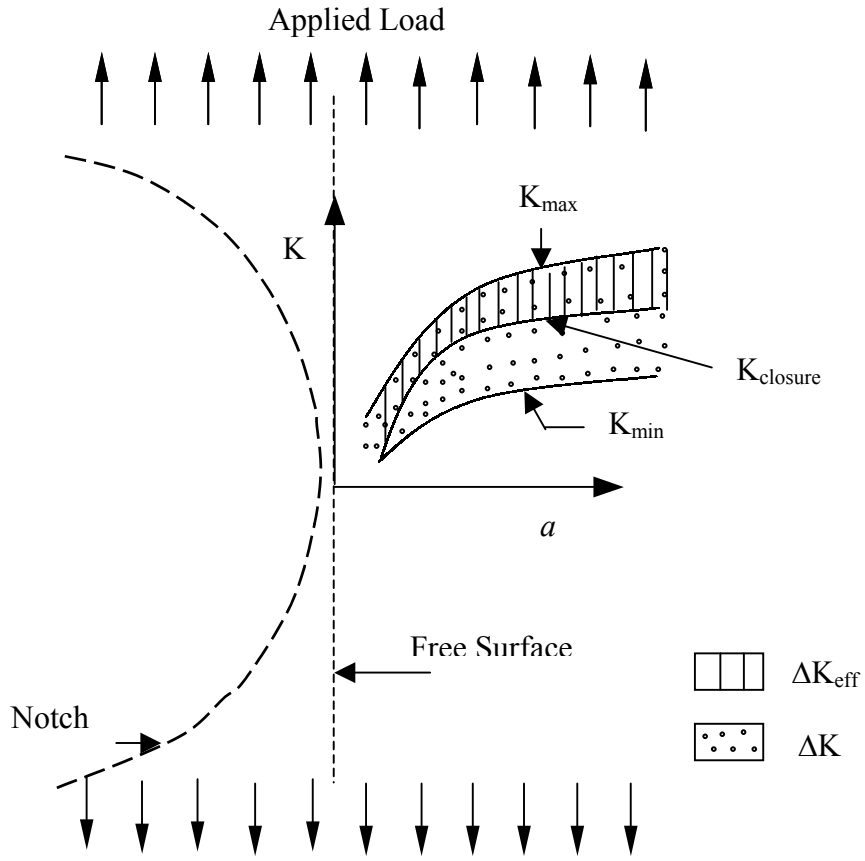

Fig.2.19 Schematic of K_{max}, $K_{closure}$, and K_{min} fields for a crack originating from a free surface or a notch subjected to constant applied load range and at low load ratios (≤ 0.5).

Hobson [137] was the first to suggest a model for short crack growth rate as given by eqns. (2.11) and (2.12) in Table 2.2. The model suggested by Hobson is based on the assumption that the effect of microstructure on a short crack remains confined only in the first grain and the crack growth depends on the distance between the crack tip and a barrier in its front. This model does not consider fluctuations in short crack growth rate once the crack crosses the first barrier. Chan and Lankford [138] proposed a model (§ equation 2.13 in Table 2.2) based upon the concept of larger plastic strain at the tip of short cracks and considered the effect of grain orientation on its growth rate. In this model the reduced crack tip strain at grain boundaries is considered to cause deceleration in crack growth rate. However, if the orientations of the adjacent grains are same, this model predicts little or no decrease in growth rate. Rios et. al.[139] suggested a model (§ equation 2.14 in Table 2.2) based on the strength of slip bands in front of short cracks. The increase in crack length with increase in number of cycles is considered to remain associated with shortening of slip band length, and the crack growth rate is considered to be a direct function of the slip band length. Later Rios et. al. [107] proposed an alternate model (§ equation 2.15 in Table 2.2), assuming that the energy at the slip band should be equal to the crack extension energy for crack propagation and the slip band energy is sufficient enough to overcome the strength of the barrier. Navarro and Rios [140] considered (§ equation 2.16 in Table 2.2) that microstructure influences crack growth rate of a material till failure in their model; but the microstructural influences are negligible when the cracks are longer. McEvily et. al. [144] have suggested an alternate model (§ equation 2.17 in Table 2.2) for fatigue crack growth considering elasticity in front of large scale plasticity. In their model the unusual growth behaviour of short cracks compared to that of long cracks is demonstrated; but the model does not deal with the commonly observed acceleration and deceleration behaviour of short cracks.

Hussain et. al. [141] suggested a modification of the model proposed by Navarro and Rios [140]. The major emphasis in this modification is that the deceleration and acceleration of crack growth remain confined solely in the first few grains. Murtaza and Akid [142] have proposed a modification for the Hobson's model [137] primarily by extending it for multiple grains in the regime of short crack growth. Angelova and Akid [145] have described the fatigue behaviour of metals by dividing crack growth rate behaviour into three regimes; these are microstructurally short cracks (MSC), physically short cracks (PSC) and long cracks (LC). Each type of crack requires a different analytical approach to characterize its propagation

behaviour, i.e. Microstructural Fracture Mechanics (MFM), Elastic-Plastic Fracture Mechanics (EPFM) and Linear Elastic Fracture Mechanics (LEFM). These investigators have proposed two types of transitions or thresholds: (i) a microstructural short shear crack to physically short tensile crack and (ii) a physically short crack to a long crack. This approach distinguishes separate independent regimes of 'microstructural short crack' and 'physically short cracks'; the latter regime lying between Microstructural Fracture Mechanics (MFM) and Linear Elastic Fracture Mechanics (LEFM). The first transition is considered to be governed by the microstructural state of the material whereas the second transition is dictated by the classical condition for fatigue threshold based on the stress intensity factor range obtained from long crack tests, and is associated with the transition of physically short crack to long crack. The formulations employed by Angelova and Akid [145] to discuss short crack growth are similar to those used by Murtaza and Akid [142].

Newman and his co-workers [143,146] have suggested modifications to estimate ΔK_{eff} in the rate relations to describe small crack growth behaviour in the near threshold region. These investigators have considered a modified Dugdale's [15] plasticity model to describe the effective stress intensity factor. Using their proposed relation they have described crack growth rate behaviour in various materials under different loading conditions. Zhang et. al. [123] have described short fatigue crack growth behaviour, by combining mechanisms of plasticity induced crack closure and fracture surface roughness induced crack closure. These investigators have proposed different stress intensity factors for crack opening and crack closure to estimate the effective stress intensity factor in the rate equations. Wei et. al. [147] have proposed a model combining the suggestions given by Newman et. al. [143,146] and Navarro and Rios [140]. These investigators have proposed an elaborate expression for crack tip plasticity displacement (ϕ). They have also suggested that crack growth rate follows a Paris law type relationship in which ΔK_{eff} is replaced by ϕ. Rodopoulos and Rios [148] have contended that the model given by eqn. (2.16) can reveal the boundaries in which growth of short crack takes place. They have also indicated that the extent of short crack growth regime is governed by a relation between fatigue limit and the cyclic yield stress of a material.

The existing analytical models for short crack growth can be broadly classified under two categories: (a) microstructure dependent and (b) microstructure independent models. All the models described in Table 2.2, except the one suggested

by McEvily et. al. [144], can be considered to belong to the first category. The models suggested by McEvily et. al. and a few others [123,143,144,147,148] do not account any microstructural parameters to describe the short crack growth behaviour in materials and thus naturally belong to the latter category.

An overview of the microstructure dependent models shows that microstructural parameters have been accounted in different ways. Hobson [137], Chan and Lankford [138], and Murtaza and Akid [142] have considered either grain size or a characteristics distance between a short crack tip and a neighbouring barrier as an essential parameter in their short crack growth models. The primary role of a grain size or a barrier ahead of a short crack tip is to decelerate the growth rate of these cracks. Rios et. al. [139], Navarro and Rios [140] and Hussain et. al. [141] have accounted the influence of slip bands on the short crack growth behaviour. As a consequence these investigators have incorporated the length and width of the slip bands and the fraction of dislocations actively participating in crack growth to describe short crack growth behaviour. Interestingly Rios et. al. [107] have suggested a model which incorporates influence of both barrier distance and slip band characteristics on short crack growth. Thus the microstructure dependent short crack growth models can be further classified as to be dependent on: (i) barrier distance, (ii) slip band characteristics, and (iii) combined barrier distance-slip band characteristics.

The models proposed by McEVily [144], Newman et. al. [143,146], Zhang et. al. [123] and Wei et. al.[147] attempt to modify K_{eff} during crack growth using crack closure concept and the plasticity associated with the crack tip. These models can be termed as mechanics-based models unlike the microstructure based models suggested by Hobson [137], Chan and Lankford [138], Rios et. al. [107,139], Navarro and Rios [140], Hussain et. al.[141] and Murtaza and Akid [142].

2.4 Fatigue thresholds: long cracks

2.4.1 Definition

The ASTM standard [8] defines: “fatigue threshold, ΔK_{th}, is an asymptotic value of ΔK at which *da/dN* approaches zero”. In practice, most experimental data do not show a clear asymptote even at the lowest growth rates that can be examined. A more practical definition of ΔK_{th} is the value of the stress intensity factor range corresponding to a specific growth rate, chosen to be low enough so that crack growth

will be negligible for all practical situations. For most materials an operational, though arbitrary, definition of ΔK_{th} is given as the value of ΔK, which corresponds to a fatigue crack growth rate of 10^{-10} m/cycle [8]. According to ASTM standard, ΔK_{th} should be determined from a linear regression of *log da/dN vs. log* ΔK curve using a minimum of five data points of approximately equal spacing between growth rates of 10^{-9} and 10^{-10} m/cycle.

2.4.2 Methods of threshold measurement

The techniques that have been used for obtaining ΔK_{th} values and/or near threshold growth rate values are: (i) load-controlled *K* reduction, (ii) strain-controlled *K* reduction, (iii) Klesnil and Lucas method, and (iv) stress-relief method. Most experimenters use the load-controlled *K* reduction system in which a crack is grown to a reasonable length, and the applied ΔK is gradually reduced until the threshold is reached. It is usual to monitor crack growth rate continuously, reducing ΔK until the growth rate drops below some specified value used to define the threshold. Then ΔK may be gradually increased to provide further data points for the growth-rate curve. In strain-controlled K reduction method, load shedding is achieved through control of some strain parameter [149] such as crack mouth opening or back-face strain.

The method proposed by Klesnil and Lucas [150] involves the deliberate application of a sudden decrease in ΔK, which causes retardation in crack growth. This enables the experimenter to measure, relatively quickly, a 'pseudo threshold'; a value of ΔK_{th} immediately following the sudden load reduction. This procedure is repeated using successively smaller values for the load reduction, giving decreasing values of the pseudo threshold.

The steps involved in stress relief method to determine ΔK_{th} are: (a) crack growth is initiated at a relatively higher ΔK and the crack is grown to a suitable length, (b) the specimen is removed from the testing machine and is stress-relieved by annealing, and (c) then testing is continued at a low applied ΔK, close to the expected threshold value. Pook and co-workers [151] have used a simple version of this method, enabling threshold values to be obtained from testing machines, which are normally used for conventional S/N-type tests. In this case the specimens are first cycled at a high load in order to initiate a crack. After initiation of cracks, the

specimens are tested at various applied stress ranges. The ΔK at which specimen has failed is the value of ΔK for crack growth. Data are recorded as a type of S/N curve, with ΔK replacing stress on the vertical axis. The 'fatigue limit' on this curve corresponds to the threshold.

Another method, developed by Taylor [152], combines the standard load-shedding procedures with stress-relief annealing. In this case, normal crack monitoring methods are used, but a period of stress relief is employed to cut out the long initial process of load reduction. It has been shown for a copper alloy that this method gives identical near-threshold data to that obtained using more conventional load shedding.

The rate of load-shedding

The standard for fatigue testing [8] suggests the procedure for load shedding in terms of a C-parameter. Load shedding is required, either continuously using constant C parameter, or in incremental steps in which the load is reduced by not more than 10%. The ASTM [8] standard recommends the expression for C parameter, which was originally proposed by Saxena et. al. [153] as:

$$C = \frac{1}{\Delta K}\frac{d\Delta K}{da} \qquad \ldots(2.21)$$

C values are always negative; numerically larger values correspond to more rapid rates of reduction. The rate of load shedding with increasing crack length shall be gradual enough to (1) preclude anomalous data resulting from reductions in the stress-intensity factor and concomitant transient growth rates, and (2) allow the establishment of about five (da/dN, ΔK) data points of approximately equal spacing per decade of crack growth rate. The above requirements can be met by limiting the normalized K-gradient, 'C' to a value algebraically equal to or greater than -0.08mm^{-1}.

Various investigators have examined the influence of C parameter on fatigue threshold [153-159]. Interestingly several investigators have obtained consistent results on fatigue thresholds for different C values used. The dependence of ΔK_{th} on ΔK-reduction rate has been shown by Brook [160] to indicate a minimum (Fig. 2.20). The data in this figure show a large variation; presumably the effect is not so great for

most materials, since different investigators using a variety of reduction rates are generally able to obtain similar results. The standard E-647 also suggests that acceptable values of C may depend on load ratio, testing conditions and environment. Taylor [161] has recommended that, for any large testing program on a new material, a range of reduction rates should be investigated at the outset in order to understand the influence of load reduction rate on ΔK_{th}.

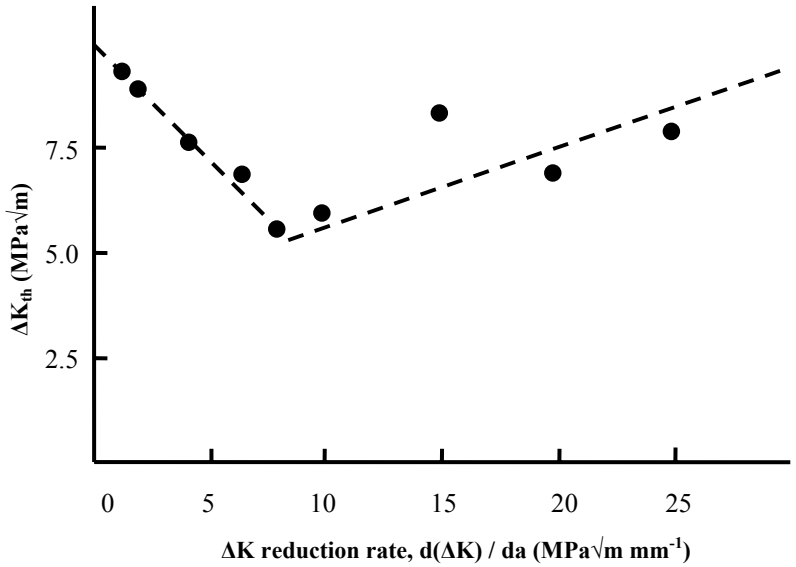

Fig.2.20 Variation of measured threshold with load reduction rate [160].

2.4.3 Factors affecting fatigue thresholds

Material properties, both mechanical and microstructural, have a strong influence on near threshold crack propagation [162,163]. Unlike the Paris region, the near-threshold crack propagation gets markedly affected by changes in mean stress, yield strength, and in microstructural parameters such as grain size [164,165]. This is because the crack tip deformation and the crack-advance rates are of a scale commensurate with the microstructural scale of the material. The influence of material properties such as yield strength and that of grain size on ΔK_{th} are illustrated by some reported results on steels as shown in Fig. 2.21 and Fig. 2.22 [162]. Figure 2.21 shows the variation of threshold with yields strength for a large number of alloy steels. Despite the scatter, a consistent relationship emerges in which decreasing yield strength increases threshold. Figure 2.22 shows some data on low-carbon mild steels, illustrating the distinct dependence of ΔK_{th} on grain size. In fact the

dependence of ΔK_{th} on yield strength also should be equally clear since the two are simply related through the Hall-Petch equation, provided the carbon content or the amount of pearlite is low. The effects of load ratio, frequency, and environment on ΔK_{th} have been discussed in section 2.6.

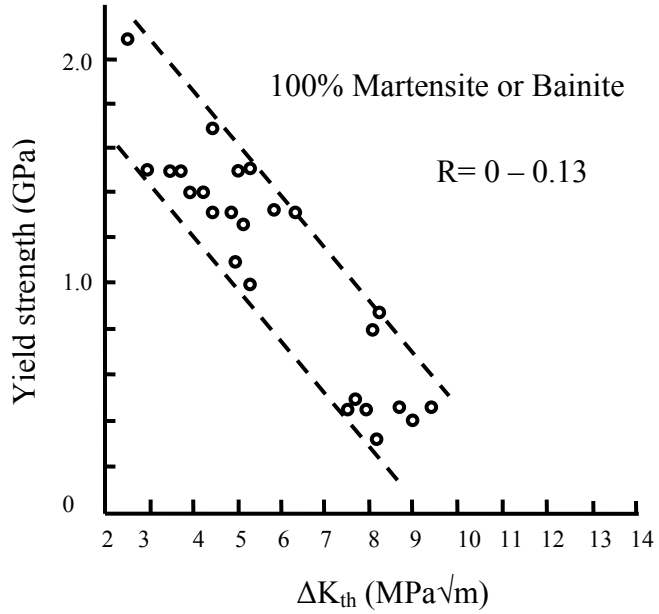

Fig.2.21 Variation of threshold with yield strength in a number of alloy steels [162].

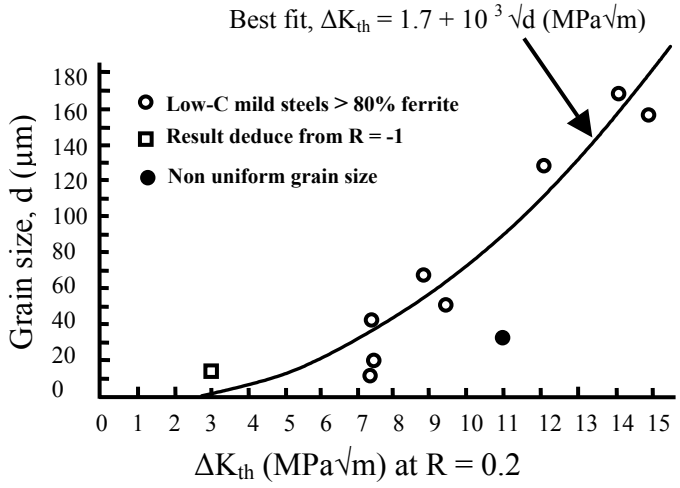

Fig.2.22 Variation of threshold with grain size in mild steels [162].

2.5 Nonpropagating cracks

Nonpropagating cracks (NPCs) are those, which initiate from a notch root but get arrested at the operating stress differential ($\Delta\sigma$) after growing for some distance. A crack gets arrested ahead of a notch when the crack driving force either remains constant or marginally increases due to increase in crack length at constant stress. Figure 2.23 shows a schematic relationship between fatigue limits and stress concentration factors typically observed for carbon steels. The magnitude of σ_i in Fig.2.23 is the fatigue limit that corresponds to the crack initiation limit and that of σ_f corresponds to the fracture limit where the NPC exists. It is generally recognized, that NPC appears at the bottom of notch root when a sharp-notched carbon steel specimen has notch root radius smaller than a critical value, ρ_c, and undergoes fatigue with an applied stress in the range of σ_I and σ_f as shown in Fig. 2.23. Typical experimental results of Tanaka and Akinawa [166] covering a wide range of notch acuities, which lead to NPCs are shown in Fig.2.24. These investigators [166] have cited examples for non-propagating cracks for both 'through', and 'part through cracks'.

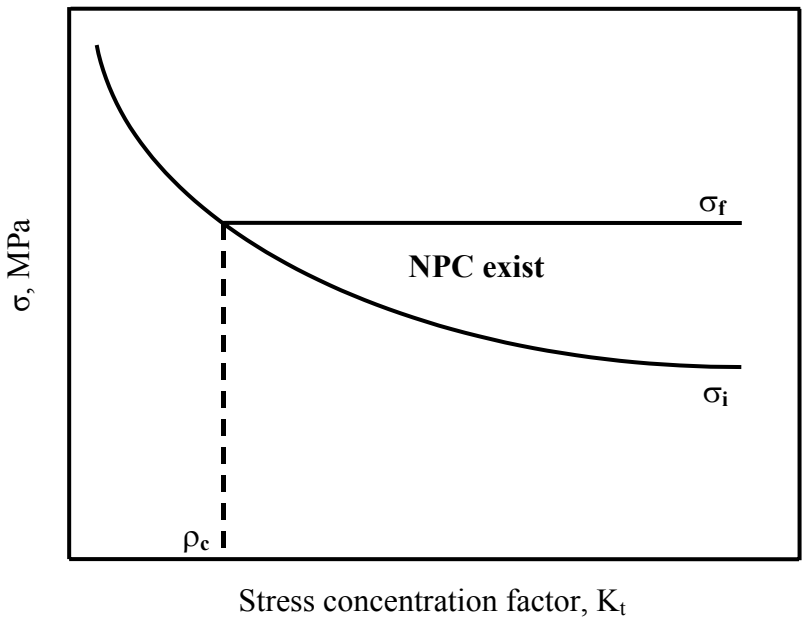

Fig.2.23 Typical relationship between stress concentration factor and fatigue limit of carbon steels in rotary bending tests.

Some of the earlier investigators have shown that there exists a critical notch root radius below which the phenomenon of NPC occurs [166-168]. Tanaka and Akinawa have shown that at low values of stress concentration factor (K_t), there exist

a small region of stress range at which NPCs would form (Fig.2.24); as K_t increases there is an increasingly large region of stress range for the formation of NPCs.

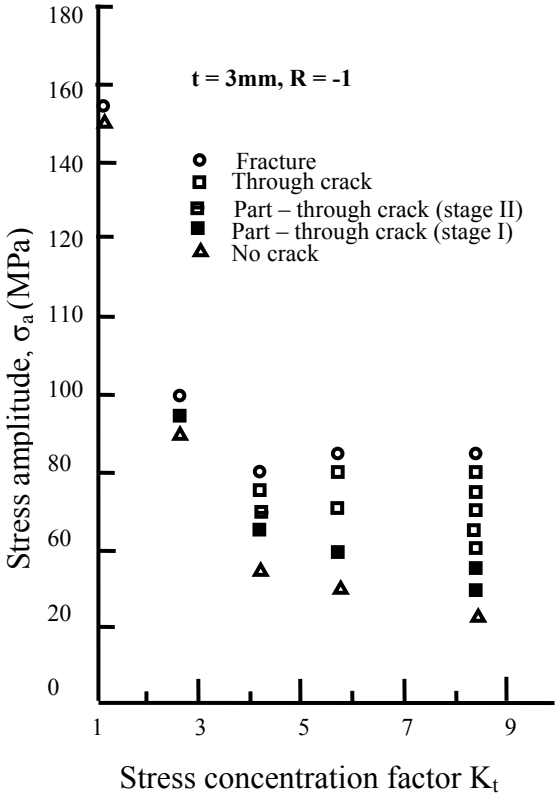

Fig.2.24 The variation of σ_{th} with K_t as reported by Tanaka and Akinawa [166].

Yates and Brown [169] and Yamada et. al. [170], have attempted to predict the length of NPCs. Plumtree [171] and Kim and Kim [168] have examined the length of NPCs in different materials. In 0.84%C steel, Yamada et. al. observed the length of NPCs to be 580 μm and 340 μm when cracks originated from artificially induced micro-pitted specimens and from smooth specimens respectively. Plumtree has examined NPCs in 2024-T351 Al-alloy and noted that the lengths of NPCs vary in a wide range and their magnitudes are dependent on specimen orientation. The length of NPC in pure titanium has been noted to be nearly 900 μm by Kim and Kim [168], but the occurrence of such NPC depends on the critical root radius of a notch from which it originates.

Yates and Brown [169], in their attempt to predict the length of NPCs, have assumed that the cracks are initially ‘short’ in the sense that the Kitagawa diagram

must be used to describe their threshold characteristics. It was assumed by these investigators that, if the crack is small enough:

$$K = 1.12 K_t \sigma \sqrt{\pi\, a} \qquad \ldots(2.22)$$

i.e. that the crack is loaded by the maximum notch-tip stress. As the crack grows, at some point the K value can be written as:

$$K = \sigma \sqrt{\pi (a + D)} \qquad \ldots(2.23)$$

Equation (2.23) is the expression for K, taking the effective crack length as the actual crack length plus the notch length, D. The variation of K with crack length is shown in Fig.2.25. By comparing this with the variation in predicted threshold with crack length as shown in this figure, a kind of 'resistance curve' for fatigue crack growth is developed. This model suggests that a crack would grow only upto the point of intersection between the K value line and the threshold line as illustrated in Fig.2.25(c).

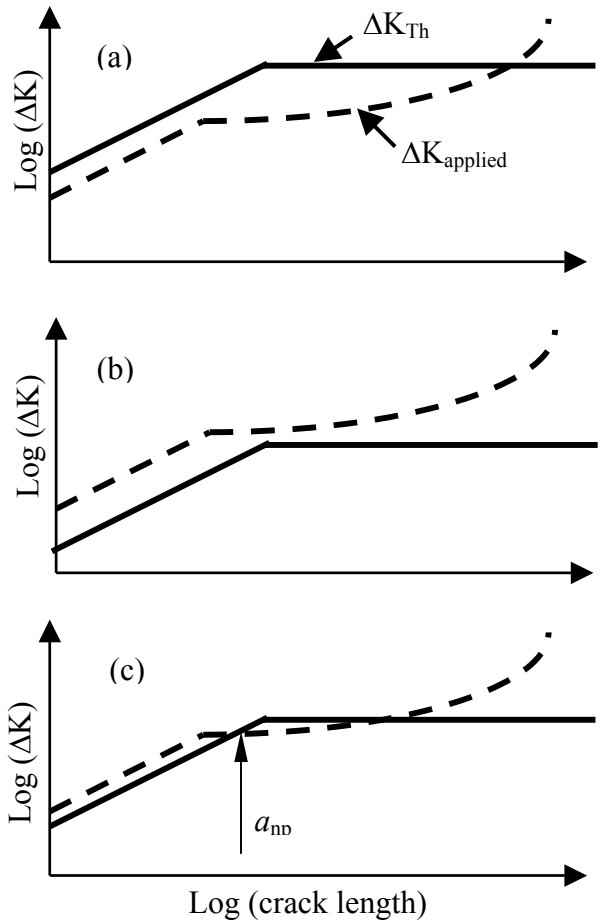

Fig.2.25 The model of Yates and Brown [169]; dashed line represent applied ΔK, solid lines represent the variation of ΔK_{th} with crack length. The three examples are for different applied stresses; (a) no crack growth; (b) crack growth continuing to failure; (c) crack growth causing a non-propagating crack, length a_{npc}.

Over the last two decades several investigations have reported the formation of NPCs and their possible mechanisms in different materials [167,168,170-180]. Taira et. al. [172] have observed that an extent of a region of dense slip bands near the crack tip decreases with crack length and they found a relation between the crack growth rate and the slip band zone size. Smith et. al. [173-175] have ascribed crack acceleration and deceleration near the notch tip due to the notch plasticity effect. Kim and Kim [168] have concluded that plasticity induced crack closure caused by compressive residual stress at the tip of a surface crack is found to be one of the major factors that give rise to the NPCs. Haddad et. al. [74,176] have described that the decreasing crack growth rate with crack length for NPCs is similar to the anomalous crack growth behaviour of a small crack within the notch plasticity. Tanaka and Nakai [124] have observed NPCs in the vicinity of sharp notches in center-notched plates of low carbon steel fatigued under stress levels near the fatigue limit.

Sadananda and Vasudevan [180] presented a different view based on their unified approach for fatigue crack propagation that considers the existence of two origins of stress intensity factors. Total stress intensity factor, according to these investigators, consists of the sum of contribution from the remote applied stress and the local internal stress. The notch-tip plasticity contributes to the changes in internal stresses. As the crack grows away from a notch, the contribution from internal stress decreases while the contribution from applied stress increases due to increasing crack length. They have shown that non-propagation of incipient cracks occur when the total stress intensity factor falls below the long crack growth threshold value in terms of K_{max}. Yamada et. al. [170] have observed NPCs in plain carbon steels. These investigators have described the reason for the appearance of NPCs as the possible effects of residual compressive stresses associated with localized plasticity at the crack tip during cyclic loading and/or from the machining of pits by EDM in their experiment.

2.6 Factors affecting fatigue crack propagation

Numerous mechanical, microstructural and environmental factors influence the fatigue crack propagation rate of long and short cracks. Some salient features of these factors are discussed in this section.

2.6.1 Mechanical factors

The mechanical factors encompass the effects of mean stress, frequency and specimen geometry on fatigue crack propagation.

Effect of mean stress on endurance limit is a well-studied phenomenon. In defect-tolerant design the effect of mean stress is usually examined in terms of stress, load or stress intensity factor ratio, R (= K_{min}/K_{max}). The influence of R is relatively less in the mid-range of growth rates but its effect on near threshold propagation is more. Studies on a wide range of structural materials in air at ambient temperature indicate that crack propagation rate increases with increasing R-ratio [13] and the fatigue threshold decreases with increasing R-value [181]. The increase of propagation rate with increasing R-value is illustrated with a typical example in Fig.2.26, whereas the decrease of ΔK_{th} with increasing R is demonstrated in Fig.2.27. Additionally several results related to influence of R on ΔK_{th} in different structural materials [13] is compiled in Table 2.3. The influence of R on fatigue crack propagation rate can be explained with crack closure phenomenon with the magnitude of K_{cl}. Higher crack closure for a fixed K_{max} leads to lower ΔK_{eff}. At low R-ratio the amount of crack closure is higher and this leads to lower crack propagation rates and higher magnitude of ΔK_{th}.

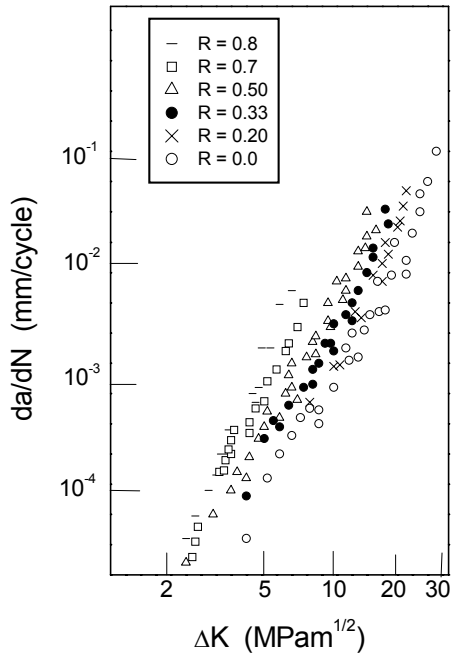

Fig.2.26 Fatigue crack propagation in 7075-T6 aluminium alloy showing effect of load ratio [13].

Table 2.3 Influence of R on ΔK_{th} in different structural materials [13].

Material	R	ΔK_{th} MPa$\sqrt{m}$
9310 Steel	0.25	~6.1
	0.90	~3.3
A533B Steel	0.10	8.0
	0.30	5.7
	0.50	4.8
	0.70	3.1
	0.80	3.0
A508	0.10	6.7
	0.50	5.6
	0.70	3.1
T-1	0.20	~5.5
	0.40	~4.4
	0.70	~3.3
Ti-6Al-4V	0.15	~6.6
	0.33	4.4
18/8 Austenitic steel	0.00	6.1
	0.33	5.9
	0.62	4.6
	0.74	4.1
Copper	0.00	2.5
	0.33	1.8
	0.56	1.5
	0.80	1.3
60/40 Brass	0.00	3.5
	0.33	3.1
	0.51	2.6
	0.72	2.6
Nickel	0.00	7.9
	0.33	6.5
	0.57	5.2
	0.71	3.6
300-M steel	0.05	6.2
(650^{o}C tempered-oil quench)	0.70	2.7
300-M steel		
(650^{o}C temper-step cooled)	0.05	6.2
2024-T3 Aluminium	0.70	2.7
2219-T851 Aluminium	0.80	1.7
	0.10	3.0
A356 Cast aluminium	0.50	1.7
	0.10	6.1
AF42 Cast aluminium	0.80	2.4
	0.50	3.4
	0.80	1.7

The number of investigations related to the examination of the role of R on fatigue crack propagation of long cracks is large. But investigations related to the influence of R on propagation rates of short cracks are limited. Higher R-ratio has been observed to shift the crack growth data to the left side of da/dN *vs*. ΔK plot just like its influence on long crack growth data. A typical result [182] illustrating the influence of R on short crack growth behaviour is illustrated in Fig.2.28.

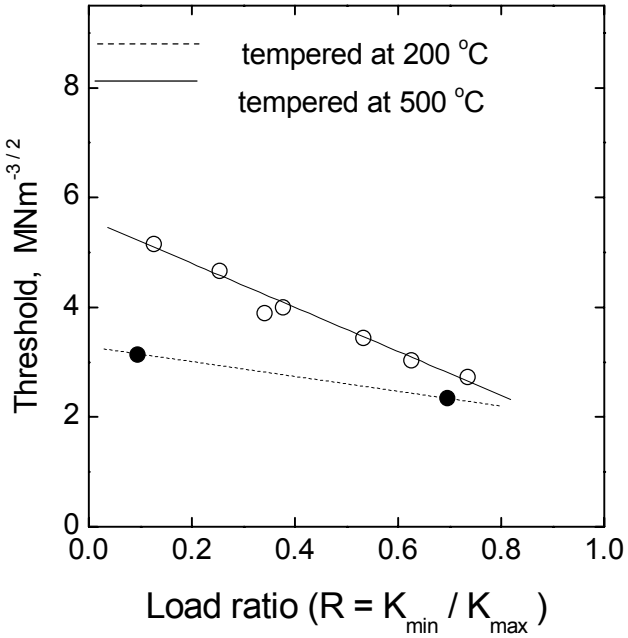

Fig.2.27 Variation of fatigue threshold with load ratio for martenstic 1.4Ni-1Cr-0.3Mo high-strength steel, tested at laboratory air [181].

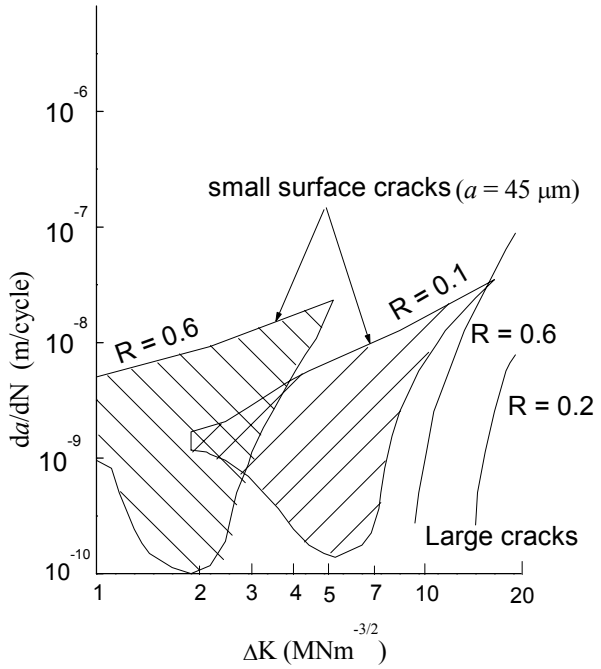

2.28 A typical result illustrating the influence of load ratio on crack growth behaviour [182].

The general effect of decreasing cyclic frequency in fatigue studies is to increase the crack growth increment per cycle in the mid-range of growth rates. This occurs primarily due to enhanced environmental effects on crack propagation [183]. Because of the time factor involved in estimating fatigue crack growth rate (FCGR) at very low frequency, limited data exists related to the effect of frequency on ΔK_{th}. Reported results on 2219-T851 aluminium alloys [184] and on D6AC steel [185] indicate no effect on near threshold growth in air over a frequency range of 25–150Hz and 100 – 375 Hz respectively. However, decreasing the frequency from 130 to 0.5Hz in aluminium alloys and stainless steels has been reported [186] to result in decrease in ΔK_{th}. The possible reason of such decrease is the influence of environment at low growth rates. Till now no reports are available on the effect of frequency on short crack growth rate to the best knowledge of the author. The effect of waveform (like sinusoidal, square and triangular) on near threshold fatigue behaviour has been examined in aluminium alloys and stainless steels in room air [186]. The alternation in waveform was found to yield no effect on the magnitude of ΔK_{th}.

The FCGR can be considered to be independent of specimen geometry provided conditions of linear elasticity remain valid. But specimen size specifically its thickness can influence FCGR owing to departure from plane strain condition. Increasing FCGR with increasing the thickness (0.3 mm to 0.65 mm) is found reported in 9Cr-1Mo steel [187], inconel [187], maraging steel [188], C-Mn steel [188] and aluminium alloys [189]. A typical set of data [190] indicating the influence of thickness on FCGR is shown in Fig.2.29. However, in certain materials the FCGR has been found to be independent of specimen thickness [191].

The crack size, on the other hand has been shown to have significant influence on the fatigue threshold as discussed earlier using Fig.2.10. The effect of crack size on ΔK_{th} is a reflection of the transition from long to short crack. Since short cracks are popularly studied on surfaces, the effect of specimen dimension is expected to have insignificant influence on its growth behaviour. But the specimen geometry and particularly the mode of loading are important in influencing short crack growth behaviour. Grabowski and Yates [192] have reported that tension geometry produces the most consistent short crack data with minimal scatter whereas three-point bend geometry yields the most inconsistent short crack data.

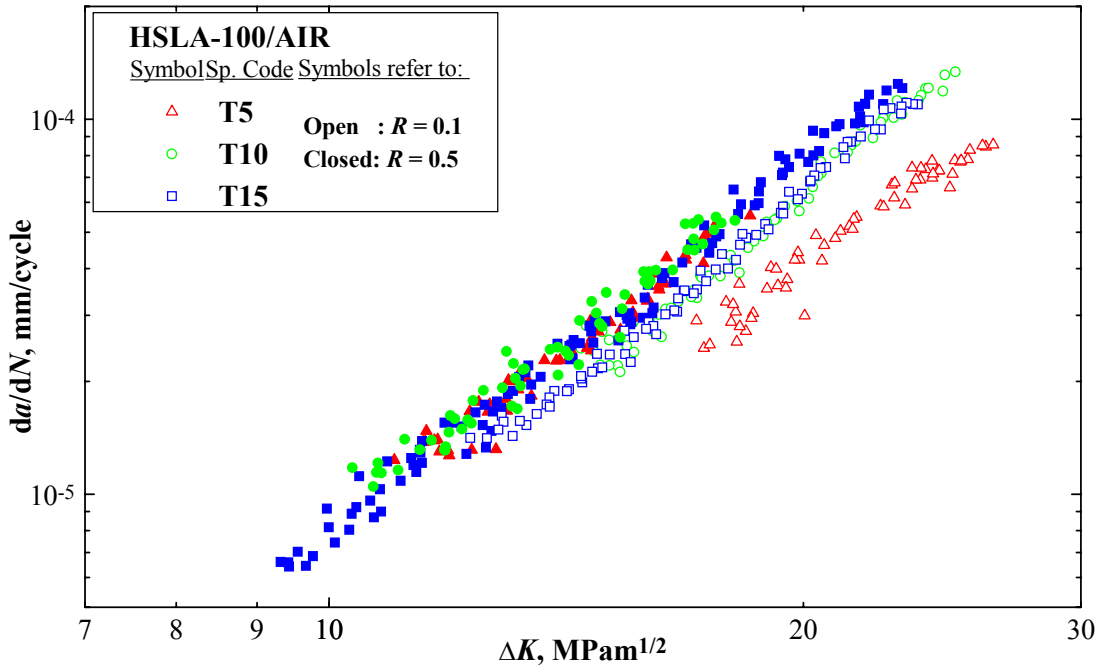

Fig.2.29 Effect of thickness on FCGR behaviour of HSLA-100 in air [190]. T5, T10 and T15 refer to specimens having thickness 5, 10 and 15 mm respectively.

2.6.2 Microstructural factors

The presence of microscopic discontinuities such as grain boundaries, interfaces of secondary phase particles or inclusions etc., significantly influences the growth of short cracks. The growth of short cracks is impeded by the presence of grain boundaries by several mechanisms e.g. the blocking of slip bands or containment of plastic zone within the grain, reorientation and re-initiation of crack as it traverses the boundary and simple cessation of growth at the boundary. Crack propagation has also been reported to be stopped by harder second phase; for example in duplex ferritic-martensitic steels cracks were observed to initiate and grow in softer ferrite, only to get arrested when these encountered the harder martensite [88].

The effect of the microscopic features on cessation and re-initiation of short cracks has been explained by Suresh [41] considering the mechanics of crack deflection. The low-restraint on cyclic slip promotes predominately a crystallographic mode of failure for short cracks. When a crack tip reaches a grain boundary it tends to reorient itself in the adjacent grain to advance by the single shear mechanism and can be considerably deflected by grain boundary. This phenomenon is schematically illustrated in Fig.2.30.

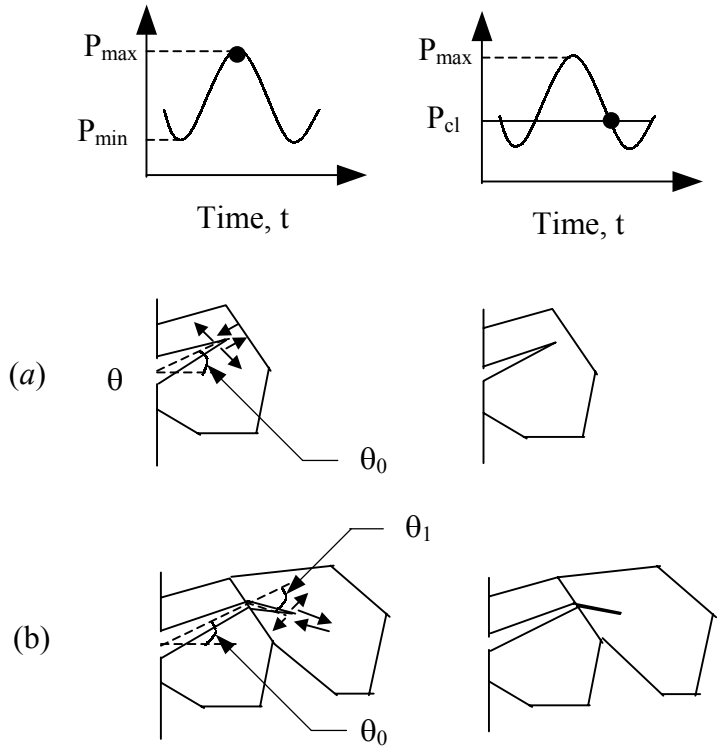

Fig.2.30 Growth and deflection of microstructurally short fatigue crack and the resultant crack tip displacement and closure; θ_0 is short crack initiation angle and θ_1 is the angle of deflection at first grain boundary. (a) Propagation into first grain; (b) Propagation across grain boundary.

The extent of crack deflection at the grain boundary is a function of the relative orientations of the most favourable slip systems in the adjoining crystals. For an elastic crack initially inclined at an angle θ_0 to the mode I growth plane and deflected at the first grain boundary through an angle θ_1 (Fig.2.30), approximate estimates of the local stress intensity factors yield the relation [41]:

$$K_1/K_I = \cos^2(\theta_0)\cos^3\left(\frac{1}{2}\theta_1\right) + 3\sin(\theta_0)\cos(\theta_0)\sin\left(\frac{1}{2}\theta_1\right)\cos^2\left(\frac{1}{2}\theta_1\right) \quad \ldots(2.24)$$

$$K_2/K_1 = \cos^2(\theta_0)\,\sin\left(\frac{1}{2}\theta_1\right)\cos^2\left(\frac{1}{2}\theta_1\right) - \sin(\theta_0)\cos(\theta_0)\cos\left(\frac{1}{2}\theta_1\right)\left[1 - 3\sin\left(\frac{1}{2}\theta_1\right)\right]$$

...(2.25)

Here K_1 and K_2 are the near-tip mode I and mode II stress intensity factors respectively, immediately following deflection at the grain boundary, whereas K_I is the nominal mode I (far-field) value. For a typical short crack emanating from the

surface at an angle of $\theta_0 \approx 45^o$ and deflected at the grain boundary by $\theta_1 \approx 90^o$, equations (2.24) and (2.25) yield $K_1 = 0.7K_I$ and $K_2 = 0.35K_I$ [41]. The effective driving force for coplanar growth can then be approximated as the square root of the sum of the squares of K_1 and K_2, such that $\Delta K_{eff} \approx 0.78\Delta K_I$. The consideration of crack deflection processes alone can account for a significant reduction in driving force as a crack tip interacts with a grain boundary when the short crack-advance is characterized by LEFM. It has been postulated that if the extent of deflection at the grain boundary is large, the effective cyclic stresses may be reduced to a value smaller than the true threshold for short crack advance (e.g. to the fatigue endurance limit) such that complete crack arrest will result. If the effective cyclic stresses after deflection are above such threshold values, there would be no crack arrest and only a temporary deceleration would occur in growth rate. The above-explained mechanism appears to provide physically meaningful explanation for the role of microstructure in influencing short crack propagation.

Crack deflection mechanisms also play an important role in enhancing the closure of short cracks. For example, irreversibility of slip steps and surface oxidation can lead to non-uniform tensile opening and shear displacements of short cracks. The presence of serrated fracture surfaces and mode II component of crack tip displacement result in premature contact between asperities leading to roughness-induced closure (Fig.2.16). Experimental measurements of closure associated with short cracks by Morris and his co-workers [135] support these approaches.

In summary, the microstructural features like grain boundaries, inclusions or second phase particles alter the crack tip driving force in a way that a short crack may cease to extend or may propagate with reduced growth (Fig.2.2). The influence of microstructure on the crack closure gets influenced by the crack length and its magnitude of deflection.

2.6.3 Environmental factors

The significance of chemically short cracks was first realised from the work of Gangloff [88] and a typical result from his work is depicted in Fig.2.18. Gangloff showed that both long fatigue cracks (a ~ 15mm) and small fatigue cracks (a ~ 0.1 to 0.8mm) are amenable to LEFM characterization and exhibit essentially the same

growth behaviour in Paris regime. But in 3% NaCl, short fatigue cracks propagate upto two orders of magnitude faster than the long cracks as shown in Fig.2.18. The effect of chemically short cracks is considered to be a consequence of the strong dependence of corrosion fatigue phenomenon on crack size. Gangloff and Wie [193] have identified the faster growth rates of short cracks due to the possibilities of oxide and roughness induced crack closure (Fig.2.16), hydrogen-enhanced crack tip straining and mass transport/reaction to produce hydrogen within the cracks. The chemical effects on short cracks have been evidenced in other ferrous and Al-alloys by Lankford [71] and Saxena [194].

2.7 Re-appraisal of the problem

The sequence of fatigue damage in a structural component i.e. crack initiation, short crack growth, stable long crack propagation and complete fracture are well documented. Several investigators have studied the phenomenon of fatigue crack initiation in laboratory made and commercial alloys. These investigations have almost established the possible mechanisms of crack initiation in conventional structural materials. But information related to role of microstructure on microcrack nucleation is limited as to provide a generalized guideline for the preferred location and the nature of the microcrack in a microstructure.

There has been an upsurge of interest to understand the anomalous behaviour of short cracks over the last two decades. That short cracks grow faster than long cracks at similar ΔK, and that these grow below the long crack fatigue threshold are firmly established facts. It is well recognized by now that fatigue lifetime of several structural components can be considerably influenced by the rate of growth of these small cracks. One finds single or multiple arrests of a short crack during its propagation and these arrest-points can be termed as short crack fatigue thresholds (SCFTH). The reasons for the occurrence of multiple SCFTH and the relation between its maximum value (i.e. the one near the long crack fatigue threshold) and the long crack fatigue threshold have not been carefully explored so far.

The determination of ΔK_{th} or crack growth studies near ΔK_{th} usually requires significant time engagement of servo-hydraulic or electro-magnetic resonance type machines. As a result, studies on fatigue behaviour at near threshold are limited compared to that of stable crack propagation. But such studies are important to

explore the mechanics and mechanisms of crack growth behaviour in structural materials designed for safe-life applications. So there exists a need to search for alternative simple techniques for studying crack growth behaviour at low da/dN values, and thereby to estimate ΔK_{th} of structural materials. In addition, attempts to carefully understand the role of the microstructural features, which results in either short or long crack thresholds, are lacking.

Numerous investigations have been carried out to understand the propagation of short and long cracks. But the role of the microstructure associated with these crack paths have not been examined so far. Studies of this nature can bring forth information about the weak-links in a microstructure through which a crack prefers to pass through or the affinity of a crack to travel through any specific phase in a microstructure.

This investigation has been directed to understand some of the above-mentioned problems.

Chapter 3

Materials characterization

3.1 Introduction

In this investigation fatigue studies have been made on five different steels having carbon content of 0.003, 0.14, 0.25, 0.47 and 0.62%. For the convenience of discussion these steels are henceforth referred to as S00, S14, S25, S47 and S62 steels respectively, where the numeric in the codes indicate the carbon content of the steels. The S00 and S14 steels were chosen for crack initiation studies whereas S00, S25 and S47 steels were selected for examinations related to short crack growth. The long crack fatigue threshold has been determined for all the steels except for S14.

Any examination of fatigue and fracture behaviour of a structural material *ab-initio* requires detailed information about the microstructural features and about some conventional mechanical properties. In the selected steels the microstructural features of importance are nature, morphology, distribution and the relative amounts of the various phases present. The conventional mechanical properties refer to hardness and tensile properties.

The aims of the investigation reported in this chapter are to generate information about the microstructure of the selected steels, to determine their hardness and tensile properties and to make a comparative assessment of the obtained results with available data on similar materials.

3.2 Experimental procedure

3.2.1 Material

Five commercial steels have been selected for this investigation. The S00 steel was obtained as courtesy of Tata Iron and Steel Company Ltd. (TISCO), Jamshedpur, India and it was available in the form of 31mm thick steel plates. The S14 and S62 steels were obtained as courtesy of the Division of Mechanical Testing and Evaluation of National Metallurgical Laboratory (NML), Jamshedpur, India. The S14 material was available in the form of either 12 or 25mm thick steel blanks of

approximate dimensions 60mm (length) × 25mm (width) or 120mm × 50mm. The S62 steel was available in the form of 30mm thick plates. The S25 steel was available in the laboratory as rods of 22mm diameter. The S47 steel was obtained from Usha Alloys and Steels Division, Jamshedpur, India and it was available in the form of rods with a diameter of 23 mm.

The compositions of the S00, S14, S47 and S62 steels were obtained as courtesy of the respective sources from where these were collected. The composition of S25 steel was determined by an X-ray fluorescence spectrometer as courtesy of Kharagpur Metal Reforming Industries, Kharagpur. The compositions of the steels are given in Table 3.1.

Table 3.1 Compositions of investigated steels (in weight percentage).

Steel	Elements									
	C	Mn	Si	P	S	Al	Cr	Ni	V	N
S00**	0.003	0.13	0.009	0.012	0.009	0.06		0.01	0.001	0.0034
S14	0.14	0.9	0.25	0.016	0.018	<0.1	0.08	0.05	<0.01	0.01
S25	0.25	0.72	0.19	0.04	0.03	--	--	--	--	--
S47	0.47	0.77	0.22	0.014	0.016	0.003	0.13	0.005	--	63ppm
S62	0.62	0.8	0.27	--	--	--	0.03	--	--	--

**Ti - 0.052, Nb - 0.001, Mo - 0.001

The S14, S62 and the S25 steels were used in the as-received condition, the S00 steel was used in the stress-relieved condition whereas S47 steel was used in the annealed condition for all subsequent microstructural examinations and studies related to mechanical behaviour. The stress-relieved condition of the S00 steel consisted of soaking specimen blanks at 400^{o}C for one hour followed by furnace cooling. The annealing of S47 steel was done by soaking the plates at 850^{o}C for one hour followed by furnace cooling.

3.2.2 Metallographic examination

Samples of approximately 10 × 10 mm cross-section or of 10 mm diameter were cut from steel blanks for metallographic examinations. All samples were initially ground upto 400 grade emery paper and were then polished, first using alundum and finally using 0.25 μm diamond paste. The polished specimens were etched with 2% Nital solution for approximately 2-10s to reveal the microstructures.

Representative microstructures of the investigated steels were photographed using a Metallograph (Model: MEF2).

The quantitative characterizations of the microstructures were carried out using an optical microscope coupled with an image analyzer. These estimations included determination of the following:

a) the volume fraction of the phases

b) the ferrite grain size, and

c) the banding index

3.2.2.1 Volume fractions of phases

The volume fraction of the phases was determined with the help of an image analyzer. The measurements were done using an optical microscope (Leica, model: 020-520-007 DM/LP) having the provision of an image analysis system (Biovis Material Plus, Revised version 2.0, Medimage Technologies Pvt. Ltd., Hyderbad, INDIA). These measurements were carried out in the following way. A representative field of an etched sample was grabbed with the help of a CCD camera. The areas covered by pearlite were marked by colouring using the threshold adjustment facility of the image analyzer. The area fraction of the pearlite was measured automatically by the image analyzer, and the numerical output was recorded. These measurements were repeated on 30 randomly selected fields of observation, from which the average volume fraction of pearlite was estimated. The volume fraction of pearlite in S14 steel estimated by the image analyzer was crosschecked by manual counting method. In the manual method, point-counting technique was done following ASTM E-562 [195] standard. In this experiment, a 21×21 grid was superimposed on a microstructure, viewed at a magnification of 200X, and random counting was made on 50 fields of observation. The volume (V_f) of a phase was calculated using the equation

$$V_f = \frac{\sum P}{nP_o} \qquad \ldots(3.1)$$

where ΣP = total number of points on a phase,

P_o = number of grid points

and n = number of fields of observations.

The data obtained from each sample was subjected to statistical analysis for computing standard deviation and standard error associated with the mean value of the volume fraction of each phase.

3.2.2.2 Grain size measurement

The average grain size of ferrite was ascertained with the help of linear intercept method following ASTM standard E-112 [196] and using the suggestions for grain size measurement of two-phase microstructure given by Vander Voort [197]. In this method, a linear test grid was superimposed on the microstructure and the number of ferrite grains intercepted by the test line was counted. Such measurements were repeated on 50 randomly chosen fields at a magnification of 400X for S14 steel, 100X for S00 steel and 200X for S25 steel. The average grain size (d) of ferrite was then calculated using the relation:

$$d = \frac{V_f L_T}{N_L} \qquad \ldots(3.2)$$

where, N_L = No. of ferrite grains intercepted by a unit true test line length. The true length L_T of a test line is defined as the length of the test line at unit magnification. This procedure was adopted for S25 and S14 steels. The microstructure of S00 steel exhibited equiaxed ferritic structure and hence grain size (d) was calculated as

$$d = \frac{L_T}{N_L} \qquad \ldots(3.3)$$

3.2.2.3 Banding parameter estimation

Microstructural banding was observed in S47 and S14 steels. The quantitative measurement of the degree of microstructural banding was carried out using stereological procedures following ASTM standard E-1268 [198].

In this procedure a linear test grid was superimposed on a representative microstructure, viewed at a magnification of 200X. The specimen was aligned on the microscope stage such that the deformation direction was horizontal on the projection screen and the test line is nearly parallel to the banding direction. The number of pearlite colonies intercepted by the line was recorded. Similar counting of pearlite colonies by a series of vertical test lines was next carried out. The observations were

repeated for 25 random fields. The degree of orientation of pearlite in a matrix of ferrite was estimated using the following equation [198]:

$$\Omega_{12} = \frac{N_{L\perp} - N_{L\,II}}{N_{L\perp} + 0.57N_{L\,II}} \qquad ...(3.4)$$

where,

$N_{L\perp}$ = mean number of feature (pearlite) interceptions per unit true test line length with test line perpendicular to the deformation direction,

N_{LII} = mean number of feature (pearlite) interceptions per unit true test line length with test line parallel to the banding direction.

The estimations of $N_{L\perp}$ and N_{LII} were carried out for S47 and S14 steel specimens and the degree of orientations (Ω_{12}) were computed using eqn. (3.4).

3.2.3 Inclusion characterization

Representative samples of approximate cross-section of 10×10 mm^2 were taken for estimation of inclusion content in the selected steels. The samples were heat treated by water quenching from austenitising temperature after soaking these for one hour. Austenitising temperature for S00, S14, S25, S47 and S62 steels were kept as 910, 877, 851, 800 and 765^oC respectively. This hardening treatment was done to achieve better surface finish during successive polishing operations. The samples were ground and polished as stated in section 3.2.2.

The volume fraction of inclusions in each steel was determined using the Japanese standard method [199]. In this technique, point counting is carried out using a 21×21 grid at a magnification of 400X on 50 fields of observation. The volume fraction of inclusions also referred as index of cleanliness, was calculated using the expression:

$$V_I = \frac{n}{P \times f} x100 \qquad ...(3.5)$$

where, V_I = index of cleanliness in percentage, P = total number of grating points in a visual field, f = number of visual fields, and n = number of grating points occupied by the inclusions.

3.2.4 Hardness measurement

Samples of approximately 10×10 mm cross-section or 10 mm diameter were cut from steel blanks for hardness examinations. The opposite surfaces of these specimens were made parallel and were polished up to 400-grade emery paper. Both macro and micro Vickers hardness measurements were carried out. The former tests were done at a load of 10 kgf using a Vickers hardness-testing machine (Fuel Instruments & Engineers Pvt. Ltd., INDIA, model: VM 50), whereas the latter tests were carried out with a Vickers indenter using a load of 25 gmf with the help of a microhardness tester (LECO, model: DM-400). Ten readings were taken in case of macro hardness measurements whereas 25 readings were taken in case of micro hardness measurements to estimate the average hardness values. Appropriate care was taken during each measurement so that the distance between two successive indentations was more than thrice the average diagonal length of the indentations.

3.2.5 Tensile testing

Round tensile specimens of 5 mm diameter and 20 mm gauge length following ASTM standard E8-93 [200] were fabricated from the as-received plates or rods. The specimens were prepared with their loading axis parallel to the rolling direction. Typical configuration of a tensile specimen is shown in Fig.3.1. All tests were carried out at a cross-head velocity of 0.5 mm/min using a Universal testing machine (Schimadzu, model: AG-5000G) at room temperature. This cross-head velocity corresponds to a nominal strain rate of 4.2×10^{-4} sec^{-1}.

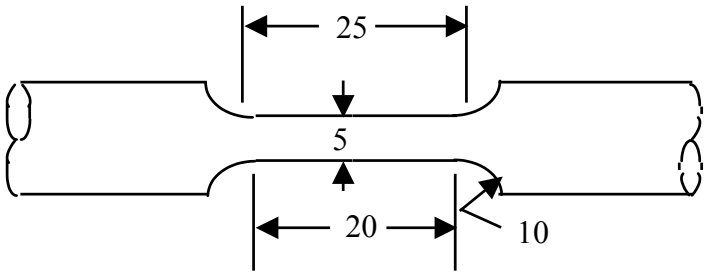

All dimensions are in mm

Fig.3.1 Configuration of round tension test specimen.

3.3 Results and discussion

3.3.1 Microstructural characterization

The compositions of the materials selected for this investigation are shown in Table 3.1. The S00 steel is almost carbon free, whereas S14, S25, S47 and S62 are plain carbon steels with carbon contents of 0.14, 0.25, 0.47 and 0.62% respectively.

The average volume fraction of inclusions were estimated as 0.06%, 0.21%, 0.09% and 0.1% in S00, S25, S47 and S62 steels respectively. It was found that in S14 steel the volume fraction of inclusion is extremely low and the amount cannot be determined with any certainty by the adopted procedure for inclusion estimation. The polished samples of S14 steel were, however, examined at 1000X and the sizes of a few inclusions could be estimated. These examinations indicated that the maximum inclusion size in this steel is of the order of 6 μm. It was found that in S00 steel, inclusions are fine in comparison to those in S25, S47 and S62 steels. The average size of inclusions in S00, S25, S47 and S62 steels were found to be 2.9, 3.4, 6.2 and 6.5 μm respectively. Most of the inclusions in S00 steel are oxides whereas sulphide inclusions are dominant in S25, S47 and S62 steels. The details of the inclusion amount and their mean size in the investigated steels are compiled in Table 3.2.

Table 3.2 Inclusion content of the investigated steels.

Material	Volume fraction (%) of inclusions	Mean size (μm)	Observed maximum inclusion size (μm)
S00 steel	0.06 ± 0.02	2.9 ± 0.4	10.3
S25 Steel	0.21 ± 0.10	3.4 ± 1.1	17.5
S45 Steel	0.09 ± 0.02	6.2 ± 0.7	12.7
S62 Steel	0.1 ± 0.04	6.5 ± 0.9	15.6

Typical microstructures of S00, S14, S25, S47 and S62 steels are shown in Fig.3.2. The S00 steel exhibits ferritic microstructure (Fig.3.2a), whereas the microstructures of the other steels reveal a mixture of ferrite and pearlite (Fig.3.2b, Fig.3.2c, Fig.3.2d and Fig.3.2e). However, the nature of distribution of ferrite and pearlite in S14, S25, S47 and S62 steels are different. The S14 and the S47 steels exhibit banded structure (Fig.3.2b and Fig.3.2d) unlike that for S25 and S62 steels.

The nature of banding in S14 and S47 steels were also examined on mutually perpendicular surfaces and some representative microstructures are shown in Fig.3.3 and in Fig.3.4. In S47 steel, the microstructure in the cross section do not exhibit any banding (Fig.3.4a), whereas the microstructure in the L-T and L-S planes indicate banding of different nature (Fig.3.3). The nature of banding was characterized in S14 and S47 steels by estimating the banding index parameter (Ω_{12}) as described in section 3.2.2.3. The values of Ω_{12} for S14 steel in L-T and L-S planes were found to be 0.21 and 0.28 respectively whereas that for S47 steel was estimated as 0.39. The banding index parameter indicates that S47 steel has severe banding than that in S14 steel. Also one can note that severity of banding is more in the L-S direction than that in the L-T direction of the S14 steel.

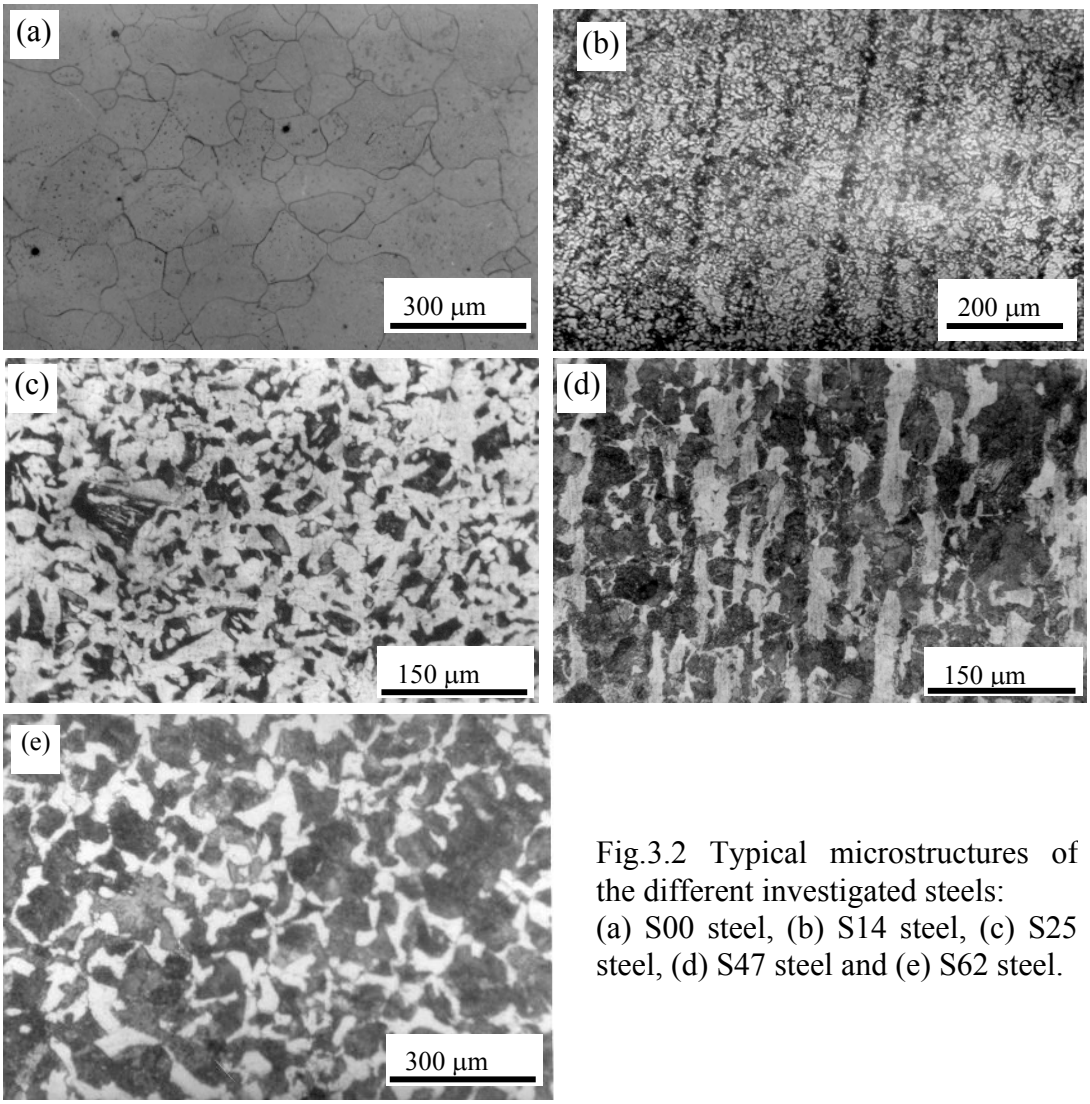

Fig.3.2 Typical microstructures of the different investigated steels:
(a) S00 steel, (b) S14 steel, (c) S25 steel, (d) S47 steel and (e) S62 steel.

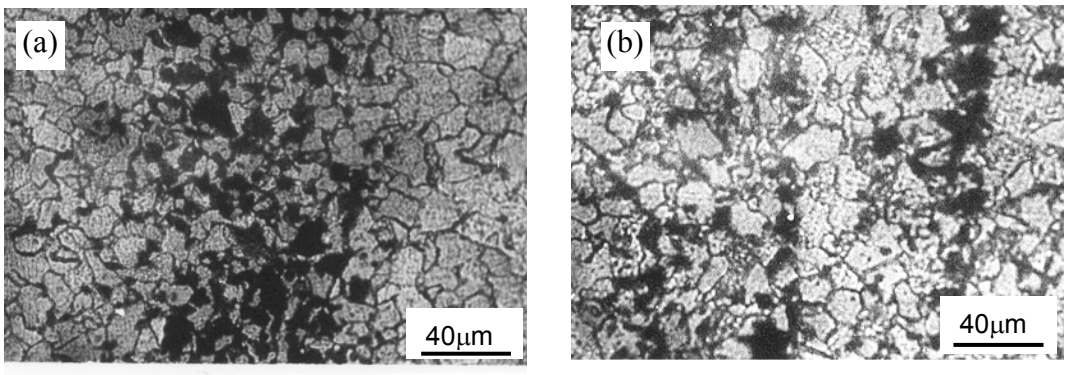

Fig.3.3 Typical microstructure of S14 steel in different orientations:
(a) L-T plane and (b) L-S plane.

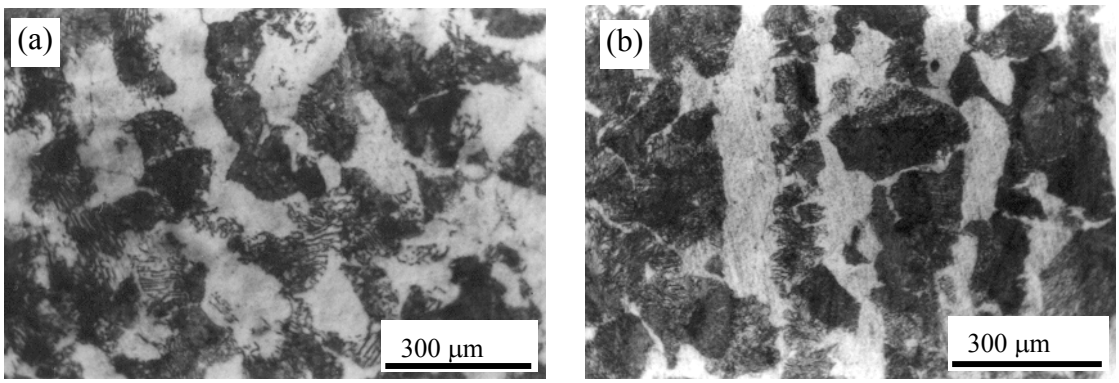

Fig.3.4 Typical microstructure of S47 steel in different orientations:
(a) Cross-sectional and (b) Surface.

The volume fractions of pearlite in S14, S25, S47 and S62 steels were found to be 15.5±1.4, 27.3±0.9, 63.0±1.6 and 78.9±1.6% respectively. The carbon content of these steels predict that the volume fraction of pearlite in S14, S25, S47 and S62 steels should be ≈ 16%, 31%, 59% and 77% respectively, following the standard iron-iron carbon diagram [201]. The difference between the theoretical and the experimental values is attributed primarily to the presence of minor alloying elements in the steels. The estimated volume fractions of pearlite in the investigated steels are compiled in Table 3.3 together with their standard deviation. The pearlite content of S14 steel was also determined by manual counting method and was found to be 14.8±1.1. One can note that the estimated pearlite content in S14 steel by image analysis (15.5±1.4) is in close agreement with that obtained by manual counting method, considering the associated standard deviation with their mean value. Hence

the measurements of volume fraction of pearlite as carried out by image analysis are considered reliable.

The ferrite grain sizes of the selected steels were obtained as described in section 3.2.2.2. The estimated values of ferrite grain size are compiled in Table 3.4. The results in Table 3.4 indicate that ferrite grain sizes in the selected steels are different.

Table 3.3 Amount of pearlite in the investigated steels.

Material	Amount of pearlite phase (%)
S00 steel	0
S14 steel	15.5±1.4
S25 steel	27.3±0.9
S45 steel	63.0±1.6
S62 steel	78.9±1.6

Table 3.4 Ferrite grain sizes of the investigated steels.

Material	Grain size (μm)
S00 Steel	64.4 ± 1.3
S14 steel	12.0 ± 0.7
S25 steel	18.0 ± 1.1
S47 Steel	NM*
S62 steel	NM*

NM*-not measured; because the steel exhibits mostly pearlitic structure

3.3.2 Related mechanical properties

The average Vickers hardness values of the different materials are reported in Table 3.5. The macrohardness values of the investigated steels were found to increase with increasing carbon content, in line with natural expectations. The microhardness of the different phases were also determined and the average microhardness values are reported in Table 3.5. For each of these estimated average values, the standard errors were also computed and their magnitudes are enlisted in Table 3.5. The ferrite of S00 and the pearlite of S62 steels indicate the lowest and the highest hardness values respectively amongst the different measurements. Interestingly the hardness of

pearlite colony is found to increase with increasing carbon percentage of the steels. The hardness of a phase in a microstructure depends on the nature and the amount of its surrounding phases in that microstructure [202,203]. The increase in hardness of pearlite with increase in carbon content has been reported by Ray and Mondal [202,203]. The above investigators have attributed the higher observed hardness of pearlite to the existence of higher hydrostatic stresses in plain carbon steels with increased amount of pearlite in their microstructure.

Table 3.5 Hardness of the investigated steels and their constituent phases.

Material	Hardness
S00 steel	$H_V = 94.4 \pm 0.1$ (at 25 gmf) – Ferrite
S14 steel	$H_V = 128 \pm 1.2$ (at 10 kgf) $H_V = 181.4 \pm 0.4$ (at 25 gmf) – Ferrite $H_V = 306.2 \pm 1.2$ (at 25 gmf) – Pearlite
S25 steel	$H_V = 157 \pm 1$ (at 10 kgf) $H_V = 224.2 \pm 1.2$ (at 25 gmf) – Ferrite $H_V = 313.3 \pm 1.9$ (at 25 gmf) – Pearlite
S45 steel	$H_V = 168.3 \pm 0.6$ (at 10 kgf) $H_V = 198.7 \pm 0.5$ (at 25 gmf) – Ferrite $H_V = 325.8 \pm 2.1$ (at 25 gmf) – Pearlite
S62 steel	$H_V = 217 \pm 1.6$ (at 10 kgf) $H_V = 322 \pm 12$ (at 25 gmf) – Pearlite

Tensile properties of the investigated steels have been studied using cylindrical samples of 5 mm diameter and 20 mm gauge length. Three specimens of each material have been tested to generate information about the average tensile properties. During these tests, the load-displacement diagrams were recorded as autographic plots and the data were stored in a computer file. A developed program was used to convert the experimental load-elongation data into the corresponding engineering stress-strain and true stress-strain values after suitable modification of the data to eliminate the machine displacement component. Typical engineering stress-strain diagrams of the investigated steels are shown in Fig.3.5. The tensile data were analyzed to estimate the yield strength, ultimate tensile strength (UTS), true uniform

elongation (ε_u), total elongation (ε_t) and reduction in area. The S14, S25, S47 and S62 steels showed distinct yield points and hence both upper and lower yield point values are shown in Table 3.6. The yield strength of S00 steel was obtained by 0.2% strain off-set procedure. The estimated total elongation values were crosschecked with the ones obtained directly from the change in the gauge marks on the specimens after the test. The average tensile parameters evaluated for each material are summarized in Table 3.6.

Table 3.6 Average tensile properties of the investigated steels.

Steel	UTS (MPa)	UYP (MPa)	LYP (MPa)	ε_t (%)	ε_u (%)	% Reduction in area
S00	238 ± 2	93.5 ± 2.5	--	45.2 ± 0.5	34.6 ± 0.8	82 ± 9.0
S14	430 ± 2	357 ± 8	291.5 ± 0.5	44.5 ± 0.5	22 ± 0	73 ± 1.0
S25	543 ± 2	338 ± 6	333 ± 5	33.4 ± 0.4	24.1 ± 0.7	58.1 ± 0.5
S47	621 ± 5	335 ± 1	327 ± 2	28.5 ± 0.3	22 ± 0.1	51.1 ± 0.1
S62*	753 ± 7	380 ± 9	376 ± 10	21.4 ± 2.0	13.4 ± 0.5	--

UTS = ultimate tensile strength, UYP = upper yield point, LYP = lower yield point, ε_t= total elongation, ε_u = uniform elongation. The results on S62* steel were obtained as courtesy of Tarafder [204].

An attempt has been made to compare the order of the estimated tensile properties of the investigated steels with those of materials of similar compositions. The compositions of S00, S14, S25, S47 and S62 steels are close to those of ASTM A366, ASME SA333 or ASTM A333, AISI 1025, AISI 1046 and AISI 1060 steels respectively. The measured tensile properties of the investigated steels are in good agreement with the reported results for their corresponding grades. For example, Singh et. al. [205] have reported the yield strength, tensile strength and percentage elongation of SA333 steel as 302MPa, 450 MPa and 36.7% respectively whereas the estimated magnitudes of these tensile parameters of S14 steel are 292MPa, 430MPa and 44.5% respectively. The minor differences between the observed tensile properties of the investigated steels and those reported for similar grades are due to minor differences in the compositions, microstructures and prior history of the materials.

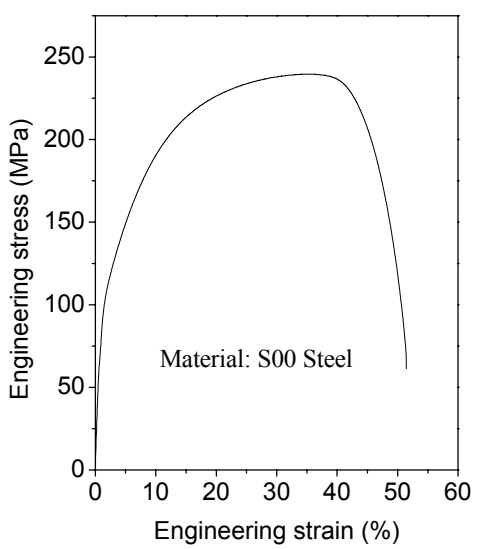

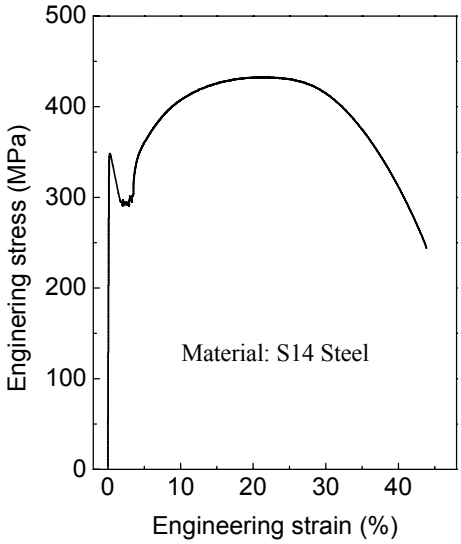

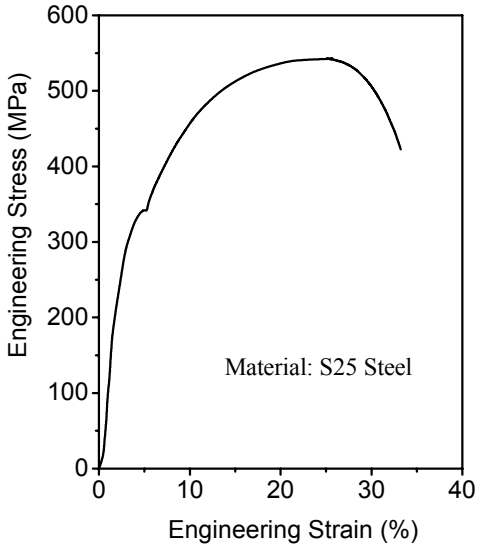

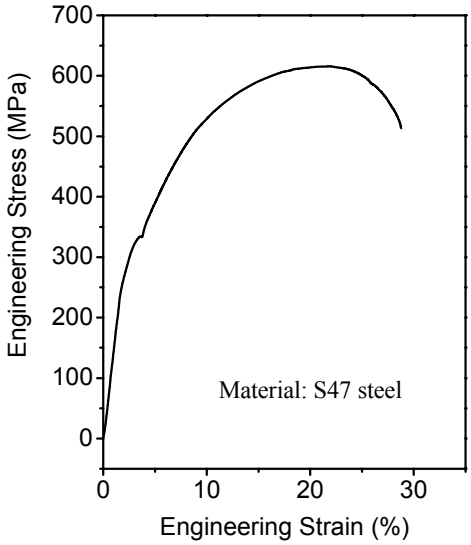

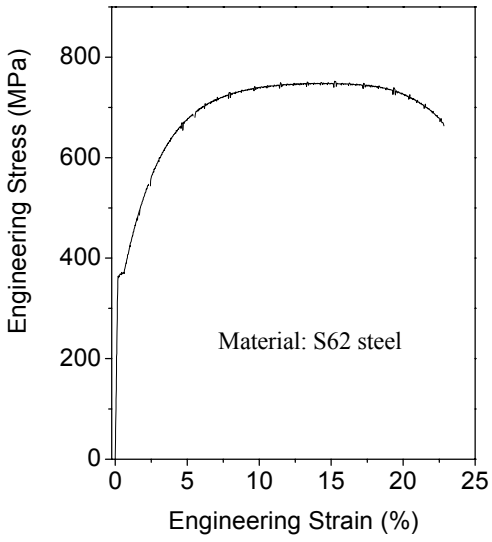

Fig.3.5 Typical engineering stress-strain diagrams of different investigated materials.

3.4 Summary

The microstructure of the S00 steel is dominantly ferritic in nature whereas the microstructures of S14, S25, S47 and S62 steels exhibit ferrite-pearlite structures. The amount of pearlite is found to increase with increasing carbon content of the steels as expected. The S00 and S14 steels can be considered relatively clean because of low inclusion contents. The S14 and S47 steels were found to show banded structure. The macrohardness values of the steels are found to increase with increasing carbon content. The hardness values of ferrite and that of pearlite in the investigated steels are not similar and appear to be function of the carbon content of the steels. The tensile strength is found to increase with increasing carbon content whereas the percentage elongation and reduction in area are found to decrease with increasing carbon content. The microstructural features, macrohardness values and tensile properties of the selected steels exhibit expected trend of variation with increasing carbon content of the selected steels. The estimated values are in good agreement with reported results for similar materials.

Chapter 4

Fatigue crack initiation in single and two-phase materials

4.1. Introduction

Micro-crack nucleation in structural materials is considered to be the first stage in fatigue damage, which is consequently followed by small/short and macro-crack propagation leading to critical fatigue fracture. A substantial body of evidences has been accumulated over the last two decades on small/short cracks behaviour [41-44,206], and these evidences are also well supplemented by a large number of investigations [107,207,208] related to the possible mechanisms of crack nucleation. By now it is well conceived that a large percentage of (high cycle) fatigue life of smooth specimens is spent in the domain of crack nucleation and small/short crack growth especially in the emerging clean (i.e. with very low inclusion content) structural materials. It is thus imperative to gather more knowledge about crack nucleation and small/short crack growth behaviour in such structural materials.

The pre-macro crack regime of fatigue damage is often termed as "fatigue crack initiation stage". It is well known by now that the microstructure of a material significantly influences this stage of fatigue damage. The existing studies which describe small/short crack growth behaviour in materials do account the microstructural features e.g. grain boundaries, precipitates, second phase particles etc. [138,140,141]; but the developments related to the mechanisms of crack nucleation, are found to be mostly associated with concepts related to sub-structural features e.g. dislocations, dislocation-vacancy complexes, dislocation dipoles etc. [2,3]. Information related to the role of microstructure on micro-crack nucleation are limited and scattered, and these have not led to any organized conceptual developments plausibly because of the numerous variety of microstructures encountered in the different investigated materials. The earlier attempts to probe this aspect have usually laid more emphasis either on the investigated material system or on the mechanics of small/short crack growth rather than trying to achieve a generalized perspective on the

effect of microstructure on the location of crack nucleation. The present study aims to achieve understanding about the location and characteristics of small cracks in single and two-phase materials. In this pursuit, this chapter deals with the formation of small cracks in two commercial steels exhibiting ferrite and ferrite-pearlite structures. The materials selected for this study are S00 and S14 steels.

The major aim of this investigation is to identify the preferred crack nucleation sites in these materials. But the selected S14 steel of engineering importance exhibits banded microstructure. The existing literature does not indicate the role of banding on the nucleation of small cracks; this has also been examined in this study. An attempt is also made to understand the possible mechanism of crack initiation in the investigated steels.

4.2. Experimental procedure

The chemical composition, microstructural parameters and mechanical properties of the investigated steels are discussed in Chapter 3. The fatigue studies were carried out on small hourglass type flat specimens as shown in Fig.4.1. One of

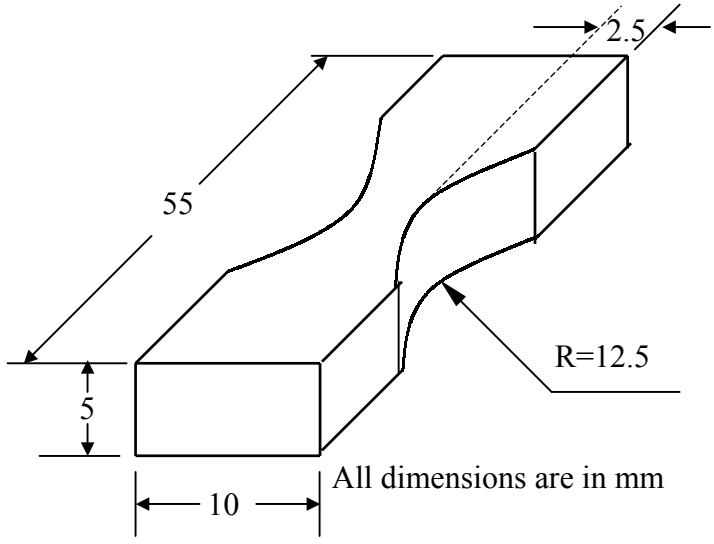

Fig.4.1 Specimen configuration used for small crack initiation studies.

the flat surfaces of each of these samples was ground, polished and etched to reveal the microstructure in a manner similar to the procedure described in Chapter 3. The fatigue tests were done with the help of an Instron machine (model: 8501) at various stress levels ranging from 0.6 to 1.0 of yield stress (σ_y) of the steel of interest

maintaining the minimum stress as zero. These tests were conducted using sinusoidal wave at a frequency of 10 Hz at room temperature (approximately 298K) in the laboratory air. The tests were carried out for 2×10^4 cycles at all applied stress levels. In addition, fatigue tests for S14 steel have been carried out with loading direction both parallel and perpendicular to the banding direction of the microstructure. The dimensions of individual specimens and the details of each test for both S00 and S14 steels are shown in Table 4.1 and in Table 4.2 respectively. After the fatigue tests, all specimens were examined under a scanning electron microscope (JEOL model: 5800) to locate the crack initiation sites. A series of micrographs with careful demarcation of the loading direction, were taken from numerous locations, which exhibited cracks. The average length of the small cracks and their location in the microstructure with respect to the loading direction were measured.

Table 4.1 Test details for crack initiation studies in S14 steel.

Sp. Code	Cross section Area (WxT) (mm×mm)	Applied stress range x σ_y	No. of Cycles applied	Banding direction w.r.t loading
S14-LR03	5.54 x 5.00	0 – 0.6	$2.0\text{x}10^4$	Parallel
S14-LR04	4.92 x 5.04	0 – 0.7	$2.0\text{x}10^4$	Parallel
S14-LR05	5.04 x 4.74	0 - 0.8	$2.0\text{x}10^4$	Parallel
S14-LR06	5.02 x 4.74	0 - 0.9	$2.0\text{x}10^4$	Parallel
S14-LR07	6.10 x 5.02	0 – 1.0	$2.0\text{x}10^4$	Parallel
S14-LR08	5.03 x 6.18	0 - 0.9	$3.0\text{x}10^4$	Parallel
S14-LR09	6.12 x 6.7	0 – 0.9	$1.0\text{x}10^4$	Parallel
S14-CL02	4.80 x 4.92	0 – 0. 6	$2.0\text{x}10^4$	Perpendicular
S14-CL03	4.88 x 4.90	0 – 0.8	$2.0\text{x}10^4$	Perpendicular
S14-CL04	4.92 x 4.90	0 – 1.0	$2.0\text{x}10^4$	Perpendicular

Table 4.2 Test details for crack initiation studies in S00 steel.

Sp. Code	Cross section Area (WxT) (mmxmm)	Applied stress range x σ_y	No. of Cycles applied
S00-CI1	5.14 x 5.02	1.0	$2.0x10^4$
S00-CI2	5.20 x 5.10	0.8	$2.0x10^4$
S00-CI3	5.12 x 4.94	0.6	$2.0x10^4$

4.3. Results and Discussion

The locations at which cracks initiate in a microstructure and the nature of such cracks after a stage of growth to a size where these can be conveniently examined by scanning electron microscopy, are the primary content of this study. The cracks thus examined may be simply termed as "small cracks". In order to understand the influence of the microstructure on the nature of the initiated cracks, the fatigue tests have been carried out in such a manner that most of the small cracks are generated with almost negligible growth. The size range of the observed cracks was found to be 1 to 96 μm, and this is considered natural. Because, under identical stress range and number of imposed fatigue cycles, when one type of cracks gets generated with the lower bound values of the above-mentioned size range, a number of alternate cracks are also found to nucleate and grow to sizes near the upper bound. A series of these cracks were photographed using a scanning electron microscope at suitable magnifications so that their maximum dimension can be measured conveniently.

4.3.1 Crack initiation in S00 steel

The SEM examinations of the polished and etched surfaces of the fatigue tested specimens of S00 steel indicated that the location at which crack initiation occurs in the microstructure of S00 steel is either at the grain boundary or in the grain body. Some typical grain boundary and grain body cracks are shown in Fig.4.2 and Fig.4.3 respectively. Interestingly no crack was observed to originate from any inclusion site, as illustrated in Fig.4.4. Thus the observed crack initiation sites in S00 steel can be categorized into two types based on the position at which these are located in the microstructure. These are: (a) grain boundary and (b) grain body cracks.

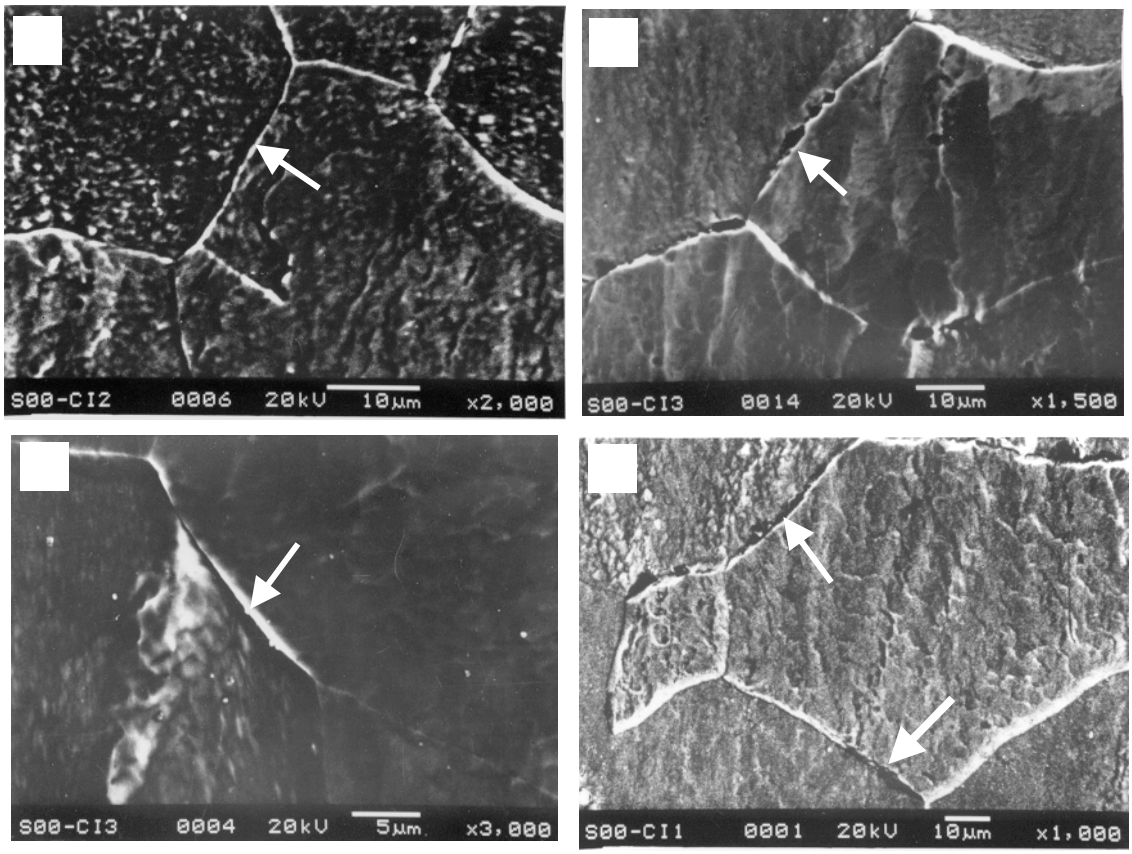

Fig.4.2 A set of typical ferrite grain boundary cracks in the investigated S00 steel.

4.3.1.1 Crack initiation at grain boundary

The size and the distribution of the grain boundary cracks were first analyzed at different fatigue stress levels and the average lengths of these cracks at 0.6, 0.8 and $1.0\sigma_y$ were found to be 14±6, 38±7 and 34±4 μm respectively. These results indicate that the average size of the initiated cracks at the lowest stress level of $0.6\sigma_y$ is considerably smaller than that at higher stress levels. These results thus naturally tend to infer that some of the initiated cracks at higher stress levels got the chance to grow. Typical distributions of the crack sizes at these stress levels are shown in Fig.4.5. An examination of the crack size distribution indicates that the 60% cracks at $0.6\sigma_y$ possesses size less than 10 μm. On the other hand, almost 60% of cracks bear size in the range 20 to 60 μm for $0.8\sigma_y$ and at $1.0\sigma_y$ about 75% of cracks have sizes in the range 20 to 60 μm. These results obviously indicate that majority of cracks at low stress level have lower size compared to that of the majority of the cracks generated at higher stress levels. The observed size distribution of the cracks thus supports the

possibility that initiated cracks get the opportunity to grow at higher stress differentials used for crack initiation studies.

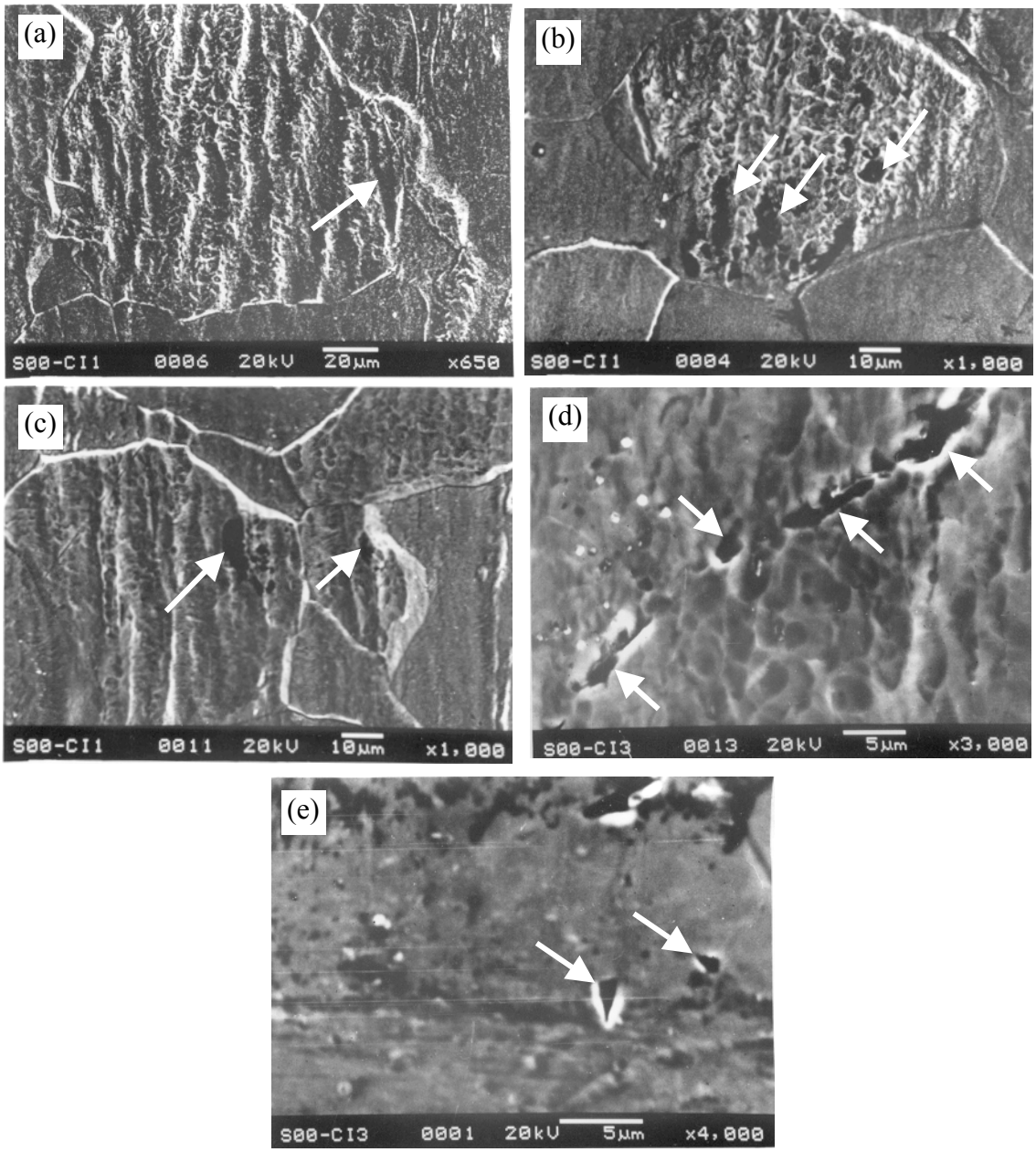

Fig.4.3 A set of typical ferrite grain body cracks in the investigated S00 steel.

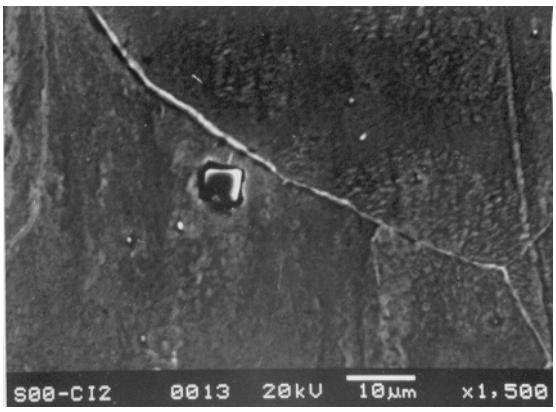

Fig.4.4 A typical inclusion in S00 steel showing no crack at applied stress of $0.8\sigma_y$.

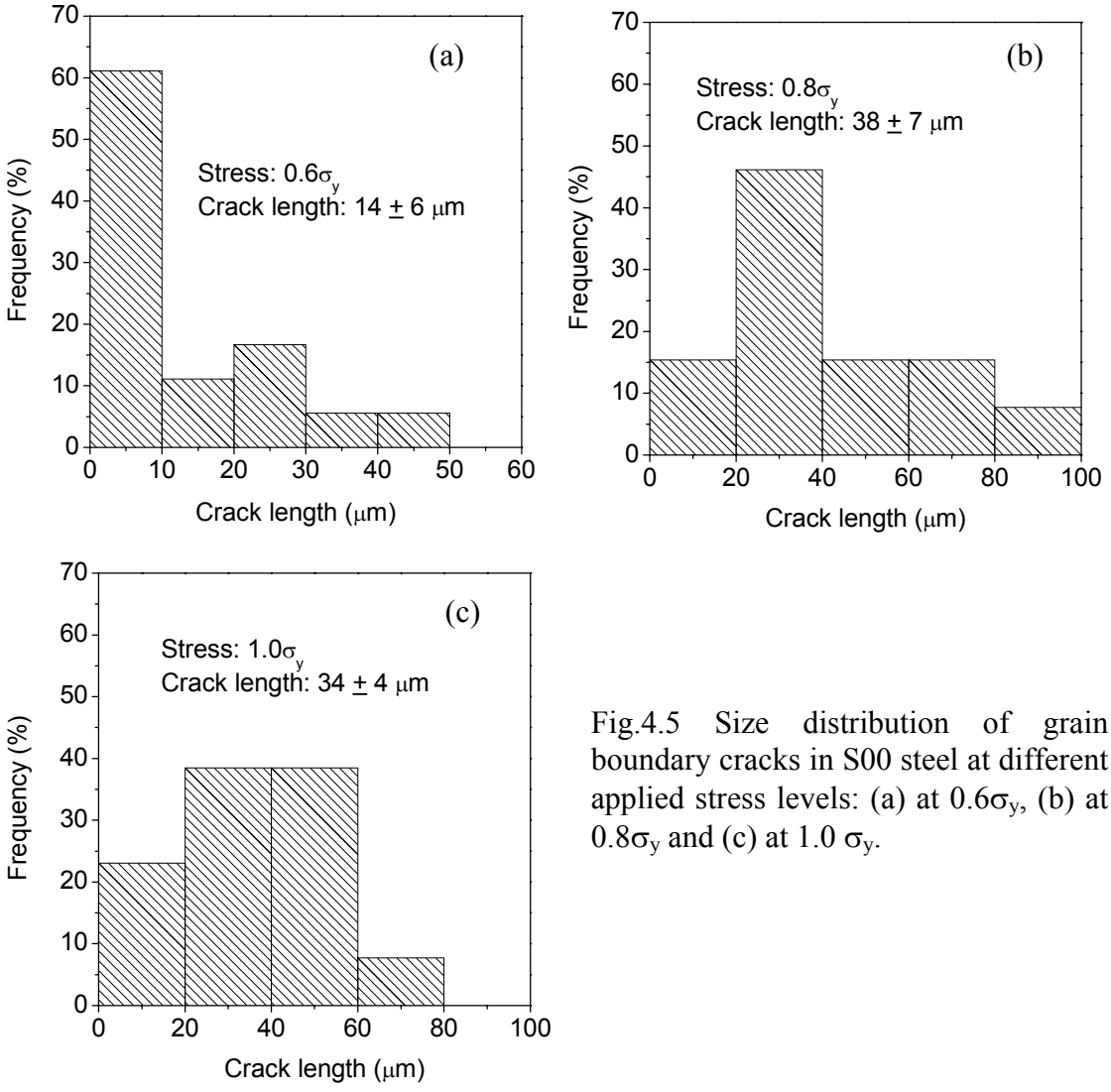

Fig.4.5 Size distribution of grain boundary cracks in S00 steel at different applied stress levels: (a) at $0.6\sigma_y$, (b) at $0.8\sigma_y$ and (c) at $1.0\ \sigma_y$.

The orientations of the observed grain boundary cracks with respect to loading axis were next analyzed and the recorded data are depicted in Fig.4.6 for the various estimations of crack initiation at different stress levels. It can be noted from this figure that the majority of cracks initiated at $0.6\sigma_y$ bear orientation between 30 to 60^o whereas at higher stress levels larger amount of cracks bear orientation greater than 60^o. The average angle of orientation of the grain boundary cracks with the loading axis for 0.6, 0.8 and $1.0\sigma_y$ fatigue stress levels were found to be 44±5 49±7 and 59±6^o respectively. These results indicate that crack initiation occurs primarily in the direction of maximum shear planes, which coincide with the available grain boundary orientations in the microstructure. The higher angle of crack orientation at higher stress levels can be attributed to the possible joining of more than one crack. In summary it can be inferred that the average size of the initiated cracks (at the lowest stress level of $0.6\sigma_y$) in S00 steel is 14±6 μm and their average orientation with the loading axis is approximately 45^o.

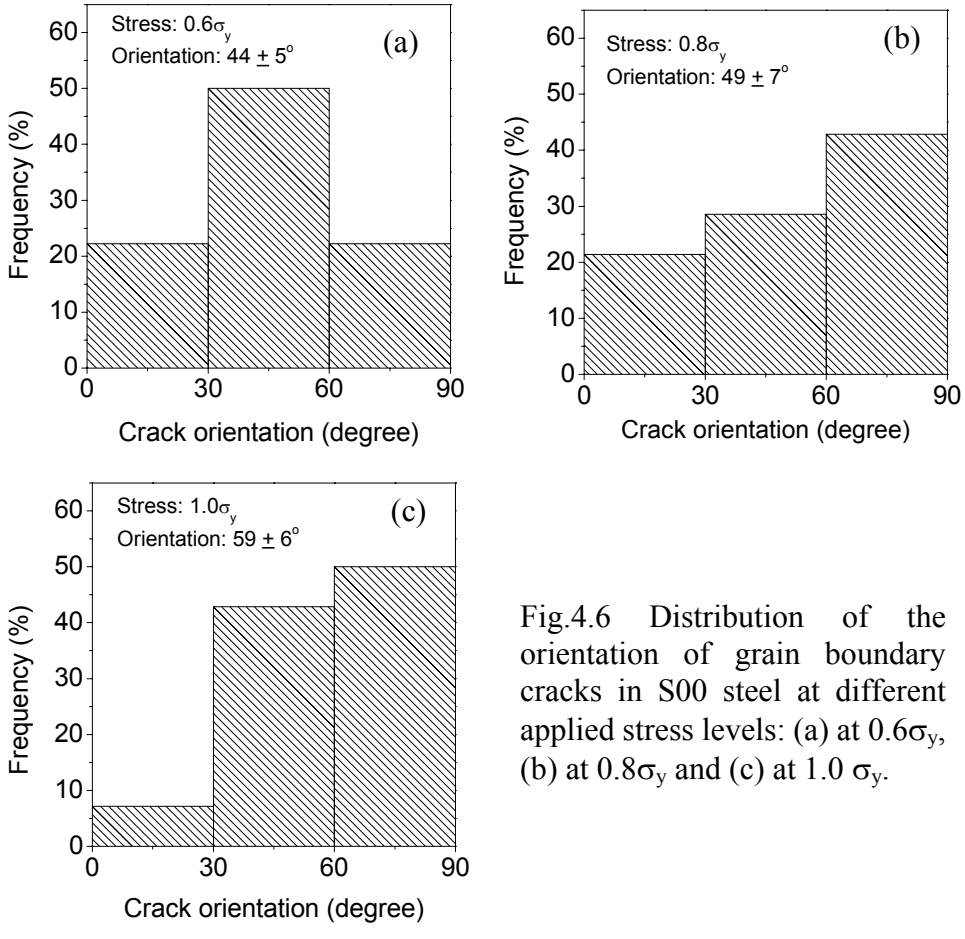

Fig.4.6 Distribution of the orientation of grain boundary cracks in S00 steel at different applied stress levels: (a) at $0.6\sigma_y$, (b) at $0.8\sigma_y$ and (c) at $1.0\ \sigma_y$.

4.3.1.2 Crack initiation in ferrite grain body

In comparison to the number of cracks encountered at grain boundaries, cracks observed inside grain body were a few in number. The average crack lengths at 0.6, 0.8 and 1.0σ_y stress levels were found to be 8±5 15±2 and 33±8 μm respectively. The average length of cracks in the grain body is thus found to be smaller than the average length of cracks at grain boundary. The average orientation of the grain body cracks with respect to the loading axis was found to be 60±16, 63±12 and 82±2^o for the applied stress levels of 0.6, 0.8 and 1.0 σ_y respectively. The higher angle of grain body crack orientation infers that crack initiation in grain body is dominated by normal stresses.

The salient features of the initiated cracks in S00 steel can be summarized as: (i) the average length of cracks initiated at grain boundaries is larger than the average length of cracks initiated inside grain body, (ii) the length of an initiated crack is small at lower applied stress, (iii) at lower stresses, orientation of grain boundary cracks is close to 45^o, whereas at higher stresses orientation of these cracks with respect to loading axis increases, and (iv) the orientation of the grain body cracks even at low stress level is greater than 45^o, and the average angle of orientation of these cracks increases like that of grain boundary cracks with increased fatigue stress.

4.3.1.3 Mechanism of crack initiation in S00 steel

The discussion in the previous sections indicates that crack initiation in S00 steel occurs both at the grain boundary and inside the grain body. The nature, size and orientation of these cracks a-priori indicate that the mechanisms of crack initiation at the grain boundary and in the grain body of S00 steel are different. The initiation of cracks in the grain body is commonly considered to occur within the slip bands in single phase material. The slip bands in BCC ferritic structure of S00 steel does not bear a systematic regular pattern like that observed in FCC materials [1,55]. The crack initiation in the investigated S00 steel was observed within the slip bands but the majority of the cracks were different than what is commonly encountered in polycrystalline metals and alloys. It is noted from Fig.4.3 that several irregular voids initiate inside the slip bands and appear to act as the origin of the grain body cracks. It is considered here that these irregular voids inside the slip bands either grow or coalesce to form cracks with low aspect ratio (length/width). As a consequence, these

cracks are not sharp and do not grow considerably. Typical slip bands in the ferritic structure are shown in Fig.4.3(a). The formation of voids and cracks with low aspect ratio marked with arrows are depicted in Fig.4.3(b) and Fig.4.3(c). The formation of voids and their gradual coalescence is illustrated in Fig.4.3(d). In addition, some cracks with sharp tips, which were occasionally observed and are not associated with any slip band are shown in Fig.4.3(e).

It has been discussed earlier that cracks at grain boundaries commonly bear an orientation approximately 45^o to the loading axis in S00 steel. Typical such cracks are described in Fig.4.2. The phenomena that maximum shear occurs at 45^o to the loading axis and that the grain boundary cracks are commonly oriented to this direction, assist to infer that grain boundary cracks are influenced by shear stresses. In Fig.4.2(b) and Fig.4.2(d) one can note the impingement of shear bands with grain boundaries, but these impingements do not significantly influence the formation of cracks at grain boundaries. It is obvious from these figures that several voids are formed at grain boundaries as shown by arrow marks in Fig.4.2(b) and Fig.4.2(d). Hence it is considered that separation of grain boundary at small segments, nucleation and growth of small voids at the grain boundary and subsequent joining of these voids lead to the formation of grain boundary cracks. The segmental separation or the void nucleation at grain boundaries may be assisted by impingement of slip lines on the grain boundaries. At low stress levels the probability of joining of the initiated cracks is low and hence one finds small average crack length at low stress levels. But at higher stress levels the neighbouring initiated cracks join with each other leading to the observed average higher crack length at 0.8 and $1.0\sigma_y$ fatigue stresses.

The mechanism of crack initiation in the grain body and at the grain boundary of single-phase materials has been discussed by several earlier investigators [2,50-52,209]. Essmann et. al. [2] have proposed crack initiation in the grain body of single phase fcc metals occurs inside slip bands. In their proposed micro-mechanism for crack initiation inside a grain body these investigators first considered that PSBs lead to protrusions (intrusions and extrusions) on specimen surface during cyclic loading. The interface between the PSB and the matrix of a material is a plane of discontinuity across which there are abrupt gradients in the density and distribution of dislocations. These interfaces were considered to serve as preferential sites for fatigue

crack nucleation. Long et. al. [209] have extended the same model for fatigue crack initiation along slip bands in bcc materials like metastable-β titanium alloy. The experimental evidence of crack initiation at the PSB-matrix-interface has been reported by Hunsche et. al. [50] and Ma et. al. [51,52] for copper. Hu et. al. [208] have suggested an alternate proposal that elastic-plastic incompatibility cause slip band crack initiation in titanium alloys. The elastic-plastic incompatibility causing crack nucleation in a grain body can be explained by the existence of an inhomogeneous stress or strain distribution inside the grain body. The inhomogeneity in the stress/strain distribution is more near the grain boundary [203,210] and this would preferably therefore cause the formation of grain body cracks near the grain boundary.

Based on the idea that grain boundaries act as obstacles to PSBs, Mughrabi [211] and Christ et. al. [212] have proposed a slip-induced intergranular crack model or PSB-grain boundary crack model. According to this model, an intergranular fatigue crack can be caused by the stress concentration due to dislocation pile-ups against a grain boundary. Zhang et. al. [207] have explained the mechanism for grain boundary crack nucleation by suggesting that slip band impingement against grain boundaries produces many micro-splits at the grain boundaries and these micro-splits join to form small cracks. Hu et. al. [208] have inferred that the elastic-plastic incompatibility is the reason for the formation of cracks at grain boundary. The mechanism of elastic-plastic incompatibility for grain boundary crack initiation has been further discussed in a subsequent section.

Several investigators [107,108,166,207,208] have examined crack initiation in different iron and iron-carbon alloys. Tanaka et. al. [166] has observed that under reversed bending and axial stresses (R = -1), cracks nucleate always at grain boundaries, but under alternating tension (R = 0), cracks nucleate along slip bands inside grains of a pure iron. Whereas, Tokaji et. al. [108] have found that the cracks generally occur in ferrite grains when the grain size is finer, but these are initiated at grain boundaries in coarse grained 0.11%C steel. Later, Zhang et. al. [207] have reported that the most favourable site for crack nucleation in 0.1%C steel is the grain boundary. Rios et. al. [107], on the other hand, have observed that crack initiation occurs only along the slip bands inside the ferrite phase of a 0.4% C steel. In bcc

single-phase titanium alloy, Hu et. al. [208] have found that fatigue cracks predominantly initiate either at grain boundaries or at slip bands in the vicinity of grain boundaries.

In the present investigation, fatigue crack initiation has been observed both at grain boundary and inside grain body in S00 steel as discussed in the previous sections. An attempt has been made to analyze the observed crack initiation behaviour in S00 steel in the perspective of the earlier studies in single-phase materials. The formation of slip band inside the grain body, slip band impingement at grain boundary and elastic-plastic incompatibility, as reported by earlier investigators, are also considered here as the main causes for crack initiation in S00 steel. The formation of irregular voids inside slip bands and their role on the formation of grain boundary cracks are considered here as some observations of interest. The observed splits at grain boundary of S00 steel due to slip band impingement is in agreement with earlier studies, but initiation and growth of small voids at the grain boundary and subsequent joining of these with other voids and splits appear specific for ductile bcc materials like S00 steel.

4.3.2 Crack initiation in S14 steel

An attempt to classify the recorded cracks in S14 steel indicated that their location in the microstructure is significantly governed by the presence of interfaces, inclusions and inhomogeneities. The observed small cracks can be broadly categorized into four types based on the position at which these are located in the microstructure. The classified different initiation sites are:

(a) ferrite-pearlite interface,

(b) ferrite-ferrite grain boundary,

(c) ferrite grain body, and

(d) inclusion-matrix interface.

4.3.2.1 Crack initiation at ferrite-pearlite interface

A random scanning of various locations (on the specimen surface) to reveal the different types of cracks during SEM examination indicated that the probability of finding ferrite-pearlite interface cracks is much higher (approximately 10 times) than

that of the other types of cracks. Some typical cracks at the ferrite-pearlite interface (FPI) are shown in Fig.4.7. The FPI cracks in this figure are indicated by arrows. The size and orientation of these cracks with respect to the loading axis were analyzed. Within the investigated stress ranges and for the applied number of cycles ($N=2.0x10^4$), the observed cracks were found to exhibit random sizes. This implies that when the stress range is changed from 0.6 to $1.0\sigma_y$ the crack-lengths do not vary significantly. But an increase in the maximum stress amplitude during fatigue cycling leads to higher number of crack nucleation sites. A set of additional experiments on S14 steel at $0.9\sigma_y$ at $N=1.0x10^4$ to $3.0x10^4$ also indicated that the number of crack nucleation sites increases with increasing N, with insignificant change in the average crack length within the domain of the present experimental conditions. All the observed cracks can be strictly termed as microstructurally small because these were not found to cross any ferrite grain boundary or ferrite-pearlite interface.

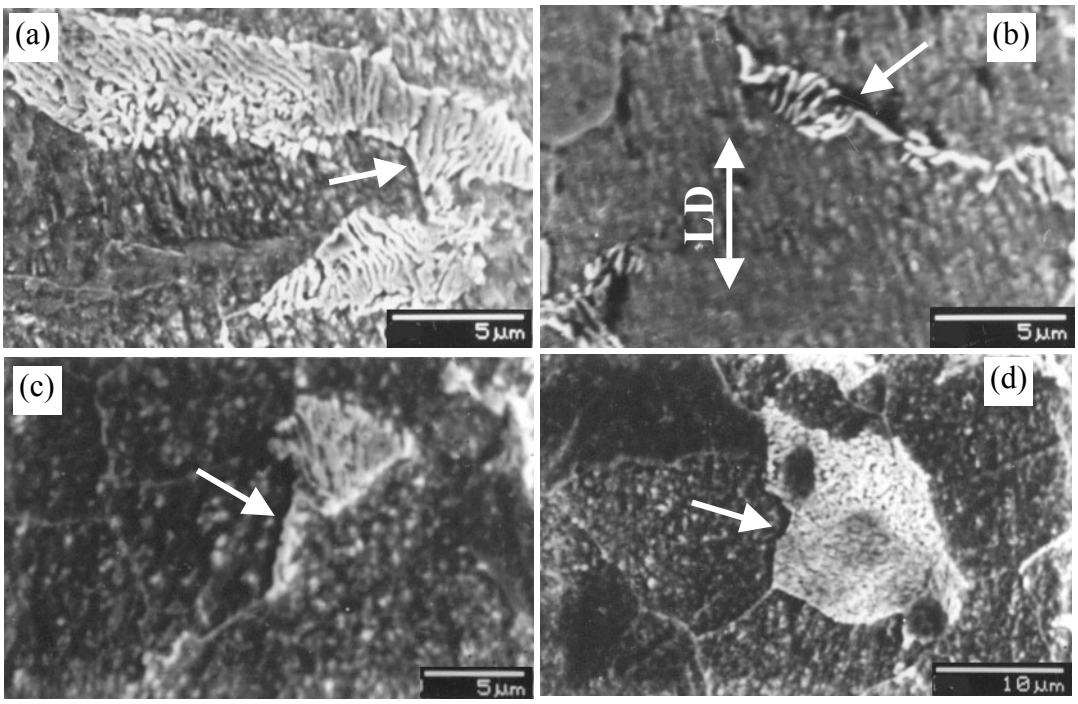

Fig.4.7 A set of typical ferrite-pearlite interface cracks in S14 steel. The loading direction (LD) common to all the figures is marked in (b).

The size distribution of the recorded ferrite-pearlite interface (FPI) cracks is shown in Fig.4.8. The average length and the associated standard error of the FPI cracks were estimated as 8.6±3.4 μm. It can be noted from Fig.4.8 that the highest

population of cracks occurs in the size range of 5-15 μm. An alternate analysis indicates that cracks generated in specimens having loading axis parallel to the banding in the microstructure are smaller compared to the crack lengths in specimens having loading axis perpendicular to the banding direction. This aspect has been illustrated using two inserts showing size distribution for these cracks in Fig.4.8. The mean sizes of cracks in specimens having banding parallel and perpendicular to loading direction are 7.0±1.9 μm and 11.0±3.8 μm respectively. Hence, it can be concluded that length of cracks in specimens having banding direction perpendicular to the loading axis is higher compared to that in specimens having banding direction parallel to loading axis.

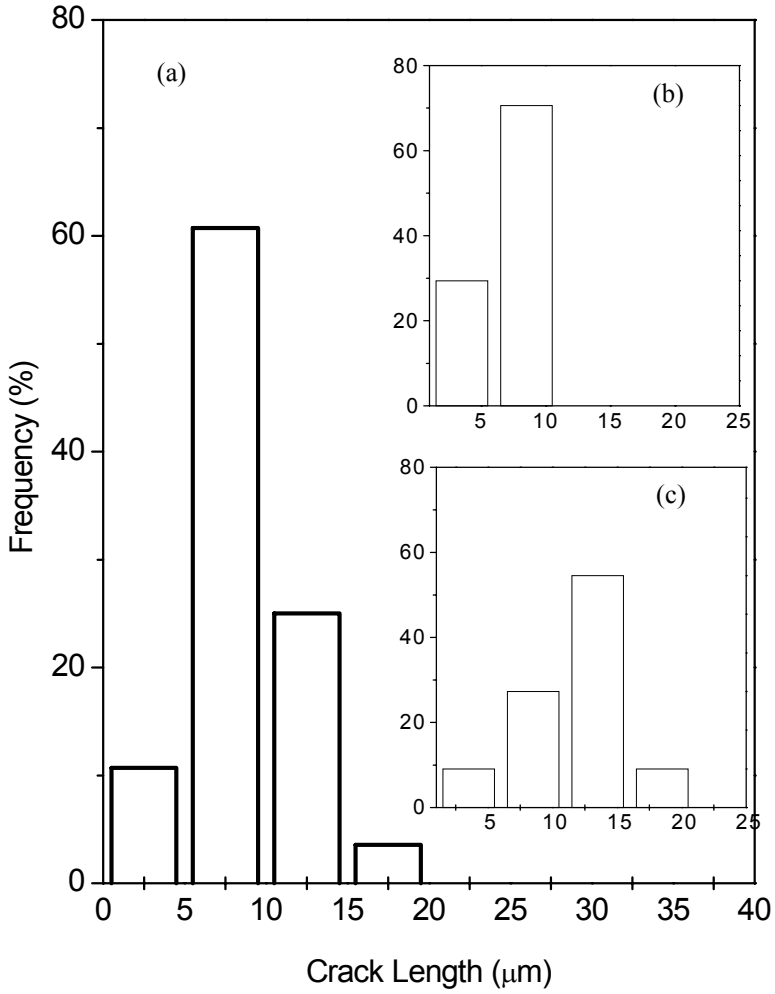

Fig.4.8 Size distribution of ferrite-pearlite cracks in S14 steel: (a) all ferrite-pearlite interface cracks, (b) cracks in samples having banding parallel to loading direction and (c) cracks in samples having banding perpendicular to loading direction.

An analysis of the orientation of the cracks with respect to loading direction in both types of specimens (i.e. parallel and perpendicular banding with respect to loading axis) indicates that these can widely vary between 0 to 90^{o}. This observation is not in agreement with the results reported by Liu et.al. [213] and Zhang et.al. [207], who have indicated that such angles primarily lie between 45 to 90^{o}. Zhang et. al. [207] have reported observations for a low-carbon steel (without having any banding), whereas Liu et. al. [213] have studied on polycrystalline copper. It is considered here that the observed difference in the nature of the crack orientation arises from the banded microstructure. In order to probe this phenomenon in depth, the distribution of the orientation of the cracks with respect to loading axis for both types specimens were examined in Fig.4.9.

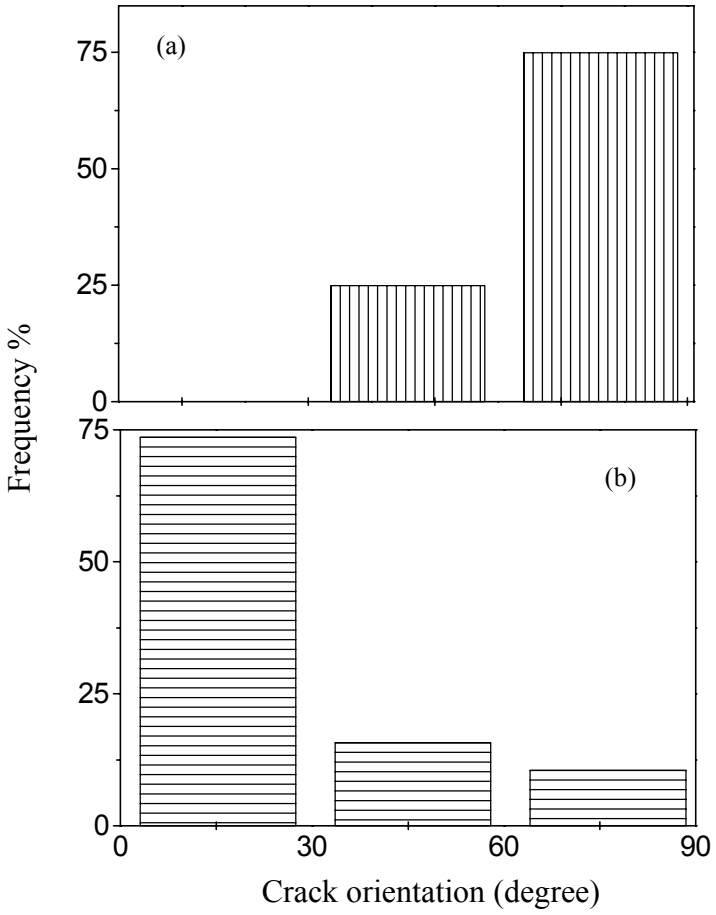

Fig.4.9 Distribution of the orientation of ferrite-pearlite interface cracks in S14 steel. (a) specimens exhibiting banding perpendicular to loading axis and (b) specimens exhibiting banding parallel to loading axis. The orientation of a crack has been estimated with respect to the loading axis.

The results in this figure reveal that (i) when banding is parallel to loading direction, cracks are mostly oriented between 0 to 45^o and (ii) when banding is perpendicular to loading axis cracks are mostly oriented between 45 to 90^o. The latter observation is in agreement with some earlier reported results [207,213]. It can thus be inferred that (a) FPI cracks are relatively smaller in size and their orientation with respect to loading direction remains between 0 to 45^o when banding is parallel to loading direction, and (b) these cracks are larger in size and their orientation with respect to loading direction remains in the range of 45 to 90^o when banding is perpendicular to loading axis. Hence it can be concluded that microstructural banding significantly influences the size and orientation of small cracks in the investigated S14 steel at the stage of their nucleation. This is the first information of its kind.

4.3.2.2 Crack initiation at ferrite-ferrite grain boundary

The preference for nucleation of fatigue cracks at ferrite-ferrite grain boundaries was found to be next to that at FPI. Some typical ferrite-ferrite grain boundary (FFGB) cracks are shown in Fig.4.10. The analyses of FFGB cracks were made in a similar manner to that of FPI cracks. The size distribution of these cracks is shown in Fig.4.11, whereas the distribution of the orientation of the cracks with respect to loading axis for both types of specimens are shown in Fig.4.12. The results in Fig. 4.12(a) and in Fig.4.12(b) correspond to observations made on specimens having banding direction perpendicular and parallel to the loading axis respectively. An analysis of the size and orientation of these cracks infer:

(i) The mean size of the estimated FFGB cracks is 8.3±4.0 μm.

(ii) The average sizes of the cracks in specimens having banding parallel and perpendicular to the loading direction are 6.0±2.2 and 10.5±4.1 μm respectively.

(iii) When banding is parallel to the loading axis, these cracks are mostly oriented with angles of 0 to 45^o to the loading axis.

(iv) When banding is perpendicular to the loading axis the FFGB cracks subtend angles between 45 to 90^o with the loading axis.

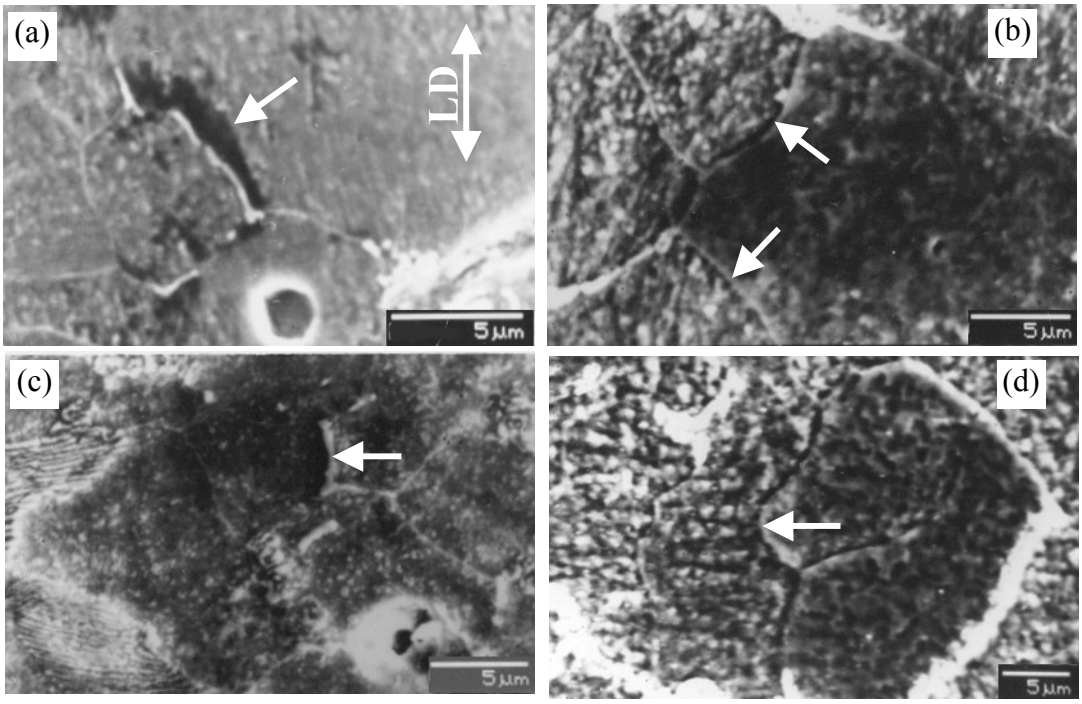

Fig.4.10 A set of typical ferrite-ferrite grain boundary cracks in S14 steel. The loading direction (LD) common to all the figures is marked in (a).

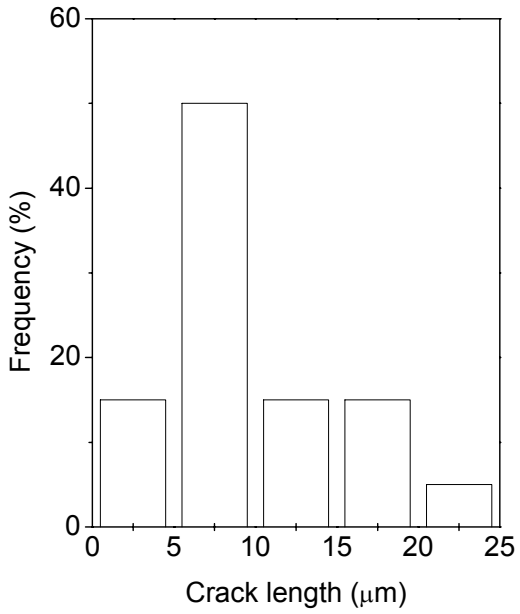

Fig.4.11 Size distribution of the ferrite-ferrite grain boundary cracks in S14 steel.

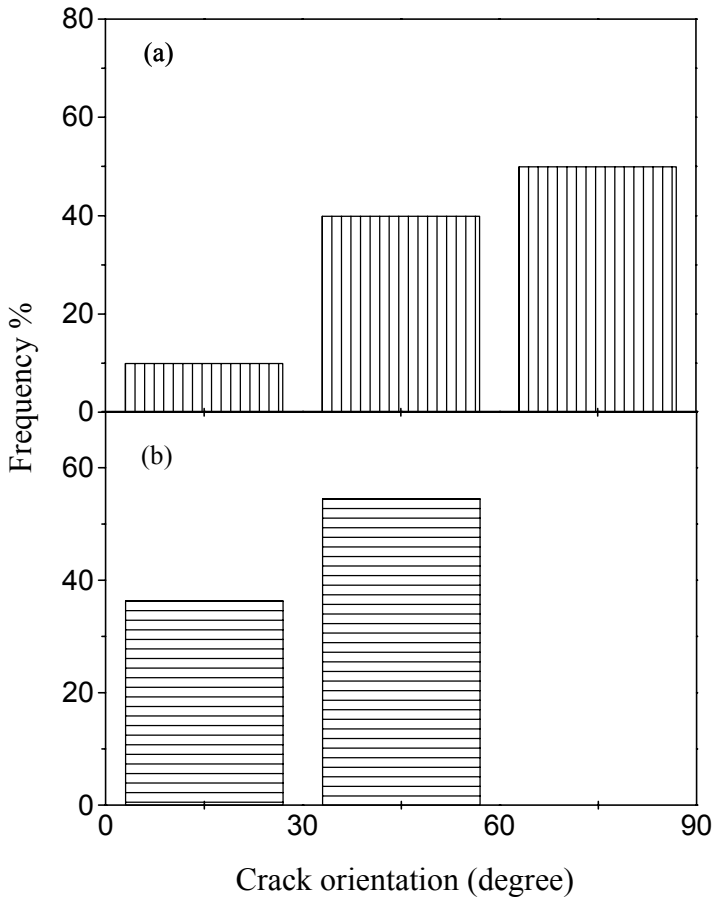

Fig.4.12 Distribution of the orientation of ferrite-ferrite grain boundary cracks in S14 steel. (a) specimens exhibiting banding perpendicular to loading axis and (b) specimens exhibiting banding parallel to loading axis. The orientation of a crack has been estimated with respect to the loading axis.

The above inferences lead to the conclusion that the effect of microstructural banding on the nature and orientation of small cracks initiated at FFGB and at FPI is similar. The observations related to FPI and FFGB cracks can thus be generalized with the contentions that (a) interface crack sizes are smaller for specimens having banding parallel to the loading axis compared to that for specimens having banding perpendicular to the loading axis, and (b) these cracks are associated with angles between 0 and 45^{o} for the former type of specimen, unlike that between 45 and 90^{o} for specimens having banding direction perpendicular to the loading axis. In general, the average length of the FFGB cracks are smaller than those initiated at FPI.

4.3.2.3 Crack initiation in ferrite grain body

In the investigated S14 steel, several cracks were also found to be nucleated in the ferrite grain body, but their number was considerably less than those initiated at FPI and FFGB. Figure 4.13 shows some typical small cracks initiated in the ferrite

grain body. The distribution of the size and the orientation of these cracks are shown in Fig.4.14 and Fig.4.15 respectively. The average crack lengths (in ferrite grain body) for both types of loading were found to be 5.8±2.5 μm, whereas the variation of the average orientation of the cracks owing to the different types of loading was found to be marginal; for the banding direction parallel and perpendicular to the loading axis, these were found to be 48.6±27.7 and 58.8±24.5^{o} respectively. Interestingly the influence of the variation of the loading axis with respect to the direction of banding was found to be negligible on the nature of the ferrite grain body cracks.

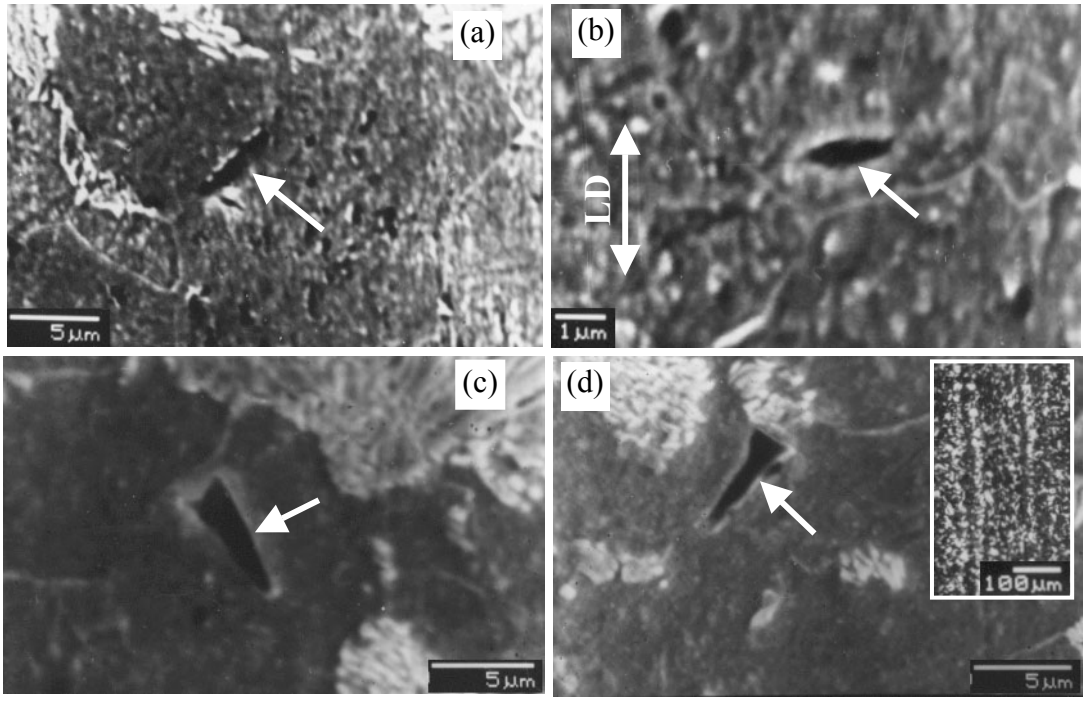

Fig.4.13 Some typical ferrite grain body cracks in S14 steel. The microstructural banding is shown as an insert to indicate its orientation with respect to loading direction (shown as a double sided arrow). The loading direction (LD) common to all the figures is marked in (c).

Some salient features of the grain body cracks are: (a) these are wider but smaller in length compared to the cracks nucleated at ferrite-ferrite or ferrite-pearlite interfaces, (b) these exhibit some specific shapes like elliptical or nail-type, and (c) one end of these cracks was almost always found near the ferrite-ferrite grain boundary or near the ferrite-pearlite interface.

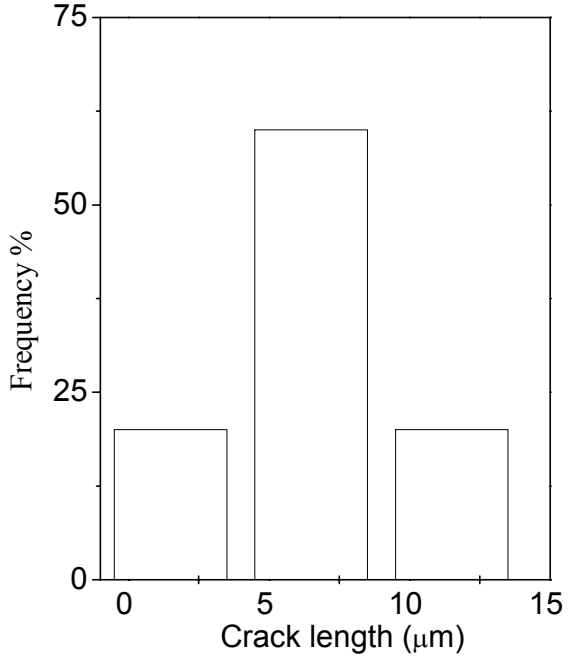

Fig.4.14 Size distribution of the ferrite grain body cracks in S14 steel.

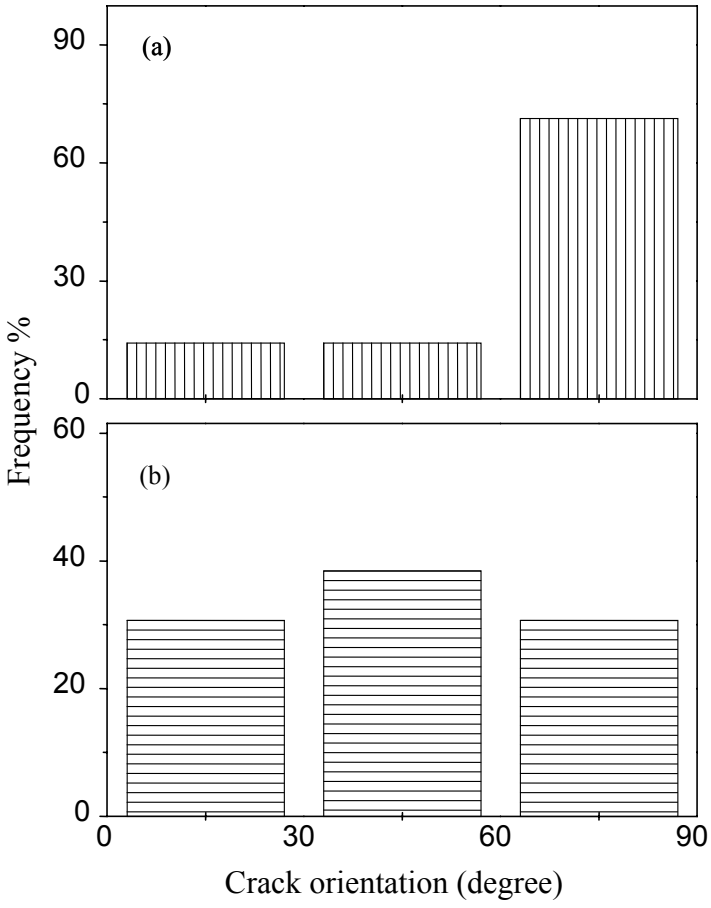

Fig.4.15 Distribution of the orientation of ferrite grain body cracks in S14 steel. (a) specimens exhibiting banding perpendicular to loading axis and (b) specimens exhibiting banding parallel to loading axis. The orientation of a crack has been estimated with respect to the loading axis.

4.3.2.4 Crack initiation at inclusions

It is considered in general that inclusions are the most preferred sites for crack nucleation. But the number of inclusion-associated cracks (IAC) was found to be negligible compared to the FPI, FFGB, and grain body cracks. As an example, in each sample approximately 40 mm^2 area was randomly scanned to locate IAC at magnifications of 2000-5000X. Such a search in 12 samples could lead to the detection of only 5 inclusion-associated cracks. This phenomenon is in agreement with the very low inclusion content of the investigated nuclear grade steel. Two typical inclusion-associated cracks are shown in Fig.4.16 and details of the size and orientation of IAC are compiled in Table 4.3. It is difficult to comment about the distribution of size and orientation of this type of cracks from these few observations. But it was found that these cracks always initiate along the inclusion length irrespective of the specific angle between the loading axis and the banding direction. Crack initiation at inclusions generally occurs by the separation of the relatively weak interface between the matrix and the inclusion. This also causes formation of this type of cracks along the longer dimension of inclusions.

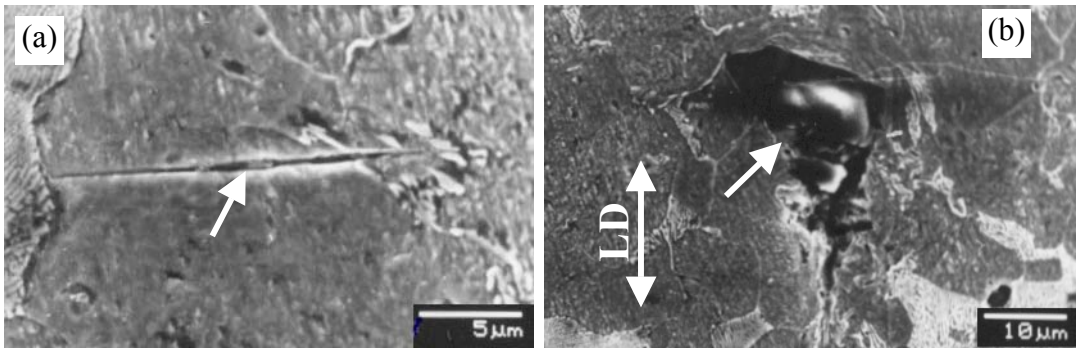

Fig.4.16 Two typical cracks nucleated at inclusions in S14 steel: (a) crack propagation perpendicular to loading direction and (b) crack propagation along the loading direction. The loading direction (LD) is common to both the figures.

Table 4.3 Details of the size and the orientation of the inclusion associated cracks in S14 steel.

Sl No	Applied stress ($x\sigma_y$)	Crack Length (μm)	Orientation* (degree)
1.	0.9	36	30
2.	0.9	18.8	90
3.	0.8	5.8	55
4.	0.8	3.6	44
5.	0.8	11.7	56

*with respect to loading direction σ_y = yield strength

4.3.2.5 On the crack initiation sites in low carbon steels

The examination of crack initiation sites in the S14 steel with ferrite-pearlite microstructure indicates the order of preference for the site of crack initiation as: ferrite-pearlite interface, ferrite-ferrite grain boundary and ferrite grain body excluding the insignificant occurrence of crack initiation at inclusion-matrix interfaces. These observations are compared with a few similar examinations by earlier investigators. Tokaji et. al. [108,117] have reported that crack initiation and propagation in low carbon steel occur through grain boundaries. However, these investigators have not distinguished between crack initiation sites at ferrite-pearlite interface and ferrite-ferrite grain boundary. Zhang et. al. [207] have observed during low cycle impact loading of a 0.1% C steel that the most favourable site for crack nucleation is grain boundary. So the present observations of preferred crack initiation at ferrite-pearlite interfaces and at grain boundaries, are in agreement with the above observations. Tokaji et. al. [108] have found that cracks usually occur in ferrite grains when the grain size is finer, but these get initiated at grain boundaries in coarse-grained materials. These inferences have been derived by Tokaji et. al. [108] from experimental results on a steel heat-treated to exhibit ferrite grain size of 24 μm (fine) and 84 μm (coarse). In the present investigation ferrite grain size is found to be only 12 μm and hence following the report of Tokaji et. al., one would expect preferred crack nucleation in grain body in contrast to what has been observed. Rios et.al. [107], on other hand, have observed that crack initiation occurs only along the slip bands inside the ferrite phase of a 0.4% C steel.

Based on the earlier and the present observations of crack initiation sites in carbon steels one can infer that preferable crack initiation site in this material can be either grain body or grain boundary/interface. But it is not clear which factors significantly govern the preference for a specific crack initiation site. It is known from some earlier studies [202,203] that the mechanical state of the ferrite phase and the pearlite colony in ferrite-pearlite structures vary with the carbon content of a steel and such variation can also be expected to get influenced by the grain size of the material. It is inferred here that the preference for grain body or grain boundary/interface cracks is governed by the mechanical state of the ferrite phase and that of the pearlite colony in a steel. It may also be expected that the formation of the slip bands in the ferrite

phase should get dictated by this aspect. In this investigation slip bands have not been observed even when the fatigue samples were examined at considerably high magnifications; for example one can examine the photograph of the ferrite grain body cracks in Fig.4.13. This is opposite to the view rendered by Rios et. al. (Fig.3 of ref. 107) and Zhang et. al. (Fig.4 of ref. 207). But observations of grain boundary/interface crack formation without being preceded by slip bands are found reported in the literature [214,215].

4.3.2.6 On the mechanism of crack initiation in the investigated S14 steel

Slip bands impingement against grain boundary or interfaces has been suggested by Zhang et. al. [207] as the primary cause for the formation of interface cracks. Such impingements usually result in several micro-splits leading to the formation of small cracks. In the current study evidence for slip line impingement causing micro-splits could not be gathered. An alternate possibility for the nucleation of the interface cracks could be due to considerable incompatibility between the elastic and the plastic deformation in the vicinity of an interface [208]. It is considered here that such incompatibility in deformation is also capable of yielding split type cracks with their subsequent coalescence to form small cracks. In Fig.4.7(b) one can observe a few split-cracks around the ferrite-pearlite interface, but no distinct slip lines. Hence it is inferred that the mechanism of formation of the small cracks at ferrite-pearlite interface in the investigated steel is predominantly governed by incompatible elastic-plastic deformation around the interfaces.

Using optical interferometric measurements of slip step heights at grain facets in fatigued copper, Kim and Laird [55] noted that fatigue cracks may nucleate at grain boundaries if: (i) the grain boundaries are separated by highly misoriented grains, (ii) the active slip system of at least one of the grains is directed at the intersection of the boundary with the specimen surface, and (iii) the traces of the high angle grain boundaries in the free surface make a large angle (30-90^{o}) with the tensile stress axis. In general, grain boundary cracking may arise from one of the two mechanisms during cyclic loading: (a) at low to intermediate plastic strain amplitude, the impingement of persistent slip bands (PSBs) at grain boundaries causes cracking [56,216], and (b) at high plastic strain amplitudes, grain boundary cracking occurs as a consequence of surface steps formed at the boundary [55]. In this study

impingement of persistent slip bands at FFGBs has not been recorded and hence the nucleation of FFGB cracks can be attributed to the possible formation of surface steps at grain boundaries. The latter can be considered to originate from elastic-plastic incompatibility strains existing at FFGBs associated with wide orientation difference between the adjacent grains.

The grain body cracks are popularly considered to occur at persistent slip bands [107,207]. Since slip bands could not be detected in the ferrite phase of the investigated steel, the formation of the grain body cracks can be explained by the existence of an inhomogeneous stress or strain distribution inside ferrite. Such inhomogeneity in the stress/strain distribution [202,203] is known to be intense near the grain boundary and this is believed to be the cause for the formation of these cracks. That one end of these cracks remains close to the interface of ferrite-pearlite or ferrite-ferrite grain boundary appear to support this hypothesis. The inhomogeneity in the stress/strain distribution has been reported by Ankem and Margolin [210] and Ray and Mondal [203] using experimental results on two-phase microstructures.

In ferrite-pearlite microstructures, the suggested major mechanisms for crack initiation are due to (a) slip bands, (b) cracking due to surface step formation and (c) incompatibility of the stress/strain along interfaces. The crack initiation inside slip bands and that due to interaction between slip bands and grain boundary/phase interface have been cited by a few of investigators [107,207]. The initiation of a crack by these mechanisms depends on the deformation behaviour of the phases present in a material and the flexibility of the slip band formation in such phases. In the investigated steel and under the employed experimental conditions, slip bands have not been observed, and naturally any operative mechanism involving slip bands is ruled out.

In order to understand crack initiation owing to elastic or elastic-plastic incompatibility near grain boundaries and at ferrite-pearlite interfaces, the local stress/strain distribution should be examined in depth. In elastically anisotropic phases like ferrite or iron-carbide, incompatibility in stress would develop across grain boundaries or phase interfaces, if the strains across these are considered continuous. The variation in local stresses can be considerable in iron since its anisotropic ratio is 2.512 [13]**;** this implies that shear modulus can vary by this factor in this metal

depending on the direction of shear elements within the lattice. The shear moduli of iron and that of iron-carbide are in the ratio 82:70 [13,217] and hence the elastic incompatibility at the iron-iron carbide or at the ferrite–pearlite interface would be considerable and would be of the order 2.94. Considering a bi-crystal of ferrite-ferrite or ferrite pearlite colony (Fig.4.17) under a uniform tensile stress, one of the compatible elastic or the plastic strain conditions can be written as

$$\Delta \in_{xx}^{e} = \in_{xx}^{e,1} - \in_{xx}^{e,2} = 0 \qquad ...(1)$$

$$\Delta \in_{xx}^{pl} = \in_{xx}^{pl,1} - \in_{xx}^{pl,2} = 0 \qquad \ldots(2)$$

where $\Delta \in_{xx}^{e}$ is change in elastic strain along x-x, $\in_{xx}^{e,1}$ is elastic strain in phase-1 along x-x, $\in_{xx}^{e,2}$ is elastic strain in phase-2 along x-x, $\Delta \in_{xx}^{pl}$ is change in plastic strain along x-x, $\in_{xx}^{pl,1}$ is plastic strain in Phase-1 along x-x, and $\in_{xx}^{pl,2}$ is plastic strain in Phase-2 along x-x.

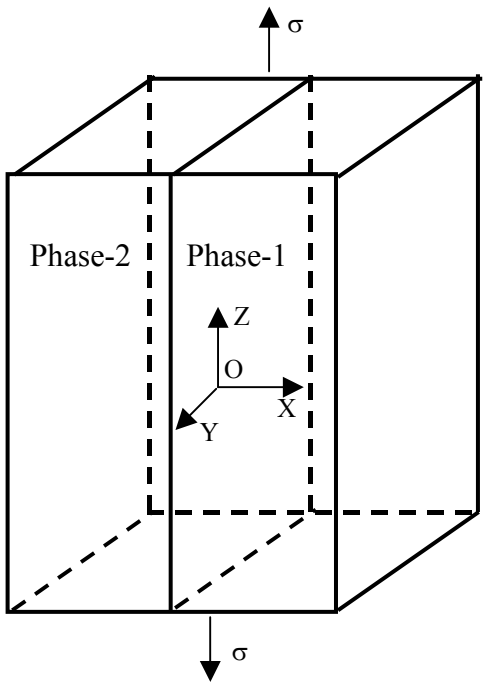

Fig.4.17 Geometry of a planar interface between two-phase domains, the interface being parallel to the loading axis.

Usually $\in_{xx}^{e,1} / \in_{xx}^{pl,1}$ is different from $\in_{xx}^{e,2} / \in_{xx}^{pl,2}$ in the vicinity of grain boundary or at the interface between ferrite phase and pearlite colony. This physical condition leads to additional internal stresses, termed here as "incompatible internal stress" to fulfill the continuity requirement. A mismatch between the incompatible internal stresses or that in strain components along a grain boundary or an interface leads to the cracking of ferrite-ferrite grain boundary or the ferrite-pearlite interface. The FPI cracks in Fig.4.7 and FFGB cracks in Fig.4.10 are considered to arise due to this reason. The observation of higher number of FPI cracks and their larger lengths compared to those of FFGB cracks is thus attributed to the fact that $\Delta \in_{xx}^{e} / \Delta \in_{xx}^{pl}$ is higher in magnitude for FPI cracks than that of FFGB cracks. The higher possible variation of shear modulus in the ferrite-pearlite interface than that along ferrite-ferrite grain boundaries supports this contention. In addition incompatible internal stresses are expected to be different when the loading axis in a specimen is parallel to the banding direction from that of the state when the loading axis is perpendicular to the banding direction. Thus the nature of the crack initiation under these two conditions would also be different as illustrated in the results given in Fig.4.9 and Fig.4.12.

A comparison of the crack initiation behaviour in S00 and S14 steels implies a comparison of this phenomenon in single and multiphase materials. The preferential sites for crack initiation in S14 steel are ferrite-pearlite interfaces and ferrite-ferrite grain boundaries, while only grain boundaries are the preferential sites for crack initiation in S00 steel. However, the highest preferential site for nucleation of fatigue cracks in multiphase materials like S14 steel is the interface between ferrite and pearlite. Initiation of irregular voids inside grains and at grain boundaries in S00 steel are its typical characteristics unlike the events associated with the fatigue crack initiation in S14 steel. Also the average sizes of cracks in S00 steel are larger compared to that in S14 steel. The orientation of the grain boundary cracks in the former is closer to 45^{o} unlike that in the latter. The observed influence of banding on the crack initiation behaviour in S14 steel indicates that in multiphase materials, the nature of distribution of second phase influences the size and orientation of the cracks initiated by cyclic loading.

4.4 Conclusions

The results of the present investigation on crack initiation and their related discussion lead to the following major conclusions:

- Cracks nucleate at grain boundary and inside ferrite grain body in S00 steel, whereas in S14 steel cracks can nucleate at ferrite-pearlite interface, ferrite-ferrite grain boundary, inside ferrite grain body and at inclusion.
- In the investigated steels ferrite-pearlite interfaces and ferrite-ferrite grain boundaries are found to be significantly preferred crack initiation sites in comparison to ferrite grain body.
- The lengths of the initiated cracks at ferrite-pearlite interfaces or at grain boundaries are usually larger in size compared to those at other locations.
- The formation of slip band inside the grain body, slip band impingement at grain boundary and elastic-plastic incompatibility synergistically influence to cause crack initiation in S00 steel.
- Elastic-plastic incompatibility is attributed to be the primary mechanism for crack initiation at the ferrite-pearlite interfaces and at the ferrite grain boundaries in the investigated S14 steel.
- At lower stresses, orientation of grain boundary cracks in S00 steel is close to 45^{o} whereas at higher stresses orientation of these cracks with respect to loading axis increases.
- The formation of irregular voids inside slip bands, initiation and growth of small voids at the grain boundary and subsequent joining of these with other voids and splits appear specific for ductile bcc materials like S00 steel.
- The direction of banding in a ferrite-pearlite microstructure with respect to loading axis exerts prominent influence on the size and orientation of the initiated cracks in S14 steel.

Chapter 5

Studies on short fatigue crack growth behaviour

5.1 Introduction

The second stage in fatigue damage is short crack growth. There has been an upsurge of interest to understand the behaviour of short cracks as it is well recognized by now that fatigue lifetime of several structural components is considerably influenced by the rate of growth of small cracks. The 'fail safe' and the 'safe life' design [1] of structural components are based on Paris law constants [9] estimated from crack growth rate *vs*. stress intensity factor range data and the fatigue threshold (ΔK_{th}) respectively. The crack configurations considered in the determination of fatigue crack growth data using the standard procedure described in ASTM E647 [8] do not always simulate those existing in engineering structures; because initiation of failure generally occurs by propagation of sub critical cracks with sizes ranging from several micrometers to a few hundred micrometers. The growth of these cracks does not follow the conventional linear elastic fracture mechanics (LEFM) approach; the cracks grow at stress intensity factor ranges lower than ΔK_{th}, exhibit fluctuating crack growth rates and are known as small or short cracks. The growth of these cracks below ΔK_{th} perturbs the basis of safe life design philosophy whereas the fatigue life time spent during the short crack growth regime may be dominating at times to bring in large deviations in the estimated results of fatigue life for fail safe design. This has led to several in-depth examinations of short cracks in different materials [44].

Most of the earlier studies are primarily related to the understanding of mechanics, mechanisms and microstructural effects on short crack growth behaviour in structural materials and these are rarely directed to explore the possibility of determining the "near long-crack fatigue threshold" (NLFTH) through short crack studies. In addition, attempts to carefully understand the microstructural features which result in either short crack or long crack thresholds are lacking. One of the primary purposes of this study is to generate small crack growth rate data in a S00, S25 and S47 steels, in order to estimate the NLFTH and to reveal the dominating

microstructural feature that leads to this phenomenon. The primary aim is preceded by the development of a new specimen configuration for which short crack growth data can be generated conveniently with the help of a rotating bending machine.

The search for a possible quantitative relation between the lengths of crack paths and their associated microstructure has not been made so far. Studies of this nature can bring forth vital information about the weak-links in a microstructure through which a crack prefers to pass through or the affinity of a crack to travel through any specific phase in a microstructure. This aspect has been examined for the first time in this investigation. In brief the main objectives of this investigation are: (a) to develop a new specimen configuration to study short fatigue crack growth in structural materials using a rotating bending machine, (b) to determine the crack growth threshold value of a few steels using short crack growth studies and (c) to examine the effect of constituents of a microstructure on the length of fatigue cracks. The steels selected for this part of the investigation are S00, S25 and S47.

5.2 Experimental procedure

The experiments consisted of fabrication of newly designed specimens and their fatigue testing. The pertinent details of these are enumerated in this section.

5.2.1 Specimen configuration

Rotating bending fatigue specimens of 12mm diameter and 120mm length with a reduced section of 11mm×5mm at a distance of 40mm from one edge of the specimen were machined from the as received rods. The surfaces of the reduced sections of the specimens were ground and polished first using emery papers and finally with 0.25μm diamond paste. Typical configuration of a specimen is shown in Fig.5.1. The purpose of this design is to continuously monitor a crack path together with its associated microstructure during a fatigue testing.

5.2.2 Short crack growth testing

The fatigue tests were performed on a 560N.m.s^{-1}(0.75hp) rotating bending machine operating at a frequency of 50Hz. These tests were carried out with an initial imposed load of 133.5N (30 lb) for S25 steel till crack initiation could be noticed by repeated interruption of a test followed by examination of the specimen under a microscope. After crack initiation, the growth studies were conducted at a reduced

load of 89N (20 lb). The initial imposed load for crack initiation in S00 and S47 steels were 84.5N (19 lb) and 146.8N (33 lb) respectively. The crack growth studies in S00 steel was carried out at a load of 44.5N (10 lb) whereas that in S47 steel was done at a load of 111.2N (25 lb). During the stage of crack growth, the tests were interrupted at each 15000 cycles or multiples of it, for recording the crack path. The crack paths were recorded by an optical microscope and their lengths were measured using an image analyzer. The fatigue testing was carried out until each crack reached a minimum length of 1200μm. After the fatigue testing the surface of a specimen was etched using 2%Nital and the entire traverse of the crack path together with its associated microstructure was recorded in several frames by using both optical and scanning electron microscopy.

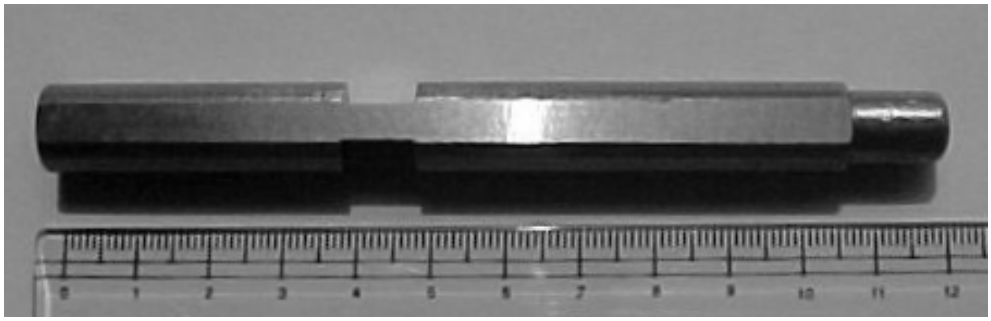

(a)

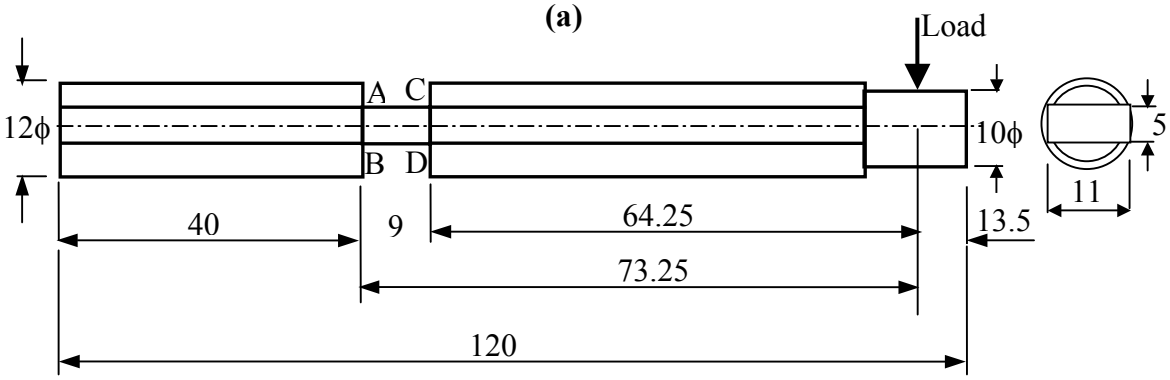

(b) All dimensions are in mm

Fig.5.1 Configuration of the specimens used for short crack growth testing (a) a typical fabricated specimen and (b) schematic diagram.

5.3 Results and discussion

The obtained results have been examined (i) to estimate the stress required to initiate small cracks in the developed specimens of the selected steels, (ii) to understand the nature of variation of crack length with number of cycles, (iii) to

reveal the influence of crack length on the crack growth rate (d*a*/dN), (iv) to determine the stress intensity factor ranges (ΔK) at which minima in d*a*/dN are encountered during crack growth in different specimens and (v) the influence of microstructure on the crack path. The results and their pertinent discussion to achieve these objectives are presented in different sub-sections. Incidentally these experiments were first carried out on S25 steel on a large number of specimens and then the suitability of the designed specimens configuration to examine short crack behaviour in S00 and S47 steels was assessed on some limited number of specimens. The obtained results and their pertinent discussion for S25 steel are thus first presented in a detailed manner in section 5.3.1. The contents of the sections 5.3.2 and 5.3.3 are concerned with the achieved results on S00 and S47 steels respectively.

5.3.1 Short fatigue crack growth behaviour in S25 steel

The initiation and growth of short cracks in S25 steel are discussed in this sub-section. For the sake of brevity, the results are often stated without indicting the name of the steel.

5.3.1.1 Crack initiation

The study of short crack growth requires an initial crack length of very small magnitude. In order to obtain such cracks, fatigue tests were carried out initially at loads of 89N (20 lb) and at 112N (25 lb). The maximum (positive) and the minimum (negative) principal stress in bending occur at the point A (or B) when it is on the top and the bottom surface respectively of the specimen during its rotation. The applied loads of 89N and 112N correspond to maximum principal stress magnitudes of 142 and 178MPa respectively in bending at locations A or B of the specimen (Fig.5.1), considering these points to be unaffected by the non-uniform stress distribution at the notch root. These stress magnitudes are sufficiently below the theoretically estimated endurance limit (σ_e=271MPa) of the steel obtained by using an approximate relationship, $\sigma_e = 0.5\sigma_t$ [1,12,13,218], where σ_t is the tensile strength of the material. During these tests, the fatigue cycling was interrupted at intervals of 10-15 kilocycles for locating any possible initiation of crack. At these stress amplitudes even almost 5×10^6 cycles did not induce crack initiation in the specimens. A load of 133.5N (30 lb) was found to induce short cracks in the fabricated specimens, and at this load the number of cycles for crack initiation was found to be approximately 2.7×10^5. The

applied stress for crack initiation at this load was estimated to be in the range of 187-212MPa depending on the position of the crack in the different specimens. These stress values for crack initiation (σ_{ini}) can be expressed as $\sigma_{ini}=(0.36 \pm 0.02)\ \sigma_t$. The micro-notches (Fig.5.2), which led to short crack initiation, were considered as semi elliptical edge flaws. The stress intensity factor for crack initiation, K_{ini} was calculated by using the expression for a semi elliptical edge flaw as [219]:

$$K_{ini} = 1.12(3\sigma)\sqrt{\frac{\pi a}{Q}}\ \sqrt{\sec\frac{\pi a}{2b}} \qquad \ldots(5.1)$$

where,

a= depth of elliptical flaw

c= half width of elliptical flaw

b= plate thickness, 5mm

surface flaw correction at point A in Fig.5.1=1.12

stress concentration effect at point A in Fig.5.1=3

Q=elliptical flaw correction = f (a/2c) obtained from standard graphs [13]

$\sqrt{\sec\frac{\pi a}{2b}}$ = finite width correction accounting for relatively large a/b ratio.

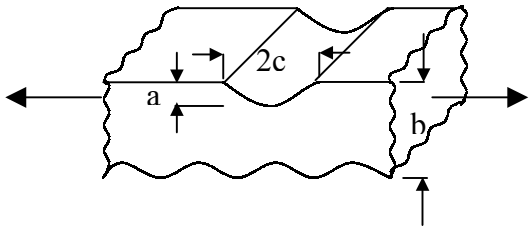

Fig.5.2 Schematic configuration of the micro-notch geometry at the edge of the reduced section of the tested specimens as shown in Fig.5.1.

A total of 10 specimens were tested and the first detected crack lengths were found to vary between 75 and 974μm. The observed wide variation in the initial crack lengths was either due to higher time interval between inspecting the specimen or due to the uncertain non-uniformity in the machined micro-notch or due to microstructural anomaly (e.g. abnormal ferrite-pearlite distribution) at the immediate vicinity of the micro-notch or due to combinations of these facts. Amongst the different possibilities, the time interval between inspecting the specimens is considered dominating. After crack initiation, if the load is not immediately reduced to a lower level, the initiated crack grows at a high rate leading to a higher starting crack length; because crack

initiation studies were carried out at 133.5N whereas crack growth studies were done at 89.5N.

Out of 10 specimens, only 5 were selected for crack growth studies at 89N load having initial crack lengths < 632μm. The geometry of the defect that introduced the first observed crack in the selected specimens was recorded, its dimensions were measured and the K_{ini} values for these cracks were estimated; the results are shown in Table 5.1. The first detected crack lengths for specimen numbers 1 and 2 were found to be 750 and 974 μm respectively, which were not suitable for short crack growth studies. The specimens 4, 5 and 6 indicated initial crack lengths of 175, 85 and 154 μm respectively. But these specimens broke while attempting to study crack growth rate at different loads >89N.

Table 5.1 Configuration of micro-notches from which the short cracks originated and the stress intensity factors for crack initiation.

Specimen No.	Depth, a (μm)	Length, 2c (μm)	a/2c	Initial stress (MPa)	Q	K_{ini} ($MPam^{1/2}$)	N_i ($\times 10^6$) (cycles)
3	19	132	0.14	211.7	1.1	5.2	0.9
7	13	103	0.13	198.4	1.05	4.2	0.27
8	12	54	0.22	204.8	1.3	3.7	0.27
9	8	25	0.32	188.2	1.6	2.5	0.27
10	13	94	0.14	187.5	1.15	3.75	0.15

The uncertainty in the length of the first observed crack is an inherent limitation of short crack growth studies, but the present results infer that one can introduce these cracks by applying a stress equivalent to $0.36\sigma_t$. The literature indicates that crack lengths of the order of 30-200μm have been considered earlier for studying short crack growth behaviour. However, in the present study higher crack lengths permissible under the definition of physically short cracks [1] have been considered.

5.3.1.2 Variation of crack length with number of cycles

The present crack growth studies were carried out by monitoring crack lengths at increasing number of cycles by interrupting the fatigue tests at several pre-selected time intervals. The crack paths for each interval of time were recorded using an image

analyzer and their lengths were measured. A compilation of the obtained *a vs. N* data for the investigated specimens is shown in Fig.5.3. The usual shape of *a vs. N* curve is one of constant rising slope for the case of long cracks [182]. But the plots in Fig.5.3 exhibit some plateau regions. These plateau regions indicate the phenomenon of crack arrest and, in turn, illustrate some typical characteristics of short crack growth behaviour. Such plateau regions have been observed in a few earlier investigations e.g. in the ones reported by Lankford [182] on a high strength steel, Liendstedt et. al. [220] on an austenitic stainless steel, Hussain et. al. [221] on a ferrite-bainite steel and Ravichandran et. al. [45] on Titanium alloys. The phenomenon of crack arrest is commonly attributed [182,220,221] to occur at microstructural barriers like grain boundaries.

The number of locations and crack lengths at which crack arrests were noted for time duration of 10-60 minutes (i.e. for 3×10^4 to 18×10^4 cycles) were found to vary in different specimens. The events of crack arrest in *a vs*. N plots in Fig.5.3 are manifested by plateau regions. These are marked with arrows in Fig.5.3. The *a vs*. N plots of specimen 7 and 8 reveal only one plateau whereas those for specimen 3 and specimen 10 exhibit two and four plateaus respectively. No plateau could be detected with certainty in specimen 9. The maximum crack lengths at which the event of crack arrest is detected with certainty in specimen 3,7,8 and 10 were found to be 539, 411, 705 and 837μm respectively. These crack lengths can be considered to represent the transition point between the short and the long cracks. The existence of a plateau region and its considerable extent signal crack arrests at barriers either due to short or near long crack threshold. Short extents of the plateau usually imply crack arrest at barriers whereas long extents are indicative of short or near long crack threshold. Since the duration of crack arrest is significant for the observed plateaus, these may be considered to reveal the threshold conditions. The variation in the maximum crack length at which crack arrest occurred in different specimens can be attributed to the nature of the cracks, and this is an inherent characteristic of short crack growth behaviour. The occurrence of crack arrest at different lengths can originate from different possibilities like local microstructural environment, extent of crack deflection, plasticity associated with crack tip, crack closure and local residual stresses [1,44,161,207,222-225].

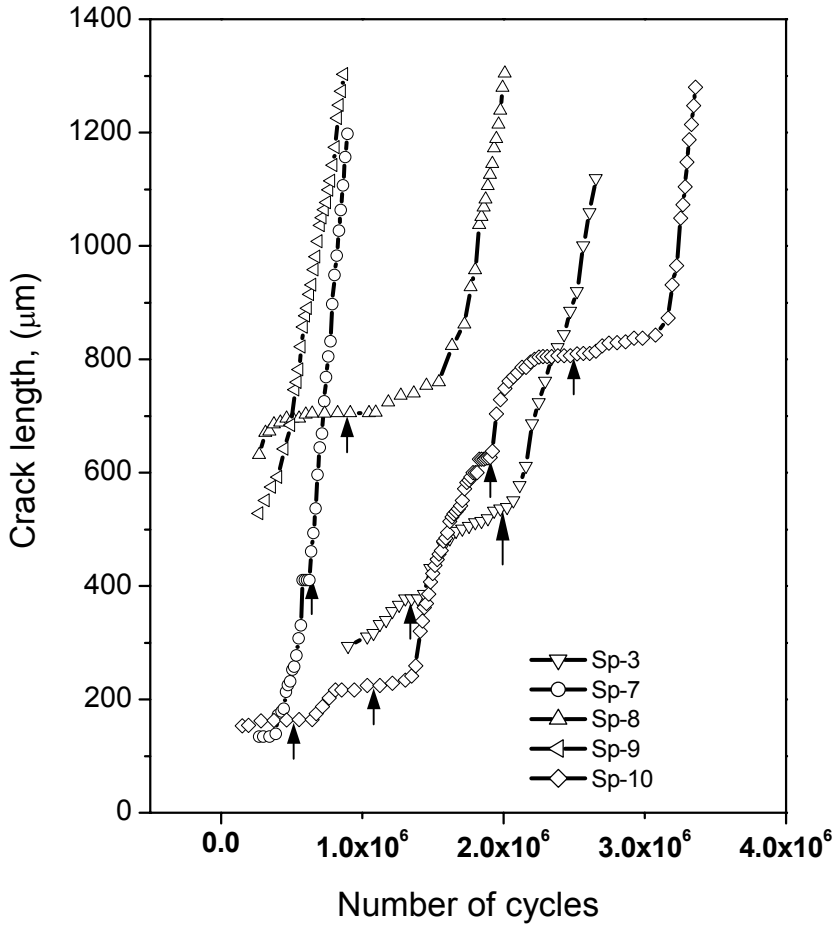

Fig.5.3 Variation of crack length with increasing number of cycles in different specimens of S25 steel.

5.3.1.3 Variation of crack growth rate with the crack length

The crack growth rate (*da/dN*) was calculated by measuring the increment in crack length (*da*) in a specific interval and dividing it by the number of fatigue cycles (dN) the specimen has been subjected to in that interval. These data were next examined by plotting d*a*/dN (in log scale) *vs*. *a*. At each plateau (Fig.5.3), the magnitude of d*a*/dN tends to zero and is not measurable; so in order to incorporate these points in the plots, d*a*/dN is arbitrarily kept at a very low value equal to 10^{-8} μm/cycle. All crack length measurements were done in the primary direction of crack growth i.e. normal to the edge of the specimen containing the micro-notch. It may be noted here that the resolution for measuring the length of a crack by the image analyzer is 0.5 μm.

A compilation of the plots of *da/dN vs. a* for different specimens is presented in Fig.5.4. These plots, in general, indicate considerable fluctuations in crack growth

rate; but the average growth rate exhibits a decreasing trend till a certain crack length followed by an increasing trend for each specimen. This typical behaviour (for specimen 8) is illustrated with an insert in Fig.5.4. The decreasing and increasing trend in d*a*/dN *vs*. *a* is found iterative for specimen 3 and 10. Figure 5.5 illustrates the crack path through the microstructure along with the plot of *da/dN vs. a* for specimen 10. The crack lengths at which large deflections in growth rate occur (Fig.5.5) correspond to microstructural locations of ferrite pearlite interface.

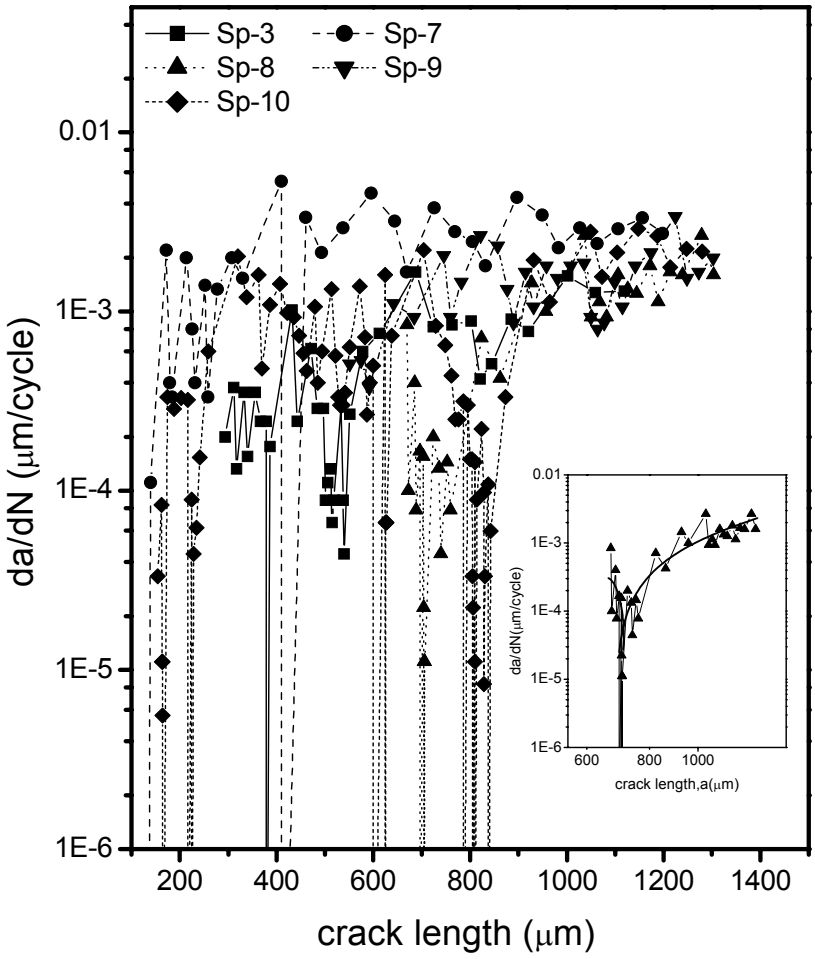

Fig.5.4 Variation of crack growth rate with crack length in the investigated specimens of S25 steel. Typical nature of crack growth is illustrated by a smooth curve in the insert for the data of specimen 8.

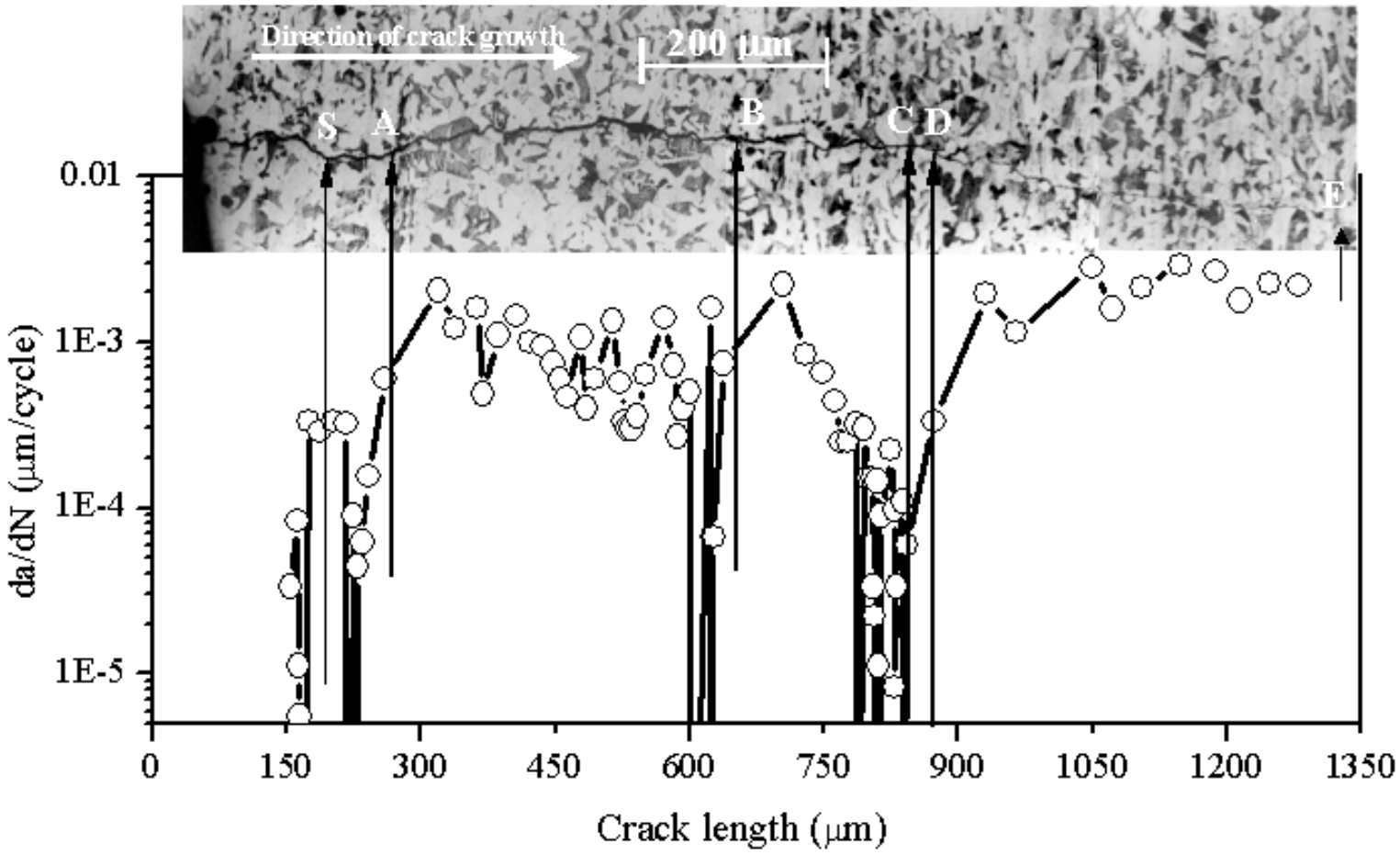

Fig.5.5 Typical profile of a crack path through the microstructure of specimen 10 of S25 steel. The crack growth rates associated along the crack path are also illustrated. Minimum crack growth rates are observed at locations A, B, C and D.

One or more minima can be observed in the *da/dN vs. a* plots. The maximum crack length at which a minimum in *da/dN* is noted in Fig.5.4 is termed here as the critical or the transition crack length. The values of transition lengths for different specimens are summarized in Table 5.2. Beyond the transition length, the fluctuations in crack growth rate decrease and *da/dN* gradually increases with *a* exhibiting lower magnitudes of scatter.

The magnitude or the order of the transition crack length for 0.25% carbon steel is not available in the existing literature, but it may be noted that the estimated values of the transition length in the investigated steel are similar to the ones reported by Shademan [226] and Tokaji et. al. [117] in titanium alloys. Typical microstructural features that are associated with the transition of short to long crack are shown in Fig.5.6. The crack in Fig.5.6 is observed to take deflection almost of the order of 90^{o} along the ferrite-pearlite interface prior to passing through the pearlite colony. The combined phenomena of large crack deflection and its passage through ferrite-pearlite interface prior to its further movement through pearlite colony can be ascribed as the reason for virtual crack arrest.

Table 5.2 Transition crack length in the investigated steel.

Specimen No.	Transition Crack length (μm)
3	539
7	411
8	705
9	592
10	837

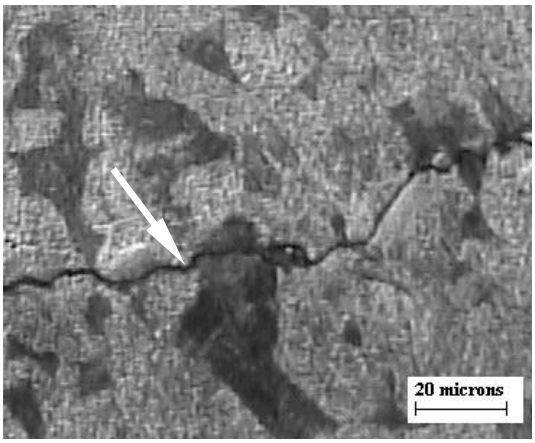

Fig.5.6 Transition points of short to long crack in specimen 3 of S25 steel.

5.3.1.4 Variation of crack growth rate with stress intensity factor range

The stress intensity factor ahead of a crack tip depends on the geometry of the specimen-crack configuration and the nature of the loading. The examination of a few fracture surfaces after short crack growth studies indicated that there is considerable amount of crack depth and cracks may be treated as quarter elliptical corner cracks. For convenience of ΔK-calculations, it was assumed that the nature of the cracks to be quarter penny edge cracks. The stress intensity factor for this type of crack is given as [219]:

$$\Delta K = (1.12)^2 \frac{2}{\pi} \sigma \sqrt{\pi a} \qquad \ldots(5.2)$$

where $(1.12)^2$ represents two surface flaw corrections and $2/\pi$ represents the correction for a quarter penny edge crack. The stress intensity factor expressed by eqn. (5.2) gives the lower bound value. The stress (σ) ahead of a crack under bend load (P) is given as,

$$\sigma = \frac{6P \times l}{wb^2} \qquad \ldots(5.3)$$

where l is the distance between the point of application of load and the location of crack in the specimen, and w and b are the dimensions of the reduced section of the specimen (Fig.5.1). Using eqn. (5.3), one finds that the magnitude of stress linearly varies from point C to A (in Fig.5.1) as 182.2 to 207.7MPa for the initial imposed load of 130 N. The stress variation between these points during crack growth studies is in the range 124.7 to 142.2 MPa corresponding to the load of 89 N. The magnitudes of the above mentioned stresses are for a specimen having w=11.0 and b=5.0 mm.

The recorded data of *da/dN vs*. *a* were converted to *da/dN vs.* ΔK using the aforementioned procedure for estimating ΔK; ΔK was taken as K_{max} following ASTM standard E647 [8]. The plots of *da/dN vs.* ΔK for the tested specimens are shown in Fig.5.7. The nature of these plots is similar to those of *da/dN vs. a*. The plots of d*a*/dN *vs.* ΔK for different specimens in Fig.5.7 reveal several minimum values which corresponding to the plateau regions in Fig.5.3. The magnitude of ΔK corresponding to the maximum crack length for a specimen at which a plateau in *a vs.* N plot is observed, is considered the transition between the short to long crack. These values

are referred here as ΔK_{scth} for the material, which take into account the implicit assumption that there is negligible difference between ΔK_{th}, estimated by standard long crack growth studies and that at the transition between a short and its long crack form. Some of the earlier studies like that of Kaynak et. al. [227] indicate that there exists some difference between fatigue threshold values determined by short and long crack growth studies. But the maximum value of fatigue threshold determined by short crack growth is usually lower than that obtained by long crack growth experiments. Hence the obtained values of ΔK_{scth} for the investigated steel can be considered as conservative estimates. The magnitudes of ΔK_{scth} for specimens 3, 7, 8, 9 and 10 were found to be 4.6, 4.7, 5.1, 4.3 and 6.9MPam$^{1/2}$ respectively. The average threshold value from all the specimens can be expressed as 5.1±1.0MPam$^{1/2}$.

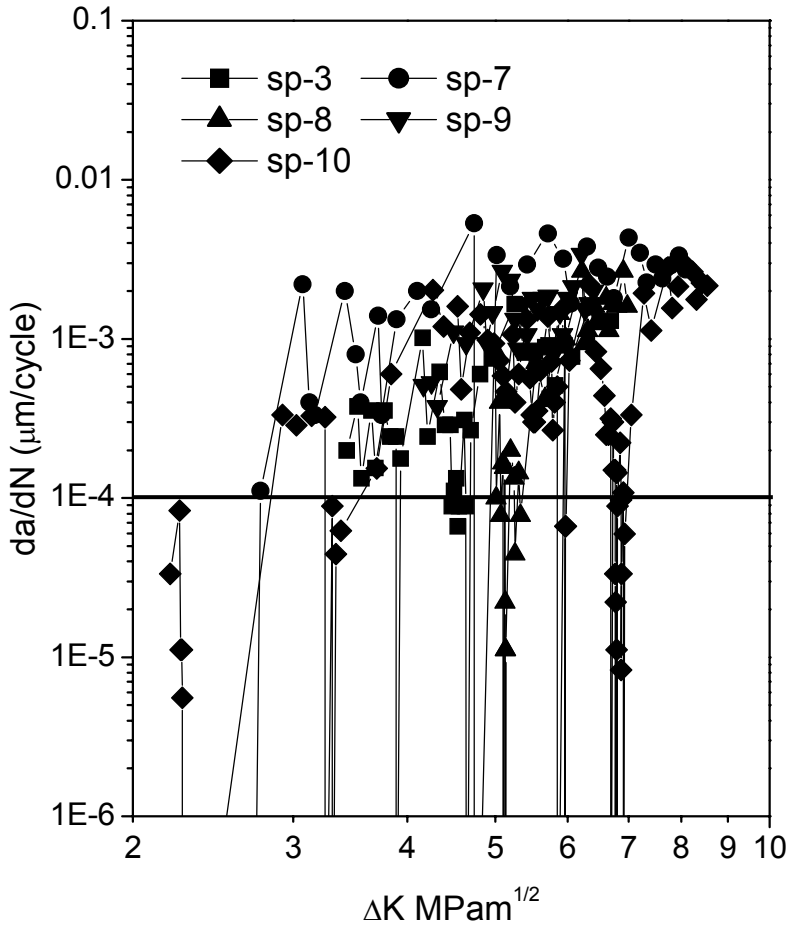

Fig.5.7 The plot of da/dN against ΔK for different specimens of S25 steel.

The transition crack length and the short crack fatigue threshold as discussed in the earlier part are schematically illustrated in Fig.5.8. One can visualize the short

and long crack behaviour by the paths A-B-D and C-D-E in Fig.5.8a. The magnitudes of ΔK corresponding to the points B and C represent the fatigue threshold for short and long crack respectively, and the point D represent the transition between short and long crack. The difference between ΔK at point B and point C primarily depends on the load ratio (R) during a fatigue test [182]. Higher value of R increases the difference between B and C whereas lower value of R almost merges the points B and C as schematically shown in Fig.5.8b. Since the present experiments have been carried out at R = -1, it is considered that the material behaviour would correspond closely to the d*a*/dN *vs*. ΔK plot as shown in Fig.5.8b. The transition crack length ideally should be at point D in case of Fig.5.8a, but it shifts to point B/C in Fig.5.8b, when one considers negligible difference between points B and C.

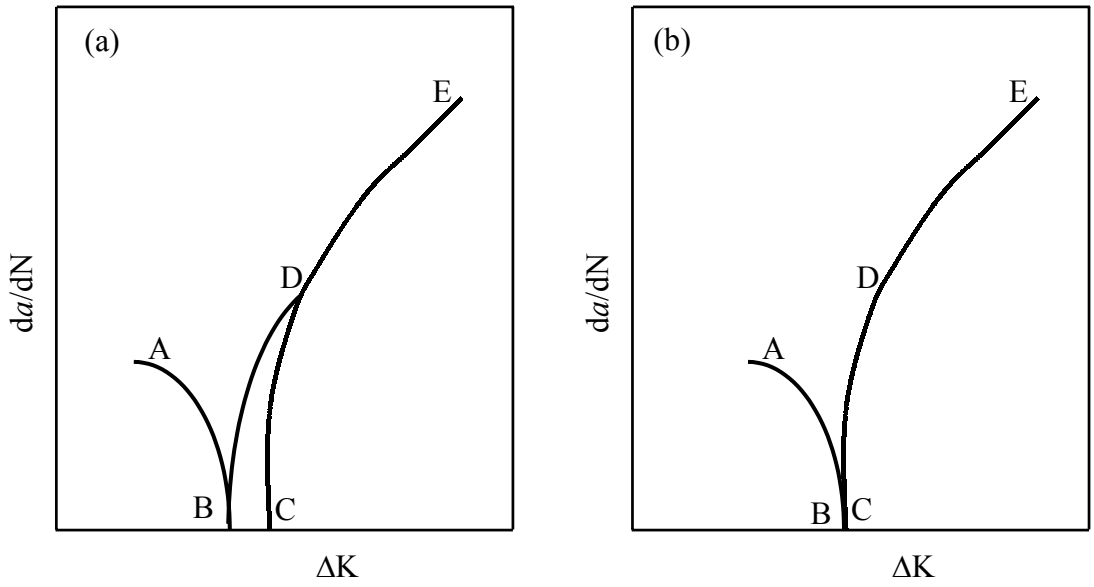

Fig.5.8 Schematic view of the critical crack length at the transition between short and long crack and their fatigue thresholds. The points B and C are the thresholds for short and long cracks. The point D (in part a) or B and C (in part b) indicates the transition length.

Further, the fatigue threshold at point C should correspond to a crack growth rate of 10^{-10} m/cycle or lower as per ASTM E-647 [8]. A horizontal line representing this crack growth rate is shown in Fig.5.7. It is obvious from this figure that the ΔK_{scth} values determined for specimens 3, 7, 8 and 10 are following this definition. The ΔK_{scth} value for specimen 9 has been taken as the one which corresponds to the minimum d*a*/dN recorded during its crack growth. In addition, the concept extended

by the Kitagawa [67] plot suggests that threshold for short crack should better be described as stress differential rather than stress intensity factor differential. The inherent assumption in the present methodology in which the difference between the points B and C in Fig.5.8 is considered negligible, indicate a point where the crack can be considered either short or long. Under this condition defining the threshold for short cracks by stress intensity factor range (ΔK) can be considered satisfactory.

An attempt has been made to compare the estimated mean ΔK_{scth} value for the investigated steel with those reported for similar materials. The reported magnitudes of ΔK_{th} values for low carbon steels are compiled in Table 5.3. This compilation indicates that the upper bound of the obtained ΔK_{scth} value from short cracks is close to most of the reported ΔK_{th} values for long cracks. A comparison of this type is difficult because, the fatigue threshold of a material depends on the chemistry and microstructure of the steel, its strength level, and the applied load ratio apart from the environmental conditions and the nature of test. Interestingly, James et. al. [118] and Kendall et. al. [228] have observed that short crack threshold and long crack threshold are in close proximity. The results of Tokaji et. al. [108] and Kaynak et. al. [228], on the other hand, indicate considerable difference between threshold values determined by short and long cracks. But the magnitudes of the long crack thresholds reported by these investigators are considerably higher compared to other reports on similar materials. An overview of the present results with those given in Table 5.3 infer that the obtained fatigue threshold is in reasonable agreement with the trend of long crack threshold values reported by most of the earlier investigators. In addition, Taylor [229] has shown that the fatigue threshold of mild steel can be approximately expressed as $\Delta K_{th} = 1.7+10^3 \sqrt{d}$ where d is in meters. The grain size of the selected steel is 18 μm; so as per Taylor's empirical formulation its fatigue threshold should be 5.9MPa$\sqrt{m}$. This theoretically estimated value of ΔK_{th} is in excellent agreement with the upper bound value of the experimentally determined fatigue threshold of the selected steel through short crack growth studies. Hence, it can be inferred that the developed test technique is capable of generating fatigue threshold of structural materials through simple rotating bending test, and that the ΔK_{scth} value of the investigated steel is $5.1\pm1.0 MPam^{1/2}$.

Table 5.3 Some reported threshold values in steels.

Sl No	%C	YS (MPa)	TS (MPa)	d (μm)	R ratio	ΔK_{scth} ($MPam^{1/2}$)	ΔK_{th} ($MPam^{1/2}$)	Ref.
1.	0.11	286	433	24	-1.0	6.03	8.12	[108]
2.	0.11	233	402	84	-1.0	6.30	8.22	
3.	0.18	301	503	-	0.1	~6**	~9**	[227]
4.	0.15	280	420	-	0.5	4.5*	4.5	[118, 228]
5.	<0.2	653	743	-	0.2	4.8*	4.8	
6.	0.21	255	545	-	0.0	-	5.5	[230]
7.	Mild steel	-	530	-	-	-	6.4	[231]
8.	Mild steel	-	430	-	0	-	6.6	
9.	Low alloy steel	-	835	-	-1.0	-	6.3	[83]
10.	Mild steel	-	430	-	-1.0	-	6.4	
11.	0.25	345	542	18	-1.0	5.1±1.0	5.1 ± 1.0	Present

* short crack threshold is within (Q1N steel) the scatter band of long crack threshold
** read from Fig.3 of ref [227], YS=Yield strength, TS=Tensile strength, d=grain size, ΔK_{scth} = short crack threshold, ΔK_{th} = long crack threshold,

5.3.1.5 Effect of microstructure on crack path

That microstructure influences the rate of short fatigue crack propagation is well known, but any quantitative relationship between the length of a crack path and the nature of the microstructural features (different phases or interfaces) through which a crack traverses, has not been examined earlier. A series of photographs of the crack profile were taken, and the lengths of various segments of a crack path passing through different microstructural features were measured. Typical segments of a crack path and its associated microstructural features are illustrated in Fig.5.9. The different microstructural features were ferrite grains, pearlite colonies, ferrite-pearlite interfaces and ferrite-ferrite grain boundaries. The segments of a crack passing through different microstructural features were first coloured according to the nature of the microstructural feature/features associated with the segment. The exact length of each coloured segment was next measured and categorized using an image analyzer. The summation of crack lengths pertaining to a particular colour revealed the relationship between the proportion of crack length with its associated microstructural feature. The results of this examination are summarized in Fig.5.10. It can be noted that 40% and 24% of crack length passes through ferrite grains and ferrite-ferrite grain boundaries respectively. The volume fraction of ferrite in the investigated steel is estimated as 73%. So it can be concluded that the amount of crack length passing through a microstructural feature is approximately proportional to its volume fraction for the

investigated steel. The total crack length passing through ferrite-ferrite grain boundary and ferrite-pearlite interface, on the other hand, was found to be 44%. This result indicates that a crack prefers to pass through the interface rather than through ferrite grains or pearlite colonies, because the interfacial area is much less compared to the area of ferrite grain body plus pearlite colony.

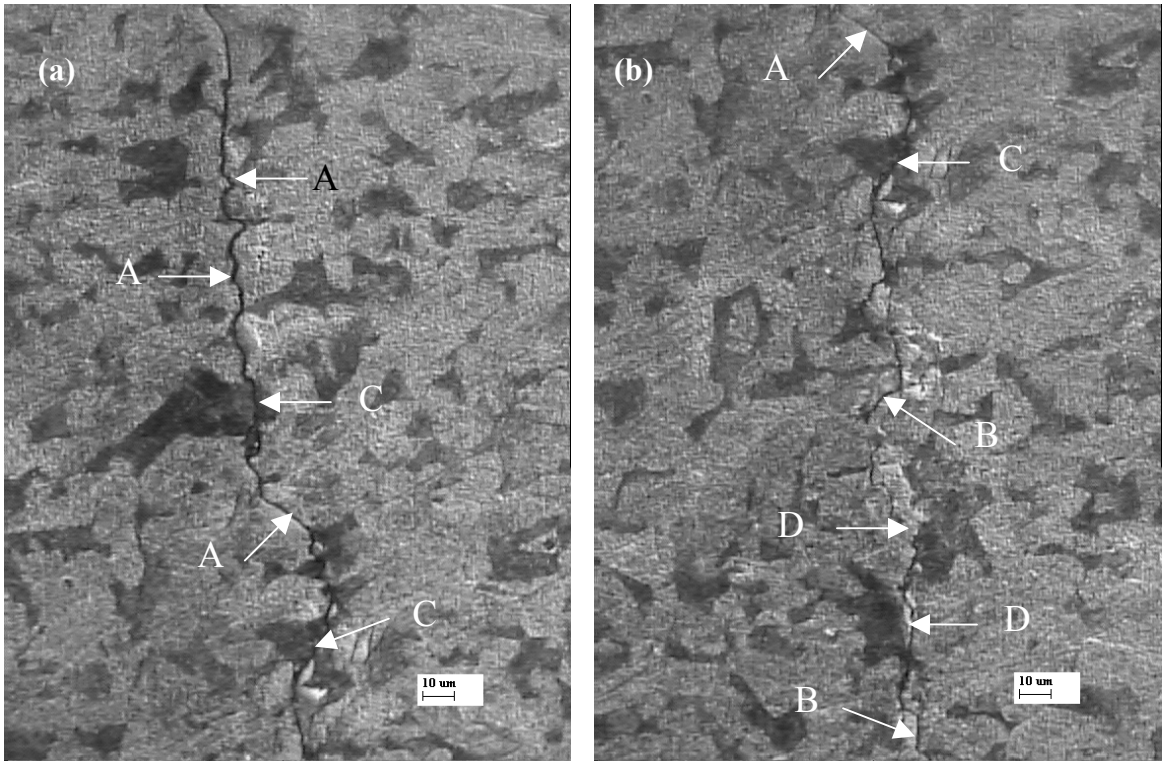

Fig.5.9 Typical crack paths and their associated different microstructural features in specimen 3 of S25 steel. Photographs (a) and (b) represent two different segments of the same crack path. A, B, C and D represent ferrite grains, ferrite-ferrite grain boundaries, pearlite colonies and ferrite-pearlite interfaces respectively.

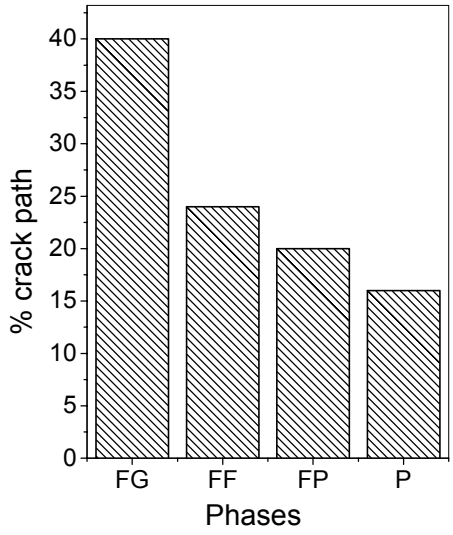

Fig.5.10 Percentage of crack path through various phases in specimen-3 (FG=ferrite grains, FF=ferrite-ferrite grain boundaries, FP=ferrite pearlite interfaces, and P=pearlite colonies.)

5.3.2 Short fatigue crack growth behaviour in S00 steel

Short crack growth study in S00 steel has been carried out in a way similar to that for S25 steel as discussed in the previous section. A load of 84.5N (19 lb), which yields a stress of 142MPa at the location of A or B (Fig.5.1), was found to induce short crack in these specimens. At this stress value the number of cycles for crack initiation was found to be approximately 1.65×10^5 and the initiation stress can be expressed as $\sigma_{ini}=(0.62\pm0.02)\sigma_t$. However, the fatigue test on this steel was started at an initial load of 44.5 N (10 lb) and the load was increased in several discrete steps to 84.5N (19 lb). At each intermediate load-steps fatigue cycling of the specimen was carried out for 5×10^6 cycles followed by optical examination to reveal any possible crack initiation in the specimen. Four specimens were considered for this study; out of which one broke during SCG studies and another resulted in a large initial crack length, which had to be naturally discarded for any further study related to SCG. The geometry of the defect that introduced the first observed crack in the fully tested specimens was recorded, its dimensions were measured and the K_{ini} values for these cracks were estimated; the results are shown in Table 5.4.

Table 5.4 Configuration of micro-notches from which the short cracks originated and the stress intensity factors for crack initiation in the tested specimens of S00 steel.

Sp. Code	Depth, a μm	Length, 2c μm	a/2c	Initial stress (MPa)	Q factor	$K_{initial}$ ($MPam^{1/2}$)	N_i ($x10^6$)
1	8	32	0.25	154	1.4	2.19	0.075
2	6	39	0.15	142	1.1	1.97	0.165

The variations of *a vs*. N, d*a*/dN *vs*. *a* and d*a*/dN *vs*. ΔK for S00 steel were obtained in the identical manner to that of S25 steel as described in section 5.3.1 and these are presented in Fig.5.11, Fig.5.12 and Fig.5.13 respectively. The different plateau in the plots of *a vs*. N in Fig.5.11 correspond to the various minima in the d*a*/dN *vs*. *a* or d*a*/dN *vs.* ΔK. The maximum crack length, at which a minimum in d*a*/dN is noted, is termed here as the transition crack length and is shown in Fig.5.12. The transition crack lengths for specimens 1 and 2 were found to be 1180 and 1160μm respectively. These crack lengths can be considered to represent the transition point between the short and the long cracks as discussed in section 5.3.1. The magnitudes of ΔK corresponding to the transition crack lengths in these specimens are referred to as short crack threshold values (ΔK_{scth}) for the material. The

magnitudes of ΔK_{scth} for specimens 1 and 2 were found to be 3.9 and 4.6MPam$^{1/2}$ respectively. The average ΔK_{scth} value can be expressed as 4.2±0.3MPam$^{1/2}$.

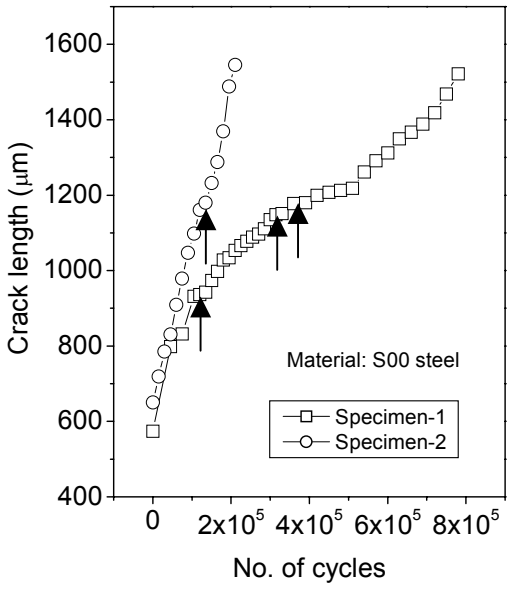

Fig.5.11 Variation of crack length with increasing number of cycles in S00 steel.

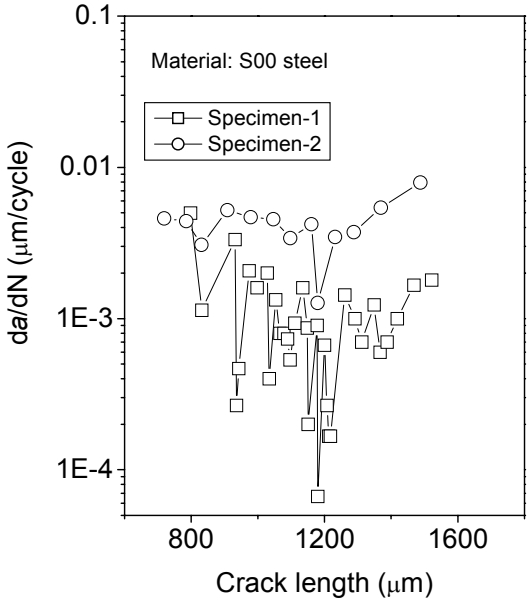

Fig.5.12 Variation of crack growth rate with crack length in S00 steel.

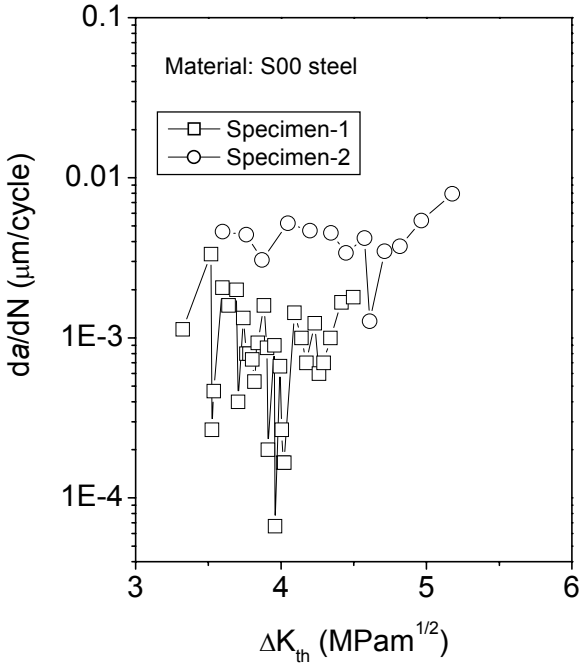

Fig.5.13 Crack growth rate against stress intensity factor range in S00 steel.

The observed lengths of transition cracks in S00 steel are larger than that of S25 steel whereas the average short-crack threshold value for S00 steel is smaller than that of S25 steel. The crack-tip, up to which the transition crack length was estimated,

was found to impinge at grain boundaries unlike the location of such crack-tips in S25 steel which were found to occur at pearlite colonies as shown in Fig.5.6. The order of the estimated short crack threshold for S00 steel is in close agreement with that of S25 steel and with most of the earlier results on plain carbon steels as compiled in Table.5.3 [83,108,118,227,228,230,231]. But it is difficult to indicate why ΔK_{scth} for S00 steel is lower than that for S25 steel. One reasoning for the above observation could be that the local residual stress field at the tip of a transition crack is possibly lower near ferrite grain boundary than that around a pearlite colony.

5.3.3 Short fatigue crack growth behaviour in S47 steel

The procedure for short crack growth study in S47 steel is identical to that as described in the previous sections. A stress of 207MPa was found to induce short cracks in the specimens of S47 steel, and at this stress the number of cycles for crack initiation was found to be approximately 2.7×10^5. The stress values for crack initiation (σ_{ini}) can be expressed as $\sigma_{ini}=(0.36 \pm 0.03)\sigma_t$. A set of six specimens were considered for this study, but the desired results could be obtained only for two specimens. The geometry of the defect that introduced the first observed crack in the selected specimens was recorded, its dimensions were measured and the K_{ini} values for these cracks were estimated; the results are shown in Table 5.5.

Table 5.5 Configuration of micro-notches from which the short cracks originated and the stress intensity factors for crack initiation in S47 steel.

Sp. Code	Depth, a μm	Length, 2c μm	a/2c	Initial stress (MPa)	Q factor	$K_{initial}$ ($MPam^{1/2}$)	N_i ($x10^6$)
1	7	45	0.15	207	1.1	3.1	0.27
2	5	37	0.13	235	1.05	3.05	0.18

A compilation of the obtained *a vs. N* data for the investigated specimens of S47 steel is shown in Fig.5.14. The plots of d*a*/dN *vs*. *a* and d*a*/dN *vs*. ΔK for specimens of S47 steel are presented in Fig.5.15 and Fig.5.16. The transition crack lengths at which the event of crack arrest is detected with certainty in specimen 1 and 2 were found to be 898 and 679μm respectively. The magnitudes of ΔK_{scth} for specimens 1 and 2 were found to be 6.6 and $7.2MPam^{1/2}$ respectively. The average ΔK_{scth} value can be expressed as $6.9\pm0.3MPam^{1/2}$. Interestingly it is noted that the ΔK_{scth} value for the three investigated steels increases with increase in carbon content

or amount pearlite or strength of the steels. Taylor [162] has reported that fatigue threshold of large cracks exhibit an increasing trend with increase in strength level of the steels. The estimated magnitudes of ΔK_{scth} for the three steels are thus found to show a trend of variation similar to that for long crack threshold and strength as reported by Taylor [162].

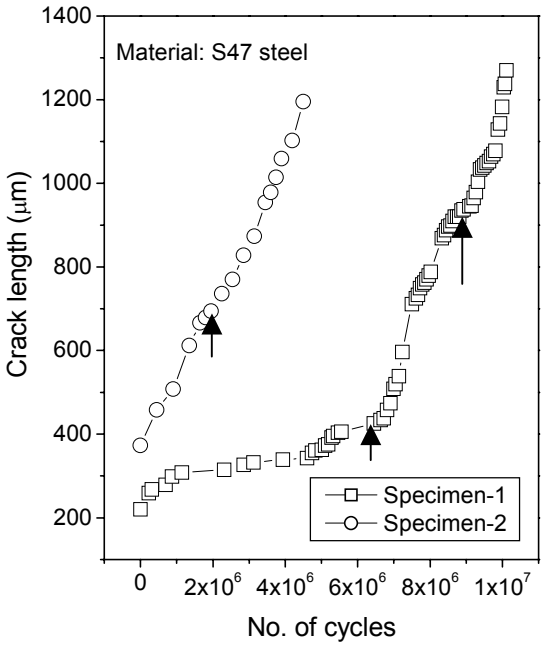

Fig.5.14 Variation of crack length with increasing number of cycles in S47 steel.

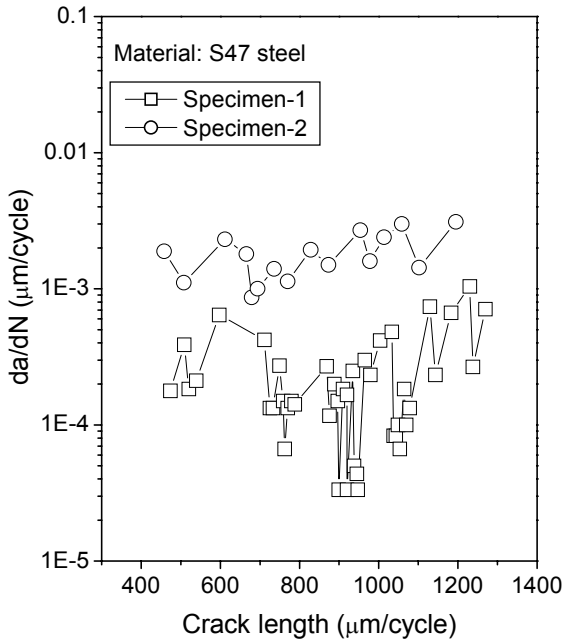

Fig.5.15 Variation of crack growth rate with crack length in S47 steel.

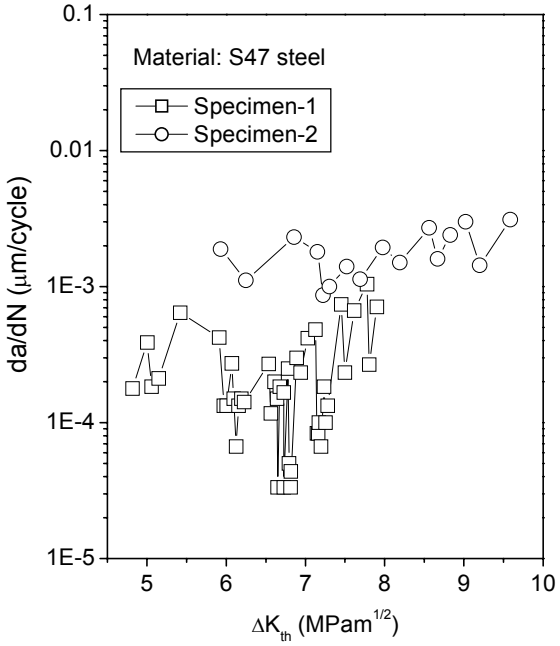

Fig.5.16 Crack growth rate against stress intensity factor range in S47 steel.

5.4 Conclusions

The following major conclusions can be drawn from the investigation on the small fatigue crack behaviour of the selected plain carbon steels:

- A new specimen configuration has been developed to study initiation and growth of short fatigue cracks using rotating bending machine.
- The number of cycles to initiate a short crack in the developed specimen configuration was found to be $\approx 2.7 \times 10^5$ at an applied stress of 210MPa for the investigated S25 steel. The stress and the number cycles required for crack initiation in S00 steel were found to be 142MPa and 1.65×10^5 respectively and those in S47 steel were 207MPa and 2.7×10^5 respectively.
- The transition crack lengths were found to be in the range of 411 to 837, 1160 to 1180 and 679 to 898 μm in S25, S00 and S47 steels respectively.
- The short fatigue crack thresholds for S00, S25 and S47 steels were found to be 4.2 ± 0.3, 5.1 ± 1.0 and 6.9 ± 0.3 $MPam^{1/2}$ respectively.
- The fatigue crack path is associated with ferrite grain body, pearlite colony, ferrite-ferrite grain boundary, ferrite-pearlite interface and occasionally with inclusion matrix interfaces for S25 and S47 steels. For S00 steel, the fatigue crack was found to pass through only grain body and grain boundary of ferrite.
- The length of a crack path through a specific phase is proportional to the volume fraction of this phase in S25 and S47 steels.
- Cracks tend to pass through the interface like ferrite-ferrite grain boundary and ferrite-pearlite interface rather than the ferrite grain body or pearlite colony.

Chapter 6

Determination of fatigue threshold of a few plain carbon steels using a rotating bending machine

6.1 Introduction

The design of structural materials against fatigue damage requires the knowledge of the nature of variation of crack growth rate (d*a*/dN) with alternating stress intensity factor (ΔK) and the magnitude of fatigue threshold (ΔK_{th}). The assessment of these engineering parameters is conventionally carried out following the ASTM standard E647. The determination of ΔK_{th} usually requires significant time engagement of servo-hydraulic or electro-magnetic resonance type machines. As a result, studies on fatigue behaviour at crack growth rates < 10^{-6} mm/cycle and around ΔK_{th} are considerably limited compared to that at d*a*/dN >10^{-6} mm/cycle. But fatigue studies at crack growth rates <10^{-6} mm/cycle and around ΔK_{th} is important to explore the mechanics and mechanisms of crack growth behaviour in structural materials designed for safe-life applications. One of the primary aims of this investigation is to search for alternative simple techniques for (i) estimating ΔK_{th} and for (ii) studying crack growth behaviour at low d*a*/dN values.

The conventional rotating bending machine can be used for the determination of ΔK_{th} provided one can measure the crack growth rate during fatigue testing. Specimens used for conventional rotating bending tests are hourglass type with circular cross section at the center. It is difficult to monitor the growth of a crack of sufficient length on the surface of circular sections. This demands specimens with sufficient region of flat surfaces, which are compatible to fix in the collet of the rotating bending machine. Though some short crack growth studies have been made earlier [232] using rotating bending machine on hourglass specimens with limited region of flat surface, no work has been reported so far on long crack growth studies using this type of specimens, possibly because of the difficulty in monitoring crack growth. An attempt has been made in this part of the investigation to overcome this problem by designing a specimen with an extended region of flat surface similar to

the specimens used for short crack growth studies as reported in Chapter 5, but with the difference of incorporating a notch. Once such a technique can be developed, the fatigue thresholds for a few materials have to be determined to gauge the appropriateness of the procedure and subsequently the results of ΔK_{th} are to be examined for their reliability in comparison to available results obtained by standard procedure. The materials selected for this investigation are S00, S25, S47 and S62 steels.

The rate of fatigue crack growth, immediately after its initiation from a notch, gradually slows down with increase in crack length, prior to its stoppage or further growth depending on the applied stress. When the propagation completely ceases to occur, the crack is referred as a "nonpropagating crack". During the investigation with the newly designed specimens, attempts were made to examine whether the similar procedure can also assist in studying non-propagating cracks.

The search for a possible quantitative relation between the segmental lengths of crack paths and their associated microstructure has not been made so far. The small cross sections of the designed specimens can be considered suitable to study crack growth together with the microstructures. Studies of this nature can bring forth information about the weak links in a microstructure through which a crack prefers to pass through or the affinity of a crack to travel through any specific phase in a microstructure.

In summary the objectives of the investigation presented in this chapter are: (i) to develop a new technique for studying crack growth behaviour using a rotating bending machine, which primarily involves the design of a new specimen configuration, (ii) to determine fatigue crack growth thresholds of a few steels using the developed technique and to examine their appropriateness, (iii) to examine the possible occurrence of non-propagating cracks in these steels, and (iv) to assess the effect of microstructure on the crack path at low crack growth rates.

6.2 Experimental procedure

This section consists of the description of two aspects related to the development of fatigue testing: (a) considerations involved in the design of a specimen suitable for testing with the help of a rotating bending machine (RBM) and that associated with the provision for crack growth measurement, and (b) the

procedure to carry out fatigue test for determining fatigue threshold of the developed specimens. The details of the test procedures for characterizing the materials selected for this investigation are already described in chapter 3.

6.2.1 Specimen configuration

Hourglass type specimens with circular cross section and reduced diameter at the center are commonly used for rotating bending fatigue tests [108,233]. Studies on crack growth require measurement of crack length, which is difficult on the surface of circular sections. Hence, to fulfill the objectives of this part of the investigation, alternate specimens with flat surfaces, which are amenable for testing with rotating bending machine (RBM), are desirable. A new type of specimen has thus been designed and fabricated to carry out fatigue crack growth threshold studies using a RBM.

The configuration of the designed specimen is shown in Fig.6.1. Both the ends of the specimen are kept circular for the purpose of holding it (end-A of the specimen) in the collet of the RBM and for load attachment (end-B of the specimen) through bearing. The length of end-A (diameter-12 mm) and end-B (diameter-10 mm) are kept as 40 and 13.5 mm respectively. In between the two circular end regions, the intermediate region is kept as rectangular in cross section with a 45^{o} notch. This section has the dimension of 12.5(W) × 12(B) mm. The notch depth is designed to be 5 mm for achieving an initial *a*/W ratio of 0.4. The specimen configuration is thus similar for the end parts of the conventional hourglass type specimen and dissimilar only in the intermediate region.

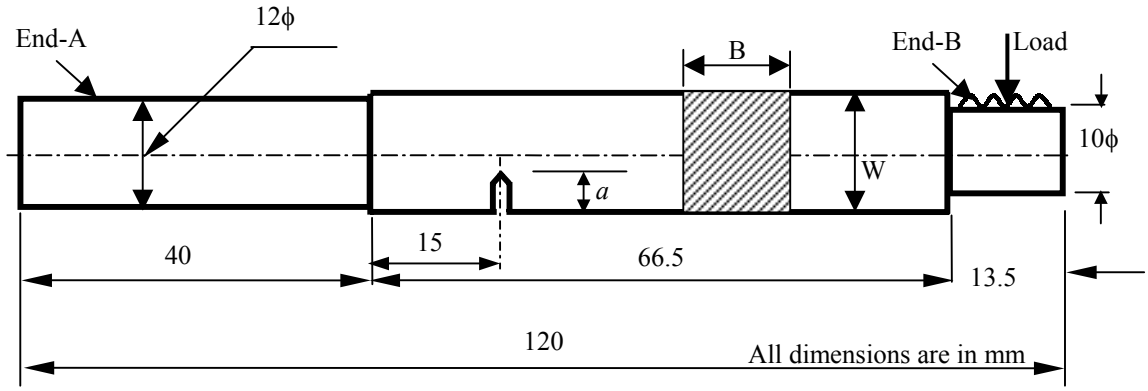

Fig.6.1 The specimen configuration used for fatigue crack growth thresholds studies.

The width of the rectangular cross-section should be long enough to examine the growth of a crack, emanated from the notch tip, for sufficient distance over the specimen surface in order to determine the fatigue threshold of a material. A notch length of 5 mm and a fatigue pre-crack of 1 mm would provide approximately a zone of 3 mm for crack growth studies before the ratio of crack length to width (a/W) of a specimen reaches approximately 0.7 for a specimen having width of 12.5 mm. This has been the primary consideration for deciding the width of the specimen. The minimum thickness (B) of a specimen must be 12 mm in order to accommodate the circular cross section of 12 mm (end-A of the specimen). Higher thickness is convenient for specimen fabrication, but it requires higher load for generating a specific stress at the notch tip. In the present specimen design, the thickness has been selected as 12 mm. In addition to the above aspects, the location of the notch in the specimen is also important for imparting required amount of stress for crack initiation at the notch tip. Higher the distance of a notch from the loading point, higher is the stress that can be induced at its tip at a particular load. Considering that a length of 40 mm is required for fixing the specimen into the RBM, the notch tip is kept at a distance of 60 mm from the point of load application. A total length of 120 mm was found to be appropriate for the fabrication of circular end parts and the intermediate rectangular cross section. The dimensions of individual specimens are shown in Table 6.1.

Table 6.1 Details of specimen dimensions used for fatigue threshold studies.

Material	Sp. code	W (mm)	B (mm)	V (mm)	l (mm)
S00 steel	LC-1	12.52	11.98	5.00	58.13
S00 steel	LC-2	12.48	12.06	5.08	58.27
S25 steel	LC-1	12.52	12.50	5.02	58.98
S25 steel	LC-2	12.48	12.52	5.12	58.13
S47 steel	LC-1	12.46	12.02	5.00	57.13
S47 steel	LC-2	12.46	12.00	5.10	57.27
S62 steel	LC-1	12.52	12.04	5.10	58.56
S62 steel	LC-2	12.52	12.06	5.10	58.24

W=width of the specimen, B=breadth of the specimen,
V = notch length, l=distance between the point of loading and the notch.

6.2.2 Testing details

A series of specimens were fabricated following the design as illustrated in Fig.6.1 from four different steels, designated as S00, S25, S47 and S62, for determining their fatigue threshold values. The fatigue tests were carried out using a 0.75 HP (560 Js^{-1}) rotary bending fatigue testing machine operating at a frequency of 50Hz. The flat surfaces of each specimen were polished upto 0.25μm surface finish using diamond paste as described in section 3.2 prior to fatigue testing. The end-A of a specimen was inserted into the chuck of the machine while end-B was fitted into the ball bearing of the RBM. The initial load for fatigue experiments was between 89 N (20 lb) and 200.2 N (45 lb) depending on the exact dimension of a specimen and its material; the details are described in section 6.3.1.

The fatigue tests were interrupted at predetermined intervals to examine the specimen surface under an optical microscope (Leica, model: 020-520-007 DM/LP) for observing possible crack initiation event. Once a crack is found to be initiated, a picture of the crack was grabbed by a CCD camera coupled to the microscope. The crack length was measured by using the software of an image analyzer (Biovis Material Plus); the length projected onto the direction perpendicular to the specimen axis was used as crack length. The cyclic loading, test interruption and crack length measurements were iterated till the crack length reached a size of approximately 1 mm. This was considered as a fatigue pre-cracked specimen.

The fatigue threshold of the materials was determined by load shedding technique [8]. In this procedure a fatigue pre-cracked specimen was subjected to cyclic loading and its crack growth was monitored while decreasing the load by approximately 10% [8] at each stage. The crack growth rate was calculated as the difference in two successive readings divided by the number of cycles elapsed between these. The procedure of load shedding was continued till the crack growth was found to be infinitesimal. At the lowest load the specimen was subjected to cyclic loading duration for approximately 10^6 cycles. The developed procedure for determining fatigue threshold of a material using a rotating bending machine is summarized as a flow chart in Fig.6.2. A series of graphs namely *a vs. N*, d*a*/dN *vs. a*

and d*a*/dN *vs. ΔK* were constructed and were subsequently analyzed for estimating different characteristics of the fatigue behaviour of the investigated materials.

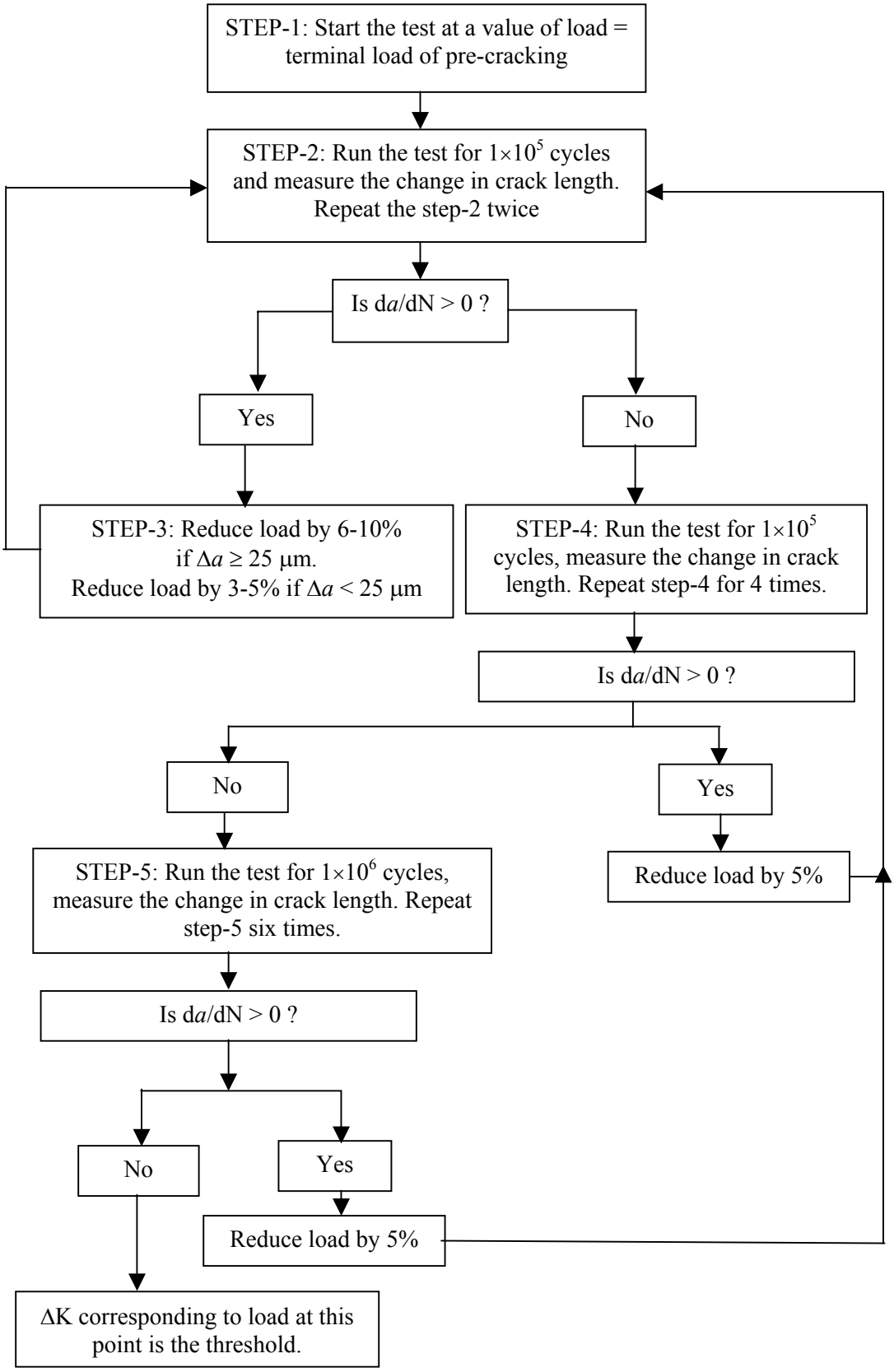

Fig.6.2 A flow chart explaining the testing procedure of developed technique.

After completion of a fatigue test, the specimen was etched and the entire crack path with its associated microstructure was photographed at different magnifications using both optical and scanning electron microscopy. In addition, a few samples were broken, and the characteristic crack growth from the notch tip was examined by the SEM.

6.3 Results and discussion

Experimental investigations related to fatigue crack growth assessment a-priori demands a fatigue pre-cracked specimen. At the outset different aspects of pre-cracking of the developed specimens have been discussed in this section. The fatigue thresholds of the selected steels have been determined using load shedding procedure. The estimation of ΔK for the new specimen, the nature of load shedding, the scatter associated with the estimated threshold values and their comparative assessment primarily with some reported data are discussed next. Since crack initiation and growth were continuously monitored from the start of the experiment, queries were intrigued to detect the occurrence of non-propagating cracks (NPCs) in the investigated steels. The results and the pertinent discussion related to NPCs follow the discussion on fatigue threshold measurements. Analyses on the role of microstructure on the fatigue crack path, which precede a small note on the fractographic features recorded on broken test specimens are the contents of the last part of this section.

6.3.1 Pre-cracking of specimens

The study of fatigue crack growth threshold requires pre-cracked specimens. According to ASTM standard [8], the length of a pre-crack shall not be less than 0.1 times the specimen thickness or 1.0 mm whichever is greater. The pre-cracking is given as to provide a sharpened fatigue crack of adequate size and straightness which ensures that (i) the effect of the machined starter notch is removed from the specimen K-calibration, and (ii) the effects on subsequent crack growth rate data caused by changing crack front shape or pre-crack load history are eliminated. The loads required for pre-cracking specimens of different materials are considered as close to those values corresponding to fatigue limits of the materials. The fatigue limit of a steel can be approximated as 0.35 to 0.50 of its tensile strength [1,12,13,218]. Based on this contention, the crack initiation in S00, S25, S47 and S62 steels should occur at

stress levels between 82-117, 190-273, 217-311 and 262-374 MPa respectively, because their tensile strengths are 235, 543, 621 and 748 MPa respectively. The estimated stress levels for crack initiation correspond to applied loads of 53.4-80.1 N (12-18 lb), 129-182.4 N (29-41 lb), 142.4-209.1 N (32-47 lb) and 164.6-235.8 N (37-53 lb) for the S00, S25, S47 and S62 steels respectively; the calculations take into account the loading configuration (Fig.6.1) of the specimens, and a stress concentration factor of 3 to be operative in front of the machined notch. The stress (σ) under bend load (P) was calculated as:

$$\sigma = \frac{6P \times l}{WB^2} \qquad \ldots(6.1)$$

where l is the distance between the point of application of load and the location of a crack in the specimen, and W and B are the dimensions of the reduced section of the specimen (Fig.6.1).

The fatigue experiments were planned first for the S25 steel. The pre-cracking in these specimens was carried out in the following manner. A specimen was subjected to cyclic loading at a starting load of 111 N (25 lb) and was examined for possible crack initiation by interrupting the test after 9×10^4 cycles. If crack initiation was not observed, the process of cyclic loading, test interruption and the examination of the specimen surface were iterated till 5.4×10^5 cycles (by interrupting the test at every 9×10^4 cycles). Then the load was increased by 8.9-13.3 N (2-3 lb) and again the specimen was subjected to cyclic loading, test interruption and notch tip examination under the microscope. The first specimen of S25 steel exhibited crack initiation at the load of 178 N (40 lb), and the length of the first observed crack was recorded. This experiment indicated that the load at which crack initiation is observed is higher than the lower bound of the estimated load for crack initiation. Based on this experience all crack initiation studies in S25, S47 and S62 steels were started with initial loads of 155.7 N (35 lb), 178 N (40 lb) and 200.2 N (45 lb) respectively. For the S00 steel the starting load for crack initiation was 20 lb but the first crack could be detected only at 138 N (31 lb). The loads at which the crack initiation occurred in each specimen and the recorded first observed crack lengths are summarized in Table 6.2. The observed stresses for crack initiation for S25, S47 and S62 steels correspond to stress levels

equivalent to $0.54\sigma_t$, $0.53\sigma_t$ and $0.42\sigma_t$ respectively; but for S00 steel it is $0.91\sigma_t$. Except for the S00 steel, stress values are in agreement with the reported correlation between fatigue limit (here estimated crack initiation stress) and tensile strength. The higher load for crack initiation in S00 steel is due to its high ductility causing extensive notch tip blunting. Thus the crack initiation stress of $0.91\sigma_t$ for S00 steel is an apparent value.

Table 6.2 Details of crack initiation.

Material	Sp. code	P_{start} (lb)	P_{ini} (lb)	σ_{ini} (MPa)	a_i (μm)	P_{max} (lb)
S00 steel	LC-1	20	32	71	409	32
S00 steel	LC-2	31	31	73	185	31
S25 steel	LC-1	25	40	89	37	45
S25 steel	LC-2	35	46	106	64	53
S47 steel	LC-1	40	45	107	118	52
S47 steel	LC-2	40	48	113	162	53
S62 steel	LC-1	40	45	106	252	45
S62 steel	LC-2	40	45	105	79	51

P_{start} = load at the start of testing, P_{ini} = load at crack initiation, P_{max} = maximum load during testing, a_i = initial crack length, σ_{ini} = stress at crack initiation.

Next the specimens were subjected to further cyclic loading for crack growth to obtain a total crack length of approximately 1.0 mm. For S00 and S62 steels the crack growth could be achieved at the load employed for crack initiation, but for S25 and S47 steels cracks stopped growing after certain number of cycles. This phenomenon required further increase in load to continue crack growth. The maximum loads required for obtaining approximately 1.0 mm of crack length in these two steels were also recorded. The events of the stoppage of the crack after initiation from a notch in S25 and S47 steels are manifestations of the existence of nonpropagating cracks in these materials. This aspect has been dealt at a later section.

6.3.2 Estimation of fatigue threshold

The fatigue threshold of the materials was determined by load shedding technique. In this procedure a fatigue pre-cracked specimen is subjected to cyclic loading and its crack growth is monitored while decreasing the load by approximately

10% [8] at each stage. The fatigue crack growth studies were carried out by monitoring crack lengths at increasing number of cycles by interrupting the fatigue tests at several pre-selected time intervals. The crack paths at each interruption were recorded as digital photographs using a CCD camera and their lengths were measured with the help of an image analyzer. All crack length measurements were done in the primary direction of crack growth i.e. normal to the edge of the specimen containing the micro-notch. It may be noted here that the resolution for measuring the length of a crack by the image analyzer is better than 1.0 μm. The variation of crack length (a) against number of cycles (N) for different specimens of the investigated steels is shown in Fig.6.3.

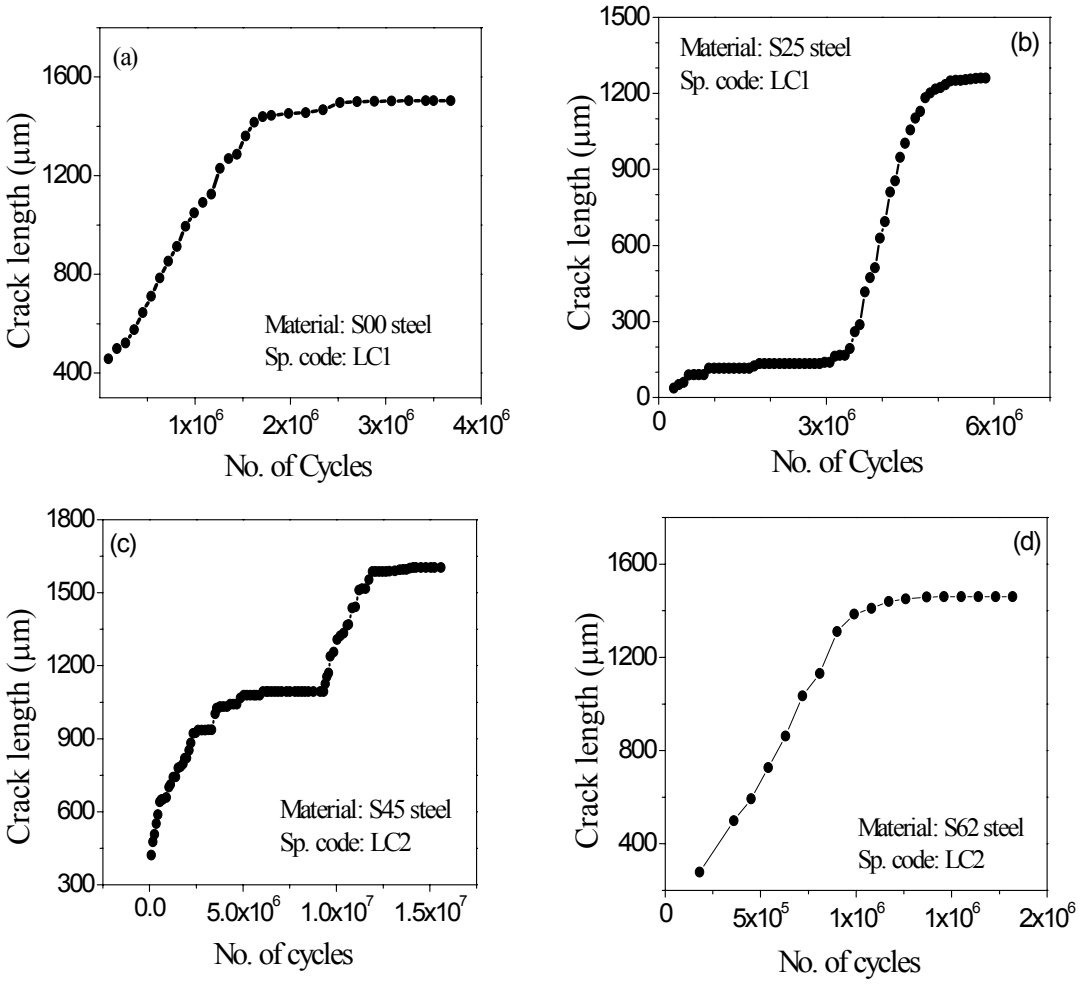

Fig.6.3 variation of crack length (a) against number of cycles (N) for different specimens of the investigated (a) S00, (b) S25, (c) S45 and (d) S62 steels.

The load shedding was carried out only when significant amount of crack growth is noticed (crack growth of the order of 100 μm at initial stages and of the order of 3 μm at near threshold was considered for load shedding). The procedure of load shedding was continued till the crack growth was found to be infinitesimal. At the lowest load the specimen was subjected to a cyclic loading duration of at least 1.08×10^6 cycles where no crack growth (i.e. the detectable limit of ≈ 1 μm) could be detected.

The stress intensity factor ahead of a crack tip depends on the geometry of the specimen crack configuration with respect to mode of loading. In this investigation the specimen is considered as single edge-notched bend type and is fixed in cantilever bending. The stress intensity factor at the crack tip was estimated following the expression suggested by Abd-Allah et. al. [234]:

$$\Delta K = \frac{M}{BW^{3/2}} f(a/W) \qquad \ldots(6.2)$$

where, M = applied bending moment = P × l

P = Applied Load

l = Distance between loading point and location of crack

B = Breadth of the specimen

W = Width of the specimen

$$f(a/W) = 1.2728 + 26.8479(a/W) - 57.6819(a/W)^2 + 88.1591(a/W)^3 \ldots(6.3)$$

The recorded data of *a vs. N* were converted to d*a*/dN *vs. ΔK* using the aforementioned procedure for estimating Δ*K* with the knowledge of load at each crack length; Δ*K* was taken as K_{max} following ASTM standard E647 [8]. The plots of d*a*/dN *vs. ΔK* for the tested specimens are shown in Fig.6.4. The magnitude of ΔK corresponding to the maximum load at which crack growth could not be observed for even 1.08×10^6 cycles is considered here as the fatigue crack growth threshold. The magnitudes of ΔK_{th} for all specimens are compiled in Table 6.3. The average fatigue threshold values for S00, S25, S47 and S62 steels are found to be as 3.8±0.1 4.2±0.1, 5.77±0.03 and 6.0±0.1 $MPam^{1/2}$ respectively.

Table 6.3 Magnitudes of ΔK_{th} for different specimens of the investigated steels.

Material	Specimen code	V (mm)	a_f (μm)	σ_{th} (MPa)	ΔK_{th} (MPam$^{1/2}$)
S00 steel	LC-1	5.00	1504	44.2	3.70
S00 steel	LC-2	5.08	1366	49.4	3.85
S25 steel	LC-1	5.02	1260	55.75	4.23
S25 steel	LC-2	5.12	1069	57.4	4.14
S47 steel	LC-1	5.00	1678	69.02	5.75
S47 steel	LC-2	5.10	1323	78.4	5.79
S62 steel	LC-1	5.10	1467	75.2	6.14
S62 steel	LC-2	5.10	1460	72.6	5.90

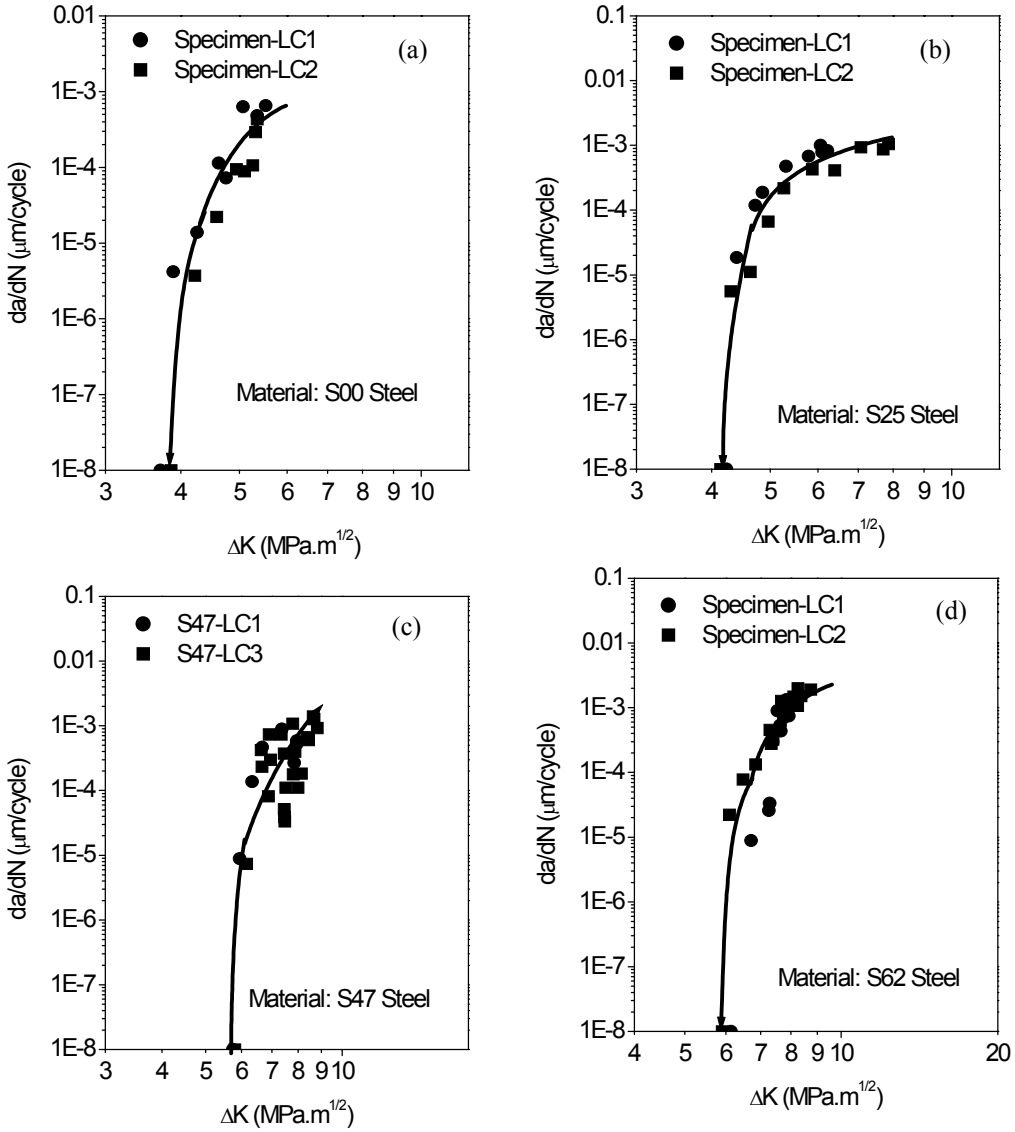

Fig.6.4 Variation of d*a*/dN with *ΔK* for the investigated (a) S00, (b) S25, (c) S47 and (d) S62 steels.

Methods of threshold measurement

The techniques for obtaining fatigue threshold (ΔK_{th}) values have been described in section 2.4. In the present investigation, determination of ΔK_{th} has been done using the standard load shedding or decreasing ΔK method. These experiments were done on pre-cracked specimens and the test-details are given in section 6.2. Load shedding is generally done either by reduction of K at constant R (decreasing ΔK by decreasing K_{max} and K_{min}), or reduction of ΔK at a constant K_{max} (decreasing ΔK by increasing K_{min}). The present study naturally follows the first method (i.e. reduction of K at constant R), because R-ratio in a rotating bending test is constant (= –1.0). The developed technique for threshold measurement follows the ASTM standard [8] with respect to load shedding, but it differs in the consideration of the specimen configuration and in the adoption of the technique for crack length measurement. The limitation of this technique is that R-ratio cannot be changed for generating fatigue data.

The rate of load shedding

The determination of fatigue threshold for the investigated materials has been carried out using the load shedding procedure. The amount of load decrement at different steps was not constant; initially load was reduced by about 10% but its magnitude was approximately 3% near fatigue threshold. The amount of load decrease for all the investigated specimens at any step was thus between 3 and 10%. Typical nature of load decrement with crack length and with number of cycles is illustrated in Fig.6.5, whereas a typical variation of ΔK with crack length is shown in Fig.6.6.

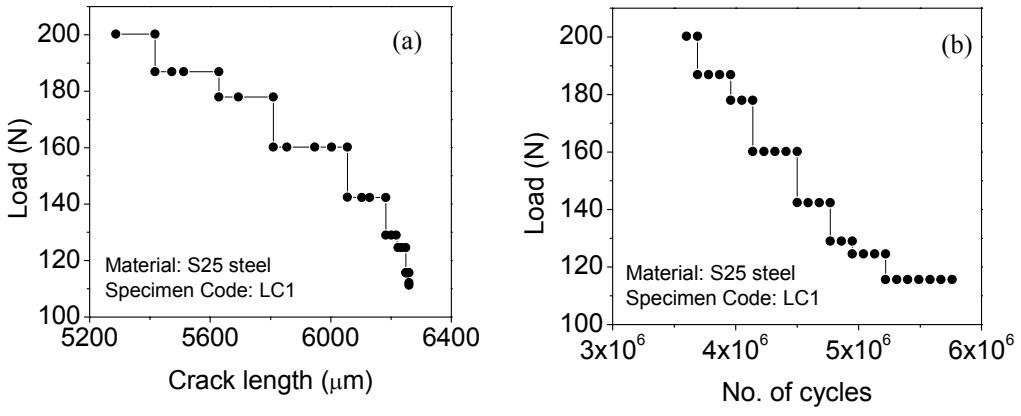

Fig.6.5 Typical nature of load decrement with (a) crack length, and (b) number of cycles.

It is clear from Fig.6.5 that crack growth is high at initial stages (order of 50 to 200 μm) and it is very low at later stages (order of 1-3 μm) for the same duration of testing. The ASTM standard E647 [8] suggests that load decrement should not be more than 10% at each step and thus the present procedure is in following this guideline.

The standard for fatigue testing [8] suggests the procedure for load shedding in terms of C-parameter, which has been defined and discussed in section 2.4. In the present investigation, the ΔK *vs. a* curve can be divided into two regimes: one for higher ΔK, termed here as regime-1, and the other for lower ΔK, termed here as regime-2, as illustrated in Fig.6.6. Considerable slope change in the ΔK *vs. a* curve occurs between regime-1 and regime-2. The magnitudes of C-parameter have been calculated using eqn. (2.21) for all samples and the estimated values were found to lie in the range of -0.07 to -0.59 mm^{-1} in regime-1 and -2.12 to -25.0 mm^{-1} in regime-2. The individual values of C-parameter for each test are summarized in Table 6.4.

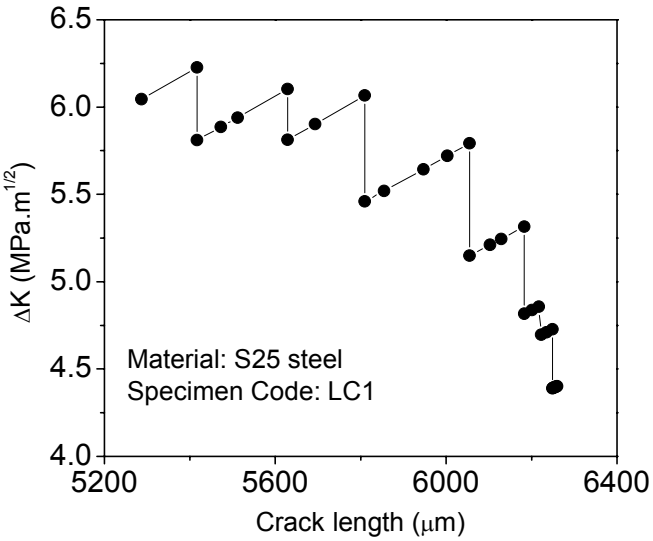

Fig.6.6 Typical variation of ΔK with crack length.

The influence of C parameter on fatigue threshold has been examined by various investigators [153-159]. Interestingly several investigators have obtained consistent results on fatigue thresholds for different C values used. Hudak et. al. [156] examined the influence of C on ΔK_{th}. These investigators observed that at high R ratio there was little change in the measured value of ΔK_{th} at different C values, but at R=0.1, the measured threshold was relatively high for the low reduction rates (C=0.02

to –0.09) and lower for the high reduction rates, up to C=-0.3. Cadman et. al. [157] also observed higher threshold values at low reduction rates. The increase in measured threshold at very low reduction rates has been popularly attributed to increased crack closure by earlier investigators [161], The phenomenon of crack closure at lower load reduction rate is considered to be caused by oxide and other debris, arising from the growth of the crack for long periods at near-threshold stress intensities. But a rational postulation for the decrease in measured threshold at higher reduction rates is lacking.

Table 6.4 Individual values of C-parameter for different specimens.

Material	Specimen code	C parameter (Regime-1)	C parameter (Regime-2)	Data range (regime-1)	Data range (regime-2)
S00 steel	LC-1	-0.59	-25.0	1-9	9-15
S00 steel	LC-2	-0.16	-17.2	1-9	9-15
S25 steel	LC-1	-0.16	-2.12	1-9	9-17
S25 steel	LC-2	-0.14	-4.19	1-9	9-19
S47 steel	LC-1	0.08	-2.03	1-7	7-15
S47 steel	LC-2	0.07	-5.21	1-11	11-15
S62 steel	LC-1	0.09	-6.47	1-9	9-13
S62 steel	LC-2	0.30	-11.46	7-10	12-19

The dependence of ΔK_{th} on ΔK-reduction rate has been shown by Brook [160] to indicate a minimum (§ Fig.2.20). The data in this diagram, however, show large variations. Presumably the effect is not so great for most materials, since using a variety of reduction rates different investigators are generally able to obtain similar results [153-156,157-159]. The standard E647 also suggests that acceptable values of C may depend on load ratio, test and environment. Values of C algebraically greater than 0.08 have been demonstrated as acceptable for use in decreasing ΔK tests of several steels and aluminum alloys tested in laboratory air over a wide range of load ratios [153,156]. Taylor [161] has recommended that, for any large testing program on a new material, a range of reduction rates should be investigated at the outset in order to understand the influence of load reduction rate on ΔK_{th}. Thus the effect of higher ΔK-reduction rate on the magnitude of ΔK_{th} needs further examination and the

recommended value of C-parameter in ASTM standard should be considered only as a guideline for a new experimental program.

In the present investigation, the values of C in regime-1 are in reasonable agreement with the order of the recommended value of -0.08 mm^{-1} [8], but the values of C for regime-2 are significantly lower compared to –0.08 mm^{-1}. The lower values of C towards the end of the experiments for determining ΔK_{th} in this study imply load reduction in terms of $d\Delta K/da$ to be faster. Imposition of slower load reduction in terms of $d\Delta K/da$ would require higher amount of crack extension at these loads but that would make the testing time unreasonably high. For example, crack growth rate at $\Delta K = 5$ $MPam^{1/2}$, for S25 specimen is found to be 1×10^{-11} m/cycle and to obtain a crack extension of 0.5 mm, as per ASTM standard would require a large number of cycles of the order of 5×10^{7}. In the present procedure threshold is considered at crack growth rate of 10^{-12} m/cycle or lower, compared to the prescribed value of 10^{-10} m/cycle [8]. Thus the developed technique indicates fatigue threshold corresponding to a considerably higher sensitivity of crack growth rate.

An alternate approach of step wise reduction of ΔK is to allow crack growth during each step to be more than the plastic zone size (at its tip) corresponding to the previous step [161]. This procedure would also take very long time to generate data at near threshold stress intensity factor range. For example, following eqn. (A.7), the plastic zone size at a ΔK of 7 $MPam^{1/2}$ for S47 steel possessing yield strength of 335 MPa, is $\approx$ 70 μm. The number of cycles required to cross this length with the crack growth rate of 1×10^{-5} μm/cycle is 0.7×10^{7}. So nearly two days would be required to get just one data point in a ΔK_{th} test with test frequency of 50 Hz. Moreover, once a crack gets extended at the crack tip, its further growth is not expected to get hindered, because the tip of a crack is the hardest location with the highest possible strain field for strain hardening materials. Considering these phenomena, load reduction has been made in the present experiments, once a crack was found to grow by a few microns near ΔK_{th} value.

On an overview it is considered that the load shedding procedure employed in the present investigation is satisfactory enough to lead to a ΔK_{th} value unaffected by the load reduction procedure.

The definition of fatigue threshold

The fatigue threshold in this investigation has been considered as the stress intensity factor at which crack growth approaches zero (i.e., below 1.0 μm, the used resolution in measurement) in 10^6 cycles. The ASTM standard [8] defines: "fatigue threshold, ΔK_{th}, is an asymptotic value of ΔK at which da/dN approaches zero". In practice, most experimental data do not show a clear asymptote even at the lowest growth rates that can be examined. A more practical definition of ΔK_{th} is the value of the stress intensity factor range corresponding to a specific growth rate, chosen to be low enough so that crack growth will be negligible for all practical situations. This definition is analogous to that of the endurance limit defined for S-N data, which do not show a clear fatigue limit. For most materials an operational, though arbitrary, definition of ΔK_{th} is given as the value of ΔK which corresponds to a fatigue crack growth rate of 10^{-10} m/cycle [8]. According to ASTM standard, ΔK_{th} is determined from a linear regression of log da/dN *vs. log* ΔK curve using a minimum of five data points of approximately equal spacing between growth rates of 10^{-09} and 10^{-10} m/cycle.

In the present technique the point of fatigue threshold has been determined by direct observation of crack growth tending. The point is considered as the one where crack does not grow even 1.0 μm for 10^6 cycles; this corresponds to a crack growth rate lower than 10^{-12} m/cycle. Thus the proposed method for the estimation of ΔK_{th} possesses higher sensitivity.

On the scatter of the estimated fatigue threshold values

The nature of variation of crack growth rate (da/dN) with stress intensity factor range (ΔK) for different specimens are given in Fig.6.4 and the estimated magnitudes of fatigue thresholds for the tested specimens are compiled in Table 6.3. The average ΔK_{th} values for S00, S25, S47 and S62 steels are found to be as 3.8±0.1, 4.2±0.1, 5.8±0.03 and 6.0±0.1 MPam$^{1/2}$ respectively. The deviations in measured threshold values are within ±0.1 MPam$^{1/2}$ for all the investigated steels. These deviations may be due to three factors: (a) errors in measurement/estimation of load, specimen-dimensions and *f(a/W)*, (b) deviation due to the procedure of estimating ΔK, and (c) deviation owing to measurement of crack length on specimen surface.

The error in ΔK_{th} due to error in measurement of input variables can be estimated in the following way:

The eqn. (6.2) can be written as

$$KBW^{3/2} = Pl\ f(a/W) \qquad \ldots(6.4)$$

On differentiation, eqn. (6.4) yields:

$$d(\Delta K) = \frac{1}{BW^{3/2}}\left(l\ f(a/W)\ dP + P\ f(a/W)\ dl + Pl\ df(a/W) - (\Delta K)W^{3/2}dB - (\Delta)B\frac{3}{2}W^{1/2}dW \right) \qquad \ldots(6.5)$$

Taking some typical values of the various parameters in eqn. (6.5) for the specimen LC2 of S25 steel, e.g.

ΔK_{th} = 4.1 MPam$^{1/2}$

P = 25 lb (112.5 N)	dP = 0.1 lb (0.45N) = 0.45×10^{-6} MN
l = 58 mm	dl = 0.1 mm
B = 12 mm	dB = 0.01 mm
W = 12.5 mm	dW = 0.01 mm
$f(a/W)$ = 11	$df(a/W)$ = 0.11 (considering 1% error)

and substituting these values in eqn. (6.5), one finds

$d(\Delta K)$ = 0.06 MPam$^{1/2}$

Deviation in threshold value due to error in measurement of load, geometrical factor and specimen dimensions is thus (0.06/4.1)×100 ≈ 1.5%.

The magnitude of ΔK_{th} for the specimen LC2 of steel S25 have been obtained at the load of 111N (25 lb). The previous load was 115.7 N (26 lb) and hence the magnitude of ΔK_{th} for this specimen has the probability to lie between any value corresponding to load ranging between 111N (25 lb) and 115.7 N (26 lb). The deviation in ΔK_{th} due to this uncertainty is termed here as procedural deviation. Since in all experiments the load shedding in the last step was 4.45 N (1 lb), uncertainty in load of 2.22 N (0.5 lb) for the determination of ΔK_{th} through eqn. (6.2) can be expected. The possible error due to this factor for specimen LC2 of S25 steel is ≈ 2%.

The crack length in a fatigue pre-cracked specimen is determined by 3 point average method [8], because the fatigue crack front is not parallel to the machined

notch. In conventional specimens [8] the crack front is concave towards the direction of crack growth; this usually indicates higher crack length at the center compared to that measured on specimen surface. A few tested samples have been broken to examine the nature of the crack front in the developed specimens. Some typical photographs of a part of the fatigue crack front around the specimen-edge are illustrated Fig.6.7. Interestingly it is noted that the fatigue crack front in the tested specimens is convex towards the direction of crack growth. These observations infer that crack length is more on specimen surface compared to that at the mid thickness of the tested specimens. The difference between the nature of crack front on tested specimens with that of conventional ones is schematically demonstrated in Fig.6.8. Some typical measurements indicated that measured crack length on the surface of a specimen is approximately 3% more than the average crack length for the specimen LC2 of S47 steel. This would result in an error in the measurement of ΔK_{th} of the order of 0.36 $MPam^{1/2}$ or approximately 5%. Hence, the total range of scatter in fatigue threshold due to the three possible variables (a), (b) and (c) as mentioned earlier could be about 8-9%.

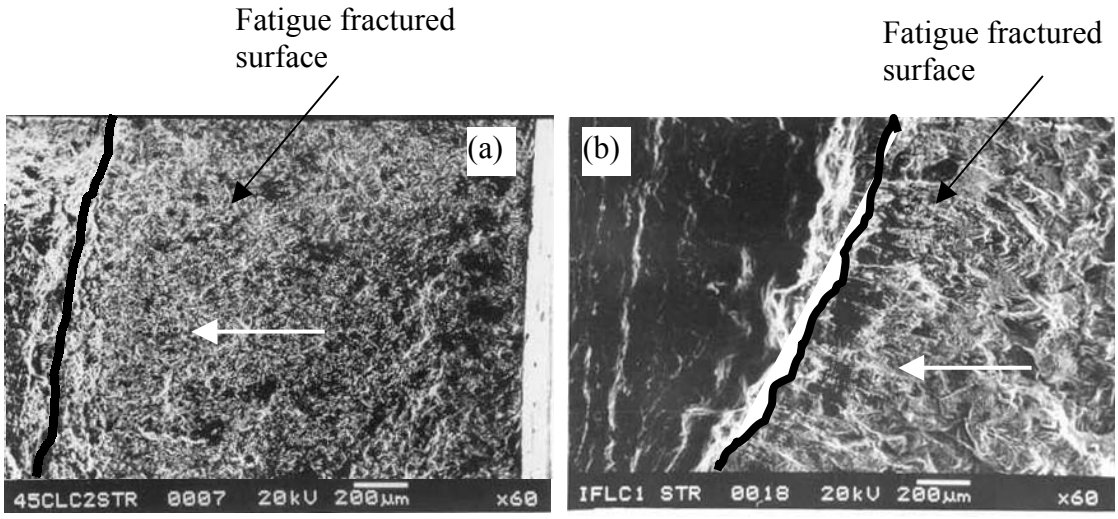

Fig.6.7 Scanning electron micrographs showing nature of crack front (marked with a black line) in a (a) S45 steel, and (b) S00 steel. Arrow indicates the direction of crack growth.

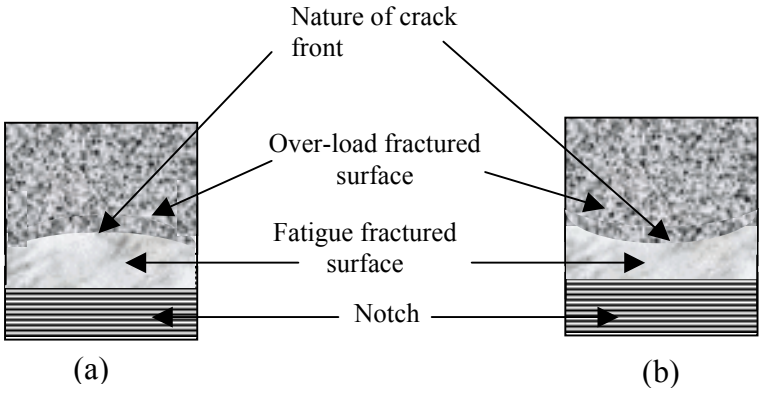

Fig.6.8 Schematic view of nature of crack front in a sample (a) tested by conventional fatigue, and (b) tested by proposed method using RBM.

But the scatter due to factor (b) and that due to factor (c) would be of opposite sign. If these deviations counteract each other, the error in ΔK_{th} should be within approximately 2% only due to factor (a). Alternatively it is expected the average value of ΔK_{th} would be associated with an error of 4-5%. The obtained results of ΔK_{th} and their scatter for all tested specimens of S00, S25, S47 and S62 are considered primarily due to factor (a). The scatter in the estimated value of fatigue threshold can also get enhanced by several other factors like microstructural differences, residual stress, change in crack tip geometry or near tip stresses influenced by crack roughness.

Comparative assessment of estimated fatigue thresholds

An attempt has been made to compare the estimated ΔK_{th} values of the investigated steels with those reported for similar materials. The reported magnitudes of ΔK_{th} values for a few steels are compiled in Table 6.5. McEvily [231] has reported that the threshold value for a low carbon steel, at R-ratio = -1.0 is 3.8 $MPam^{1/2}$. The estimated threshold value of S00 steel at the same R-ratio is in excellent agreement with the above one. In addition, for mild steel, the value of ΔK_{th} is reported [231] to decrease with increasing R-ratio; at R=0.13, ΔK_{th} = 6.6 $MPam^{1/2}$ and at R = 0.75, ΔK_{th} = 3.8 $MPam^{1/2}$. The estimated results in S00 steel can thus be considered comparable to ΔK_{th} estimated at relatively high positive R-ratio. Indirectly this observation suggests that crack closure at R = -1.0 may be insignificant.

Table 6.5 Some reported threshold values in steels.

Material	YS (MPa)	TS (MPa)	R ratio	ΔK_{th} (MPam$^{1/2}$)	Ref.
Low carbon steel	-	-	-1	3.8	[231]
0.15%C steel	280	420	0.5	4.5	[118,228]
<0.2%C steel	653	743	0.2	4.8	
0.21%C steel	255	545	0.0	5.5	[230]
Low alloy steel	-	835	-1.0	6.3	[83]
0.11%C steel	286	433	-1.0	8.12	[108]
0.11%C steel	233	402	-1.0	8.22	
Mild steel	-	530	-	6.4	[231]
Mild steel	-	430	0	6.6	
9310 steel	-	-	0.25	~6.1	[13]
	-	-	0.90	~3.3	[13]
A533B steel (0.25%C)	485	620-795	0.10	8.0	[13]
			0.30	5.7	[13]
			0.50	4.8	[13]
			0.70	3.1	[13]
			0.80	3.0	[13]
A508 steel (0.16%C)	-	-	0.10	6.7	[13]
	-	-	0.50	5.6	[13]
	-	-	0.70	3.1	[13]
Mild steel	-	430	0.13	6.6	[231]
			0.35	5.2	[231]
			0.49	4.3	[231]
			0.64	3.2	[231]
			0.75	3.8	[231]
1080 steel (0.81%C steel)	476	979	0.1	9.1	[235]
			0.7	6.0	[235]
0.15-0.20%C steel (AISI 1018)	255	441	0.05	6.2	[236]
0.33-0.38% steel (SAE 4135)	1500	1690	0.05	3.7	[236]

YS=Yield strength, TS=Tensile strength, ΔK_{th} = long crack threshold.

The reported threshold value of A533B steel (0.25%C) at R=0.5 is 4.8 MPam$^{1/2}$ [13]. And also the reported threshold value of 0.15%C steel at R=0.5 is 4.5 MPam$^{1/2}$ [118]. The estimated threshold of S25 steel (ΔK_{th} = 4.2 MPam$^{1/2}$) is in good agreement with the reported results. Pook [83] has observed that the threshold value of a low alloy steel, having tensile strength of 855 MPa, is 6.3 MPam$^{1/2}$ (at R=-1.0). The threshold value (ΔK_{th} = 6.0 MPam$^{1/2}$) of S62 steel, having tensile strength of 750 MPa, is in close agreement with the results reported by Pook. The estimated threshold of S47 steel could not be compared because of the lack of any

available ΔK_{th} data on steels of similar carbon content. The above comparative assessments of ΔK_{th} values for S00, S25 and S62 steels can be considered as apparent because fatigue data of similar materials with similar tensile properties and under similar test conditions specifically at identical R-ratios should only be taken into consideration for this type of comparison. However, the comparisons made above strongly support the appropriateness of the order of the magnitudes of the estimated ΔK_{th} values and hence the ΔK_{th} determined by the developed technique are considered satisfactory in nature. Since these values are found to be close to ΔK_{th} values of materials at a high positive R-ratio, one may also infer that these are closer to the effective threshold of a material.

The results obtained through any developed technique demand comparison with those estimated by some established or standard procedures to check their validity and reliability. The results generated on S62 steel in this investigation by the developed technique have been compared with some available results on this material generated by the standard procedure. The fatigue threshold of S62 steel has been determined by Tarafder [204] following the ASTM standard. These tests are reported to have been done on CT specimens (B=20, W=50mm) at load ratio of 0.1.

The results obtained by Tarafder [204] on S62 steel are summarized in Fig.6.9 as plots of da/dN *vs.* ΔK and ΔK_{eff} . The magnitudes of ΔK and ΔK_{eff} have been estimated by linear fitting of 5 points towards the lower end of the reported data and considering the extrapolated value at the da/dN = 10^{-10} m/cycle following ASTM standard E-647 [8]. The threshold values of S62 steel by the standard test procedure resulted in ΔK_{th} = 10.9±1.0 MPam$^{1/2}$ and ΔK_{effth} = 5.5±0.5 MPam$^{1/2}$. The fatigue threshold of this steel estimated by the present technique is 6.0±0.1 MPam$^{1/2}$ and is close in magnitude to the ΔK_{effth} value reported by Tarafder [204].

The minor difference between the estimated fatigue threshold by the developed technique and ΔK_{effth} reported by Tarafder using standard test procedure can be attributed to three possibilities: (i) the present estimate of fatigue threshold with measurement sensitivity of da/dN = 10^{-12} m/cycle assumes insignificant crack closure and so inherently considers the value to be similar to ΔK_{effth}; but some amount of crack closure may be possible. Any possible crack closure associated with the

present estimate would indicate it to be higher than the estimate of ΔK_{effth} made with the consideration of crack closure, (ii) The trend of the data presented in Fig.6.9 indicates that the d*a*/dN *vs.* ΔK_{eff} plot exhibits considerable scatter than d*a*/dN *vs.* ΔK plot. This may arise because of the uncertainties associated with the estimation of closure stress intensity factor, ΔK_{cl}. Higher estimate of ΔK_{cl} would result in lower value of ΔK_{eff} and would automatically show the ΔK_{effth} on the standard specimen to be lower than that obtained by the present technique, (iii) The present experiments have been carried out using 12 mm thick specimens whereas Tarafder [204] has used 20 mm thick specimens for determining ΔK_{th}. Any effect of specimen thickness on K_{th} may also lead to the observed difference. In short, from the above discussion on the comparison between threshold value obtained by the developed technique and that by using standard specimens, it can be inferred that the fatigue thresholds obtained in this investigation are reliable and the obtained magnitudes of threshold represent the effective threshold value. This also indirectly infers that crack closure at R = -1.0 in the investigated specimens is negligible.

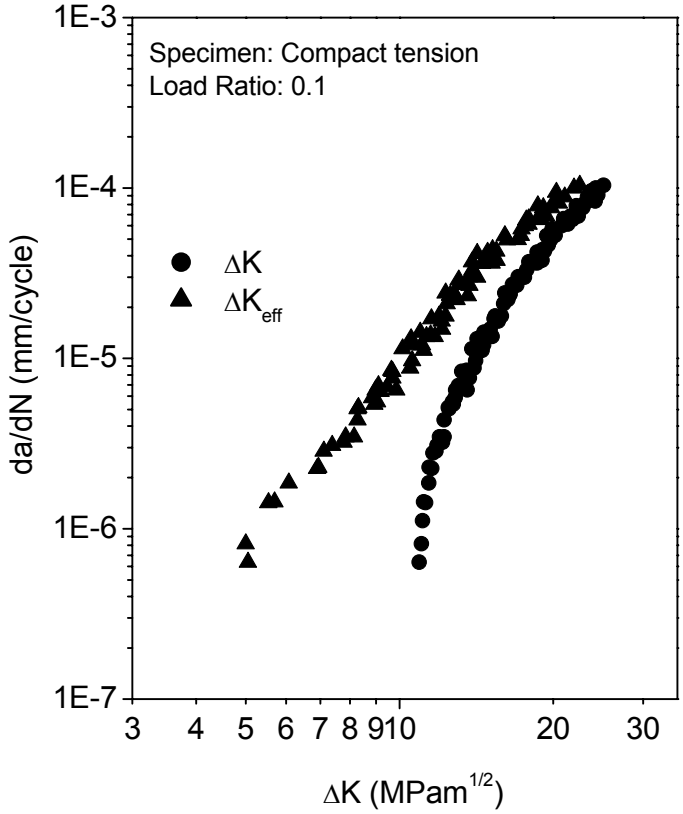

Fig.6.9 Plots of d*a*/dN *vs.* ΔK and ΔK_{eff} for S62 steel obtained following standard procedure [204].

6.3.3 Non-propagating cracks

The crack growth behaviour during the pre-cracking of the notched specimens has been examined. It was observed that the initiated cracks from a notch root get arrested after some amount of crack propagation. These cracks are referred in the literature [124,167,168,170-180] as non-propagating cracks (NPCs). The term "non-propagating cracks" has been used for cracks that grow under an applied crack driving force but come to complete arrest. A crack gets arrested ahead of a notch when the crack driving force either remains constant or marginally increases due to increase in crack length at constant stress. Thus the phenomenon of NPC can be studied by examining the variation of crack length (originated from a notch) with number of cycles at some specific stress magnitudes. The presence of NPCs in the investigated S25 steel is illustrated in Fig.6.10.

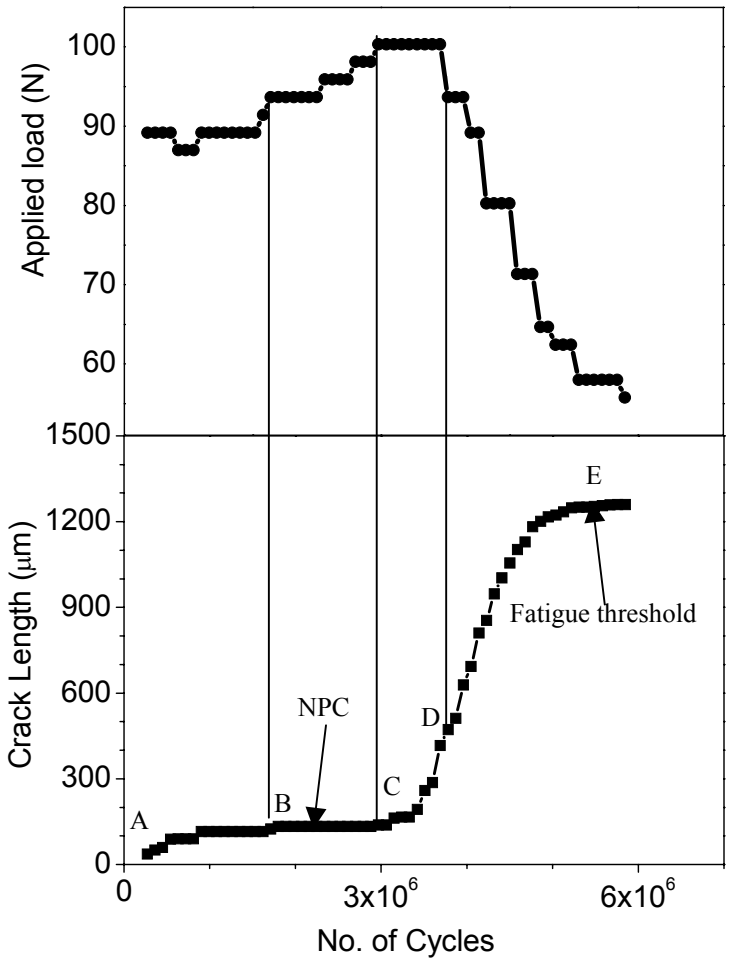

Fig.6.10 Load spectrum during crack growth in S25 steel indicating the presence of NPCs.

The variations of crack length and load with number of cycles are shown in the lower and the upper parts of this figure. The point A in Fig.6.10 represents the first observed crack after interrupted fatigue test; and the existence of NPC can be realized between points B and C. The NPCs were also encountered during pre-cracking of S47 steel specimens while determining their fatigue threshold. A typical result related to NPC of S47 steel are shown in Fig.6.11. But unlike ferrite-pearlite steels, the interstitial free steel did not indicate any NPCs within the applied stress domain.

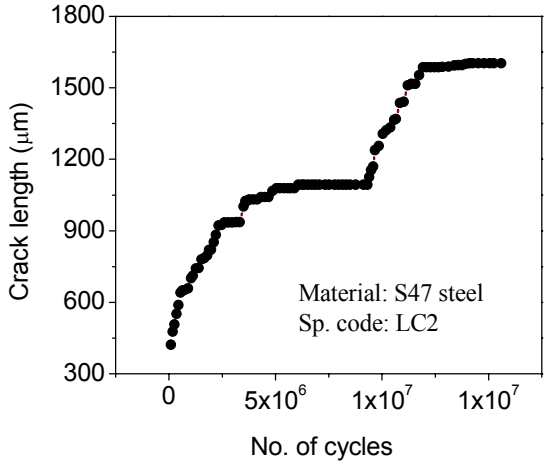

Fig.6.11 Crack growth in S47 steel indicating the presence of NPCs.

Over the past two decades several investigations have been reported on the formation of NPCs and their possible mechanisms in different materials [124,167,168,170-180]. Taira et. al. [172] observed that the extent of a region of dense slip bands near the crack tip decreases with crack length and they found a unique relation between the crack growth rate and the slip band zone size. Smith et. al. [173-175] have ascribed the crack acceleration and deceleration near the notch tip to the notch plasticity effect. Kim and Kim [168] also concluded that plasticity induced crack closure caused by compressive residual stress at the tip of the surface crack is found to be one of the major factors that give rise to the NPCs. Haddad et. al. [176,237] have described the decreasing crack growth rate with crack length for NPCs as similar to the anomalous crack growth behaviour of a small crack within the notch plasticity. Tanaka and Nakai [124] have observed NPCs in the vicinity of sharp notches in center-notched plates of low carbon steel fatigued under stress levels near the fatigue limit. Tanaka and Nakai [124] have concluded that crack

closure was the main factor responsible for the decreasing crack growth rate with crack length for a NPC near a sharp notch tip.

Sadananda and Vasudevan [180] presented a different view based on their unified approach for fatigue crack propagation that considers the existence of two origins of stress intensity factors. Total stress intensity factor, according to these investigators, consists of the sum of contribution from the remote applied stress and the local internal stress. The notch-tip plasticity contributes to the changes in the internal stresses. As the crack grows away from a notch, the contribution from internal stress decreases while contribution from applied stress increases due to increasing crack length. They have shown that non-propagation of incipient cracks occur when the total stress intensity factor falls below the long crack growth threshold value in terms of K_{max}. Yamada et. al. [170] have observed NPCs in plain carbon steels. These investigators have described the reason for the appearance of NPCs as the possible effects of residual compressive stresses associated with localized plasticity at the crack tip during cyclic loading and from the machining of pits by electro discharge machining (EDM).

Kitagawa et. al. [167], and Kim and Kim [168] have found that the formation of NPCs depends on the notch root radius of a specimen of a material. Kim and Kim [168] have found that the critical root radius for the formation of a NPC from a notch in titanium is between 0.04 and 0.06 mm. Kitagawa et. al. [167], on the other hand, have found that the critical notch root radii for the formation of NPCs in steels ranges from 0.1 to 0.6 mm depending on carbon percentage and the strength of the material.

Yamada et. al. [170], Plumtree [171] and Kim and Kim [168] have examined the length of NPCs in different materials. In 0.84%C steel Yamada et. al. observed the length of NPCs to be 580 μm and 340 μm when cracks originated from artificially induced micro-pitted specimens and from smooth specimens respectively. These investigators have attributed the occurrence of large NPCs in artificially pitted specimens to residual compressive stress associated with notch tip plasticity and that arising during the artificial pitting of specimens by electro discharge machining (EDM). They have demonstrated that the length of a NPC decreases when the residual stresses due to EDM are removed. These investigators have also reported that the length of NPCs varies in different steels. Plumtree has examined NPCs in 2024-T351

Al alloy and noted that the lengths of NPCs vary in a wide range and their magnitudes are dependent on specimen orientation. Typical lengths of NPCs in LS, LT, ST, SL, TS and TL specimens were reported as 2-435, 4-70, 2-17, 4-67, 6-8 and 5-77 μm respectively. The length of NPC in pure titanium has been noted to be nearly 900 μm by Kim and Kim, but the occurrence of such NPC depend on the critical root radius of a notch from which it originates.

Formation of NPCs thus depends on the nature of a material, applied stress, notch root radius, notch tip plasticity and internal stresses induced at the notch tip during its machining. In the present investigation NPCs have been observed only in S25 and S47 steels but this phenomenon was not encountered in S00 steel under the applied experimental conditions. An overview of the suggested mechanisms for the occurrence of NPCs in different materials by the earlier investigators indicates that notch tip plasticity is usually the major factor to give rise to NPCs. The notch tip plasticity induces compressive residual stresses at the tip of an initiated crack and thus the growth of a crack depends on the relative magnitudes of the applied stresses and compressive residual stresses. Sadananda and Vasudevan [180,225] have suggested that the notch tip plasticity induces a gradient internal stress field, and the latter interacts with the applied stress field to cause NPCs or short cracks. Experimental verification and justification for the compressive stress field, which may lead to closure, or the nature of internal stress field are not sufficient enough to generalize the exact phenomenon which leads to the formation of NPCs. It is considered here that a NPC results in due to the interaction between the primary applied stress field with a secondary stress field, which could be termed as compressive or internal stress field. The nature of the latter depends on the experimental conditions, the type of material and the geometry of the specimen being investigated. Thus the observed NPCs in S25 and S47 steels are attributed to the favourable secondary stress field due to the very nature of these materials associated with their specimen conditions.

Some of the earlier investigators have shown that there exists a critical notch root radius below which the phenomenon of NPC occurs. In the present investigation notch root radius has been kept constant as 0.25 mm for all the investigated specimens. The employed notch root radius is within the reported range (0.1-0.6 mm) of critical crack tip radius by Kitagawa et. al. [167] for the existence of NPCs in

steels. The notch root radius of 0.25mm could be more than the critical radius required for the formations of NPCs in S00 steel. The notch root radius may further increase due to crack tip blunting in a low strength material like S00 steel. Tanaka and Akinava [166] have shown that at low value of stress concentration factor (K_t) there is a small region of stress range at which NPCs would form (Fig.2.24); as K_t increases there is an increasingly large region of stress range for the formation of NPCs. In the fabricated specimens K_t is approximately 3. At this K_t value, the applied stress may not be falling in the small region of stress range required for the formation of NPCs in S00 steel. The nature of a material also affects the formation of NPCs. In addition to the specimen geometry effect, when a crack attempts to cross over from ferrite to the harder pearlite in ferrite-pearlite steels (like S25 and S47), the harder phase may act as a barrier for crack growth due to sharp localized internal stress field. Thus the microstructural condition may also be a controlling factor for the formation of NPCs in S25 and S47 steels unlike that in S00 steel.

The lengths of the NPCs were found to be 133 to 196 μm in S25 steel and 787 to 1094 μm in S47 steel. The expected lengths of NPCs, stresses and stress intensity factor ranges at the tip of NPCs are summarized in Table 6.6; the size and notch geometry for all the specimens were identical as described in section 6.2.

Table 6.6 Details of the observed non-propagating cracks in S25 and S47 steels.

Material	Specimen code	a_{npc} (μm)	P_{npc} (lb)	$\Delta\sigma_{npc}$ (MPa)	ΔK_{npc} (MPa$\sqrt{m}$)	r_p (μm)
S25 steel	LC-1	133	44	98.1	5.7	420
S25 steel	LC-2	196	52	119.4	7.0	632
S47 steel	LC-1	787	45	107.1	7.1	675
S47 steel	LC-2	1094	41	100.4	7.4	733

a_{npc} = length of non-propagating crack, P_{npc} = applied load at the length of NPC, $\Delta\sigma_{npc}$ = applied stress range at the length of NPC, ΔK_{npc} = applied ΔK at the length of NPC, r_p = plastic zone size

The estimated magnitudes of NPCs are compiled with the available values in different materials in Table 6.7. The results in Table 6.7 indicate that the lengths of NPCs vary in a wide range. The lengths of NPCs are expected to depend on the nature of a material, the applied stress, size and geometry of a notch, notch tip plasticity and

internal stresses prevailing ahead of a notch. Yamada et. al. [170] have reported that the local residual stresses around micropits increase the size of NPCs. Taylor [161] has suggested that the length of a NPC should be expected to be greater than the notch tip plastic zone size, since a crack which is contained within the plastic zone would experience cyclic loading at high stress levels of the order of the yield strength of a material. Plastic zone size in front of a notch has been calculated for the investigated materials using the expression:

$$r_p = \frac{1}{2\pi}\left(\frac{\Delta K_{npc}}{\sigma_y}\right)^2 \qquad \ldots(6.6)$$

where, r_p = plastic zone size in front of a notch, σ_y is the yield stress of material, $\Delta K_{npc} = K_t \Delta K$, ΔK is given by eqn (6.2), and K_t is taken as 3 for the investigated notch geometry. The estimated r_p values are compiled in Table 6.6. The magnitudes of NPCs in S25 steel are smaller than its notch tip plastic zone size whereas the values of NPCs in S47 steel are higher than its calculated r_p. Plumtree [171] has also observed that NPCs possess length smaller than the plastic zone size. Thus the obtained results related to length of NPCs in S47 steel is in following the suggestion of Taylor whereas that in S25 steel is in agreement with the results observed by Plumtree. It is, therefore, difficult to draw a generalized conclusion on the length of NPCs in a material.

A comparison of the threshold values of NPCs (ΔK_{npc}) was made with those of long crack fatigue thresholds (ΔK_{th}) in Fig.6.12. This indicates that the critical stress intensity factor for NPCs is larger than the long crack fatigue threshold values by 51% and 26% in S25 and S47 steels respectively. These results together with the length of the NPCs in these steels infer that higher difference between ΔK_{npc} and ΔK_{th} leads to smaller length of NPCs in a material. The absence of NPC in the S00 steel may have resulted due to unfavourable difference between ΔK_{npc} and ΔK_{th} for this material.

Table 6.7 Estimated magnitudes of NPCs values are compiled with those reported for different materials.

Sl. No.	Material	Testing details	Length of NPC (μm)
1	Pure Ti [168]	Notch root radius = 0.02 mm Rotary bending (R=-1)	900
2	2024-T351 Al-alloy [171]	R=-1, Specimen Orientation: LS	2-435
		Specimen Orientation: LT	4-70
		Specimen Orientation: ST	2-17
		Specimen Orientation: SL	4-67
		Specimen Orientation: TS	6-8
		Specimen Orientation: TL	5-77
3	0.84%C steel [170]	Rotary bending (R=-1) Artificial induced micropit	580
		Smooth specimen	340
		Annealed after insertion of micropit	107
4	0.55%C steel [170]	Rotary bending (R=-1) Annealed after insertion of micropit	42
5	0.36%C steel [170]	Rotary bending (R=-1) Annealed after insertion of micropit	172
6	0.25%C steel [current]	Rotary bending	96-133
7	0.47%C steel [current]	Rotary bending	787-1094

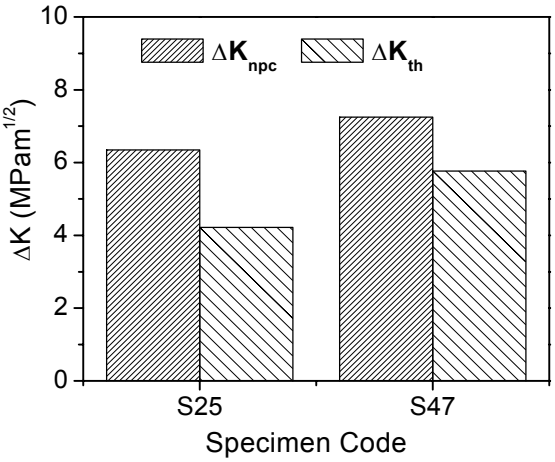

Fig.6.12 Comparison of stress intensity factor values of NPCs with those of long crack fatigue thresholds.

6.3.4 Effect of microstructure

The entire crack paths for one specimen of each of the investigated steels are shown in Fig.6.13 to Fig.6.16. Enlarged views of some typical crack-tips, where fatigue thresholds were encountered, are shown in Fig.6.17. In S00 steel, crack-tips were naturally arrested in ferrite whereas in S25 and in S47 steels cracks were found arrested either in ferrite or in pearlite. The location of crack-tip where the threshold value was encountered in these steels was found either in pearlite or in ferrite indicating no preference for microstructural features unlike that for locations where short crack thresholds have been observed (as discussed in chapter 5). These phenomena lead to infer that the crack-tip location at which the long crack fatigue threshold occurs is independent of microstructural features unlike that for short cracks.

Figure 6.18 shows the variation of fatigue threshold with change in pearlite percentage and with change in carbon content of the investigated steels. The results in Fig.6.18 indicate that fatigue threshold increases with increasing carbon content or pearlite percentage in ferrite-pearlite steels.

Quantitative relations between the length of a crack path and the amount of the different associated microstructural features (different phases or interfaces) through which a crack traverses, has not been examined earlier. Using crack profiles as shown in Fig.7.13 to Fig.7.16, the segments of a crack passing through each microstructural features were measured using an image analyzer. The results of this examination are summarized in Table 6.8, which infer that the amount of crack length passing through a specific microstructural feature is approximately proportional to its volume fraction in the investigated steel.

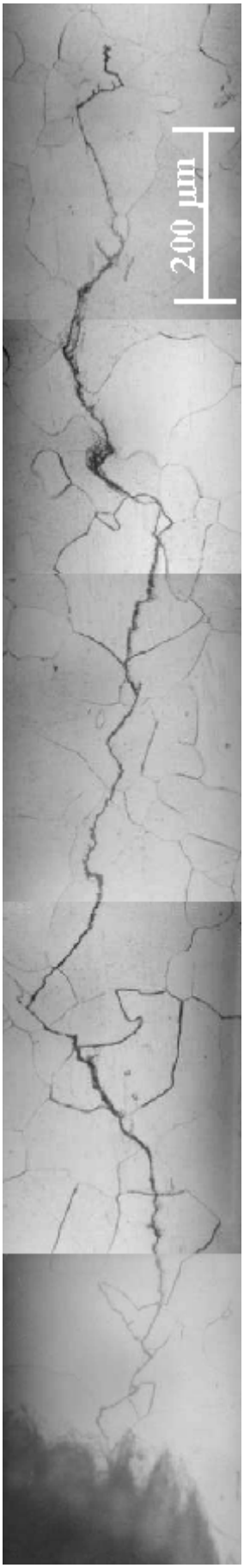

Fig.6.13 Crack path in the investigated S00 steel (Specimen code: S00-LC1).

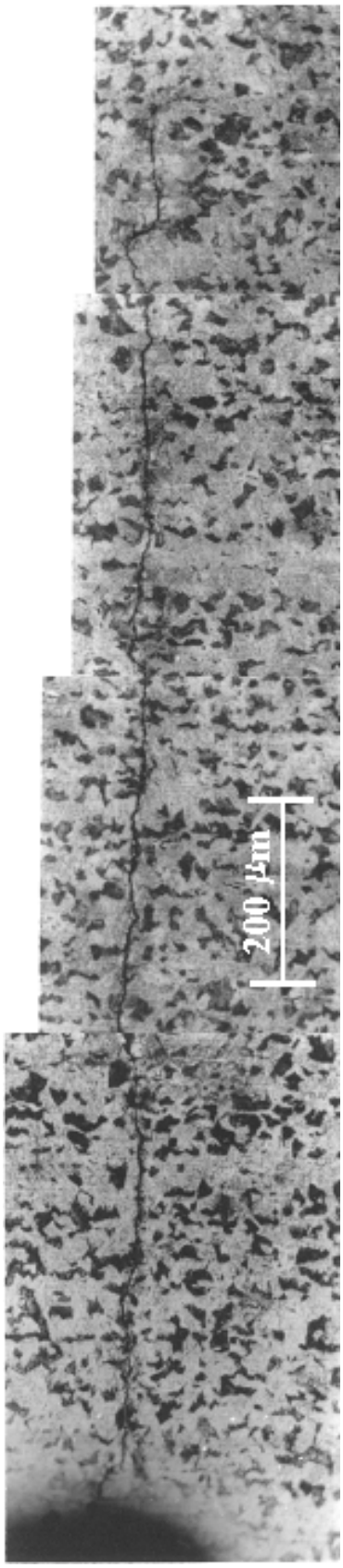

Fig.6.14 Crack path in the investigated S25 steel (Specimen code: S25-LC1).

Fig.6.15 Crack path in the investigated S47 steel (Specimen code: S47-LC1).

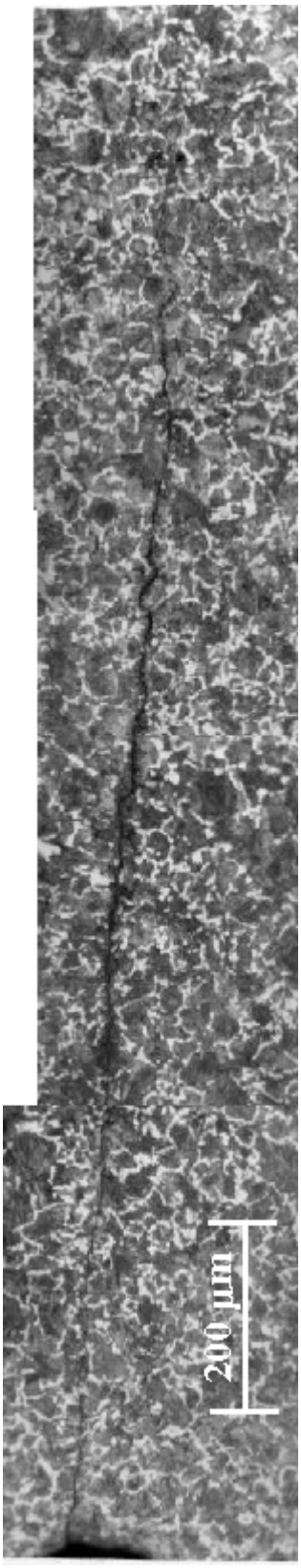

Fig.6.16 Crack path in the investigated S62 steel (Specimen do: S62-LC2).

Table 6.8 The percentage of crack passing through different microstructural features in different materials.

Material	% of crack through ferrite	% of crack through ferrite-pearlite interface	% of crack through pearlite	% pearlite in the steel
S00	100	--	--	--
S25	69	8	23	27
S47	35	13	52	63
S62	18	14	67	79

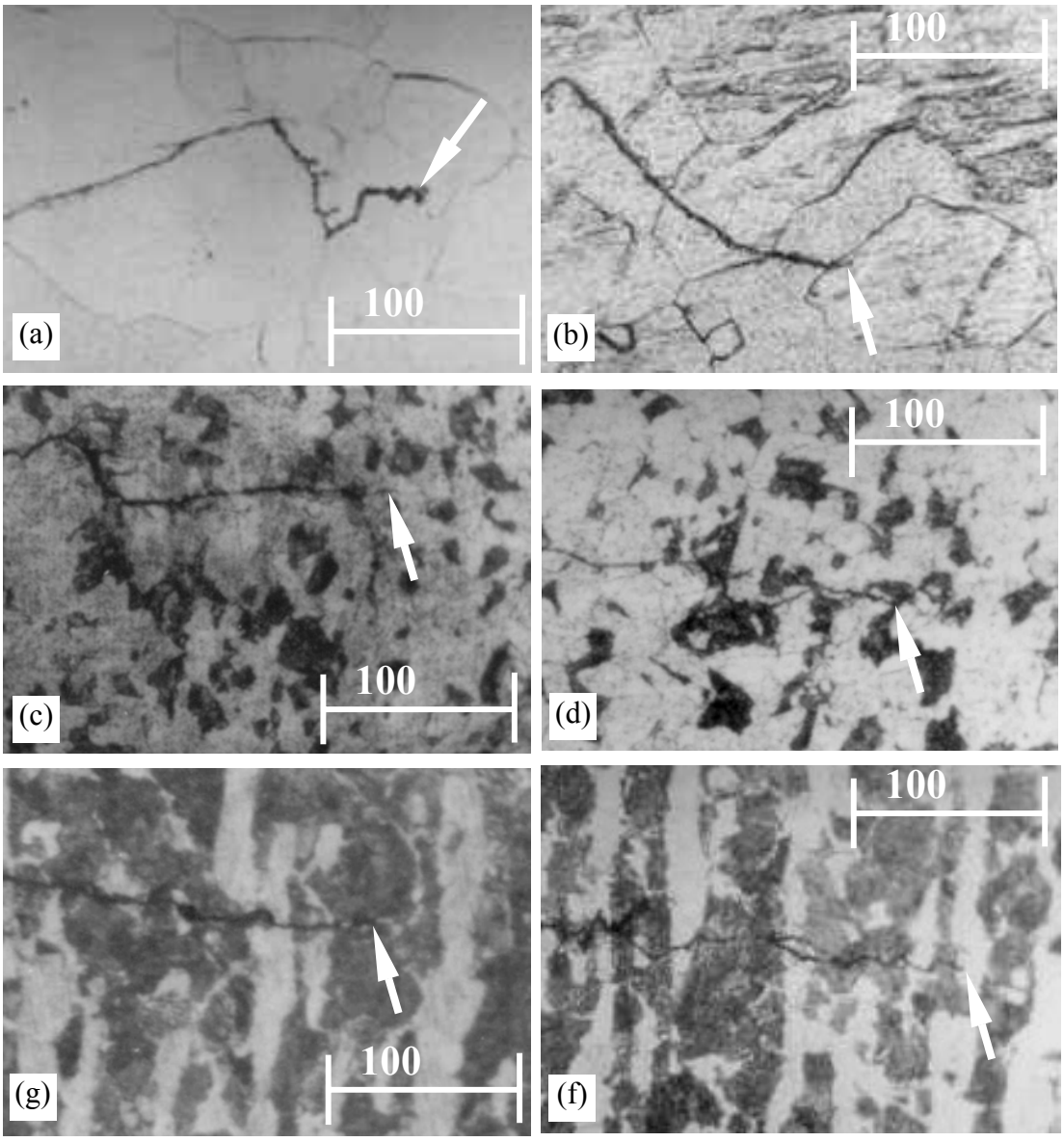

Fig.6.17 Some typical photographs showing locations of tips of cracks at the point of threshold. Arrow mark shows the tip of the crack. (a) S00 steel: inside ferrite (sp. code: S00-LC1), (b) S00 steel: inside ferrite (sp. code: S00-LC2), (c) S25 steel: inside ferrite (sp. code: S25-LC1), (d) S25 steel inside pearlite (sp. code: S25-LC1), (e) S47 steel: inside pearlite (sp. code: S47-LC1), and (f) S47 steel: inside ferrite (sp. code: S47-LC2).

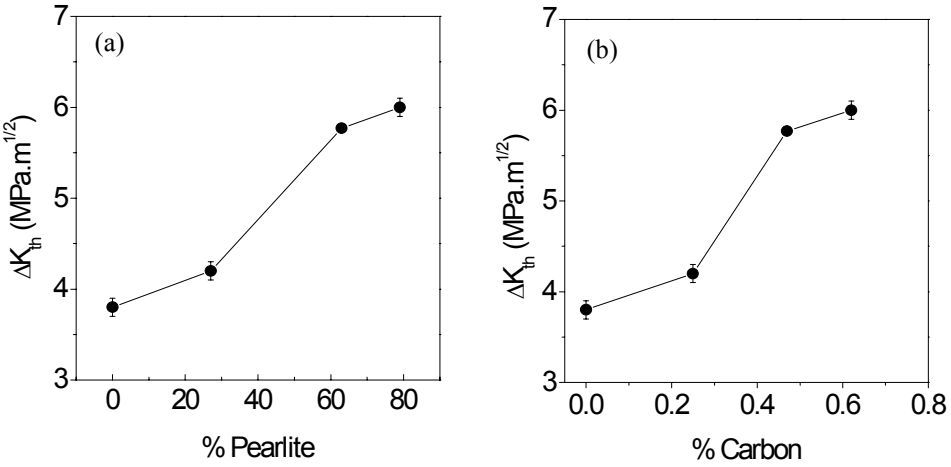

Fig.6.18 Variation of threshold with change in (a) % pearlite and (b) % carbon.

6.3.5 Fractographic examination

To examine the fractographic features on the surfaces of the fatigue cracked regions of the investigated steels, a few tested samples were broken by loading these in three point bending. The characteristics of the fatigue fractured surfaces were examined at different magnifications using SEM. The observed fractographic features in S47 and S00 steels are presented in Fig.6.19 and Fig.6.20 respectively. The domains of fatigue and overload fracture for S47 steel are distinguished in Fig.6.19(a). Higher magnification views of the fatigue and overload fracture morphology in Fig.6.19(b) and Fig.6.19(c) respectively indicate poorly developed fatigue striations and quasi-cleavage fracture for S47 steel. The fatigue striations exhibit wavy undulations, but each striation appear to resemble wavy slip lines in BCC materials as shown by an arrow in Fig.6.19(d).

Similar observations were also made on the fractured surfaces of S00 steel. The fatigue and overload fractured regions in S00 steel are illustrated in Fig.6.20(a). Figure 6.20(b) shows distinct river line marks and poorly developed fatigue striations in S00 steel. Figure 6.20(c) and Fig.6.20(d) depict typical examples of river lines fatigue striations in S00 steel at two different magnifications. The nature of the striations could be clearly revealed only at higher magnifications and is demonstrated in Fig.6.20(d).

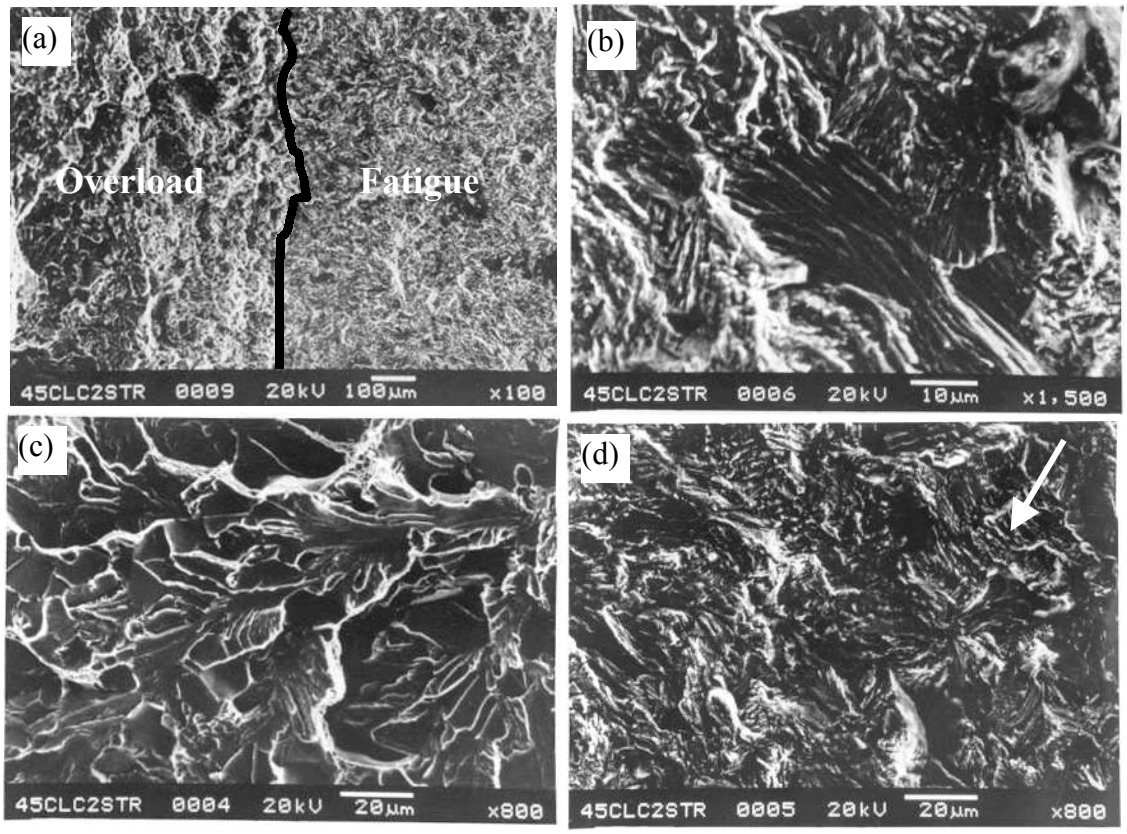

Fig.6.19 Characteristics of fatigue fractured surfaces of S45 steel: (a) the domains of fatigue and overload fracture, (b) poorly developed fatigue striations, (c) quasi-cleavage fracture, and (d) undulations associated with features similar to wavy slip lines (shown by an arrow).

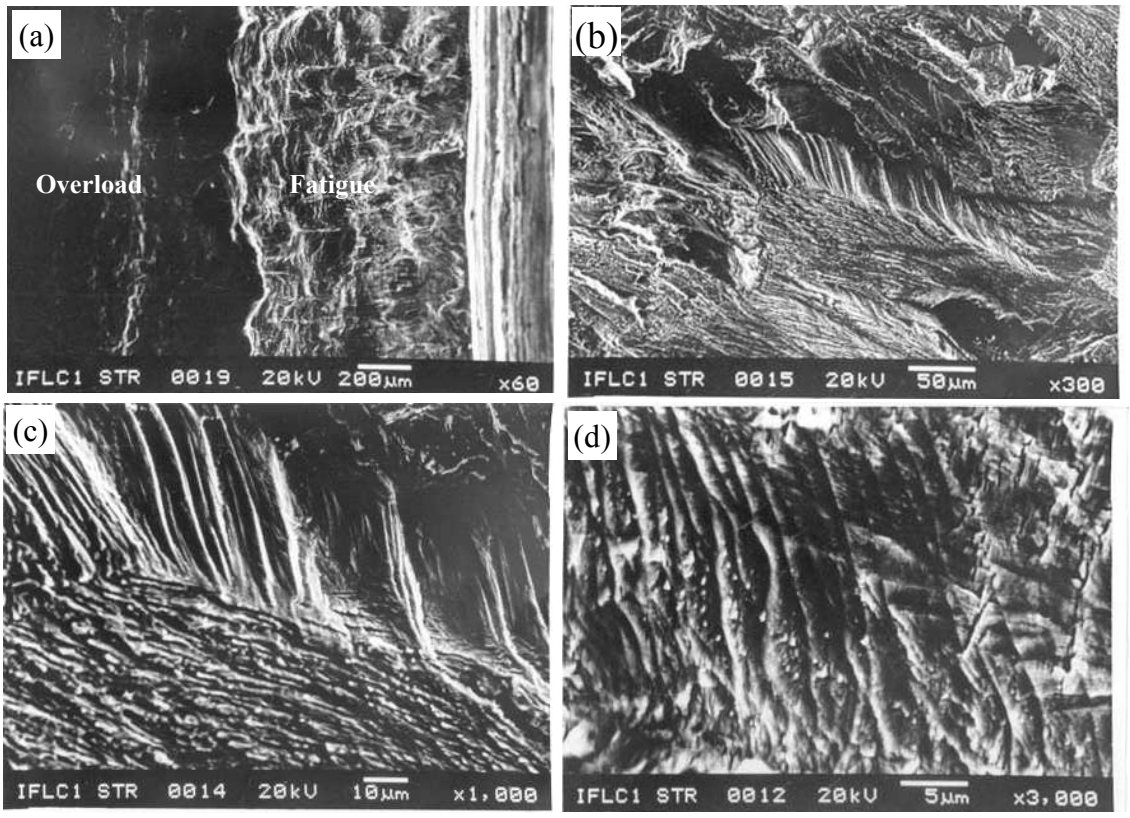

Fig.6.20 Characteristics of fatigue fractured surfaces of S00 steel: (a) fatigue and overload fractured regions, (b) river lines on a cleavage facet, (c) magnified view of a part show in (b) and (d) striations at higher magnification.

6.4 Conclusions

The major conclusions derived from the results of the investigation carried out in this chapter are:

- A reliable technique has been developed for fatigue crack growth studies using rotating bending machine with the design and fabrication of a specimen with a new configuration.
- The fatigue thresholds of four steels with carbon contents 0.003, 0.25, 0.47 and 0.62 were found to be 3.8, 4.2, 5.8 and 6.0 $MPam^{1/2}$ respectively
- The reliability of ΔK_{th} measurement with the developed technique is high as all the obtained average threshold values were found to be associated with standard deviation of $\pm$ 0.1 $MPam^{1/2}$
- The developed procedure is based on measurement of d*a*/dN with high sensitivity of the order of 10^{-12} m/cycle and the obtained threshold values appear to represent effective fatigue thresholds determined by conventional technique.
- Analysis of the crack growth behaviour near the notch indicates occurrence of non-propagating cracks only in S25 and S47 steels. The occurrence of non-propagating cracks has been attributed qualitatively to the nature of some secondary stress field present at the crack tip.
- Fatigue threshold at R = -1 for plain carbon steels increases with increasing carbon content or with increasing pearlite content.
- The sum of the segmental lengths of a crack passing through different constituents in a microstructure is approximately proportional to the volume fractions of the constituents in the investigated steels.

Chapter 7

A phenomenological model for short fatigue crack growth rate

7.1 Introduction

Considerable emphasis has been laid over the last two decades to understand the nature, as well as the mechanics, mechanism and microstructural interactions of short cracks in structural materials. These cracks are known to exhibit higher growth rate compared to that predicted by Paris-Erdogan type equation [9] at a nominal stress intensity factor range and are known to be capable of propagating below the threshold stress intensity factor range ΔK_{th}, for long cracks. As discussed in chapter-2, a unique generalized physical phenomenon is considered insufficient to distinguish these from the long cracks. Short crack behaviour is anticipated: (a) when cracks are comparable in length to the scale of local plasticity, (b) when cracks are small in length with respect to some microstructural parameters and (c) when cracks are long in terms of microstructural parameters and local plasticity, but still exhibit higher growth rate. The short cracks under category (a), (b) and (c) are usually referred [238] as 'mechanically short cracks', 'microstructurally short cracks' and 'physically short cracks' respectively as schematically illustrated in Fig.2.8. The possible reasons that are often attributed to the anomalous behaviour of short cracks are: (i) failure to achieve crack closure, (ii) sensitive interaction with microstructure, (iii) deviation from mode-I loading in micro-scale and (iv) breakdown of similitude concept [41]. The varied definitions and the multiple reasons inherent in describing the characteristics of short cracks have led to the development of a number of models; but a unified picture is yet to crystallize.

The existing models [107,137-142,144] for describing short crack growth behaviour consider different physical parameters. These are: (a) the distance between the tip of a short crack and the immediate neighboring barrier [137,138,144], (b) the deflection of a crack for its further growth after it crosses a barrier [107,138], (c) the number of barriers a short crack has to overcome before its length reaches the size of the transient crack [141,142], (d) the crack closure effect [123,143,144] etc. The

existing models are capable of predicting experimental short crack growth data to a reasonable extent. But their applicability at times may be questionable because these do not account some significant aspects of short crack propagation. For example, the mean plane of a short crack may have considerable deviation from the perpendicularity with respect to the loading axis or the tip of a propagating short crack may experience variable surface characteristics in terms of defect population. These aspects may be significant particularly for physically short cracks rather than for microstructurally short cracks.

In this part of the investigation, a model has been suggested for the growth of physically short cracks considering primarily the possible deviation of the mean plane of a short crack with respect to its loading axis. The model also accounts the possible variation in the crack-tip material characteristics till it reaches a transition crack length (a_o). The effect of the new factors, considered in this model, has been illustrated using several simulated results. The applicability of the model to the generated short crack growth data and to some available experimental data highlights its potential.

7.2 The proposed model

The sequential development of the proposed model is discussed in the following subsections. The limitations of existing models to describe short crack growth behaviour precedes the proposition of the model based on the two new considerations.

7.2.1 Some limitations of the existing models

The existing models which attempt to describe short crack growth behaviour have taken into account several physical phenomena to describe the acceleration and deceleration of short crack growth behaviour. The predictions by these models are schematically shown in Fig.7.1. But two significant factors have not been systematically taken into account in the existing models for predicting short crack growth. First the nucleation and growth of a short crack can not be implicitly assumed to occur perpendicular to the loading direction. This is evident from the fact that crack initiation usually occurs at an angle of 45^o with respect to the loading axis. When the growth of such cracks gets retarded at a barrier and the subsequent movement takes place with some deflection, the mean crack plane can be considered to remain at some

fluctuating angle to the direction of the applied load. As a consequence, the tip of a short crack is not governed by pure mode-I loading and one should consider the influence of mixed mode loading for the growth of short cracks. A few earlier investigations related to short crack growth do deal with mixed mode phenomenon [239,240], but the present consideration is different in the fact that the mean plane of a short crack gets subjected to varying deviations with respect to the loading axis along its path.

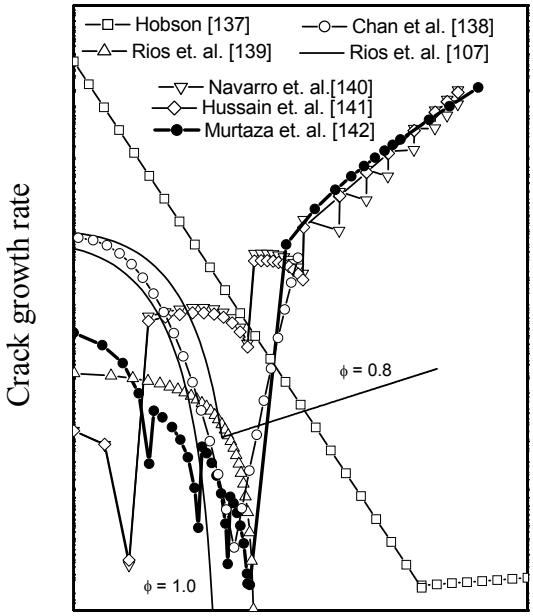

Fig.7.1 A schematic view of acceleration and deceleration of short crack growth rate predicted by the earlier models.

Secondly short cracks are generally considered to nucleate inside slip bands. The stress field around the tip of a short crack may vary from that prevailing inside the bulk of a specimen or in surface domains far away from the short crack tip. The difference in the surface stress level from that of the bulk of a specimen is due to micro-notches. The magnitude of surface stress at regions around the tip of a short crack gets considerably influenced by differential plastic deformation. A specimen surface can be assumed to possess a specific density of dislocations prior to crack initiation. But initiation and subsequent growth of short cracks can be considered to alter the line defect density around the crack tip on the specimen surface by their annihilation and/or multiplication. The alteration of the defect density at the surface would naturally influence the crack growth rate.

7.2.2 Phenomenological considerations in the proposed model

The discussion related to the physical phenomena in the preceding section demands consideration of two major aspects. These are: (a) dynamic variation in the mean angular orientation of a short crack with respect to the loading axis, and (b) variation in surface characteristics ahead of a short crack tip in a specimen when the crack extends. These two phenomena henceforth would be referred as 'mixed mode factor' (ξ) and the 'surface energy factor' (ψ) for convenience of discussion in the subsequent sections.

7.2.3 Model based on mixed mode factor

It is well established that a fatigue crack usually initiates along the plane of maximum shear stress [1], which is oriented at an angle to the direction of the applied cyclic loading. The growth of a crack immediately after its initiation is referred here as stage-I*a* to distinguish it from the three stages of crack growth for long cracks, especially stage-I in Paris-law. It is assumed here that the end of stage-I*a* overlaps with the starting position of stage-I in a d*a*/dN vs. ΔK plot. In stage-II (of Paris-law), a crack is considered to propagate with its mean plane perpendicular to the direction of the applied load in mode-I loading. While stage-II crack growth is dictated by only mode-I loading, the stage-I or below threshold (stage-I*a*) crack growth may remain under mixed mode loading. It may be considered that there exists a gradual transition from mixed mode loading to mode-I loading and the nature of this transition distinguishes short crack growth from long crack growth behaviour. Alternatively once a crack length attains a size which exhibits stage-II crack growth, the effect of mixed mode loading becomes insignificant, and a crack grows only due to K_I. The rate of this change can be gradual or fluctuating in nature depending on the crack profile. Considering θ to be the angle between the loading axis and the mean crack plane, the above phenomenology indicates short crack growth when $\theta < 90^o$ unlike that for the growth of long crack when $\theta = 90^o$. The mixed mode short crack growth behaviour is differentiated from mixed mode long crack growth with the condition that θ varies along the short crack profile whereas it possesses a constant value in the latter.

The regimes of short and long cracks described in terms of $\theta < 90^o$ and $\theta = 90^o$, imply that the contribution of applied stress gets divided into two crack

driving forces K_I and K_{II} for short cracks. Thus the estimation of ΔK in a fatigue cycle for short cracks would not be identical to the conventional calculation of ΔK for long cracks. It is considered here that the short crack growth derives some crack driving force below the transition crack length or the fatigue threshold because it is under mixed mode loading. This condition can be mathematically expressed as:

$$\Delta K_{eff} = \Delta K(1-\xi) = \Delta K\left(1-\xi_o \frac{a}{a_o}\right) \qquad \ldots(7.1)$$

Equation (7.1) indicates that the effective stress intensity factor differential (ΔK_{eff}) is minimum when a crack length 'a' attains the value of 'a_o'; this is the condition for the threshold condition for long cracks i.e., at $a \rightarrow a_o$, $\Delta K_{eff} = \Delta K_{th}$. The constant ξ_o is considered as a function of mode mixicity factor or the orientation of a crack with respect to the loading axis. Several trial and error formulations to incorporate mode-mixicity factor, ξ_o, leads to a formulation of ΔK_{eff}, which can describe short cracks growth as:

$$\Delta K_{eff} = \Delta K\left[1-(2/\pi)\left\{\tan^{-1}(K_{II}/K_I)\right\}(a/a_o)\right] \qquad \ldots(7.2)$$

where
$$K_I = \sigma\, Sin^2\theta \sqrt{\pi a} \qquad \ldots(7.3)$$

$$K_{II} = \sigma\, Sin\theta\, Cos\theta \sqrt{\pi a} \qquad \ldots(7.4)$$

The function $\tan^{-1}(K_{II}/K_I)$ is commonly known as the mode mixicity factor [141]. The mode mixicity factor is zero in pure mode-I loading and is $\pi/2$ in case of pure mode-II loading. Considering a short crack under mixed mode loading, the crack growth rate can be expressed as:

$$da/dN = C[\Delta K(1-\xi)]^m \qquad \ldots(7.5)$$

where
$$\xi = (2/\pi)\left[\tan^{-1}(K_{II}/K_I)\right](a/a_o) \quad \text{for } a < a_o, \qquad \ldots(7.6)$$

$$\xi = 0 \quad \text{for } a \geq a_o$$

The applicability of eqn. (7.5) is illustrated with a series of computations for different short cracks, which exhibits varied initial angular deviations between the crack plane and the loading axis in Fig.7.2.

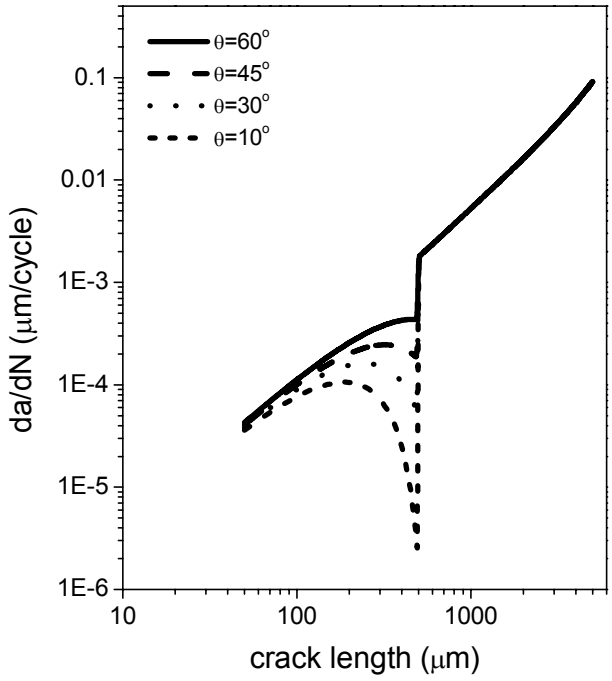

Fig.7.2 Effect of mode mixicity factor on short crack growth.

One can note the similarity in the nature of variation of crack growth rate against crack length in the present results and that predicted by Navarro et. al. [140] and Murtaza et. al. [142] by comparing Fig.7.1 and Fig.7.2. But the present results (Fig.7.2) describe a gradual deceleration of the short crack till threshold unlike the fluctuating crack growth rate predicted by Murtza et. al. in the short crack regime. The variation of crack growth rate beyond long crack threshold predicted by both the approaches is similar. The difference in the crack growth rate between the one predicted by the present formulation and that given by the earlier work [140,142], originates from the nature of the theoretical simulation. In the simulated results shown in Fig.7.2 it has been considered that ξ monotonically increases with short crack length, having a constant value of ξ_o; the latter implies a fixed angular deviation of the mean plane of the short crack assumed in the calculation. In reality the mean plane of a short crack fluctuates during its growth and hence initial θ value assumed in a simulation has to be altered following the profile of the crack. This is expected to yield the crack growth rate fluctuations in the short crack regime. One may note that the physical parameter incorporated for predicting the short crack growth in the present model takes into account the nature of the crack profile, whereas that incorporated in the models by Navarro et. al. [140], Hussain et. al. [141] and

Murtaza et. al. [142] is the barrier distance between the crack-tip and the nearest obstacle (a grain boundary or a precipitate etc.).

7.2.4 Model based on surface energy factor

When a specimen is subjected to cyclic loading, stresses at the surface of a specimen are different than that prevailing inside its bulk. This leads to differential plastic deformation from the exterior to the interior of a specimen as well as from the crack-tip to regions away from it on the surface. The nature of variation of stress on the surface of a specimen can be attributed to plane stress condition and the existence of micro-notches; these factors would enhance plastic deformation on the specimen surface. A specimen surface possesses a specific density of dislocations prior to crack initiation. But initiation and subsequent growth of short cracks can be considered to alter the initial defect density on the surface by processes like annihilation and multiplication of dislocations, redistribution of vacancy dipoles on crack surfaces etc. These phenomena would influence the growth of short cracks. It is *a*-priori considered that such defect interaction with the crack-tip is significant only for small cracks and that its extent varies with the growth (or size) of short cracks. This aspect is termed here as 'surface energy factor (Ψ)' and its magnitude is assumed as an exponential function of the relative crack length with respect to transition crack length. The rate of decrease of surface energy factor with increase in crack length may be expressed as:

$$\psi = \left[\exp\left(\frac{a_o - a}{a_o}\right)\right] \qquad \text{for } a < a_o, \qquad \ldots(7.7)$$

$$\psi = 1 \qquad \text{for } a \geq a_o \qquad \ldots(7.8)$$

Considering surface energy factor, the crack growth rate can be expressed as:

$$da/dN = C(\Delta K)^m (\psi)^n \qquad \ldots(7.9)$$

where, n is a constant like m and C.

The nature of short crack growth predicted by the eqn. (7.9) is illustrated in Fig.7.3. The results in Fig.7.3 indicate that by increasing the exponent of surface energy factor, n, the crack growth rate increases. In stage-I*a*, 'ψ' has similar effect on the predicted nature of the variation of crack growth against crack length (Fig.7.3) like that of ξ (Fig.7.2). In the latter case (ξ-effect) the crack growth decelerates to a minimum value and then jumps to stage-II crack growth. But in the former case

(ψ-effect) crack growth rate slowly decelerates and directly merges with stage-II crack growth. The predicted results of short crack growth rate considering only surface energy factor are also similar in nature to those predicted by earlier investigators [140-142].

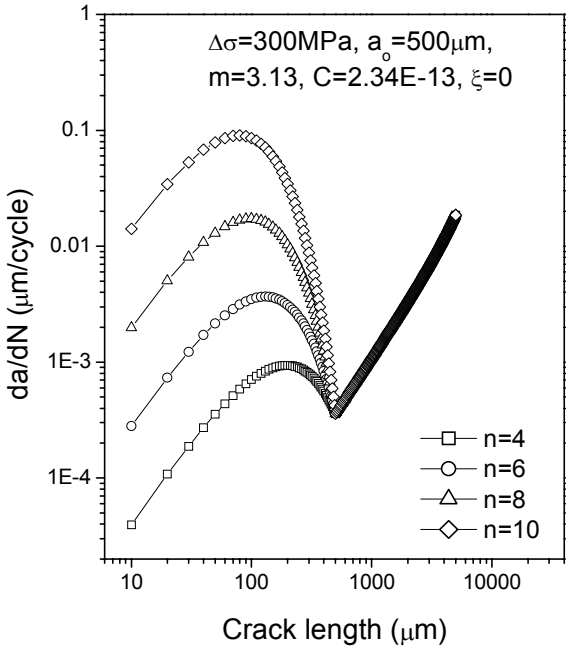

Fig.7.3 Effect of surface energy factor on short crack growth.

7.2.5 Model based on combined 'mode mixicity' and 'surface energy factor'

The mode mixicity and the surface energy factor simultaneously influence the growth of a short crack. Thus the effects of both these factors should be concurrently taken into account to obtain a model for short crack growth. Incorporating both 'mixed mode factor (ξ)' and the 'surface energy factor (ψ)', through eqn. (7.5) and eqn. (7.9), the proposed model can be written as:

$$da/dN = C\left[\Delta K\left(1-\xi\right)\right]^{m}\left(\psi\right)^{n} \qquad \ldots(7.10)$$

For LCG: $a \geq a_o$, $\xi = 0$ and $\psi = 1$

For SCG: $a < a_o$, $\xi = \left(2/\pi\right)\left[\tan^{-1}\left(K_{II}/K_{I}\right)\right]\left(a/a_o\right)$

$$\psi = \left[\exp\left(\frac{a_o - a}{a_o}\right)\right]$$

The crack growth rate predicted by eqn. (7.10) is shown in Fig.7.4 for varying values of ψ with constant ξ and assuming C = 2.34×10^{-13}, m = 3.13, a_o = 500 μm and n = 0.5m to 2.0m. The results in Fig.7.4 depict trend of crack growth rate similar to that predicted by most of the earlier models as illustrated in Fig.7.1. But the results in Fig.7.4 do not indicate any fluctuating crack growth rate in stage-I*a*.

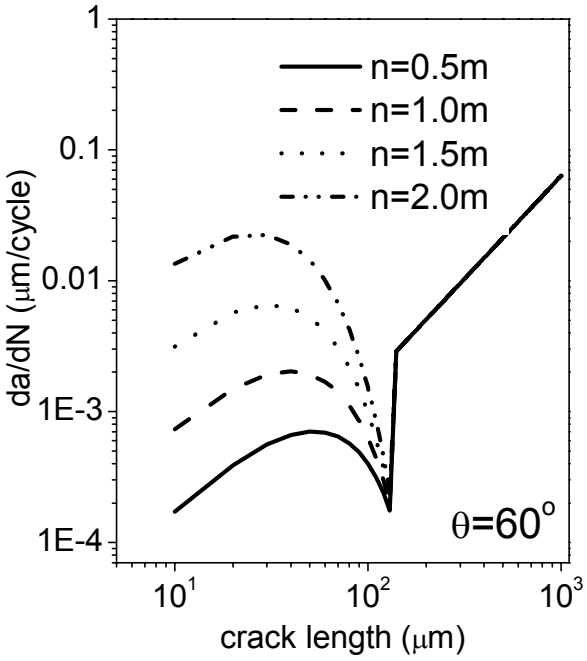

Fig.7.4 The crack growth rate for varying values of ψ with constant ξ.

The smooth variation of d*a*/dN vs. *a* in Fig.7.4 is due to the inherent consideration that the orientation of the mean plane of a crack with respect to loading axis remains constant. In reality as short crack extends with varied deflections at the barriers that it encounters, the orientation of its mean plane should also vary. Assuming θ to be randomly varying between 0 to 90° in stage-I*a*, another crack growth data was simulated in Fig.7.5. The fluctuating behaviour of short crack in Fig.7.5 unlike that in Fig.7.4 leads to the inference that variation in mode-mixicity during short crack growth can explain its characteristic behaviour. The major difference of the proposed model from the existing ones is that it considers the nature of the crack path rather than the microstructural barriers.

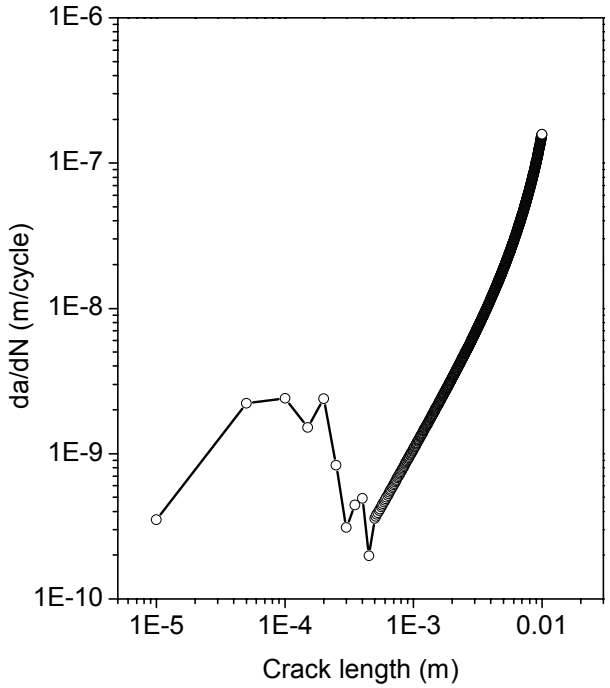

Fig.7.5 The proposed model describing fluctuating behaviour of short crack growth.

7.3 Proposed model vis-à-vis generated experimental data

An attempt has been made to describe the generated short crack growth data of the investigated steels (as discussed in chapter 5) by the proposed model. The description of the short crack growth behaviour by the present model requires the magnitudes of m, C, n and ξ of eqn. (7.10). The magnitudes of ξ can be obtained from the knowledge of a_o and θ following eqns. (7.3), (7.4) and (7.6). The Paris law constants, m and C, have been estimated by a linear fit of the data in the long crack regimes of log d*a*/dN *vs.* log ΔK curves. The slope and the intercept of the fitted line yielded the value of m and C respectively. The magnitudes of θ have been measured from the obtained crack paths with the help of an image analyzer. The transition crack length (a_o) has been obtained from the analyses of the experimental data as mentioned in chapter-5. The applied stress for crack growth and the estimated Paris law constants (m and C), a_o and θ values of the investigated materials are compiled in Table 7.1. The only unknown parameter in the eqn (7.10) was thus the value of 'n'. A series of d*a*/dN values were simulated with different values of n (between 0.2m to 4m at intervals of 0.1m) and the known magnitudes of the other parameters shown in Table 7.1. Next for each value of m, the magnitude of ∑ was estimated where ∑ is given as:

$$\sum = \sum \left[\left(\frac{da}{dN} \right)_{simulated} - \left(\frac{da}{dN} \right)_{experimental} \right]^2 \quad \ldots(7.11)$$

The value of n at which $\sum$ is found to be minimum is considered to describe the experimental results in the best manner. The obtained n values for the three investigated steels are also shown in Table 7.1. The graphical description of the experimental data of short crack growth by the proposed model are depicted in Fig.7.6 for S00, S25 and S47 steels.

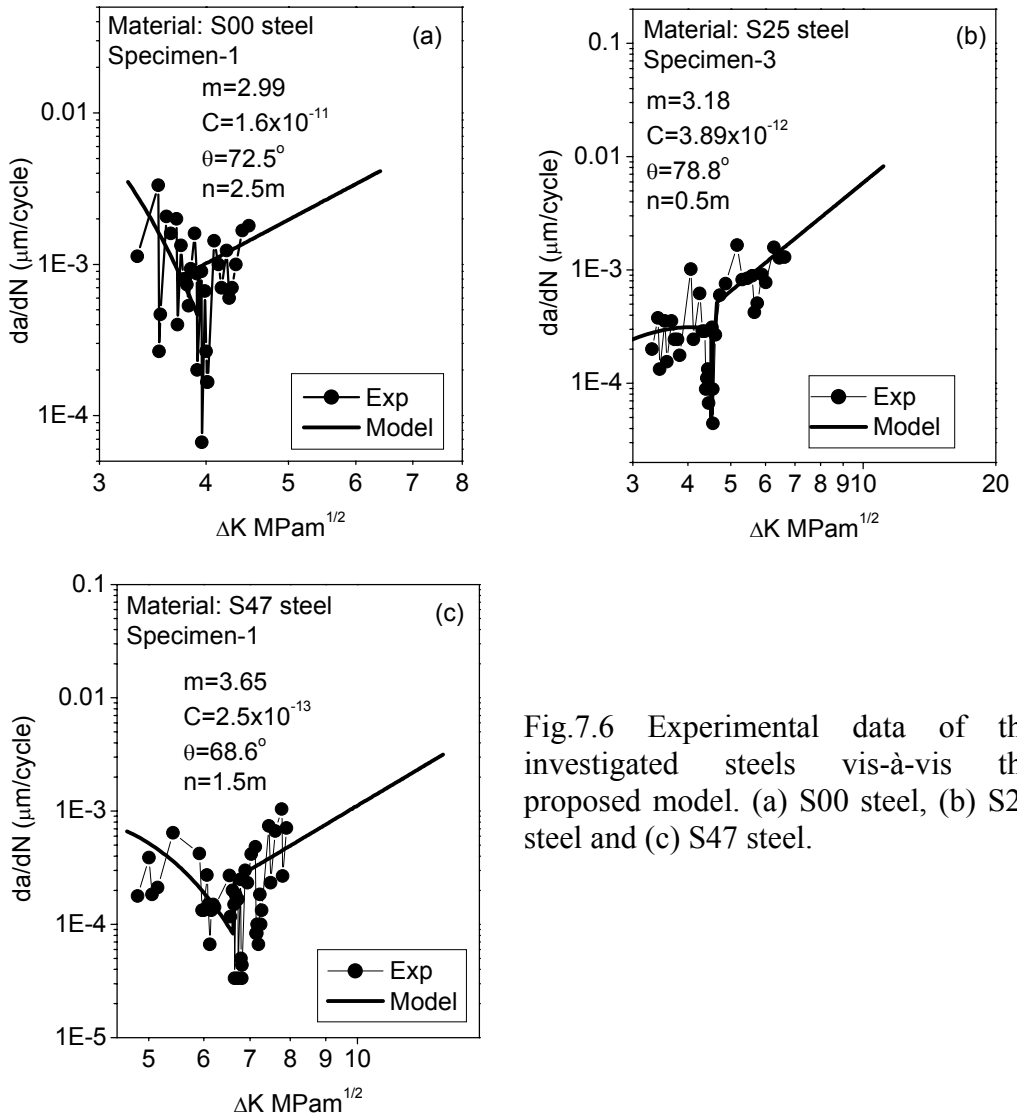

Fig.7.6 Experimental data of the investigated steels vis-à-vis the proposed model. (a) S00 steel, (b) S25 steel and (c) S47 steel.

Table 7.1 Parameters of short crack growth model for the investigated steels.

Material	Paris law constant (m)	Paris law constant (C)	a_o (μm)	Applied stress (MPa)	θ (degree)	n
S00	2.99	3.89×10^{-11}	1160	81.5	72.5	2.5m
S25	3.18	3.89×10^{-12}	540	141.5	78.8	0.5m
S47	3.65	2.5×10^{-13}	898	156.8	68.6	1.5m

7.4 Proposed model vis-à-vis some reported data

The applicability of the proposed model is also illustrated in this section with the help of an available set of experimental data of 'd*a*/dN vs. *a*' reported by Murtaza and Akid [142]. The experimental data is known to have been generated for 0.56%C low alloy steel using fully reversed torsional loading on smooth hourglass type specimen at an applied stress = 1106 MPa. At the outset the 'd*a*/dN vs *a*' data were converted to 'd*a*/dN vs. ΔK' using the stress intensity factor expression suggested by Newman and Raju [146]. This expression is:

$$K_I = \left(\sigma_t + H\sigma_b\right)\sqrt{\pi\frac{a}{Q}} \quad F\left(\frac{a}{t},\frac{a}{c},\frac{c}{b},\phi\right) \qquad \ldots(7.12)$$

where σ_t = remote uniform tension stress, σ_b = remote uniform bending stress on outer fiber, *a* = depth of surface crack, c = half length of surface crack, t = plate thickness, b = half width of cracked plate, ϕ = parametric angle of the ellipse and Q = shape factor for elliptical crack. Details of the parameters used in this expression are available in the original report [146]. The entire experimental data of 'd*a*/dN *vs*. ΔK' was categorized into three regimes as, A to B (Stage-I*a*), B to C (Stage-I), and C to D (Stage-II) depending on the nature of the data. The Paris-law constants 'm' and 'C' were first calculated from long crack growth experimental data (regime C to D) and the values were obtained as m = 3.13 and $C = 2.34\times10^{-13}$. Next a series of calculations were done considering different values of 'θ' to predict the data in stage-I*a* assuming n = 2m. The proposed model well describes the experimental data when θ is 60^o as shown in Fig.7.7.

The proposed model attempts to describe both short and long crack growth, but it has several limitations: (a) the variation of the mean crack plane has been

assumed to alter in monotonic way, (b) the expression to describe the variation of surface energy factor in its present form does not correlate with any physical parameter related to variation in surface defects and (c) it does not exhibit multiple short crack thresholds or fluctuations in the d*a*/dN values. The possibility of describing the fluctuations in the short crack growth data exists as shown by some typical calculations in Fig.7.5. Further refinement of the proposed model with respect to correlations between ξ and ψ with physical parameters is expected to bring forward a satisfactory description for physically short cracks.

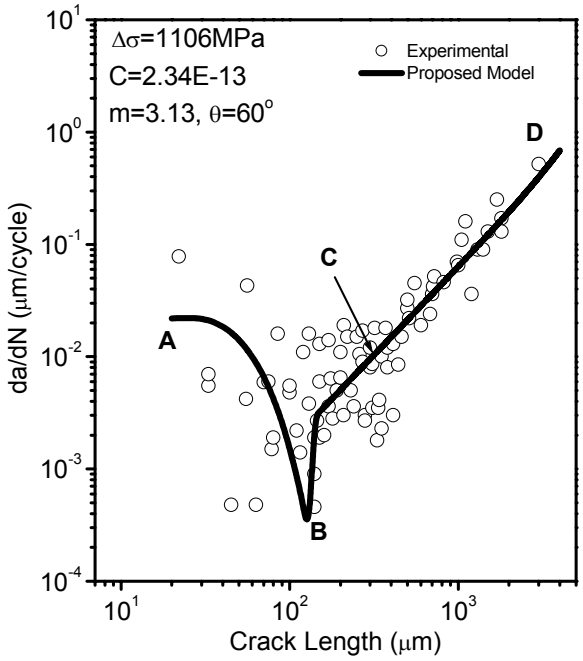

Fig.7.7 Reported data vis-à-vis the present model (data has been taken from ref. 142).

7.5 Conclusions

The major conclusions from this part of investigation are:

- A new model has been proposed for short fatigue crack growth considering mode-mixicity factor and specimen-surface characteristics around short cracks. Some reported experimental results have been satisfactorily described using this model.
- A single Paris-Erdogon type equation can be used for predicting both short and long crack growth using some additional constants related to the mean plane of a short crack with respect to its loading axis.

Chapter 8

Concluding remarks and scope for future research

In this chapter, the major conclusions listed at the end of chapter 4 to chapter 7 have been reviewed and the implications of the experimental design, the obtained results and their analyses have been overviewed. The major findings of this investigation have been highlighted and the experience acquired from this work has been used to indicate some guidelines for future research.

All critical engineering applications demand assessment of the structural integrity of components in the employed service conditions for their safe operation. One of the major components in the assessment of structural integrity is the evaluation of the fatigue behaviour of the structural materials. The present investigation deals with this component and is aimed to strengthen the understanding of fatigue damage below and near fatigue threshold values in structural materials. The phenomena of fatigue crack initiation, short crack growth (SCG) and fatigue thresholds for short and long cracks have been studied using five plain carbon steels. Some salient aspects of this investigation are: (i) the developments of new specimen configurations to study short crack growth behaviour and to determine long crack fatigue thresholds using rotating bending machine, (ii) examination of crack initiation in predominantly ferrite and ferrite-pearlite plain carbon steels, (iii) examination of fatigue crack path vis-à-vis microstructural features and (iv) modeling growth of physically short cracks.

The investigation related to crack initiation on two clean commercial steels exhibiting ferritic and ferrite-pearlite structures was directed to understand the sites for crack initiation in these materials and to reveal the mechanisms associated with the crack initiation process. These studies have shown that ferrite-pearlite interfaces and/or ferrite-ferrite grain boundaries are significantly preferred crack initiation sites in the investigated steels. The formation of slip band inside the grain body, slip band impingement at grain boundary and elastic-plastic incompatibility are attributed as the main causes for crack initiation in ferritic (S00) steel. Elastic-plastic incompatibility, on the other hand, is attributed to be the primary mechanism for crack initiation at the ferrite-pearlite interfaces and at the ferrite grain boundaries in the ferrite-pearlite

(S14) steel. The formation of irregular voids inside slip bands, initiation and growth of small voids at grain boundaries and their subsequent joining are some new observations for the process of fatigue crack initiation in the ferritic (S00) steel. It is observed here for the first time that the angle between the direction of banding and the loading axis, has pronounced effect on the orientation and on the size of the initiated cracks in the investigated ferrite-pearlite (S14) steel.

Earlier studies on short cracks are primarily directed to understand the mechanics and mechanisms of SCG and how SCG gets influenced by the microstructure of a material. Short cracks are known to exhibit several thresholds unlike long cracks. The highest value amongst these has been termed here as 'near long crack fatigue threshold (NLFTH)'. The major aim of the investigations related to SCG in the selected steels (S00, S25 and S47) is to determine their NLFTH values and to understand whether the microstructure of the investigated materials influence their NLFTH. These studies have revealed that NLFTH for steels increases with increasing pearlite content in the microstructure. The part of a fatigue crack path through a phase is found proportional to the volume fraction of the latter in the microstructure. The primary aim in this part of the investigation is preceded by the development of a new specimen configuration for which short crack growth data can be generated conveniently with the help of a rotating bending machine. The developed technique is relatively simple, inexpensive and provides satisfactory generation of short crack growth data.

The ASTM standard E647 suggests the procedure for determining crack growth rate and long crack fatigue threshold (ΔK_{th}). But determination of ΔK_{th} usually requires significant time engagement of servo-hydraulic or electro-magnetic resonance type machines. A simple technique has been developed for fatigue crack growth studies using rotating bending machine and specimens having new configurations to overcome the above experimental difficulties. Fatigue thresholds of four steels (S00, S25, S47 and S62) have been determined using the developed technique and the average threshold values were found to be associated with standard deviation of $\pm$ 0.1 $MPam^{1/2}$. Also the developed procedure is based on measurement of da/dN with the order of 10^{-12} m/cycle. The results generated by the developed technique have been compared with those generated by ASTM standard procedure.

The threshold values measured by the developed technique appear to represent effective fatigue thresholds determined by the standard procedure. Thus the developed technique is reliable, sensitive and it possibly helps to obtain effective fatigue threshold. The threshold value of the investigated steels was found to increase with increasing pearlite content. The sum of the segmental lengths of a crack passing through different constituents in a microstructure is found approximately proportional to the volume fractions of the constituents in the investigated steels. Analyses of the crack growth behaviour near the notch also indicate occurrence of non-propagating cracks in two steels. The occurrence of non-propagating cracks has been attributed qualitatively to the nature of some secondary stress field present at the crack tip.

There exist several attempts to describe short crack growth behaviour through modeling. But most of these models are focused to illustrate growth of microstructurally short cracks. An empirical model has been suggested here to describe growth of physically short cracks. This model considers: (i) the deviation of the mean plane of a short crack with respect to its loading axis and (ii) an assumed variation in the crack-tip material characteristics till it reaches a transition crack length. The effect of the above factors on crack growth characteristics has been demonstrated using several simulated results. The applicability of the proposed model has been verified with some typical results generated on the investigated steels as well as with some reported data.

Two new techniques, one to study short crack growth behaviour and the other to determine long crack fatigue thresholds both using rotating bending machine, have been developed. As long crack fatigue threshold is an important design parameter to ensure safe-life of structural components, it is expected that the developed techniques would be used in the coming days to generate threshold data for various materials. Future studies in this direction are expected to establish the potentials of the developed techniques for fatigue studies. The long crack fatigue threshold value estimated by the developed technique for a steel appear to represent its effective fatigue threshold determined by the standard test procedure. This aspect demands re-examination in other materials in future work. The length of a crack path through a phase has been found to be proportional to its volume fraction in the microstructure. Future work should be directed to examine the inter-relation between fatigue crack path and their associated microstructure in alternate multiphase systems.

References

1. S. Suresh, *Fatigue of materials*, 2nd ed., University of Cambridge, United Kingdom, p.141, 222, 541, 1998.
2. U. Essman, U. Gosele and H. Mughrabi, *Phil. Mag. A*, vol.44, p.405 (1981).
3. J. G. Antonopoulos, L. M. Brown and A. T. Winter, *Phil. Mag.,* vol.34, p.549 (1976).
4. S. Pearson, *Engg. Fract. Mech.*, vol.7, p.235 (1975).
5. W. L. Morris, *Metall. Trans*., vol.10A, p.1117 (1980).
6. K. J. Miller, M. F. E. Ibrahim, *Fatigue Eng. Mater. Struct.*, vol.4, p.263 (1981).
7. J. C. Newman Jr., *ASTM STP* 748, p.53, Philadelphia, (1981).
8. E647-93, *Annual Book of ASTM Standards*, vol. 03.01, P. 679, 1993.
9. P. C. Paris and F. Erdogan, *J. Basic Eng*., vol.85, p.528 (1963).
10. A. Saxena, *Nonlinear fracture mechanics for engineers*, CRC press, New York, 1998.
11. T. L. Anderson, *Fracture mechanics – fundamentals and applications*, 2nd edition, CRC press, New York, 1995.
12. G. E. Dieter, *Mechanical Metallurgy*, SI Metric Edition, McGraw Hill Publishing Co. Place, London, 1988.
13. R. W. Herzberg, *Deformation and fracture mechanics of engineering materials*, 4th ed., John Wiley & Sons, Singapore, p.327, 542 (1996).
14. G. R. Irwin, *Handbuch der Physik*, VI, Springer, Berlin, p.551 (1958).
15. D. S. Dugdale, *J. Mech. Phys. Solids*, vol.8, p.100 (1960).
16. G. T. Hahn and A. R. Rosenfield, *Int. J. Fract. Mech*., vol.4, p.79 (1968).
17. S. Banerjee, *Engg. Fract. Mech.*, vol.15, p.343 (1981).
18. J. A. Jacobs, *Phil. Mag*., vol.F41, p.349 (1950).
19. F. A. McClintock, *J. Appl. Mech.*, vol.25, p.582 (1958).
20. J. R. Rice and G. F. Rosengren, *J. Mech. Phys. Solids*, vol.16, p.1 (1968).
21. A. Well, *Brit. Welding Journal*, vol.10, p.563 (1963).
22. J. N. Goodier and F. A. Field, *Fracture of Solids*, D. C. Dunker and J. J. Gilman (eds.), p.103, Wiley, New York 1963.
23. F. M. Burdkin and D. E. W. Stone, *J. Strain Analysis*, vol.1, p.145 (1966).
24. D. P. Rooke and F. J. Bradshaw, *Fracture*, p.46, Chaman & Hsll, UK, 1969.
25. D. Broek, *Elementary Engineering Fracture Mechanics*, Martinus Nijihoff Publ., The Netherlands, p.224, 1979.

26. *British Standards Institution Document BS5762*: Methods for Crack Opening Displacement (COD) Testing, 1979.

27. E 1290-89, Standard Test Method for Crack Tip-Opening Displacement (CTOD) Fracture Toughness Measurement, *Annual Book of ASTM Standards*, 1994, vol.03.01, p.946, ASTM, Philadelphia, PA.

28. J. N. Robinson and A. S. Tetelman, *ASTM STP* 559, p.139 (1974).

29. D. J. Hayes and C. E. Turner, *Int. J. Fract. Mech.*, vol.10, p.17 (1974).

30. J. R. Rice, *J. Appl. Mech*., vol.35, p.379 (1968).

31. J. W. Hutchison, *J. Mech. Phys. Solids*, vol.16, p.13 (1968).

32. J. D. Eshelby, *Solid State Physics*, F. Seitz and D. Tumbull (Eds.), Academic Press, New York, vol.3, p.79 (1956).

33. G. P. Cherepanov, *J. Appl. Mech. Translation*, vol.31, p.504 (1967).

34. J. A. Begley and J. D. Landes, *ASTM STP* 514, p.1, Philadelphia, 1972.

35. J. D. G. Sumpter and C. E. Turner, *Int. J. Fract. Mech*., vol.9, p.320 (1973).

36. G. R. Irwin, *ASTM Bulletin*, p.29 (1960).

37. J. M. Kraft, S. M. Sillivan and R. W. Boyle, *Conf. Proc. Crack-Propagation Symposium*, vol.1, p.8, Cranfield, 1961.

38. E 561-92a, Standard Practice for R-curve determination, *Annual Book of ASTM Standards*, vol.03.01, p.597, ASTM Philadelphia PA, 1994.

39. E 1151-87, Standard test method for determining J-R curves, *Annual Book of ASTM Standards*, vol.03.01, p.847, ASTM Philadelphia PA, 1994.

40. E 399-90, Standard test method for plane-strain fracture toughness of metallic materials, *Annual Book of ASTM Standards*, vol.03.01, p.407, ASTM Philadelphia PA, 1994.

41. S. Suresh and O. Ritchie, *Int. Met. Rev.*, vol.29, p.445 (1984).

42. K. J. Miller and E. R. de los Rios, (eds), "*The Behaviour of Short Fatigue cracks*", EGF1, Mechanical Engineering Publications, London, 1986.

43. R. O. Ritchie and J. Lankford, (eds.), "*Small Fatigue Cracks*", The Metallurgical Society Inc., New York, 1986.

44. K. S. Ravichandran, R.O. Ritchie, Y. Murakami, (eds), *Small Fatigue Cracks: Mechanics, Mechanisms and Applications*, Elsevier Science Publications (1999).

45. K. S. Ravichandran and Xu-Dong Li, *Acta Mater.*, vol.48, p.525 (2000).

46. S. J. Hudak, D. L. Davidson, K. S. Chan, A. C. Howland and M. J. Walsch, *Growth of small cracks in aero-engine disc materials*, Report No. AFWAL-TR-88-4090, Dayton: Air force wright aeronautical laboratories.

47. P. J. E Forsyth and A. Stubbington, *J. Inst. Metals*, vol.84, p.173 (1955).

48. W. A. Wood, *Phil. Mag.*, vol.3, p.692 (1958).

49. N. F. Mott, *Acta Metall.*, vol.6, p.195 (1958).

50. A. Hunsche and P. Neumann, *Acta Metall.*, vol.34, p.207 (1986).

51. B. T. Ma and C. Laird, *Acta Metall.*, vol.37, p.325 (1989).

52. B. T. Ma and C. Laird, *Acta Metall.*, vol.37, p.337 (1989).

53. K. Katagiri, A. Omura, K. Koyanagai, J. Awatani, T. Shiraishi and H. kaneshiro, *Met. Trans.*, vol.8A, p.1769 (1977).

54. J. Porter and J. C. levy, *J. Inst. Metals*, vol.89, p.86 (1960).

55. W. H. Kim and C. Laird, *Acta Metall.,* vol.26, p.789 (1978).

56. J. C. Figueroa and C. laird, *Mater. Sci. and Eng*., vol.60, p.45 (1983).

57. T. Wantanabe, *J. de Physique,* vol.C4, p.555 (1985).

58. H. Mughrabi, R. Wang, K. Differt and U.Essmann, *In quantitative measurement of physical damage*, STP 811, p. 5-45, Philadelphia, PA: American society for testing and materials (1983).

59. F. Guiu, R. Dubniak and R. C. Edward, *Fat. Eng. Mater. Struct*., vol.5, p.311 (1982).

60. H. Mugrhabi, K. Herze and X. Stark, *Int. J. Fracture*, vol.17, p.193 (1981).

61. J. Lankford and F. N. Kusenberger, *Met. Trans.*, vol.4A, p.553-9 (1973).

62. J. C. Grosskreutz and G. C. Shaw, In *fracture 1969,* P. L. Pratt (ed.), p. 620 (1969).

63. J. M. Hyzak and I. M. Berstein, *Met. Trans.*, vol.13A, p.33 (1982).

64. H. J. Gough and D. G. Sopwith, *J. Inst. Metals*, vol.49, p.93 (1932).

65. N. Thompson, N. J. Wadsworth and N. Louat, *Phil. Mag*., vol.1, p.113 (1956).

66. C. Laird, *ASTM STP* 415, p.131, Philadelphia, 1967.

67. H. Kitagawa and S. Takahashi, *Proc. second international conference on mechanical behaviour of materials*, p. 627, Metals Park, American society for Metals, 1976.

68. K. Tanaka, Y. Nakai and M. Yamashita, *Int. J. Fract*., vol.17, p.519 (1981).

69. D. Taylor and J. F. Knott, *Fat. Eng. Mater. Struct.*, vol.4, p.147 (1981).

70. J. Lankford, *Fat. Eng. Mater. Struct*., vol.5, p.233 (1982).

71. J. Lankford, *Fat. Fract. Eng. Mater. Struct.,* vol.6, p.15 (1983).

72. C. W. Brown and M. A. Hicks, *Fat. Fract. Eng. Mater. Struct.*, vol.6, p.67 (1983).

73. L. Wagner, J. K. Gregory, A. Gysler and G. Lutjering, *In small fatigue cracks,* R. O.Ritchie, and J. Lankford (Eds.), p.117, Warremdae: The metallurgical Society of the American Institute of Mining, Mineral and Petroleum Engineers (1986).

74. M. H. El Haddad, T. H. Topper and K. N. Smith, *Eng. Fract. Mech*., vol.11, p.573 (1979).

75. H. Ohuchida, S. Usami, A. Nishioka, *Bulletin of the Japan society of Mech. Engineers*, vol.18, p.1185 (1975).

76. T. Kunio and K. Yamada, *ASTM STP* 675, p.342, Philadelphia, (1979).

77. S. Usami, In *Fatigue Thresholds*, J. Baklund, A. F. Blom and C. J. Beevers, (eds.), p. 205, Engineering Materials Advisory Services, Warly, West Midlands, 1983.

78. H. Suzsuki and A. J. McEvily, *Metall. Trans.* vol.10A, p.475 (1979).

79. V. B. Dutta, S. Suresh and R. O. Ritchie, *Metall. Trans.*, vol.15A, p.1193 (1984).

80. A. Saxena and Jr. S. J. Hudak, *Int. J. Fract.*, vol.14, No.5 (1978).

81. V. Bachman and D. Munz, *Eng. Fract. Mech*., vol.11, p.61 (1979).

82. G. A. Hartman and D. A. Johanson, *Expl. Mech.*, p.106, (1987).

83. L. P. Pook, *J. Strain Analysis*, vol.10, p.242 (1975).

84. R. P. Wei and R. L. Brazill, *ASTM STP* 738, p.103, Philadelphia, 1981.

85. K. K. Ray, "Crack growth measurement" in *"Encyclopedia of Materials: Science and Technology"*, ed. K.H.J. Buschow, R.W. Cahn, M.C. Flemings, B. Illschner, E.J. Kramer and S. Mahajan, publ. Amsterdam, Elsevier: p.1741, 2001.

86. G. P. Sheldon, T. S. Cook, T. W. Jones, and J. Lankford, *Fat. Eng. Mater. Struct*., vol.3, p.219 (1981).

87. C. Blochwitz and W. Tirschler, *Mater. Sci. Eng*. vol.A276, p.273 (2000).

88. R. P. Gangloff, In *Fatigue Thresholds*, J. Baklund, A. F. Blom and C. J. Beevers, (eds.), p.175, Engineering Materials Advisory Services, Warly, West Midlands, 1983.

89. R. P. Gangloff, *ASTM STP* 738, p.120, Philadelphia, (1981).

90. R. P. Gangloff, *Res. Mech. Lett*., vol.1, p. 299 (1981).

91. M. T. Resch, D. V. Nelson, J. C. Shyne and G. S. Kino, in *Fatigue Thresholds*, J. Baklund, A. F. Blom and C. J. Beevers, (eds.), p.473, Engineering Materials Advisory Services, Warly, West Midlands, 1983.

92. W. Baxter, *Int. J. Fatigue*, vol.5, p.37 (1983).

93. A. K. Zurek, James, M. R. and Morris, W. L., *Metall. Trans.*, vol.14A, p.1697 (1983).

94. E. Heuaum and M. E. Fine, *Scripta Metall.*, vol.18, p.1235 (1984).

95. Robert S. Vecchio and R. W. Hertzberg, *Eng. Fract. Mech*, vol.22, p.1049 (1985).

96. N. M. Grinberg, *Int. J. Fatigue,* vol.13, p.370 (1991).

97. J. C. Healy, *Int. J. Fatigue*, vol.13, p.133 (1991).

98. J. W. Provan, *Int. J. Fatigue*, vol.13, p.99 (1991).

99. K. S. Ravichandran, *Int. J. Fatigue*, vol.18, p.9 (1996).

100. R. L. Carlson, *Int. J. Fatigue*, vol.19, p.S119 (1997).

101. J. D. Costa, C. M. Branco and J. C. Radon, *Int. J. Fatigue*, vol.19, p.161 (1997).

102. De-Guang Shang, *Int. J. Fatigue*, vol.20, p.683 (1998).

103. W. L. Morris, *Int. J. Fatigue*, vol. 8A, p.589 (1977).

104. R. R. Stephens, *Int. J. Fatigue*, vol.15, p.273 (1993).

105. M. D. Halliday, *Int. J. Fatigue*, vol.19, p.273 (1997).

106. K. Obrtlik, *Int. J. Fatigue*, vol.19, p.471 (1997).

107. E. R. De Los Rios, Hussain, J. Mohamed and K. J. Miller, *Fat. Fract. Engg. Mater. Struct*., vol.8, p.49 (1985).

108. K. Tokaji, T. Ogawa and Y. Harada, *Fat. Fract. Engg. Mater. Struct*., vol.9, p.205 (1986).

109. K. T. Venkatewara Rao, W. Tu and R. O. Ritvhie, *Scripta Metall.*, vol.20, p.1459 (1986).

110. D. J. Nicholls, *Int. J. Fatigue*, vol.13, p.469 (1990).

111. D. A. Gerand, *Int. J. Fatigue*, vol.13, p.345 (1991).

112. M. Levin, *Int. J. Fatigue*, vol.15, p.377 (1993).

113. D. Taylor, J. Li and A. Giese, *Int. J. Fatigue*, vol.17, p.201 (1995).

114. S. Beretta and S. Matteazzi, *Int. J. Fatigue*, vol.18, p.451 (1996).

115. M. N. James, *Int. J. Fatigue*, vol.13, p.169 (1991).

116. Zhou Jingen, Zhong Jianyun, Feng Zhongxin and Li Nian, *Int. J. Fatigue*, vol.15, p.141 (1993).

117. K. Tokaji, *Int. J. Fatigue*, vol.16, p.571 (1994).

118. M. N. James and J. F. Knott, *Fat. Fract. Eng. Mater. Struct*., vol.8, p.177 (1985).

119. K.Tanaka and P. P .Wei, *Engg. Fract Mech.*, vol.21, p.293 (1985).

120. O. Jim and S. Mail, *Mater. Sci. Eng.,* vol.359A, p.356 (2003).

121. W. Elber, *Eng. Fract. Mech.*, vol.2, p.37 (1970).

122. W. Elber, *ASTM STP* 486, p.230 (1971).

123. X.-P. Zhang, J.-C. Li, C.H. Wang, L. Ye and Y.-W. Mai, *I. J. Fatigue* vol.24, p.529 (2002).

124. K. Tanaka and Y. Nakai, *Fat. Eng. Mater. Struct*., vol.6, p.315 (1983).

125. K. Tanaka and Y. Nakai, *J. Eng. Mater. Tech.,* vol.106, p.192 (1984).

126. W. L. Morris, and O. Buck, *Metall. Trans.*, vol.8A, p.597 (1977).

127. J. Lankford and D. L. Davidson*, Acta Metall*., vol.31, p.1273 (1983).

128. J. Lankford and D. L. Davidson*, Fat. Eng. Mater. Struct.*, vol.6, p.241 (1983).

129. R. O. Ritchie, S. Suresh, and C. M. Morris, *J. Eng. Mater. Tech.*, vol.102, p.293 (1980).

130. A. T. Stewart, *Eng. Fract. Mech*., vol.13, p.463 (1980).

131. S. Suresh, G. F. Zamiski, and R. O. Ritchie, *Metall. Trans*., vol.12A, p.1435 (1981).

132. V. Sinha, C. Mercer and W. O. Soboyejo, *Mater. Sci. Eng.*, vol.A287, p.30 (2000).

133. S. Suresh and R. O. Ritchie, *Metall. Trans*., vol.13A, p.1627 (1982).

134. S. Suresh, *Scripta Metall*., vol.16, p.995 (1982).

135. M. R. James and W. L. Morris, *Metal. Trans.*, vol.14A, p.153 (1983).

136. P. K. Liaw and W. A. Logsdon, *Eng. Fract. Mech*., vol.22, p.115 (1985).

137. P. D. Hobson, *Fat. Fract. Eng. Mater. Struct*., vol.5, p.323 (1982).

138. K. S. Chan and J. Lankford, *Scripta Metall.*, vol.17, p.529 (1983).

139. E. R. De los Rios, Z. Tang, and K. J. Miller, *Fat. Fract. Eng. Mater. Struct*., vol.7, p.97 (1984).

140. A. Navarro and E. R. de los Rios, *Fat. Fract. Engg. Mater. Struct.* vol.11, p.383 (1988).

141. K. Hussain, E. R. de los Rios and A. Navarro, *Eng. Fract. Mech.,* vol.44, p.425 (1993).

142. G. Murtaza, and R. Akid, *Int. J. Fatigue*, vol.17, p.207 (1995).

143. J. C. Newman Jr., E. P. Phillips and M. H. Swain, *Int. J. Fatigue*, vol.21, p.109 (1999).

144. A. J. McEvily, D. Eifler and E. Macherauch, *Eng. Fract. Mech*., vol.40, p.571 (1991).

145. D. Angelova and R. Akid, *Fat. Fract. Eng. Mater. Struct*., vol.21, p.771 (1998).

146. J. C. Newman Jr., and I. S. Raju, *Eng. Fract. Mech*., vol.15, p.185 (1981).

147. L. W. Wei, E. R. De los Rios, and M. N. James, *Int. J. Fatigue*, vol.24, p.963 (2002).

148. C. A. Rodopoulos and E. R. De los Rios, *Int. J. Fatigue*, vol.24, p.719 (2002).

149. W. F. Deans and C. E. Richards, *J. Testing and Evaluation*, vol.7, p.147 (1979).

150. M. Klesinl and P. Lukas, *Eng. Fract. Mech*., vol.4, p.77 (1972).

151. L. P. Pook, *ASTM STP 513*, p. 106 (1972).

152. D. Taylor, *Eng. Fract. Mech*., vol.32, p.177 (1989).

153. A. Saxena, S. J. Hudak Jr., J. K. Donald, and D. W. Schmidt, *J. Testing and Evaluation*, vol.6, p.167 (1978).

154. C. Bathias, *Fat. Eng. Mater. Struct.*, vol.4, p.1 (1981).

155. G. Mingda, D. Chuanfu, Z. Wei and Y. Minggao, *Fatigue 84*, EMAS, Warley, UK, p.287 (1985).

156. S. J. Hudak, A. Saxena, R. J. Bucci and R. C. Malcolm, Report No. AFML/TR/78/40, Air Force Materials Laboratory, USA, 1978.

157. A. J. Cadman, R. Brook, and C. E. Nicholson, *In Fatigue Thresholds*, EMAS, Warley, UK, p.59, 1981.

158. R. W. Hertzberg, G. Miller, K. Donald, R. J. Stofonak and J. Jaccard, Proceedings ICF5 (Cannes, France, 1981).

159. R. S. Williams, P. K. Liaw, M. G. Peck and T. R. Leax, *Eng. Fract. Mech.*, vol.18, p.953 (1983).

160. R. Brook, *Fatigue crack growth threshold concepts*, TMS-AIME, USA, p.417, 1983.

161. D. Taylor, *Fatigue thresholds*, Butterworths and Co., London, p.58, 135, 167, 1989.

162. D. Taylor, *In Fatigue* 84, EMAS, Warely, UK p.327, 1985.

163. B. Holper, H. Mayer, A.K. Vasudevan and S.E. Stanzl-Tschegg, *Int. J. Fatigue*, vol.25, p.397 (2003).

164. B.L. Boyce and R.O. Ritchie, *Eng. Fract. Mech*., vol.68, p.129 (2001).

165. J. Zhang, X. D. He and S. Y. Du, *Int. J. Fatigue*, vol.25, p.935 (2003).

166. K. Tanaka and Y. Akinawa, *In Fatigue 87*, EMAS, Warley, UK, p.739 1987.

167. H. Kitagawa, H. Nisitani and T. Matsuoto, *Trans. JSME* 42-356, p.996 (1973).

168. J. H. Kim and M. G. Kim, *Mater. Sci. Engg*., vol.A346, p.216 (2003).

169. J. R. Yates and M. W. Brown, *Fat. Fract. Eng. Mater. Struct.*, vol.10, p.187 (1987).

170. K. Yamada, M. G. Kim and T. Kunio, in: *The behaviour of short fatigue cracks*, K. J. Miller and E. R. de los Rios (eds.), p.261, EGF Pub. 1, Mechanical engineering publications, London, 1986.

171. A. Plumtree, *Mater. Sci. Eng*., vol.A234, p.236 (1997).

172. S. Taira, K. Tanaka and J. G. Ryu, *Proc. 16th Japan Cong. Mater. Res*, p.36 (1973).

173. M. M. Hammouda, R. A. Smith and K. J. Miller, *ASTM STP* 668, p.703, Philadelphia, (1979).

174. M. M. Hammouda, R. A. Smith and K. J. Miller, *Fat. Engg. Mater. Struct.*, vol.2, p.139 (1979).

175. R. A. Smith and K. J. Miller, *Int. J. Mech. Sci.*, vol.20, p.201 (1978).

176. M. H. Haddad, K. N El. Smith and T. H. Topper, *ASTM STP* 677, p.274 Philadelphia, (1979).

177. Xu Kewei, Hu Naisai and Zhou Huijiu, *Engg. Fract. Mech.*, vol.50, p.417 (1995).

178. De-Guang Shang, Wei-Xing Yao and De-Jun Wang, *Int. J. Fatigue*, vol.20, p.683 (1998).

179. P. Cacciola and G. Muscolino, *Comp. Struct.*, vol.80, p.2387 (2002).

180. K. Sadananda and A. K. Vasudevan, *Non-propagating incipient cracks from sharp notches under fatigue*, Private communication.

181. R. O. Ritchie, In *Small Fatigue Cracks: Mechanics, Mechanisms and Applications*, Proceedings of the Third Engineering Foundation International Conference, Turtle Bay Hilton, Oahu, Hawali, December 6-11, 1998; Ravichandran, R. S., Ritchie, R.O. Murakami, Y, Eds.; p.233, Elsevier: New York, 1999.

182. J. Lankford, *Fatigue Fract. Eng. Mater. Struct.*, vol.8, p.161, (1985).

183. W. J. Plumbridge, *J. Mater. Sci*., vol.7, p.939 (1972).

184. S. J. Hudak, A. Saxena, R. J. Bucci, and R. C. Malcolm: *Third Semi-Annual Report to AFML*, Westinghouse Research and Development Laboratories, Pittsburgh, May 1977.

185. J. Mautz and V. Weiss, *ASTM STP* 601, p.154 (1976).

186. C. Bathias, A. Paneau, J. Pluvinage, and P. Rabbe: *'Fracture 1977'*, D. M. R. Taplin (ed.), vol.2, p.1283, London, Institution of Mechanical Engineers, 1977.

187. H. Bao and A. McEvily, *J. Fatigue'96*, Sixth international fatigue congress, Vol.1 Berlin, Germany, May 6-10, 1996, Elsevier Science Inc., New York, p.381 (1996).

188. K. Fujitani, T. Sakai, A. Nakagawa and T. Tanaka, *Bull. Japan Soc. Mech. Eng*., vol.25, p.1195 (1982).

189. W. D. Dover and N. F. Boutle, *Jr. Strain Anal*., vol.13, p.129 (1978).

190. S. Sivaprasad, Ph.D thesis, 1998, I. I. T. Kharagpur, Inida.

191. K. Tokaji, Z. Ando, T. Amai and K. Morikawa, *J. Sci. Mater. Sci*., vol.31, p.51 (1982).

192. L. Grabowski, *Int. J. Fatigue*, vol.14, p.227 (1992).

193. R. P. Gangloff and R. P. Wei, In *Small Fatigue Cracks* (eds. R. O. Ritchie & J. Lankford), P. 239, Warrendale: The Metallurgical Society of the American Institute of Mining, Metallurgical and Petroleum Engineers, 1986.

194. A. Saxena, W. K. Wilson, L. D.Roth and P. K. Liaw, *Int. J. Fract.*, vol.28, p.69 (1985).

195. E 562-89, *Annual Book of ASTM Standards*, vol. 03.01, p 612**,** 1993.

196. E112-88, *Annual Book of ASTM Standards*, vol. 03.01, p.297**,** 1993.

197. G. E. Vander Voort, in "*Metallography princeples and practice*", Mc-Graw Hill Book Co., New York, 1984.

198. E1268-88, , *Annual Book of ASTM Standards*, vol. 03.01, p.918**,** 1993.

199. Japanese standard JISG-0555, *Microscopic testing method for the non-metallic inclusions of steels*, 1992.

200. E8-93, *Annual Book of ASTM Standards*, vol.03.01, p.130**,** 1993.

201. T. B. Massalski (ed-in-chief), H. Okamoto, P. R. Subramanian and L. Kacprzak (eds.), *Binary alloy phase diagrams*, second edition, vol.1, p.843, ASM International, Materials Park, Ohio, USA, 1990.

202. K. K. Ray and D. Mondal, *Acta Metall. Mater.,* vol.39, p.2301 (1991).

203. K. K. Ray and D. Mondal, *Metall. Trans. A,* vol.23A, p.3309 (1992).

204. S. Tarafder, Private communication.

205. P. K. Singh, J. Chattopadhyay, H. K. Kushwaha, S. Tarafder and V. R. Ranganath, *Int. J. Pressure Vessels and Piping*, vol.75, p.271 (1998).

206. K. J. Miller and E. R. de los Rios, (eds), "*The Short Fatigue Cracks*", ESIS-13, Mechanical Engineering Publications, London (1992).

207. M. Zhang, P. Yang, T. Yuxu, *Int. J. Fatigue*, vol.21, p.823 (1999).

208. Y. M. Hu, W. Floer, U. Krupp and H. J. Crist, *Mater. Sci. Engg*., vol.A278, p.170 (2000).

209. M. Long, R. Crooks and H. J. Rack, *Acta Mater.*, vol.47, p.661 (1999).

210. S. Ankem and H. Margolin, *Metall. Trans. A*, vol.17A, p.2209 (1986).

211. H. Mughrabi, in: G. C. Sih, J. W. Provan, M. Nijhoff (Eds.), Defects, Fracture and Fatigue, p.139, The Hugue, 1983.

212. H. J. Christ, H. Mughrabi, C. Witting-Link, in: P. Lukas, J. Polak (Eds.), *Basic Mechanism in Faitgue of Metals*, Elsevier, Amsterdam, p.83, 1988.

213. H. W. Liu, M. Bayerlein, H. Mughrabi, A. Day and P. N. Quested, *Acta Metall. Mater.*, vol.40, p.1763 (1992).

214. S. Kocanda, *Fatigue failure of metals*, Sijthoff and Noordhoff International Publishers, p.113, 1978.

215. J. Awatani and K. Katagiri, *Bulletin JSME*, vol.12, p.10 (1969).

216. H. Mughrabi, R. Wang, K. Differt and U. Essman, in J. Lankford, D. L. Davidson, W. L. Morris and R. P. Wei (eds.), *STP* 811, , Philadelphia, P.A: American Society for Testing and Materialspp., p.5-45, 1993.

217. H. Mizubayashi, S.J. Li, H. Yumoto and M. Shimotomai, *Scripta Mater.*, vol.40, p.773 (1999).

218. Craig Jr Roy R, *Mechanics of Materials*, 2nd ed, John Wiley and Sons, New York, p.747 (2000).

219. H. Tada, P.C. Paris and G. R. Irwin, *The stress analysis of cracks handbook*, Del research, Hellertown, Philadelphia, 1973.

220. U. Liendstedt, B. Karlsson and M. N. Nystrom, *Fat. Fract. Eng. Mater. Struct.,* vol.21, p.85 (1998).

221. K. Hussain, A. Tauqir, F. H. Hashmi and A. Q. Khan, *Metall. Trans*., vol. A25, p.2421 (1994).

222. K. Nakajima, K. Terao and T. Miyata, *Mater. Sci. Eng*., vol.A243, p.176 (1998).

223. G. Murtaza and R. Akid, *Int. J. Fatigue*, vol.18, p.557 (1996).

224. L. Edwards and Y. H. Zhang, *Acta. Metall. Mater.,* vol.42, p.1413 (1994).

225. K. Sadananda and A. K. Vasudevan, *Int. J. Fatigue,* vol.19, p.S99 (1997).

226. S. Shademan and W. O. Soboyejo, *Mater. Sci. Eng*., vol.335A, p.116 (2002).

227. C. Kaynak, A. Ankara and T. J. Baker, *Int. J. Fatigue*, vol.18, p.17 (1996).

228. J. M. Kendall, M. N. James and J. F. Knott, in: *The behaviour of short fatigue cracks*, K. J. Miller and E. R. de los Rios ER (eds.), p. 241, EGF pub, Mechanical Engineering Publications, London, 1986.

229. D. Taylor, *In Fatigue* 84, EMAS, Warley, UK, p.327, 1984.

230. S. Usami, in: *Fatigue thresholds-fundamentals and engineering applications*, J. Backlund, A. F. Blom and C. J. Beevers (eds.) vol-1, p.205, EMAS, Warley, UK, 1981.

231. A. J. McEvily, *Fatigue crack thresholds. Fatigue and Fracture*, ASM Handbook vol.19, p.134 (1996).

232. K.K. Ray, N. Narasaiah and R. Sivakumar, *Mater. Sci. Eng.A* **(**In Press**).**

233. D. L. Davidson, K. S. Chan and R. C. McClung, *Metall. Trans.*, vol.27A, p.2540 (1996).

234. N. M. Abd-Allah, M. M. Megahed and A. M. Eleiche, *J. Testing and Evaluation*, vol.30, No. 2, p.124 (2002).

235. Adel B. El-Shabasy and John J. Lewandowski, *Int. J. Fatigue*, vol.26, p.305 (2004).

236. K. Minakawa and A. J. McEvily, On near-threshold fatigue crack growth in steels and aluminium alloys, J. Backlund, A. F. Blom and C. J. Beevers (eds.) *Fatigue thresholds-fundamentals and engineering applications*, vol.1, p.373, EMAS, Warley, UK, 1981.

237. M. H. Haddad, K. N El. Smith and T. H. Topper, *Eng. Fract. Mech*., vol.11, p.573 (1979).

238. R. O Ritchie, *Int. Metals Review*, Nos. 5 and 6, p.205 (1979).

239. J. P. Campbell, and R. O. Ritchie, *Engg. Fract. Mech*. vol.27, p.229 (2000).

240. R. K. Nalla, J. P. Campbell and R. O. Ritchie, *Int. J. Fatigue*, vol.24, p.1047 (2002).

241. M. Y. He, H. C. Cao and A. G. Evans, *Acta Metall. Mater*., vol.38, p.839 (1990).

Appendix-A

Some terminologies in fracture mechanics

The defect-tolerant approach of fatigue analysis relates fatigue crack growth rate (FGCR) with stress intensity factor range. The concept of stress intensity factor is derived from the principle of linear elastic fracture mechanics (LEFM), which considers a unique distribution of stress ahead of a crack in a body under load [1,10-13]. The amplitude of such a stress distribution is defined as the stress intensity factor, the magnitude of which provides the driving force for crack propagation. The critical value of the stress intensity factor, which causes crack initiation in monotonic loading, is termed as the fracture toughness of a material (K_{IC}). The stress field ahead of a crack in an infinite specimen (Fig.A1) is usually described as:

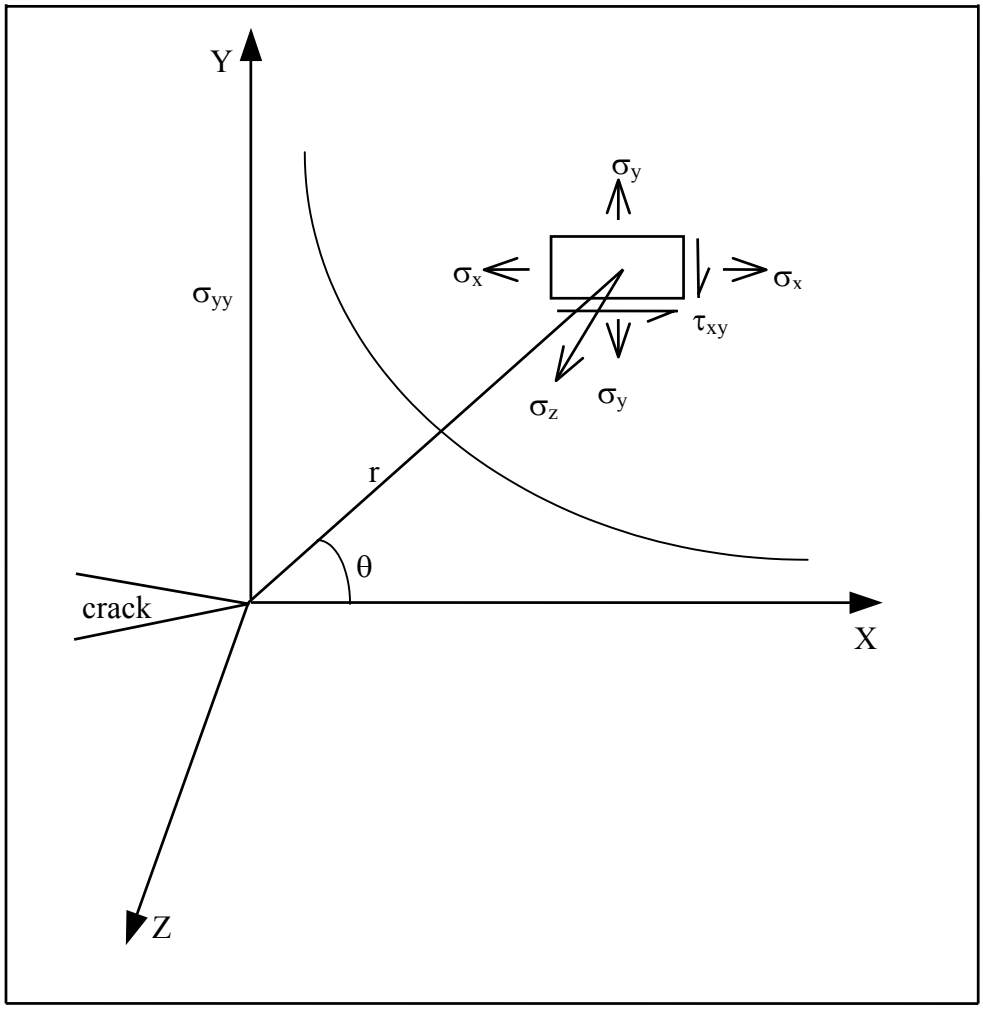

Fig.A1 Schematic representation of the stress distribution ahead of a Crack Tip.

$$\sigma_{ij} = \frac{K}{\sqrt{2\pi r}} f_{ij}(\theta) \quad \ldots(A.1)$$

where (r, θ) indicate polar co-ordinates of a point around the crack tip, f_{ij} are characteristic functions obtained from linear elasticity analysis. The magnitude of K for finite specimens in mode-I loading is given as:

$$K = \sigma \sqrt{\pi a}\ f\left(\frac{a}{W}\right) \quad \ldots(A.2)$$

where σ is the applied stress on a component, *a* is crack length, W is width of specimen and *f(a/*W*)* is a characteristic function which depends on the specimen geometry. The magnitude *f*(*a/*W) for an infinite specimen is unity.

In fatigue analysis, one considers the magnitudes of stress intensity factors K_{max} and K_{min} corresponding to the maxima and minima of the loading cycles, P_{max} and P_{min}, respectively with employment of eqn. (A.2). The fatigue crack is considered to be driven by a stress intensity factor range ΔK, which is given by

$$\Delta K = K_{max} - K_{min} \quad \ldots(A.3)$$

In addition to ΔK, the description of the cyclic stress state also incorporates the terminologies R-ratio and K_{mean} which are described as follows:

$$R = \frac{\sigma_{min}}{\sigma_{max}} = \frac{K_{min}}{K_{max}} \quad \ldots(A.4)$$

$$K_{mean} = \frac{K_{max} + K_{min}}{2} \quad \ldots(A.5)$$

It is well established that the region ahead of a crack tip is plastically yielded and this region is termed as plastic zone. The use of LEFM remains valid as long as the plastic zone is very small compared to the dimension of a crack length. The size of a plastic zone in monotonic loading for $\theta = 0$ (Fig.A1) is given as:

$$r_p = \alpha \left(\frac{K}{\sigma_y}\right)^2 \quad \ldots(A.6)$$

where α is a constant and depends on the state of stress i.e. plane stress or plane strain condition. The plastic zone ahead of a crack under cyclic-loading consists of an

intensely deformed region termed as reversed plastic zone. The magnitude of the reverse plastic zone (r_{rpz}) is given as [1]**:**

$$r_{rpz} \approx \frac{1}{\pi}\left(\frac{\Delta K}{2\sigma_y}\right)^2 \qquad \ldots(A.7)$$

The phenomenon of reverse plastic zone is illustrated in Fig.A2.

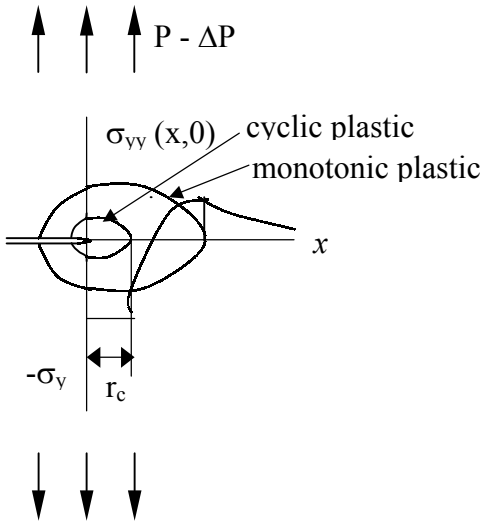

Fig.A2 Concept of reverse plastic zone.

Elastic-plastic fracture mechanics

The employment of LEFM remains valid as long as the size of the plastic zone is insignificantly small in comparison to significant dimensions of the cracked specimen geometry. In materials where the size of the plastic zone is large, fracture conditions are controlled by EPFM. EPFM often uses the concept of non-linear elasticity to obtain solutions for equivalent plastic problems. Unlike LEFM, EPFM demands a careful understanding of the crack tip plasticity and currently this discipline provides three established procedures for obtaining fracture criteria [1,10]. These are: (i) Crack Tip Opening Displacement (CTOD), (ii) J-integral and (iii) R-curve analysis.

Crack tip plasticity

The presence of larger plastic zone induces a higher displacement field than that calculated by elasticity theory. Irwin [14] was the first to provide a measure of such plastic zone, and suggested that the presence of a larger plastic zone makes a

crack behave as if it were longer than its actual size, which lowers the stiffness of the component. A series of refined calculations [10,11,15-20] later followed to predict the shape and the size of the plastic zone associated with crack tips. These investigations have established that the size and shape of a plastic zone depends on (a) mode of fracture, (b) yield criterion and (c) strain hardening rate of the material.

CTOD Parameter

Wells [21] proposed the concept of CTOD as a fracture criterion which was improved upon by Goodier and Field [22] and Burdekin and Stone [23]. Using the Dugdale [15] formulation for plastic zone size given by

$$\frac{a}{\mathrm{C}} = \cos\left(\frac{\pi\sigma}{2\sigma_y}\right) \qquad \text{...(A.8)}$$

where a is half the crack length, and C is equal to a+d, where d denotes the length of the plastic zone at the crack tip, the expression for CTOD (δ) suggested by the above investigators [23] is

$$\delta = \frac{8a}{\pi\sigma_y}\log\left(\sec\frac{\pi\sigma}{2\sigma_{\mathrm{y}}}\right) \qquad \text{...(A.9)}$$

Equation (A.9) can be simplified for $\sigma << \sigma_y$ as,

$$\delta = \frac{\mathrm{K}^2}{\mathrm{E}\sigma_{\mathrm{y}}} \qquad \text{... (A.10)}$$

For constrained yielding eqn.(A.10) can be written as,

$$\delta = \frac{\mathrm{K}^2}{\mathrm{m_1 E}\sigma_{\mathrm{y}}} \qquad \text{...(A.11)}$$

where m_1 is a constant and its value lies between 1 and 2.

Equation (A.10) and eqn. (A.11) indicate that as $K \rightarrow K_C$, $\delta \rightarrow \delta_C$, and hence a critical value of CTOD (δ_C) is a material property which depends only on microstructure of the material apart from temperature and the loading rate used for testing. In addition, if the size of plastic zone is insignificantly small, $K \rightarrow K_C$, and $\delta \rightarrow \delta_C$. Thus, CTOD parameter is applicable in both LEFM and EPFM domains.

The major difficulty associated with the determination of CTOD lies in its experimental measurement. Several procedures like optical method, extraction of replica, paddle device, infiltration technique [24,25], etc., have been used to measure CTOD in the early stages of development of this concept. Currently the recommendations given by the British and the ASTM standard test procedures [26,27] prescribe the use of clip gauge to measure displacement at the crack mouth and subsequently converting the crack mouth opening displacement (CMOD) to δ (CTOD). Such conversions can be obtained by experimental, theoretical and finite element analyses [28,29].

J-Integral parameter

The J-integral characterizes the elastic-plastic stress field near the crack tip in the same way as K describes the crack tip elastic stress field. A path independent contour integral introduced by Rice [30], and subsequently adopted by Hutchinson [31], Rice and Rosengren [20] and others [32,33] provides a description of the crack tip mechanical environment for the elastic-plastic situation.

The two dimensional form of the line integral proposed by Rice [3068RIC1] can be written as

$$J = \int_{\Gamma} W\, dy - T \frac{\partial u}{\partial x} ds \qquad ...(A.12)$$

where Γ is closed contour around the crack tip followed counter clockwise in a stressed solid and the other parameters are defined in Fig.A3.

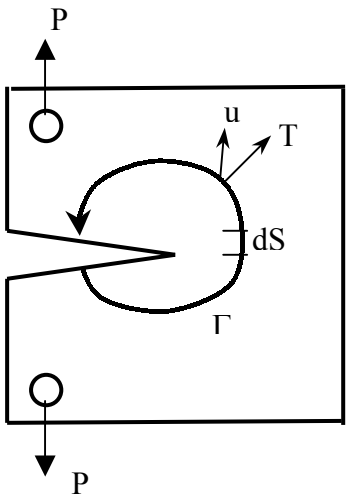

Fig.A.3 A contour around a crack-tip and nomenclature used in the definition of J-integral.

Rice [30] has shown that the J-integral as defined above is the change in potential energy for a virtual crack extension of ∂a, and J can be defined as

$$J = -\frac{\partial V}{\partial a} \qquad ...(A.13)$$

where V represents potential energy.

The significance of path independence lies in the fact that the value of J evaluated remote from the crack tip can be used to describe conditions near the crack tip.

During deformation through incremental plasticity, the potential energy term is no longer available for crack propagation since a portion of the energy is dissipated in plastic deformation. The physical meaning of J as energy release rate given by eqn. (A.13) is thus lost in real materials [34,35]. Therefore for an elastic-plastic situation eqn. (A.13) should be written as [30]

$$J = -\frac{1}{B}\frac{\partial U}{\partial a} \qquad ...(A.14)$$

where U is the strain energy, B is the component thickness and $\partial U/\partial a$ represents the elastic and plastic work done per unit crack growth.

The R-curve

In addition to J-integral and CTOD criteria, R-curve analysis is an alternative technique for determining the fracture resistance of a material in the EPFM domain. Unlike the earlier two approaches the emergence of R-curve technique is based on an extension of LEFM concept to the EPFM regime.

Irwin [36] proposed that there is a continuous balance between the released and the consumed energy during slow stable crack growth, and failure occurs when the rate of change in the elastic energy rate, $\partial G/\partial a$, equals the rate of change in the material resistance to such crack growth, $\partial R/\partial a$. This phenomenon of instability is illustrated using Fig.A4 as the point of tangency between G and R when plotted against crack length. Knowing a material's R curve and using the correct stress and crack length dependence of G for a given specimen configuration, it is possible to determine G_C or K_C. Kraft et. al. [37] suggested that R is invariant for a given

material-specimen-environment system, and the R curve is a function of the magnitude of the crack extension Δa irrespective of the initial crack size.

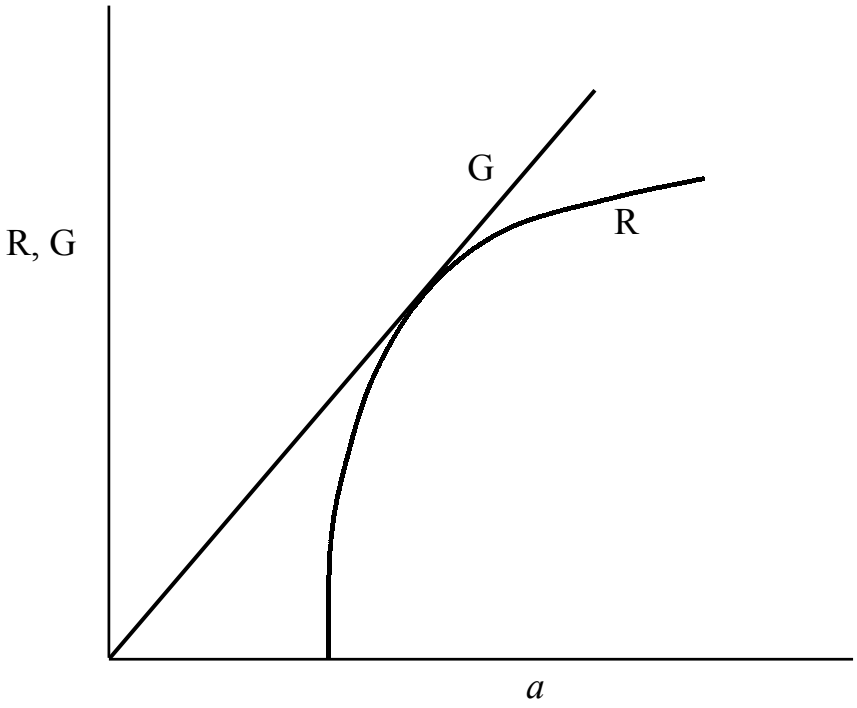

Fig.A4 A typical schematic diagram of G-R curve.

ASTM has recommended standard procedures for the construction of R curve using K concept [38], according to which

$$K_R = \frac{P}{B\sqrt{W}} f(a/W) \qquad ...(A.15)$$

where $f(a/W)$ is a polynomial function dependent upon the specimen geometry.

The R-curve describes the entire fracture behaviour of a material, incorporating both crack initiation and crack propagation. This method also provides an alternative way to analyze fracture behaviour of an elastic-plastic material where determination of valid J_{IC} is not possible. The recommended procedure for J-R analysis given by ASTM standard [39] divides the J-resistance of a material into elastic and plastic components.

$$J_R = J_e + J_p$$

The elastic component is given by

$$J_e = \frac{K^2\left(1-\nu^2\right)}{E} \qquad ...(A.16)$$

in which the value of K is computed in a similar fashion to the computation of stress intensity factor described in the ASTM standard E399 [40], and the plastic component of J is given by

$$J_p = \frac{2A}{Bb} \qquad \text{(for TPB specimen)} \qquad ...(A.17)$$

where A is the area under the load-displacement curve during the J-integral test, b is the remaining unbroken ligament and B is the specimen thickness. The magnitude of J_p can also be obtained from the measurement of CMOD.

Publications and presentations

Publications

1. **N. Narasaiah** and K. K. Ray
   Design against fatigue failure of spheroidal graphite cast iron
   Indian Foundry Journal, Vol. 7, No. 5, pp. 17-25 (May, 2001).

2. A. K. Dutta, **N**. **Narasaiah**, A. B. Chattopadhyaya, K. K. Ray
   The load dependence of hardness in alumina-silver composites
   Ceramics International, Vol. 27, No. 4, pp. 407-413 (June 2001).

3. A K. Dutta, **N. Narasaiah**, A. B. Chattopadhyaya & K. K. Ray
   "The role of microstructure on the relationship between wear resistance and mechanical properties of ceramic cutting tools"
   in "Advances in Materials and Materials Processing", Tata McGraw-Hill Publishing Limited, New Dehli, pp. 282-286 (2002).

4. A K. Dutta, **N. Narasaiah**, A. B. Chattopadhyaya and K. K. Ray
   "Influence of microstructure on wear resistance parameter of ceramic cutting tools**",** Materials and Manufacturing Processes, vol. 17, No. 5, pp. 651-670 (2002).

5. **N. Narasaiah** and K. K. Ray
   Modelling of Short Fatigue Crack Growth Behaviour
   Transactions of Indian Institute of Metals, Vol. 56, No.4, pp. 421-428 (Aug 2003).

6. K. K. Ray, **N. Narasaiah** and R. Sivakumar
   Studies on small fatigue crack growth behaviour of a plain carbon steel using a new specimen configuration
   Materials Science and Engineering A **(**In Press**).**

7. **N. Narasaiah** and K. K. Ray
   Small crack formation in a nuclear grade low carbon steel with banded ferrite-pearlite structure
   (To be Communicated).

8. **N. Narasaiah** and K. K. Ray
   Estimation of long fatigue crack thresholds using a rotating bending machine
   (To be Communicated).

9. **N. Narasaiah** and K. K. Ray
   Effect of microstructure on fatigue crack growth behaviour
   (Under preparation).

Presentations

1. **N. Narasaiah** and K. K. Ray
   Influence of microstructure on fatigue crack growth in cast iron
   Presented at the National conference on cast iron technology, 04 November 2000, Kulti, West Bengal, India.

2. **N. Narasaiah,** K. K. Ray
   A new model for short fatigue crack growth using mixed mode fracture mechanics
   Presented at 55th Annual Technical Meeting, Indian Institute of Metals, 18-21 November, 2001, Bhubaneswar, India.

3. A. K. Dutta, **N. Narasaiah**, A. B. Chattopadhyaya & K. K. Ray
   The role of microstructure on the relationship between wear resistance and mechanical properties of ceramic cutting tools
   Presented at International Conference on Advances in Materials and Materials Processing, 1-3 February, 2002, Indian Institute of Technology, Kharagpur, India.

4. **N. Narasaiah** and K. K. Ray
   Modelling of Short Fatigue Crack Growth Behaviour
   Presented at Fourth National Symposium of Research Scholars, 27-28 September, 2002, Indian Institute of Technology, Chennai, India. (**Best Technical Paper Award**)

5. **N. Narasaiah** and K. K. Ray
   The effect of banding on the nucleation of small cracks in SA333 steel
   Presented at 56th Annual Technical Meeting, Indian Institute of Metals, 14-17 November, 2002, Baroda, India.

6. S. S. Hazra, **N. Narasaiah**, S. K. Kudari and K. K. Ray
   Fracture toughness of thin sheets of 316 stainless steel
   Presented at 56th Annual Technical Meeting, Indian Institute of Metals, 14-17 November, 2002, Baroda, India.

7. R. Sivakumar and **N. Narasaiah**
   Short crack growth behaviour in a plain carbon steel
   Presented at IX National Meet, Congress of Metallurgical Professionals Involving Students, Industry and Teachers (COMPOSIT), 11-12 January, 2003, Indian Institute of Technology, Kharagpur India.

8. A. K. Dutta, **N. Narasaiah** and K. K. Ray
   Fatigue of cast components – A perspective through short crack behaviour
   Presented at Frontiers On Casting And Solidification Technology (FOCAST), 1-2 March, 2003, Indian Institute of Technology, Kharagpur India.

9. **N. Narasaiah** and K. K. Ray
   Characterization of near threshold fatigue crack behaviour in notched specimens under rotating bending
   Presented at Conference of Research Scholars on Materials Science and Engineering (CRSMSE), 30-31 August, 2003, Indian Institute of Technology, Kharagpur, India. **(Best Paper Award)**

10. **N. Narasaiah** and K. K. Ray
    Studies on fatigue crack growth thresholds using a rotating bending machine
    Presented at 57th Annual Technical Meeting, Indian Institute of Metals, 14-16 November 2003, Kolkata, India.